A Study of Unsteady Flow Wave Attenuation in Partially Filled Pipe Networks

A Thesis submitted for the degree of Doctor of Philosophy

by

Sarah Bridge

Department of Mechanical Engineering,

Brunel University

May 1984

A Study of Unsteady Flow Wave Attenuation in Partially Filled Pipe Networks

Abstract

The attenuation of unsteady flow in building drainage systems must be fully considered if water conservation proposals involving changes in flush volume or pipe diameter are not to lead to solid deposition and subsequent blockage of the drainage system. Empirical methods of studying attenuation are limited in their application and there is a need for a time-dependent numerical model to simulate flow in the building drainage system.

A number of numerical solutions to the time-dependent unsteady flow equations were considered and the method of characteristics was chosen for its suitability and proven usefulness. Full-scale flow tests were undertaken in the laboratory to validate the use of the method of characteristics and the results justified the development of a network model incorporating subsections to simulate end boundaries, junctions and multiple inflows. The final computer model of the building drainage system was completed using a representation of flow in a vertical stack based on work published elsewhere.

The program is capable of simulating multi-storey drainage systems with multiple flow inputs and variable boundary and junction types. It is restricted to level invert junctions and requires the steady-flow depth characteristics of each type of junction within the program. The program can be used to output depth or flow rate through time at any point in the system and could therefore be used by a designer to evaluate the performance of new systems. The program could also be used to determine the effects of water conservation legislation on system design.

Acknowledgements

The author would like to thank Dr. John Swaffield of the Mechanical Engineering Department, Brunel University for his unfailing optimism and support and Dr. Lawrence Galowin of the National Bureau of Standards, Washington D.C. for his encouragement.

Contents

Notation

A	cross-sectional area of flow (m^2)
A	point on the characteristic grid (chapter four)
A_W	non-dimensional wave amplitude
a	actual wave amplitude (m) (chapter seven)
a	area of the delivery tube (m^2)
B	point on the characteristic grid (chapter four)
b	translation coefficient
C	point on the characteristic grid (chapter four)
C	Chézy coefficient
C1	correction coefficient
C2	correction coefficient
C^+	positive characteristic
C^-	negative characteristic
c	wave speed (m/s)
D	pipe diameter (m)
D_a	attenuation coefficient
D_p	non-dimensional pipe diameter
DL	drainage line
E	specific energy of flow (m)
E_s	given by $g(S_f - S_o)$
Fr	Froude number
f	Darcy resistance coefficient
g	acceleration due to gravity (m/s^2)
h	depth above datum (m)
i	subscript for pipe or section number
i	row identifier (chapter twelve)

j	column identifier (chapter twelve)
K	loss coefficient at base of stack
k	roughness coefficient
k	number of upstream dead-end nodes (chapter twelve)
l	length (m)
N	number of nodes in tree
n	Manning's coefficient
P	wetted perimeter (m)
P	point on the characteristic grid (chapter four)
Pn	number of pipes connected to each node
Q	discharge (m^3/s)
q	lateral inflow per unit length (m^2/s)
R	hydraulic radius (m)
R	point on the characteristic grid (chapter four)
R_e	Reynold's number
S	point on the characteristic grid (chapter four)
S'	point on the characteristic grid (chapter four)
S_f	slope of the energy grade line
S_o	slope of the pipe
T	water surface width (m)
T_w	non-dimensional wave duration
t	time (s)
t	annular thickness (chapter twelve)
t_w	actual wave duration (s)
U	reaction force ($kg/m/s^2$)
u	water jet velocity (m/s)
V	velocity of flow (m/s)
V_{crit}	critical velocity (m/s)

V_e flow velocity between floors (m/s)

V_{norm} normal velocity (m/s)

V_{sub} subcritical velocity (m/s)

V_t terminal velocity (m/s)

V_w velocity of steep-fronted wave (m/s)

X distance (m)

X non-dimensional distance (chapter seven)

x distance along pipe (m)

Y depth just upstream of junction (m)

Y relative depth (chapter seven)

y depth (m)

y_c critical depth (m)

y_e depth of flow for energy entry boundary condition (m)

$\bar{y}$ depth to centroid (m)

z point on the characteristic grid

z height above datum

α counter

θ given by $\Delta t / \Delta x$

θ angle between the main and branch channels (chapter ten)

ν kinematic viscosity (m^2/s)

ρ density (kg/m^3)

τ_o mean shear stress (kN/m^2)

ω stage variable

List of Figures

1. Introduction

1.1 The Design of Building Drainage Systems

Research conducted over the last fifty years has been largely responsible for the development of the modern single stack building drainage system which has considerably reduced the complexity of pipe networks leading to cost and visual benefits. Swaffield (1980) reviewed the work which led to the design of the single stack system and described the close link which exists between research objectives and current design needs. The mechanism of operation of the one pipe system was studied by Hunter (1924) and Dawson and Kalinske (1937) and was introduced to Britain from the USA in the 1930s. The single stack system was developed during the 1950s at the Building Research Station and the results of this work were reported by Wise (1952) and Wise and Croft (1954).

The principal area of interest in drainage research at present is the effect on building drainage systems of water conservation proposals and it is clear that future designs should be based upon the results of the type of research which led to the design of the single stack system. Methods of conserving water are being studied in virtually all western countries at present, in many other parts of the world there is a basic shortage of water and any practical research which would assist in conserving water is likely to prove very useful.

One important consequence of reduced water consumption due to the application of conservation measures would be a diminution in the flow through building drainage systems. This would lead to a reduction in the depth and velocity of the flow through the system which could lead to failure due to solid deposition and subsequent blockage. As a

flow hydrograph propagates along a pipe there is a general attentuation in the maximum depth and discharge observed at any downstream point. The hydrograph may be thought of as a series of waves of individual depth possessing an individual wave velocity c which increases with depth. Deeper waves travel faster than shallow waves on the trailing edge of the hydrograph thus extending the profile. The converse occurs at the leading edge and the flow profile steepens; however, frictional forces act to reverse this effect and the leading edge may also be drawn out. Attenuation is a complex phenomenon and depends upon channel parameters such as pipe size, roughness coefficient and gradient. It is clear therefore that in parallel with research into improved appliance design, necessary to enable appliance operation at reduced volumes, there should also be an investigation into the importance of wave attenuation in long drainage pipes and the effect of reduced flows on this attenuation.

A number of studies of the hydraulics of drainage systems have been made. Wyly (1964) produced empirical equations which can be used to estimate the hydraulic capacity of drains subject to unsteady flows or unsteady flows with a steady baseflow. Wise (1973) reviewed some aspects of fluid mechanics applied to drainage installations in buildings and Burberry (1978) studied the attenuation of flushes within single pipes and devised an approximate empirical technique for estimating the effect of attenuation in sections of drain remote from the main stack. In order to take the effect of attenuation fully into account Burberry recommended that a time dependent method of calculation would have to be used.

The current trend towards water conservation increases the importance of accurately estimating the effect of flow attenuation in

drainage systems. Proposals to reduce the w.c. flush volume increase the probability that solid deposition will take place as flow depth and velocity decrease. There is a need to develop a time-dependent predictive method that will provide depth and velocity estimates at any point in the system so that the effect of attenuation and the implications for water conservation proposals can be studied.

1.2 Time-Dependent Modelling

The influence of attenuation upon flow in drainage systems is considerable and it would be unrealistic to ignore the effect it has on flow depth and velocity along the pipe network. Conventional methods of estimating flows in drainage systems cannot cope with the problem of time-dependent inputs occurring at a number of points in the system. Any technique which could adequately deal with such inputs would inevitably involve solving the time-dependent equations describing unsteady flow. There is clearly a need to develop a method which will solve the equations of unsteady flow and provide depth and velocity profiles at any point along a building drainage network.

The development of a mathematical model for unsteady flow computation follows the path suggested by Weinmann and Laurenson (1979) and illustrated in Figure 1.1. The first step in the development of the model is to select the flow characteristics which are of most importance in simulating building drainage systems. The depth and velocity are the best measures of attenuation and the unsteady flow model must be able to predict these two characteristics of the flow at any point in the system. The next stage in the development of the model is to describe the physical processes involved using the principles of hydraulics, this involves defining the equations of

unsteady flow in terms of depth and velocity. The third step is to decide how the equations are to be solved; this will involve an analytical, numerical or approximate treatment of the basic equations and forms the foundation for the mathematical model.

Once it has been decided how the equations are to be solved then a particular solution technique must be chosen. At this stage the characteristics of the channel and type of flow must be specified as these factors will influence the choice of solution technique. Certain methods are more useful for subcritical flow than supercritical flow, others can handle steep inflows more easily and the type of channel, its approximate size, roughness, etc. will also influence the choice of solution technique. The initial conditions in the pipe network must be specified as well as the range of boundary conditions to be expected at the entrance and exit to the system. Any stationary or moving boundaries within the system, such as hydraulic jumps or junctions, must also be enumerated. It is now possible to build up a detailed hydrologic or, in this case, hydraulic model incorporating the range of geometry and flow conditions associated with a building drainage network.

The next step is to convert the model into a computer program using an appropriate programming technique and to decide upon the form of the input and output. When the program is complete the initial flow conditions, the unsteady flow profile and the channel characteristics may be input, the distance and time intervals chosen and the result of the unsteady flow routing obtained in whatever form is desired. In order to investigate attenuation the results will be in the form of depth and perhaps velocity profiles at points throughout the network.

Figure 1.2 illustrates the type of building drainage system

which can be modelled to provide information about the attenuation of time-dependent inputs and assess the effect of reduced flows or changes in pipe diameter. The characteristics of the pipe, such as length, diameter, roughness coefficient and slope can be varied and a number of entry boundary conditions are necessary in order to model the input from w.c.s, baths, basins, etc. The input profiles can be of any shape or duration and information about the depth and velocity can be output for any point. Junctions must be adequately modelled as they strongly influence the flow through a drainage system due to the relatively short runs between junctions or boundaries.

1.3 The Flow Régime

No previous attempt has been made to model the building drainage network using the equations of unsteady flow; all other work in the field has been within the areas of storm sewer, canal or river modelling. There is one fundamental difference between these areas and building drainage and that is the nature of the flow régime. Virtually all of the unsteady flow modelling reported in the literature is primarily concerned with the subcritical case (sub-and supercritical flow are described in Appendix I); the supercritical case is either not considered or treated superficially as it is only of interest for a very small percentage of the time.

Figure 1.3 shows that for the range of gradients and discharges relevant in building drainage the flows are predominantly supercritical. A typical 9 l w.c. flush will have a maximum flow rate of about 1.4 l/s (Wise, 1973) and at gradients between, say, 1/50 and 1/200 this will result in supercritical flow throughout the entire passage of the wave. In a small number of cases, particularly where

the pipe has been laid very flat, then subcritical flow may occur and so any unsteady flow model must be able to deal with both types of flow.

The principal difference between the two flow régimes is that in subcritical flow disturbances can propagate upstream and in supercritical flow they cannot. It is well known in drainage research that backflow occurs at junctions; it is clear therefore that subcritical flow must exist at the junction. It is also clear that supercritical flow exists upstream of the junction,therefore a transition between the two types of flow is necessary. Most other unsteady flow models consider the whole pipe to be subcritical and so the effect of a junction is easily modelled. In the small number of models where supercritical flow is simulated junctions are trivial since no backflow can occur and the calculation simply proceeds downstream through the junction.

The nature of the flow régime and the importance of backflow combine to make the task of simulating unsteady flow in building drainage systems a very interesting problem. Workers in similar fields have not adequately addressed themselves to the particular problems associated with a system containing both supercritical and subcritical flow in the same pipe.

1.4 Time-Dependent Input

The flow carried by a building drainage network is not only dependent upon attenuation but also upon the discharge characteristic of the appliances served by the system. The design of drainage networks cannot be undertaken without allowance for the time-dependent frequency of use.

The fixture unit method combines appliance discharge rate data

with reasonable design decisions on the intervals between usage and usage satisfaction levels to provide a design flow. The current fixture unit method was developed by Burberry and Griffiths (1962) and is a method for estimating design flows based upon the application of probability theory which allows the likelihood of a given number of independent events occurring coincidentally to be calculated if the likely occurrence of each event is known. It is highly unlikely that flow from all sanitary appliances will occur simultaneously in a drainage network and it would therefore be unrealistic to design a system to cater for the maximum possible load. Probability theory allows an estimate to be made of the number of appliances likely to be contributing to the flow at any given time. Assuming that the frequency of use of individual appliances has been correctly identified, this method works well in sections of pipe where the duration and rates of flow are closely related to the flow in the sanitary appliances. Once attenuation has begun to take place this method does not work well and the more sophisticated approach of mathematical modelling using the unsteady pipeflow equations should be used. The fixture unit methods do allow an estimate to be made of the pattern of inflow into a building drainage system.

The fixture unit methods (Wise, 1979) have been widely used in the design of building drainage systems but the amount of data on usage patterns in buildings is small. Wise and Croft (1954), Webster (1972) and Courtney (1976) all presented usage data which has been widely used and Courtney suggested that the current design techniques consistently over-estimate demand and lead to over-provision of drainage services. Courtney also felt that this extended to the drainage system itself and could have serious implications as the ability of a gravity driven

drain to remain clear is a function of the relationship between the flow rate, depth, pipe diameter and pipe gradient. It is clear that further research into the frequency of use of sanitary appliances is necessary if the most economic systems are to be installed.

The development of a mathematical model for unsteady flow in partially-filled building drainage networks requires the discharge profiles expected from common sanitary appliances to be available. Wise (1973) presents the discharge characteristic of a low-level washdown w.c. with a 9.1 l flush (Figure 1.4a) and similar results were obtained by Uujamhan (1981) for a variety of flush volumes (Figure 1.4b). Pink (1973) gives discharge curves for a variety of sanitary appliances; Figure 1.5 presents the results from both a low-level and a high-level washdown w.c. These discharge hydrographs have a time base of between 8s and 12s and a maximum flow rate of about 1.0 l/s to 2.4 l/s which is reached in 1-2s. Adesanya (1983) gives the discharge characteristics of a number of wash hand basins; these are illustrated in Figure 1.6. The time base is generally about twice that for a w.c. with a maximum discharge of approximately 0.8 l/s achieved in the first 3-5s. Pink also gives discharge curves for both wash basins and kitchen sinks (Figure 1.7).

Obviously the exact nature of the discharge characteristic of a particular appliance may fall outside of these limits but these examples provide an insight into the magnitude, rate of rise and time base of typical discharge profiles. Any mathematical model for unsteady drainage flow must be able to cope with a maximum flow rate of at least 2.4 l/s and possibly greater as the combination of flow from several input locations in a complex pipe network may result in a combined peak flow which exceeds the original unattenuated flow. The

rate of rise of the flow profile will also effect the operation of the model. While the sharpest increase to be expected would be a rise to about 1.5 l/s in 1s, this may be exceeded in some cases.

1.5 Conclusion

In order to fully understand the consequences of the water conservation measures currently under consideration in most western countries, there is a need for further research into the accurate estimation of flow attenuation in complex building drainage networks. Any study of attenuation must necessarily involve the solution of the time-dependent unsteady flow equations for partially-filled pipe flow using one of a number of possible solution techniques. The mathematical model must be able to simulate the variable conditions found in a building drainage network; these will include the pipe characteristics, the boundary conditions at the entrance and exit, the effect of junctions, bends, etc., and also the flow down a vertical stack. The inputs to the system are user-dependent and although a number of methods exist for estimating frequency usage more research is needed in this field. Research into the type of output to be expected from typical sanitary appliances allows an assessment of the range of flow rates and rates of flow increase which must be dealt with by the mathematical model. The following chapters outline the development of a mathematical model suitable for building drainage network simulation that meets these criteria.

2. Unsteady Flow Models

2.1 The Unsteady Open Channel Flow Equations

The theory used in the numerical modelling of flow in partially filled pipes is expressed mathematically in the equations of unsteady flow in open channels. The equations are a simplified model of the actual processes at work, only those processes which are thought to be important in modelling are included. The physical limitations of the equations remain no matter how they are subsequently manipulated in numerical simulation models (Cunge, Holly and Verwey, 1980). The extent of these limitations should be borne in mind when considering the application of the theory of unsteady flow to a real situation.

The equations derived by de St. Venant (1870) are based upon the following set of assumptions,

(i) the flow is one-dimensional, the flow velocity is uniform over the cross-section and the water level across the section is horizontal.

(ii) the curvature of the streamlines is small and the vertical acceleration is negligible. The flow is gradually varied and the pressure is hydrostatic.

(iii) the effects of boundary friction and turbulence can be modelled using the resistance laws for steady-state flow.

(iv) the channel bed slope is small so the cosine of the slope may be replaced by unity.

Obviously, true one-dimensional flow does not occur either in natural or fabricated open channels and care must be taken to ensure that a flow régime can be modelled without seriously violating this assumption. The principal limitation is that no sudden change of depth

may occur within the cross-section of the channel; it would not be possible for instance to incorporate a berm into a canal model. If the curvature of the streamlines increases then the flow becomes rapidly varied and the vertical acceleration must be considered. Rapidly varied unsteady flow can be modelled,as will be seen later,but only with increased complexity and greater computational time. It is sometimes simpler to approximate a solution to rapidly varied flow by using the gradually varied flow equations, accepting the loss of accuracy.

One-dimensional flow can be described by two dependent variables, velocity and depth are used here, which define the state of the flow in both space and time. Two equations are therefore required, both of which must characterise actual physical laws. The equations used here are the conservation of mass (continuity equation) and the conservation of momentum (dynamic equation); the conservation of energy could be used but it is only valid for continuous flow,which introduces difficulties when discontinuities such as steep-fronted waves are modelled (Cunge, Holly and Verwey, 1980).

2.1.1 Continuity Equation

The continuity equation may be established by considering the conservation of mass in a very short length Δx of the flow (Figure 2.1). In unsteady flow the discharge varies with both distance and time and the discharge in and out of the infinitesimal section may be written thus,

$$Q_2 - Q_1 = \frac{\partial Q}{\partial x} \Delta x \qquad (2.1)$$

where Q_1 = discharge into the section (m^3/s)

Q_2 = discharge out of the section (m^3/s)

x = distance along the channel (m)

This expression gives the rate at which the discharge between the two sections is changing.

The storage of water between sections 1 and 2 is changing at the rate

$$\frac{T\partial y}{\partial t}\Delta x \qquad (2.2)$$

where T = mean water surface width of the element (m)

y = mean depth of water of the element (m)

t = time (s)

Since water is incompressible, the net change in discharge plus the storage should be zero, therefore,

$$\frac{\partial Q}{\partial x} + \frac{T\partial y}{\partial t} = 0 \qquad (2.3)$$

This is the equation of continuity for unsteady flow.

At a given section Q = VA, where V is the velocity of flow (m/s) and A is the cross-sectional area (m^2), so the previous equation becomes

$$\frac{\partial(VA)}{\partial x} + \frac{T\partial y}{\partial t} = 0 \qquad (2.4)$$

which may be rewritten

$$\frac{V\partial A}{\partial x} + \frac{A\partial v}{\partial x} + \frac{T\partial y}{\partial t} = 0 \qquad (2.5)$$

2.1.2 Dynamic Equation

The dynamic equation is derived by considering the forces acting on the infinitesimal element of length Δx and the changes in momentum these cause (Henderson, 1966).

The horizontal force due to hydrostatic pressure acting on the

element is given by the term

$$- \rho g A \Delta y \qquad (2.6)$$

where ρ = density of the fluid (kg/m^3)

g = acceleration due to gravity (m/s^2)

Δy = different in water depth between sections 1 and 2 (m)

(Figure 2.1)

This force is resisted by a shear force which is assumed to act in a direction parallel to the hydrostatic pressure. The total force in the direction of flow is equal to

$$- \rho g A \Delta Y - \tau_o P \Delta x \qquad (2.7)$$

where τ_o = mean shear stress acting over the perimeter of the section (N/m^2)

P = mean wetted perimeter of the section (m)

The mass of the element is given by

$$\rho A \Delta x \qquad (2.8)$$

and the acceleration of the element including both convective and local terms is expressed thus

$$\frac{dV}{dt} = V\frac{\partial v}{\partial x} + \frac{\partial v}{\partial t} \qquad (2.9)$$

Now, the force on the element is a product of the mass of the element and its acceleration, therefore

$$- \rho g A \Delta y - \tau_o P \Delta x = \rho A \Delta x \left(V\frac{\partial v}{\partial x} + \frac{\partial v}{\partial t}\right) \qquad (2.10)$$

The slope of the total energy line S_f (Figure 2.1) is given by

$$S_f = - \frac{\partial}{\partial x}\left(h + \frac{V^2}{2g}\right)$$

$$= - \left(\frac{\partial h}{\partial x} + \frac{V}{g}\frac{\partial V}{\partial x}\right) \qquad (2.11)$$

where h = depth of flow above the datum line (m)

The mean shear stress τ_o may be written,

$$\tau_o = \frac{\rho g A S_f}{P} \qquad (2.12)$$

therefore,

$$S_f = \frac{\tau_o}{\rho g R} \qquad (2.13)$$

where R = hydraulic radius (m) = A/P

Equation 2.11 is substituted into Equation 2.10,

$$\tau_o = -\rho g R\left(\frac{\partial h}{\partial x} + \frac{V}{g}\frac{\partial V}{\partial x} + \frac{1}{g}\frac{\partial V}{\partial t}\right) \qquad (2.14)$$

2.14 gives,

$$-S_f = \frac{\partial h}{\partial x} + \frac{V}{g}\frac{\partial V}{\partial x} + \frac{1}{g}\frac{\partial V}{\partial t} \qquad (2.15)$$

The slope of the channel bed S_o is given by $-\partial z/\partial x$ where z is the height of the bed above datum and since h = y + z,

$$(S_f - S_o) + \frac{\partial y}{\partial x} + \frac{V}{g}\frac{\partial V}{\partial x} + \frac{1}{g}\frac{\partial V}{\partial t} = 0 \qquad (2.16)$$

This is the general dynamic equation for gradually varied unsteady flow. The equation of continuity and the dynamic equation are known collectively as the St. Venant equations.

2.2 Techniques for Solving the Unsteady Flow Equations

The St. Venant equations provide a model for unsteady flow which is a simplification of the real situation, despite this the equations are too complex to solve analytically. The equations can be modified or simplified further to allow approximate solutions to be obtained, the most common of these procedures is the hydrologic flood-routing technique known as the Muskingham-Cunge method (Figure 2.2). Hydrologic methods suffer a loss of accuracy due to the simplifying assumptions made but this may be offset by the speed and

economy of the calculations. Since computers are now widely used in this country to obtain engineering solutions to complex problems it is possible to solve the St. Venant equations numerically, thus achieving a high level of accuracy (within the limits of the model). The general flow laws are used to allow discrete values of, say, depth and velocity at a finite number of points to be calculated using one of a wide range of numerical methods. The range of techniques based on the solution of the fundamental differential equations for gradually varied unsteady flow in open channels are known as hydraulic methods (Figure 2.2).

2.2.1 Hydrologic Methods

A large number of hydrologic methods have been developed and described in the literature and these are well reviewed by Chow (1959) and Weinmann and Laurenson (1979). Approximate models produce results which are limited in their generality and accuracy compared to hydraulic models but are considerably less expensive which is often a significant factor in engineering applications. Hydrologic models are essentially of two types based either on an analogy with the differential equations of gas dynamics (diffusion wave analogy) or on a kinematic wave model.

2.2.1.1 Diffusion Wave Analogy

By neglecting the acceleration terms in the dynamic equation and then combining the remains with the continuity equation a single equation expressed in terms of discharge may be derived (Weinmann and Laurenson, 1979),

$$\frac{\partial Q}{\partial t} + b\frac{\partial Q}{\partial x} = D_a\frac{\partial^2 Q}{\partial x^2} + bq \qquad (2.17)$$

where b = translation coefficient

D_a = attenuation coefficient

q = lateral inflow per unit length (m^2/s)

This equation is analogous to the differential equation which may be written for the diffusion of an unsteady stream of particles by applying the classical statistical theory of flow diffusion in gases. The coefficients can either be constant or vary with discharge, depending upon the complexity of the model. As with all hydrologic routing techniques the methods used to calculate the value of the coefficients is fundamental to the accuracy of the solution.

Isaacson, Stoker and Troesch (1958) used the diffusion wave analogy to model floods in various rivers in the USA; this is one of the earliest uses of the computer for routing unsteady flows through river channels. Barnes (1967) also used the technique and noted that a primary disadvantage is the inability of the model to maintain a stable initial steady-state water surface profile. This study was undertaken using experimental results from a 1 m diameter pipe with a length of 800m and an input profile with a duration of one to two minutes.

The diffusion wave analogy is a useful technique but it has a number of serious drawbacks. By ignoring the acceleration terms in the general dynamic equation the method tends to overestimate the speed of the leading edge of the wave profile. Another disadvantage is that the two coefficients, b and D_a, must be found empirically by analysing the movement of an observed flood; the method cannot be used for design calculations (Henderson, 1966).

2.2.1.2 Kinematic Wave Model

The definition of a kinematic wave is that the discharge Q is

always a single valued function of the depth y so that the discharge is always equal to the normal discharge (Weinmann and Laurenson, 1979). Using this relationship and the equation of continuity then the kinematic wave equation may be written,

$$\frac{1}{c}\frac{\partial y}{\partial t} + \frac{\partial y}{\partial x} = 0 \qquad (2.18)$$

where c = wave speed (m/s)

The kinematic wave speed is defined thus,

$$c = \frac{1}{T}\left(\frac{dQ}{dy}\right) \qquad (2.19)$$

The properties of the kinematic wave are derived principally from the equation of continuity and thus the wave travels without attenuation. Models based on kinematic wave theory do not allow for subsidence of the wave as it travels along the open channel unless weighting coefficients are included in the model to create a numerical distortion which simulates the attenuation of the wave.

The Muskingham-Cunge flood routing method provides a solution to the kinematic wave model. In order to simulate the attenuation of a wave using the method,a weighting coefficient is introduced into the finite-difference form of the kinematic wave equation. The choice of this coefficient is important and is usually based upon observed discharges for the channel section in question. A further parameter may also be introduced which models the translation of the wave.

Ponce and Yevjevich (1978) showed that the technique used to calculate the value of the parameters representing attenuation and translation definitely affects the accuracy of the model. Varying the parameters with discharge offers a more accurate solution than the original constant parameter technique. Koussis (1980) and Jones (1981) also comment on the importance of accurately simulating the translation

and attenuation of the wave by proper attention to the appropriate coefficients. The primary disadvantage of using the kinematic wave model is that the St. Venant equations are reduced to discharge as a simple function of depth and continuity.

2.2.2 Hydraulic Methods

Hydraulic methods of simulating unsteady flow are based on the numerical solution of the complete St. Venant equations using one of a variety of finite-difference techniques. Three major categories of solution can be identified (Figure 2.2),

(i) method of characteristics.

(ii) explicit finite-difference schemes.

(iii) implicit finite-difference schemes.

All of these methods give a more accurate prediction of the translation and attenuation of a wave passing through an open channel than the hydrologic methods described in the previous section but at far greater cost in terms of computational effort and expense.

Finite-element methods have been described by a few authors (Keuning, 1976, Cooley and Moin, 1976) but for the one-dimensional problem of unsteady flow the technique has no particular advantage so no further description is given (Cunge, Holly and Verwey, 1980).

2.2.2.1 Method of Characteristics

The St. Venant equations are a pair of quasi-linear hyperbolic partial differential equations which may be transformed into their characteristic forms in a number of ways. The method described here is that given by Fox (1977).

The continuity equation is expressed,

$$V\frac{\partial A}{\partial x} + A\frac{\partial V}{\partial x} + T\frac{\partial y}{\partial t} = 0 \qquad (2.20)$$

Assuming that the channel is prismoidal and that A/T = y (which is true for a rectangular channel and nearly so for a broad channel) then the continuity equation becomes,

$$V\frac{\partial y}{\partial x} + y\frac{\partial V}{\partial x} + \frac{\partial y}{\partial t} = 0 \qquad (2.21)$$

The depth y is related to the wavespeed c by the following equation,

$$y = \frac{c^2}{g} \qquad (2.22)$$

therefore

$$\frac{\partial y}{\partial x} = \frac{2c}{g}\frac{\partial c}{\partial x} \qquad (2.23)$$

and

$$\frac{\partial y}{\partial t} = \frac{2c}{g}\frac{\partial c}{\partial t} \qquad (2.24)$$

Substitute Equations 2.23 and 2.24 into Equation 2.21 and divide by c/g,

$$2V\frac{\partial c}{\partial x} + c\frac{\partial V}{\partial x} + 2\frac{\partial c}{\partial t} = 0 \qquad (2.25)$$

Substitute Equations 2.23 and 2.24 into the dynamic equation,

$$g(S_f - S_o) + 2c\frac{\partial c}{\partial x} + V\frac{\partial V}{\partial x} + \frac{\partial V}{\partial t} = 0 \qquad (2.26)$$

Add Equations 2.25 and 2.26,

$$g(S_f - S_o) + 2(V + c)\frac{\partial c}{\partial x} + 2\frac{\partial c}{\partial t} + (V + c)\frac{\partial V}{\partial x} + \frac{\partial V}{\partial t} = 0 \qquad (2.27)$$

Let $E_s = g(S_f - S_o)$, then

$$\left((V + c)\frac{\partial}{\partial x} + \frac{\partial}{\partial t}\right)(V + 2c) + E_s = 0 \qquad (2.28)$$

Subtract Equation 2.26 from Equation 2.25, let $E_s = g(S_f - S_o)$

and multiply through by -1,

$$\left(\left((V - c)\frac{\partial}{\partial x} + \frac{\partial}{\partial t}\right)(V - 2c) + E_s = 0\right) \qquad (2.29)$$

Equations 2.28 and 2.29 may be written,

$$\left(\left((V \pm c)\frac{\partial}{\partial x} + \frac{\partial}{\partial t}\right)(V \pm 2c) + E_s = 0\right) \qquad (2.30)$$

The basic equation of partial differentiation may be written,

$$\frac{dy}{dt} = \frac{\partial y}{\partial x}\frac{dx}{dt} + \frac{\partial y}{\partial t}$$

therefore

$$\frac{dy}{dt} = \left(\frac{dx}{dt}\frac{\partial}{\partial x} + \frac{\partial}{\partial t}\right)y \qquad (2.31)$$

Compare Equation 2.30 with Equation 2.31 (E_s is treated as a constant for ∂t) then,

$$\frac{dt}{dx} = \frac{1}{(V \pm c)} \qquad (2.32)$$

and

$$\frac{d}{dt}(V \pm 2c + E_s t) = 0 \qquad (2.33)$$

$$\frac{dt}{dx} = \frac{1}{V + c}$$

defines a positive (C^+) characteristic along which $V + 2c + E_s t$ is constant,

$$\frac{dt}{dx} = \frac{1}{V - c}$$

defines a negative (C^-) characteristic along which $V - 2c + E_s t$ is constant (Figure 2.3).

These equations can now be written in finite-difference form and solved numerically with either a fixed rectangular grid or a variable characteristics grid. The characteristics grid method uses graphical techniques and was developed before computers were available. The method has been programmed for the computer (Amein, 1966 and Liggett, 1968), but requires two-dimensional interpolations in

order to obtain solutions on a regular rectangular space-time grid, which is wasteful and inefficient (Sevuk and Yen, 1973). Wylie (1970) presents a comparison between the characteristics grid and the rectangular grid which clearly sets out the advantages and disadvantages of both methods. Generally the rectangular grid method is favoured as it allows results to be obtained where they are needed (although they may suffer interpolation errors) and also allows flow inputs at user defined times.

Most studies (e.g. Baltzer and Lai, 1968, Harris, 1970 and Fox, 1977) are carried out using a regular rectangular grid which is imposed on the computational domain before the calculations begin (Figure 2.3). Generally two different schemes are in use which allow the characteristic curves to be used to locate the points R and S on Figure 2.3. In the first-order scheme the characteristics are assumed to be straight lines and the non-derivative terms of the equations are evaluated at points R and S. The second-order scheme evaluates the non-derivative terms using points R, S and P, making the scheme implicit and therefore more costly of computer time. When the position of points R and S has been found, linear interpolations are made between the grid points to find the depth and velocity at R and S. Finally, by using the equations along the characteristics the depth and velocity at P may be obtained.

The time-step size is chosen to conform to the Courant stability condition (Courant, Isaacson and Rees, 1952) which may be expressed,

$$\Delta t < \frac{\Delta x}{(V + c)_{max}} \qquad (2.34)$$

This ensures that the solution points fall within the domain of

dependency of point P. Sivaloganathan (1979) investigated the effect of relaxing the Courant condition and concluded that for small values of Δx little loss of accuracy occurred if time steps with large Courant numbers were used. However,no obvious saving in computer time can be made due to the reduction in the size of the distance step Δx. Goldberg and Wylie (1983) used interpolations in time rather than space by projecting the characteristics back to the previous time step, an extension of this technique is to implicitly interpolate by projecting the characteristic equation into the current time step,thus allowing the Courant condition to be relaxed. This method may be useful for modelling systems which previously required common time steps to be used at boundaries which resulted in simulation difficulties. Strelkoff (1970) also examines the stability of solutions using the method of characteristics.

Almost all of the literature describing unsteady flow models is fundamentally concerned with the subcritical régime, although reference is often made to the boundary conditions etc. necessary for modelling supercritical flow. As shown in Chapter One the predominant type of flow to be expected in a building drainage network is supercritical although allowance must also be made within the numerical model for any subcritical flows which may occur. Zovne and Martin (1979) presented both characteristic grid and rectangular grid solutions for supercritical flows but concluded that only the rectangular grid method could be used for this régime. They also noted that for severely transient flows when a steep-fronted wave (or bore) might be expected to form the rectangular grid method forces a solution, which is often adequate for engineering purposes, without attempting to solve the rapidly varied flow equations themselves.

Many variations on the basic method of characteristics have been reported (e.g. Sivaloganathan, 1978, Abbott and Verwey, 1970) and the method has been used in many network models (see Chapter Three). The regular rectangular grid method is the most useful as it allows depth and velocity to be calculated for a predetermined net of points and flow profiles to be input at specific times. The method is amenable to solution by computer and by using the Courant condition a reasonable degree of stability is assured. Supercritical flows can easily be modelled using this technique,which makes it suitable for simulating flow in building drainage networks.

2.2.2.2 Explicit Schemes

The St. Venant equations are expressed in finite-difference form and solved explicitly. The dynamic equation becomes (Figure 2.4),

$$S_{fi}^{j} - S_{oi} + \left(\frac{y_{i+1}^{j} - y_{i-1}^{j}}{2\partial x}\right) + \frac{v_i^j}{g}\left(\frac{v_{i+1}^{j} - v_{i-1}^{j}}{2\partial x}\right) + \frac{1}{g}\left(\frac{v_i^{j+1} - v_i^{j}}{\partial t}\right) = 0 \qquad (2.35)$$

The continuity equation is expressed,

$$\frac{(AV)_{i+1}^{j} - (AV)_{i-1}^{j}}{2\partial x} + T_i^j\left(\frac{y_i^{j+1} - y_i^{j}}{\partial t}\right) = 0 \qquad (2.36)$$

Equations 2.35 and 2.36 are linear in unknown v_i^{j+1} and y_i^{j+1}; the solution is executed point by point from one time level to the next. Despite the ease of computation of this scheme and the directness of the solution,it suffers from serious computational instability even if the space and time steps are based upon the Courant condition. Strelkoff (1970) recommends a staggered rectangular grid in which Equations 2.35 and 2.36 are solved at every other node in the x direction in order to stabilise the calculation. Other schemes,

including the leap-frog method (Cunge, Holly and Verwey, 1980), diffusion scheme (Sevuk and Yen, 1973) and the Lax-Wendroff scheme (Murota, Kanda and Eto, 1973), have been suggested in order to improve the stability of the explicit schemes. The Lax-Wendroff scheme includes second-order derivatives in order to approximate the solution at a particular point by using a non-linear expression which should give a more accurate solution,since the principal limitation on any finite-difference technique is the linearity of the approximation between points. Barnes (1967) suggests that the Lax-Wendroff scheme may not easily be used for supercritical flow régimes,which is a major drawback and renders the method unusable for building drainage network modelling.

A further disadvantage of all explicit schemes is the difficulty experienced in handling boundary conditions. Explicit schemes are also known to be prone to instability when the transient flows start to become rapidly varied (Sevuk and Yen, 1973 and Sivaloganathan, 1980),unlike the method of characteristics which will force a solution even if a steep-fronted wave (or bore) develops.

2.2.2.3 Implicit Schemes

The St. Venant equations are expressed in finite-difference form as a set of non-linear algebraic equations from which the unknowns are solved simultaneously. A number of different implicit schemes have been suggested, the four-point non-central method described here is given by Sevuk and Yen (1973).

The finite-difference operators are written thus (Figure 2.4),

$$\frac{\partial U}{\partial t} = \frac{1}{2\Delta t}\left((U_i^{j+1} + U_{i+1}^{j+1}) - (U_i^{j} + U_{i+1}^{j})\right) \qquad (2.37)$$

$$\frac{\partial U}{\partial x} = \frac{1}{\Delta x} (U_{i+1}^{j+1} - U_i^{j+1}) \qquad (2.38)$$

$$U = \frac{1}{2} (U_i^{j+1} + U_{i+1}^{j+1}) \qquad (2.39)$$

where U represents any function (V, y, etc.). By substituting Equations 2.37, 2.38 and 2.39, the two St. Venant equations may be written,

$$C\ (V_i^{j+1}, V_{i+1}^{j+1}, y_i^{j+1}, y_{i+1}^{j+1}) = 0 \qquad (2.40)$$

$$D\ (V_i^{j+1}, V_{i+1}^{j+1}, y_i^{j+1}, y_{i+1}^{j+1}) = 0 \qquad (2.41)$$

where C and D represent the finite difference form of the continuity and dynamic equations respectively. For i = 1 to n there are 2n + 2 unknowns (the depth and velocity at each node) which may be found by solving the 2n non-linear equations and the two boundary equations using the generalised Newton iteration method (Amein and Fang, 1970).

Implicit finite-difference schemes are unconditionally stable and the Courant condition can be ignored, thus allowing large time steps to be used which reduces the computational time required (Baltzer and Lai, 1968, Sevuk and Yen, 1973). However, the maximum values of Δt and Δx which can be used are limited by convergence considerations. Convergence is the ability of the finite-difference solution to approach the analytical solution of the partial differential equations; as no analytic solution of the St. Venant equations is possible other representative criteria are usually used.

A number of other implicit schemes are described in the literature, all of which have various advantages and disadvantages. Evans (1977) uses the four-point implicit operator of Preissman which is also discussed by Cunge, Holly and Verwey (1980), whilst a four-point central method is proposed by Amein and Chu (1975). Six-point central and non-central schemes and a staggered method have also been

suggested. The implicit scheme is usually preferred for models having an input profile with a long time base because of the large values of Δt which can be used; it is often found to be unsuitable for flow inputs with short durations (Sevuk and Yen, 1973).

2.3 Conclusions

This short survey of some of the numerical methods which have been used to solve the unsteady flow equations is not exhaustive but does describe the main categories of solution techniques. The St. Venant equations are not a complete representation of the physical situation so no solution will give an accurate description of the unsteady flow phenomenon. The hydrologic methods are approximate and thus most suitable for large scale open channels such as rivers; they require less computational effort than hydraulic methods and are often used for this reason. The techniques based on the full St. Venant equations offer a more complete solution and are most frequently used for storm-sewer models where greater accuracy is required and can be paid for in terms of computer time. Flow and channel parameters can be measured with far greater accuracy in fabricated channels than in rivers,which is a further reason for preferring the more complex hydraulic methods.

Explicit schemes are attractive because they are easily calculated; however,the disadvantages of instability and difficulty in handling both boundary equations and supercritical flow render the schemes impractical. Implicit schemes and the various methods of characteristics offer computational stability, as long as the Courant condition is observed, flexibility in dealing with boundary conditions and the ability to model supercritical flow. If sufficient

computational effort is available then these schemes offer the most accurate and flexible numerical solution to the unsteady flow equations.

3. Network Simulation Models

3.1 Introduction

This chapter reviews some of the ways in which the numerical methods described in the previous chapter have been used to model unsteady flows in rivers, pipes, sewers, etc. The method of characteristics, usually using a rectangular grid, is the most popular technique and is used by the largest proportion of modellers. Hydrologic schemes are widely used due to their simplicity and ease of computation whilst few schemes utilise either explicit or implicit schemes (although the Lax-Wendroff technique is quite popular).

3.2 Models Using the Method of Characteristics

The method of characteristics is a hydraulic method of flood routing based upon the solution of the basic partial differential equations for unsteady flow in open channels. The partial differential equations are transformed into four ordinary differential equations which are then treated as finite-difference equations for which solutions of the unsteady flows at each time level on the space-time grid can be calculated.

The Illinois Storm Sewer (ISS) System Simulation Model (Sevuk, Yen and Patterson (1973) was developed to simulate unsteady flows in dendritic storm sewer networks using the method of characteristics to solve the wave equations. The model may either be used to predict flows in existing sewer networks or to assist in the design of new systems by assessing the effect of changes of pipe diameter, pipe slope, etc. A small but negligible initial baseflow is necessary to start the calculations as a dry pipe (with zero depth and velocity) causes a

computational singularity; this is a necessary precondition for any model based on the numerical solution of partial differential equations. Two methods of modelling junctions were used and the authors concluded that the junction condition must be carefully simulated if the effect of using complex methods of analysing unsteady flow in straight pipes is not to be undermined by large errors at the junctions. The ISS model was designed for networks with a subcritical flow régime and it cannot handle flows with a Froude number greater than two or regions of flow containing hydraulic jumps. Results presented for a number of sewer systems confirm the belief that the maximum discharge does not usually coincide with the maximum depth of flow so that networks based on estimates of maximum discharge may surcharge (Sevuk and Yen, 1973). This model is a powerful and advanced tool for the analysis of unsteady flows in storm sewer systems.

Joliffe (1981) presents a flood-routing model for urban drainage which is capable of simulating flows in both dentritic and looped networks. The solution technique is based upon the method of characteristics and was chosen after a number of other methods had been considered, particularly for speed of computation. Unlike most sewer network models this one is capable of dealing with looped networks, which is a useful attribute in a small number of cases. Junctions are modelled using the point-type formulation even though this is known to be inadequate and to produce errors which may be considerable. No laboratory or field evidence is presented to demonstrate the accuracy of this model or to validate any of the techniques used. The results from the two example pipes that are presented demonstrate the potential usefulness of such complex numerical models but fail to show that the model itself can simulate real events. The type of flow régime for

which this model was devised (e.g. subcritical, supercritical) is not disclosed although the shallow pipe gradient used in the two examples suggest that a subcritical flow régime was expected.

The procedure described by Pinkayan (1972) was developed to route storm water through a very simple storm drainage system consisting of a single circular pipe with one branch pipe set at right-angles to the main channel. The method of characteristics with a fixed interval space-time grid is used to calculate the velocity and depth of flow at each node on the x-t plane. Equations are presented to deal with all three flow conditions; subcritical, critical and supercritical. A power-loss equation is used to model the effect of the junction box based upon the power upstream and downstream of the junction. The initial flow condition in the pipe is assumed to be steady non-uniform flow and must be set up before the unsteady flow computation can begin. Boundary conditions for the entry and exit as well as the junction box are also incorporated into the numerical solution. The computer model was validated using observations from a full-size physical model in a laboratory, agreement between the observed and predicted data is generally good and the discrepancies found in the results are attributed to the junction model used,which does not take account of the backwater effect of the confluence. The author concluded that in order to give better results the junction model used should be reconsidered, particularly if a storm drain with more branch pipes is to be modelled.

Baltzer and Lai (1968) conducted an extensive investigation into a number of methods of solving the partial differential equations describing unsteady flow including using the method of characteristics with specified time intervals. The investigation was concerned with

transient flows in rivers and therefore certain boundary conditions considered (such as river braiding) are peculiar to natural waterways. Comparison of the predicted flows with a number of unsteady flows measured in the field indicated that the model gave generally good results. The authors also found that if a calculation was begun with an initial discharge with a large error then the effect of channel friction was to cause the computed discharge to rapidly converge to a unique solution. This model was designed to be used as a tool in the investigation of river pollution, sediment transport, navigation and hydroelectric power-scheme design and management. It could also be used to predict the effect of design floods, flood protection schemes, channel excavations,etc. Although unsteady flow models for rivers deal with flows greater than those which occur in piped systems the difference between the two is one of magnitude not of type.

The method of characteristics is a widely used technique for modelling transient flows in partially-full pipe networks, it has also been used to simulate flows in natural waterways. Most of the work which has been carried out is for storm-sewer systems where pipe diameters are measured in metres and the discharge profile varies over hours rather than seconds. Building drainage networks are on a smaller scale than storm-sewer systems but the fundamental nature of the flow is the same and is most completely described by a hydraulic flood-routing method.

3.3 Other Hydraulic Models

A number of open-channel network simulation models are based upon hydraulic methods other than the method of characteristics. Some of these procedures are described in Chapter Two and in this section a

few of the models which utilise these techniques are described.

Murota, Kanda and Eto (1973) present a model for flood routing through urban river networks consisting of a main channel with both tributaries and distributaries. Although the main channel is usually a natural waterway many of the tributary streams are piped so that a procedure for simulating the hydraulic conditions at junctions is necessary. A further consideration is tidal changes at the model boundary which interact with the flood wave and whose effects may be felt at a considerable distance upstream. The computational technique used is a modified one-step Lax-Wendroff scheme which is claimed to simplify programming, reduce computer time and produce results with a high degree of accuracy. A simplifying assumption is made in order to calculate the cross-sectional area of flow which may adversely affect the accuracy of the results. This scheme appears to be suitable for large urban rivers but probably does not accurately model the many piped inflows into the system.

The hydraulic model developed for rivers by the Hydraulics Research Station, Wallingford (Price, 1977 and Price and Samuels, 1980) is primarily intended for single channel rivers but it is included here due to its importance in Britain. The model, known as FLUCOMP, cannot be used in the region near the confluence of two major streams but minor tributaries can be modelled. The numerical solution of the unsteady flow equations is obtained by using a four-point finite difference representation of the basic flow equations and then solving the resulting implicit equations using a two-step iterative method. This scheme is not always stable so a small artificial viscosity is included to damp any unnecessary fluctuations. The initial flow conditions are set up using a standard backwater profile calculation

and this can also be used as a method of calculating a value of Manning's n for the whole channel if discharge and depth data are available. FLUCOMP has been tested with data from a number of rivers and the major problem is accurately describing the channel conditions although the model appears to reproduce depth hydrographs quite adequately. Models such as these cannot be expected to provide accurate simulations of river flows in the same way as a sewer system model; their use is as tools to assist the engineer in exercising judgement in the design of urban drainage systems, flood protection schemes,etc.

Baltzer and Lai (1968) use the implicit method as one solution in their investigation of a number of techniques for simulating unsteady flow in waterways. The fundamental unsteady flow equations are used to produce a set of finite-difference equations. A further set of equations, equal in number to the number of dependent variables in the system, is then produced and a numerical solution found by solving the equations implicitly. Since the solution must be found by iteration the use of a computer is essential; however,the Courant condition which restricts the size of the time-step in the method of characteristics may be relaxed so longer time-steps between calculations may be used. Flows predicted using this method generally agreed well with those observed in a number of waterways.

Although these models are all primarily intended for use in natural waterways they use methods which can readily be applied to unsteady partially-filled pipeflow. Of all the hydraulic methods implicit schemes tend to be favoured for large-scale modelling because of their stability when long time-steps are used.

3.4 Hydrologic Models

The diffusion analogy method is an approximate hydraulic approach to flood routing in open channels which was used by Akan and Yen (1981) in their model for open-channel network flow simulation. The diffusion wave approach is based upon the statistical theory of flow diffusion in which a differential equation is used to describe the unsteady flow of particles with time. The technique is more often used in heat transfer problems but when used as an approximation to the St. Venant equations the diffusion wave model is more accurate than a kinematic wave model (Chow, 1959). Results from the diffusion wave method proposed by Akan and Yen were compared with results obtained by using an implicit dynamic wave model (similar to that proposed by Baltzer and Lai (1968)) and with results from a kinematic wave model. The results for the diffusion wave model agreed closely with those obtained from the dynamic wave model but the results from the kinematic model contained a far greater error. Akan and Yen concluded that the diffusion wave model can simulate the backwater effect of a channel in both the main and branch channels, that it is nearly as accurate as the more complex dynamic wave model and that it is faster to run on a computer than the simpler kinematic wave model. The method is suitable for large open-channel networks and is also applicable to storm-sewer systems when flowing partially full.

The kinematic wave method of flood routing is based upon the concept that the rate of change of storage within the channel reach is equal to the average inflow less the average outflow from that reach for a fixed time period (Chow, 1959). The dynamic effects of the flow are assumed to be negligible,therefore the effects of downstream boundaries (such as junctions) or flow disturbances (such as surges)

are not simulated using this approach. For channels with shallow slopes the hydrologic method will give approximate results but for channels with a slope greater than about 1/400 the dynamic effect is important and cannot be ignored. The kinematic wave model is inherently linear since it is based upon the relationship described above and this is not always immediately obvious when some of the more complex techniques such as the Muskingham-Cunge method are used.

Price and Kidd (1978) presented a model which was developed at the Hydraulics Research Station, Wallingford,and uses the Muskingham-Cunge flood routing method. The model was developed for partially full pipe networks with a gradient of less than about 1/500 so it was felt that the backwater effect of junctions could be ignored and a simple hydrologic routing method used. The model also calculates surface runoff into the pipe network so a routing method which needed minimum computer time was required in order to make the whole package commercially useful. The model was tested on two catchments and then used to redesign the pipe network on one catchment; the authors concluded that the model is a useful design tool.

Bettess, Pitfield and Price (1978) used the same routing technique for a storm-sewer model which takes surcharging into account. The Muskingham-Cunge method was used for the sections of pipe flowing part full and it was chosen as the most acceptable compromise between accuracy and speed. The flood routing through the pipe network only forms part of the complete model which also takes into account surface runoff into the sewer system. The Muskingham-Cunge method is ideal for systems which have a shallow gradient and where the inaccuracy incurred by not using the dynamic wave equation is small compared to the scale of the complete model. The method is less

suitable for open-channel networks at steeper gradients or where the backwater effect of junctions is important as is the case in building drainage networks.

An interesting extension to current popular methods of hydrologic flood routing is the lumped mathematical model proposed by Mays and Tung (1978) based upon state-variable modelling theory. The authors comment that since most of the approximate hydrologic methods, such as the diffusion wave model and the kinematic wave model,do not accurately predict backwater effects then a lumped mathematical model may be just as useful and computationally quicker. State-variable modelling is based upon the system concept which "considers an input flow medium which enters the structure of the system where it is modified by physical processes within the system until it leaves the system as output" (Mays and Tung). The system (i.e. the pipe) is divided into a number of reaches; within each reach the flow is assumed to be uniform,which gives an approximation to the continuous flow profile which actually exists. The model is lumped in time by averaging variables over a discrete time interval and in space by taking average values of the parameters within each reach. The equation of continuity and Manning's equation (which is used since the flow is assumed to be uniform within each reach) form the basis for the state equation of the lumped flow model. Results from the model were compared with results from a kinematic wave model and were found to be broadly similar. The state variable modelling technique for pipe flow in sewers has the same drawbacks and limitations as the other hydrologic methods and is not therefore suitable for building drainage network modelling.

4. The Single Pipe Program

4.1 Introduction

The method of characteristics using a regular rectangular grid was chosen to model unsteady flow in partially filled drainage pipe networks because it is the most suitable of all the techniques described in Chapter Two. The hydrologic methods ignore most of the terms of the dynamic equation and only provide an approximate solution which is inadequate for analysing unsteady flow in small bore pipes. The explicit hydraulic methods suffer from computational instability which may not be improved by using the Courant condition and, more importantly, they are not suitable for the supercritical flows which predominate in drainage networks. The real choice lies between the method of characteristics in one of its many forms or an implicit method. Implicit schemes were rejected because they are most useful for slowly varying input profiles with a long time base which is the reverse of the type of flow input expected in a drainage system. The principal advantage of the method of characteristics is its ability to deal easily with the supercritical flow régime (Cunge, Holly and Verwey, 1980) and varying boundary conditions. The method of characteristics using a regular rectangular grid imposed upon the computational domain before the calculation commences was used as other characteristics methods (e.g. variable grid) require greater computational time and effort.

4.2 The Method of Characteristics Using a Rectangular Grid

The technique described here for solving the unsteady flow equations using the method of characteristics is that propounded by

Fox (1977) and subsequently described in greater detail by Swaffield (1980, 1981).

Equations 2.31 and 2.32 from Chapter Two describing the positive (C^+) and negative (C^-) characteristics are written,

$$\frac{d}{dt}(V \pm 2c + E_s t) = 0 \qquad (4.1)$$

$$\frac{dt}{dx} = \frac{1}{V \pm c} \qquad (4.2)$$

where V = velocity of flow (m/s)

c = wave speed (m/s)

t = time (s)

x = distance along the channel (m)

Since

$$E_s = g\,(S_f - S_o) \qquad (4.3)$$

where g = acceleration due to gravity (m/s^2)

S_f = slope of the energy grade line

S_o = slope of the pipe

and

$$\frac{dy}{dt} = \frac{2c}{g}\frac{dc}{dt} \qquad (4.4)$$

where y = flow depth (m)

then Equations 4.1 and 4.2 may be rewritten,

$$\frac{dV}{dt} \pm \frac{g}{c}\frac{dy}{dt} + g(S_f - S_o) = 0 \qquad (4.5)$$

$$\frac{dx}{dt} = V \pm c \qquad (4.6)$$

With reference to Figure 4.1, if the velocity and depth are known at points R and S at time level t - Δt then the following equations may be written in terms of the unknown depth and velocity at point P at time level t,

$$V_p - V_R + g \int_{y_R}^{y_P} \frac{1}{c}\, dy + \int_{t_R}^{t_P} g(S_f - S_o)dt = 0 \qquad (4.7)$$

$$x_p - x_R = \int_{t_R}^{t_P} (V + c)dt \qquad (4.8)$$

$$V_p - V_s + g \int_{y_S}^{y_P} \frac{1}{c} dy + \int_{t_S}^{t_P} g(S_f - S_o)dt = 0 \qquad (4.9)$$

$$x_p - x_s = \int_{t_S}^{t_P} (V - c)dt \qquad (4.10)$$

where the subscripts refer to points P, R and S.

Equations 4.7 and 4.8 describe the positive characteristic and Equations 4.9 and 4.10 describe the negative characteristic. Applying a first-order approximation to Equations 4.7 to 4.10,

$$V_p - V_R + \frac{g}{c_R}(y_p - y_R) + g\,(S_R - S_o)\,\Delta t = 0 \qquad (4.11)$$

$$x_p - x_R = (V_R + c_R)\,\Delta t \qquad (4.12)$$

$$V_p - V_s + \frac{g}{c_s}(y_p - y_s) + g(S_s - S_o)\,\Delta t = 0 \qquad (4.13)$$

$$x_p - x_s = (V_s - c_s)\,\Delta t \qquad (4.14)$$

These equations are paired so Equation 4.11 is only true if Equation 4.12 is satisfied and similarly for Equations 4.13 and 4.14.

In order to be assured of a stable solution,the size of the time step Δt must be determined using the Courant condition to ensure that the solution points R and S fall within the domain of dependency of point P. Since the velocity and celerity both vary throughout the duration of the analysis,the maximum value of each is found at every time step and used to calculate the minimum time step necessary to ensure stability,using the following equation,

$$\Delta t = \frac{\Delta x}{(V + c)max} \qquad (4.15)$$

The depth and velocity at points R and S are found by linearly interpolating between points A, C and B. The error introduced by the assumption of linearity may be minimised by applying the Courant

condition to find the time step size.

4.2.1 Non-Rectangular Cross-Sections

The method of characteristics can be extended to channels of uniform non-rectangular section by using the stage variable ω introduced by Escoffier and Boyd (1962). The equation

$$c = \sqrt{\frac{gA}{T}} \tag{4.16}$$

where A = cross-sectional area (m^2)

T = water surface width (m)

is only true for rectangular channels and to overcome this difficulty the stage variable ω is used to replace y as a measure of depth in the pipe. It is defined as,

$$\omega = \int_0^A c \frac{dA}{A} = \int_0^Y \sqrt{\frac{gA}{T}} \frac{T dy}{A} = \int_0^Y \sqrt{\frac{gT}{A}} dy \tag{4.17}$$

It therefore follows that,

$$d\omega = \sqrt{\frac{gT}{A}}\, dy \tag{4.18}$$

The value of ω for any given depth may be found by establishing a table of values at the beginning of the calculation (Henderson, 1966).

4.2.2 Subcritical and Supercritical Flow

Open-channel flow is divided into two régimes, those of subcritical and supercritical flow. In subcritical flow the local wave celerity c is greater than the flow velocity V and it is therefore subject to downstream control. In supercritical flow the wave celerity is less than the flow velocity and so no disturbance may be propagated upstream. The Froude number, which is the ratio of the flow velocity to the wave celerity, is less than unity for subcritical flow and

greater than unity for supercritical flow.

For subcritical flow the conditions at P (Figure 4.1) are determined by the C^+ and C^- characteristics PR and PS. For supercritical flow the conditions downstream of point P in grid section CB cannot affect the conditions at point P. Since the flow velocity is greater than the wave celerity the gradient of the C^- characteristic becomes positive and falls within the section AC. For critical flow, when V and c are equal, the gradient of the line becomes zero and the characteristic falls on the grid line CP.

4.2.3 Internal Nodes

A further set of equations are required in order to interpolate between A, C and B and obtain the depth, velocity and celerity at points R and S (or S' in the supercritical case).

For subcritical flow the following equations may be written,

$$\frac{V_C - V_R}{V_C - V_A} = \frac{x_C - x_R}{x_C - x_A} = (V_R + c_R)\frac{\Delta t}{\Delta x} \qquad (4.19)$$

$$\frac{c_C - c_R}{c_C - c_A} = \frac{x_C - x_R}{x_C - x_A} = (V_R + c_R)\frac{\Delta t}{\Delta x} \qquad (4.20)$$

$$\frac{Y_C - Y_R}{Y_C - Y_A} = (V_R + c_R)\frac{\Delta t}{\Delta x} \qquad (4.21)$$

Now $x_p - x_R = (V_R + c_R)\,\Delta t$ and also $x_p = x_c$. The subscripts refer to points A, C and R.

The solution of these equations gives the following expressions for V_R, c_R and Y_R,

$$V_R = \frac{V_C + \theta(c_C V_A - V_C c_A)}{1 + \theta\,(V_C - V_A + c_C - c_A)} \qquad (4.22)$$

$$c_R = \frac{c_C(1 - \theta V_R) + \theta c_A V_R}{1 + c_C\theta - c_A\theta} \qquad (4.23)$$

$$Y_R = Y_C - \theta(Y_C - Y_A)(V_R + c_R) \qquad (4.24)$$

where $\theta = \frac{\Delta t}{\Delta x}$

Similar expressions may be derived for the depth, velocity and celerity at point S,

$$V_S = \frac{V_C - \theta(V_C c_B - c_C V_B)}{1 - \theta\ (V_C - V_B - c_C + c_B)} \qquad (4.25)$$

$$c_S = \frac{c_C + \theta V_S (c_C - c_B)}{1 + \theta\ \ (c_C - c_B)} \qquad (4.26)$$

$$Y_S = Y_C + \theta(V_S - c_S)(Y_C - Y_B) \qquad (4.27)$$

For supercritical flow a new set of equations must be written for the flow conditions at S',

$$V_{S'} = \frac{V_C(1 + \theta c_A) - \theta V_A c_C}{1 + \theta(V_C - V_A + c_A - c_C)} \qquad (4.28)$$

$$c_{S'} = \frac{c_C + \theta V_{S'} (c_A - c_C)}{1 + \theta\ \ (c_A - c_C)} \qquad (4.29)$$

$$Y_{S'} = Y_C - \theta\ (y_C - y_A)(V_{S'} - c_{S'}) \qquad (4.30)$$

Using the equations described above it is now possible to calculate the conditions at P at time t in the following way,

(i) the conditions at all nodes within the computational domain are known at time t - Δt (the initial flow conditions at time t = 0 are set up as described below).

(ii) the depth, velocity and celerity are found at points R and S (or S') by interpolation using Equations 4.22 to 4.30.

(iii) the depth and velocity at point P at time t are found by using the C^+ and C^- characteristics (Equations 4.11 to 4.14).

The celerity at P is calculated from the following equation.

$$c = \sqrt{\frac{gA}{T}} \qquad (4.31)$$

where A = cross-sectional area of flow (m^2)

T = surface water width (m)

(iv) the steps are repeated for each node at time t. The conditions

for all nodes within the space-time grid at time t are known so calculations for time t + Δt may proceed. (Boundaries are discussed below).

4.2.4 Initial Flow Conditions

The method of characteristics requires that the flow conditions at time t = 0 be known before the computation can begin. The depth and velocity at each of the nodes within the space-time grid are found by assuming steady-state flow at time t=0. The uniform flow depth is found using Chézy's equation,

$$V = C\sqrt{RS_o} \qquad (4.32)$$

where R = hydraulic radius (m)

C = Chézy coefficient = $R^{1/6}/n$

n = Manning's coefficient

which is solved using the bisection technique described by Wylie and Streeter (1978) given a known discharge, pipe slope and value for Manning's n (Chow (1959) suggests values between 0.009 and 0.02 for building drainage pipe materials). The equation must be satisfied by a depth which is less than the diameter of the pipe and greater than zero. This interval is bisected and the depth obtained used to evaluate Equation 4.32. If the equation is positive then the real depth is less than the midpoint and the upper depth is moved to the midpoint and the interval bisected again. A similar procedure is followed if the equation is negative. This is repeated until an acceptable solution is found.

The uniform flow depth is compared to the critical flow depth found by solving the equation describing critical flow,

$$Q = \sqrt{\frac{gA^3}{T}} \qquad (4.33)$$

where Q = discharge (m^3/s)

using the bisection method.

If the flow is supercritical then the effect of the downstream boundary cannot propagate upstream and the uniform flow depth and velocity apply throughout the length of the pipe. If the flow is subcritical then the effect of the downstream exit will propagate upstream. The pipe exit is assumed to act as a free overfall (Henderson, 1966) with a section of critical flow an infinitesimal distance upstream of the actual boundary. The depth then rises upstream of the discharge point until it achieves the normal steady flow depth at a distance specified by the equation for gradually varied flow. This equation allows the depth profile between the two points to be calculated by describing the local head loss at each section in terms of the steady flow loss equation.

This may be written,

$$\frac{d}{dx}\left(z + y + \frac{V^2}{2g}\right) = -S_f \qquad (4.34)$$

where z = elevation of pipe above datum (m)

The slope of the energy grade line S_f may be determined either from the Chézy equation or from the Manning equation.

Equation 4.34 may be rewritten,

$$\frac{dE}{dx} = S_o - S_f \qquad (4.35)$$

where E = specific energy of flow (m)

and $\frac{dz}{dx} = -S_o$

Now

$$E = y + \frac{V^2}{2g} = y + \frac{Q^2}{A^2 g} \qquad (4.36)$$

The minimum specific energy is given by,

$$\frac{dE}{dy} = 1 - \frac{Q^2}{gA^3}\frac{dA}{dy} \qquad (4.37)$$

Now dA = Tdy where T is the water surface width in metres so,

$$\frac{dE}{dy} = 1 - \frac{Q^2 T}{gA^3} = 1 - \frac{V^2 T}{gA} \qquad (4.38)$$

Substitute this expression into Equation 4.35,

$$\frac{dy}{dx}\left(1 - \frac{V^2 T}{gA}\right) = S_o - S_f \qquad (4.39)$$

$$\Delta x = \int_{Y_0}^{Y_1} \frac{1 - V^2 T/gA}{S_o - S_f}\, dy \qquad (4.40)$$

Simpson's Rule is used to integrate the solution numerically and calculate the flow depth profile. The numerator of this equation is the expression for critical depth and when it is equal to zero then the flow is at critical depth and there is no change in x for a change in y. The denominator of the equation is the expression for the uniform flow depth and when this takes a value of zero,uniform depth is achieved and there is no change in y for a change in x.

Once the initial flow depth, velocity and celerity are known for each grid point within the computational domain at time zero then the method of characteristics solution may proceed.

4.2.5 Boundary Conditions

4.2.5.1 Entry Boundary

In the supercritical flow case the depth at the entry boundary is found from the inflow profile since the downstream conditions cannot affect the depth or velocity at the boundary (Figure 4.2). The inflow is given as a function of time, Q = f(t), and this is solved with the

equation for normal depth (Equation 4.32) using the bisection technique to find the depth at each time step.

In the subcritical flow case the downstream conditions do affect the depth at the entry boundary. The inflow profile is solved together with the C^- characteristics, again using the bisection technique (Figure 4.2).

4.2.5.2 Exit Boundary

Since the flow velocity exceeds the wavespeed in supercritical flow, the exit boundary conditions may be found in the same way as at internal nodes. Points R and S' (Figure 4.1) both lie upstream of point P and so are not affected by the presence of the pipe exit. The forward and backward characteristics are solved in the usual way to calculate the depth and velocity at the end of the pipe (Figure 4.2).

The exit depth for subcritical flow is given by the critical flow equation (Equation 4.33) which may be solved with the C^+ characteristic by using the bisection method to calculate the flow conditions at the final node in the space-time grid (Figure 4.2).

4.2.6 Steady-State Loss

The slope of the local energy grade line S_f is evaluated at points R and S (or S') using Chézy's steady-state formula,

$$S_f = \frac{V^2}{C^2 R} \tag{4.41}$$

The loss due to channel resistance represented by the expression $g(S_f - S_o)$ can then be found at each node. S_f is not always positive and must be allowed to take the sign of the flow velocity by replacing V^2 with $V|V|$.

4.3 The Computer Program

The computational techniques described in this chapter were used to create a computer program to solve the St. Venant equations numerically. Initially the program was designed to model the passage of a single wave through a straight pipe with entry and exit conditions dependent upon the flow régime. Figure 4.3 is a flow chart of the program showing how the method of characteristics was used in the simple case of a single pipe. This program represents the starting point in the attempt to produce a network model which is capable of simulating the effect of variable entry conditions, bends, junctions, etc.,and thus provide a design tool for the construction of efficient building drainage systems. Subsequent chapters examine different aspects of the drainage network and the original computer program is then modified to incorporate any changes required. A fundamental revision was necessary to convert the single pipe program to a multi-level network program capable of dealing with multiple inflows.

A computer program is only a tool so no detailed description is given within the main text. However, an appendix is included which gives details of the individual subroutines used and the data necessary to run the program,which should be sufficient to allow the program to be used by others and permit it to be modified to suit the user's requirements. Cunge, Holly and Verwey (1980) offer an interesting discussion on the nature of computer programs written essentially as research tools and the difficulties involved in making them usable in the wider context of commercial engineering.

5. Laboratory Apparatus and Instrumentation

5.1 Introduction

The Drainage Research Group laboratory rig at Brunel University was constructed to provide experimental verification of the flow attenuation in partially filled pipe networks predicted by the computer model outlined in Chapter Four. The equipment originally consisted of a single run of glass or cast iron pipe,but as the work progressed an additional section of pipe was constructed to allow bends and junctions to be tested. Many of the techniques in building this test rig were originally used by other members of the Drainage Research Group when constructing equipment for earlier test programmes.

Figure 5.1 illustrates the general layout of the test facility including the instrumentation used for measuring steady and unsteady flows and for measuring the changing depth of flow within the pipe at a number of points. Two methods of producing unsteady flow within the pipe were used, firstly the controlled outflow from a pressure vessel and secondly a drop-valve cistern.

5.2 The Pipe

The glass pipe used was standard Schott Kem borosilicate glass drainline supplied in standard lengths of 2m, 1m and 0.5m with a nominal internal diameter of 100mm, although this was generally found to average about 106mm. Glass pipe was used because it is transparent and can easily be seen through. UPVC (unplasticised polyvinylchloride) was the obvious alternative but its opacity is a serious disadvantage when, for instance, analysing the effect of junctions on the flow pattern. Schott also produce a wide range of pipe fittings such as

bends, junctions, expansions,etc.,which facilitated the construction of the experimental apparatus. When dropped or cracked glass pipe tends to splinter into long dagger-like shards which are potentially dangerous, and so great care was exercised when using glass pipe on the scale reported.

The pipe work was jointed by single bolt couplings comprising a stainless-steel outer shell, a rubber compression liner and a PTFE (polytetrafluoroethylene) insert to seal the joint securely. The joints remained leak free when deflected up to 4 degrees and had a recommended maximum pressure rating of 210 kN/m^2. The only problem found with the pipe couplings was that at shallow gradients, when the flow was subcritical, local depth changes occurred which propagated upstream for about 0.5m; at steeper gradients this problem was not encountered.

A few tests were carried out using cast-iron pipe in order to assess the effect of a rougher pipe material. The cast-iron drainpipe was available in 2m and 1m lengths, coupled by cast iron clamps with a rubber insert. The effect the joints had on the flow could not be seen, illustrating the primary disadvantage of cast-iron pipe. The weight of the pipe was a further practical difficulty encountered. The majority of the laboratory test work was carried out using the glass drainline and the cast-iron pipe was only used to investigate the effects of pipe roughness.

5.3 The Pipe Support

The pipe was supported by two lightweight heavy duty aluminium ladders hanging horizontally on edge from a Dexion angle framework which was clamped to the roof beams for support. The ladders were

chosen because they offer high rigidity with least weight due to the nature of their construction. Experimental laboratory pipes or flumes are often supported by massive rolled steel I-beams in order to ensure that the gradient of the pipe or flume remains stable; however, observations over many years by the Drainage Research Group have shown that hanging the pipe from a rigid structure (such as a ladder) is equally effective in this application and simpler to construct. The ladders were hung from the Dexion framework at three points (the centre and either end) by turn-buckles (or bottle screws) which could easily be adjusted in order to change the gradient of the pipe.

The pipe was suspended underneath the ladder using pipe clamps with rubber linings which were attached to lengths of 8mm studding fed through the hollow rungs of the ladder and kept in place by nuts and washers above and below the ladder. These nuts could be adjusted in order to level the pipe. A surveyor's level was used to level the lower outer surface of the pipe to the horizontal with an accuracy of about 0.5mm being achieved; the pipe could then be dropped to the required gradient by adjusting the turn-buckles at the centre and downstream end of the pipe. Checks made on the pipe gradient showed that it remained stable over quite long periods of time although minor adjustments sometimes had to be made to maintain the accuracy of the gradient settings.

A free standing "A frame" Dexion framework was built to support the branch pipe needed to model bends and junctions, the framework could be moved to allow different angles of bends and junctions to be tested (Figure 5.1). The 6m of pipe was hung from the framework using the technique described above, although only one ladder was necessary, supported by a turn-buckle at either end. The gradient of the branch

section required more careful attention than the main pipe as the free-standing framework was not as rigid as the Dexion framework supporting the main pipe, which was clamped to the roof trusses. However the slope of the branch pipe could still be accurately set using a surveyor's level and regular checks ensured errors did not go unnoticed.

5.4 Steady Flow

Steady flow was provided from a reservoir of water open to the atmosphere. The water flowed full-bore through a horizontal 100mm diameter glass pipe at ground level and then up a vertical glass riser (100mm diameter) to a junction with either the main or branch glass pipe (Figure 5.1). Two pumps provided the steady flow, a small central heating pump was used for flows up to about 12 l/min and a second larger pump provided flow rates up to 200 l/min. The actual flow rate was measured using appropriate range Rotameters. Two Rotameters were used, the first measuring flow up to 200 l/min and the second flows up to 50 l/min; the accuracy of both was checked using a stop watch to measure a known volume of water. Both are accurate to within 6% of the actual flow rate,which was acceptable for this investigation. A system of valves (Figure 5.2) was used to ensure that any rate of flow can be supplied to either or both the main and branch pipes although there was clearly a limit to the maximum combined flow rate due to the size of the pumps.

Early attempts to feed the steady flow into the vertical riser with only a very short length of horizontal pipe at ground level showed that the flow tended to jet into the glass pipe from the reinforced plastic tube connected to the valve and pump system. This jet action distorted flow velocity profiles across the vertical riser so the

horizontal pipe at ground level was extended by 2m to allow the jet action to be damped out by the full-bore flow in the 100mm pipe. This successfully cut down the serious distortion of the flow velocity profile in the vertical riser and allowed the flow to well into the main or branch pipe at a steady rate.

Steady flow was required as a baseflow for the unsteady flow tests because the numerical method used in the computer program required that an initial steady flow existed within the pipe before subsequent calculations could begin. A variable value steady-state flow was also used to analyse the effect of bends and junctions on the flow régime and to calculate the roughness characteristics of a particular pipe material.

5.5 Unsteady Flow

An unsteady flow profile could be produced in one of two ways at the head of both the main and branch channels. A drop-valve cistern was used to produce a high energy wave which simulated the type of unsteady flow to be expected near the head of a drainage system; the cistern was flushed automatically using a compressed air-operated piston and the baseflow was supplied by allowing the cistern to overflow after it had been filled by flow from the small pump. The second type of wave was provided by a pressure vessel which could be pressurised to about 700 kN/m^2; the shape of the unsteady flow profile was controlled by a valve on the tank discharge,which was again driven by a compressed air piston, allowing the rate of rise and fall of the flow to be adjusted. The piston was connected to a linear voltage displacement transducer and the output from this was recorded on a chart recorder so that the exact movement of the piston, and hence

the valve motion, was known and could be accurately adjusted (Figure 5.3). The peak flow rate was a function of the head in the pressure vessel and therefore dependent upon the pressure in the compressed air system. This pressure was usually sufficient to give a maximum flow rate in the region of 2.5 l/s. The base flow was provided by the small pump which fed into the ground level pipe through a different set of pipework to that of the wave produced by the pressure vessel (Figure 5.3). The unsteady flow profiles produced in this way represent the type of waves to be expected in pipes remote from the head of the drainage network.

5.5.1 Unsteady Flow Measurement

The measurement of unsteady flow is a long established problem in hydraulics (Katys, 1964); the best method currently available is probably the laser technique which uses the Doppler effect to continuously monitor the velocity of flow past a fixed point. This method has many advantages; it does not obstruct the flow, it does not need calibration and the velocity is measured at a precisely defined point; however, the instrument is complex to operate and very expensive and was therefore not available for this study. Two types of flowmeter, as opposed to velocity meter, were considered, electromagnetic and ultrasonic, but were also rejected on grounds of cost. Electromagnetic flowmeters work on the principle that when a conductor (e.g. water) moves across a magnetic field a voltage is induced in the conductor and the magnitude of the voltage is directly proportional to the velocity of the conductor. Ultrasonic flowmeters either use the Doppler effect or the fact that sound waves travel faster with the current than against it (Hayward, 1979). Hot-film

anemometry is a cheaper alternative velocity metering system and this was used for the early experiments but was found to be very sensitive to even small changes in the water temperature and the results obtained were not reliable.

The method finally chosen to measure the mean velocity of the unsteady flow profile was the Streamflo miniature current flowmeter system which is designed for measuring low velocities of conducting fluids such as water. The system consists of a measuring head with a five-bladed rotor on a stainless-steel pivot with jewelled bearings to reduce frictional torque and produce a linear output over a wide range of velocities (Figure 5.4). The head is mounted on a stainless-steel tube which contains an insulated gold wire at a distance of 0.1mm away from the rotor blades. When the rotor revolves the passage of each blade past the gold wire slightly varies the impedance between the tip of the gold wire and the stainless steel tube; this variation is used to produce a current signal in the digital indicator proportional to the velocity of the flow turning the rotor. This signal is output to a chart recorder and using the calibration chart supplied with each probe the velocity of the flow throughout the passage of the unsteady wave can be found. The probe used for these tests was able to measure velocities between 0.025 m/s and 1.5 m/s; given that the discharge was measured flowing full bore in a vertical riser with a diameter of 100mm and assuming a uniform velocity distribution then flow rates between 0.19 l/s and 11.8 l/s could be measured.

The Streamflo meter was used to measure the discharge from the pressure vessel but could not be used on the wave from the drop-valve cistern due to the presence of aerated water which changes the conductivity of the fluid surrounding the probe and renders it

inoperative. The discharge from the drop-valve cistern was found by recording the cistern water level as the cistern emptied and suitably distributing the known volume of water flushed through time to create an input profile.

5.6 Flow Depth Measurement

In order to measure the depth of flow in the 100mm diameter glass pipe a small hole was made in the pipe wall and a short piece of 6mm outside diameter glass tubing welded on perpendicular to the outside of the glass pipe. This tapping point was connected to one side of a differential pressure transducer with a length of plastic tubing; the other side of the transducer was left open to atmosphere (Figure 5.5). A tap placed before the pressure transducer allowed the tubes to be balanced so that the tube open to atmosphere had a pressure head equal to the invert level of the glass pipe; the depth of flow within the pipe could then be measured as a head above invert level. The pressure transducers were rated for pressures between 0 and 35 kN/m^2 and the output from them was measured in volts with a linear relationship between voltage and pressure (i.e. head) differential. The pressure transducers were calibrated by noting the voltage produced for a known difference in head; there is a linear relationship between voltage and pressure head.

Originally seven tapping points were fitted to the pipe at intervals of approximately 1.5m and the output from the differential pressure transducers was measured on a number of chart recorders. This method was slow and inflexible as the observed flow depths could not be easily compared with those predicted by the computer program for unsteady flow. A second system was developed which allowed data from

the laboratory rig to be fed into an Apple microcomputer and thence to the University's Honeywell mainframe computer where graphical comparison between observed and predicted data could be made. The number of tapping points was reduced to six when the automatic logging system was introduced and the position of these could be altered to maximise their effectiveness.

5.7 Solartron Logging System

5.7.1 Hardware

The output from the pressure transducers was input to a Solartron Microprocessor voltmeter which was used as an analogue to digital signal converter. Depending upon the range of functions and accuracy required,up to 330 readings per second could be collected by the voltmeter and output to the microcomputer. The computer used was an Apple II with a purpose-built card which read the binary output directly from the voltmeter and stored it on disk.

5.7.2 Software

The software was written specifically for the purpose of recording data output from the Solartron digital voltmeter and included all the features required.

The program on the microcomputer allowed four options to be chosen. The first was for logging data from the digital voltmeter and allowed the user to specify the range over which voltages were to be logged and the number of samples per channel per second which were to be recorded. The range was specified as the maximum voltage to be expected but the system would not fail unless a voltage was received which was greater than twice the maximum specified. If this did occur

then the current run would be aborted and a higher maximum voltage specified before a new test was started. The logging rate input by the user was used to calculate the actual logging rate in integer thousandths of a second, the actual rate logged was always equal to or greater than that specified by the user up to the maximum logging rate which the Solartron offered. For instance,if a user specified a logging rate of 12 samples per channel per second for 5 channels then the actual number of samples per second was 62 rather than 60. The length of time for which logging could take place was limited by the capacity of the Apple and was usually about 30 seconds (depending upon the logging rate). When logging finished the program automatically dumped the results to disk in binary form for maximum speed and another test run could be started. The digital voltmeter sampled the channels sequentially so there was a lag between the time logging started for each channel. The lag depended upon the number of samples per channel per second which were to be collected but it should be taken into consideration when the results of each run are interpreted.

The second option converted data stored in binary into decimal form and sorted the file into an easily readable format. Converting a text file takes a considerable length of time (about 7.5 minutes for 2000 samples) which was why the data was initially collected in binary form. The punch option allowed the converted data files to be output onto punched tape which could be read into the University's Honeywell mainframe and the review option printed converted data files onto the Apple printer.

During the course of the work described herein a link was made between an Apple microcomputer and the Honeywell mainframe so that by using the Apple as an intelligent terminal data files could be read

directly to the mainframe. This facility considerably improved the speed at which data could be transferred and reduced the number of errors which occurred.

Comparisons could be made between results collected by the automatic logging system and transferred to the mainframe and those predicted by the simulation program. The graphics facility available on the mainframe allowed the comparison between the observed and predicted data to be clearly illustrated.

6. Verifying the Single Pipe Program

6.1 Introduction

The computer program described in Chapter Four predicts the attenuation of flow depth and velocity of an unsteady flow profile in a long drainage pipe. If this theoretical simulation is to be useful it must be shown to be a reasonably accurate representation of the conditions within the glass pipe of the laboratory apparatus. Verification of the accuracy of the program by comparing depths of flow predicted by the model with depths of flow measured along the pipe was therefore the first step in the construction of a building drainage network model.

6.2 Normal Depth At Entry

Unsteady flow tests were carried out on the rig at pipe gradients of 1/60, 1/100, 1/150 and 1/200. The pressure vessel was used to produce an unsteady wave which was delivered to the pipe through a vertical riser. These tests were conducted before the automatic logging system was installed so depths were measured using chart recorders at seven tapping points along the rig. The pipe characteristics and flow profile were input to the computer program and depth profiles at the nearest node to each of the tapping points predicted. The node separation for these simulations was 0.25m so the greatest error between the actual position of a tapping point and the node used to represent it was 0.125m. This error will obviously slightly affect the results,but given wave velocities of the order of 1 m/s the timing error will only be measurable in tenths of seconds, which was considered negligible. Comparisons were then made between

the depths predicted by the computer program and the depths observed on the laboratory rig.

Figure 6.1 and Figure 6.2 illustrate the results of two example runs each at a gradient of 1/100. The observed and predicted depth profiles are shown together with the measured input unsteady flow profile; the predicted results are consistent with those observed on the test rig in both cases. The depth profile is underestimated at both the first and second tapping points and this is due to the entry boundary condition which is based on normal depth at pipe entry; alternative conditions are described below to deal with this anomaly. The depth is unusually great at the entrance to the pipe due to the vertical velocity component of the water in the vertical riser leading to the horizontal glass pipe. Changing the boundary condition at the pipe entrance from normal depth to a more suitable model allowed a better prediction to be made of the depth profiles at the first two tapping points.

The observed depth profiles have a steeper leading edge than those predicted by the computer program, this is partly a result of the greater depth at entry which causes the wave to attenuate more slowly but is also a result of the use of pressure transducers to measure the depth of flow. The sudden change in depth as the leading edge of the wave profile passes over the tapping point causes pressure transients within the water-filled plastic tubing which connects the pressure transducer to the tapping point on the glass pipe and causes the pressure transducer to "bounce" and record a steeper rise than is actually occurring. Attempts were made to damp out this effect but the response time of the system was then reduced and realistic results could not be obtained. However, despite the over-steepening of the

leading edge, the attenuation of the depth profile can be clearly seen and is mirrored by the predictions from the computer program. From the comparisons which were made between observed and predicted flows the program appeared to provide a good prediction of the attenuation of surge profiles at a number of points along the drainage pipe.

Figure 6.3 illustrates the effect of changing the gradient to 1/150, the attenuation is more marked than at steeper gradients and again the depth at the first two tapping points is under-estimated, this is a boundary problem and is discussed later. Generally the observed and predicted profiles are in agreement and the attenuation of the wave can clearly be seen.

Figure 6.4 shows a test run at a gradient of 1/60 with a large steep wave running over a low steady flow. The attenuation of the flow is well predicted by the computer model except towards the end of the pipe.

These examples illustrate the application of the Brunel test apparatus in providing experimental verification of the attenuation of unsteady flow in long pipes predicted by the computer program developed which incorporated the normal depth at pipe entry boundary condition. Certain problems with entry boundary conditions were discovered and new boundary equations were developed to deal with the difficulties presented as a result of the test rig design.

6.3 Critical Depth At Entry

Normal depth at entry was the boundary condition used for the initial analysis but it has been shown that this led to an underestimate of the predicted depths at the first two pressure tapping points compared with the depths observed on the test rig. It may be

argued that this was an unrepresentative condition in any case. The normal flows are all supercritical at the gradients currently being considered and therefore downstream conditions are determined solely by the upstream boundary condition. As the wave speed is always less than the velocity in supercritical flow,nothing which occurs downstream can affect the conditions at the entrance to the pipe. In order to predict the depth profiles at the first two pressure tapping points it was therefore necessary to postulate one or more alternative entry boundary conditions. The construction of the Brunel test facility, a vertical riser leading to a horizontal pipe, suggested that depths above normal depth would be experienced at the entrance to the pipe and that this effect would propagate downstream thus affecting depth profiles near the pipe entrance.

The first alternative entry boundary condition to be considered was that of critical depth with a gradually accelerating flow giving a return to normal depth over the first few metres of the pipe. The flow depth at the pipe entrance was set to the critical depth, determined using the bisection method (described in Chapter Four) to solve the following equation iteratively;

$$X = 1 - \frac{Q^2 T}{gA^3} = 0 \qquad (6.1)$$

where X = distance, positive in initial flow direction (m)

Q = flow rate (m^3/s)

T = surface width of flow within partially filled channel (m)

g = acceleration due to gravity (m/s^2)

a = cross-sectional area of flow (m^2)

Downstream conditions cannot affect this depth as supercritical flow velocity exceeds the wave speed and thus the critical depth

boundary condition is independent of pipe gradient.

In the original program, with a normal depth entry boundary condition, two lines of slopes respectively $1/(V + c)$ and $1/(V - c)$ (where V is the local mean velocity (m/s) and c is the wave speed (m/s)) are constructed through point P (Figure 4.1) to give points R and S (or S' in the supercritical case). A linear interpolation is then made between A and C to find the velocity and wave speed at point R and between C and B to find the velocity and wave speed at S (S' in the supercritical case). This linear interpolation cannot be made if the alternative entry boundary condition of critical depth is applied since the velocity and wave speed do not vary linearly between the two nodes. A suitable approximation is to allow the velocity to vary in proportion to the square root of the distance along the pipe. The following equation is used and applied over the first two metres of the pipe gradually increasing the velocity from critical velocity at the entrance to normal velocity at two metres along the pipe (Figure 6.5);

$$V = V_{crit} - (V_{crit} - V_{norm}) L^{0.5} \qquad (6.2)$$

with $0 < L < 1.0$

and where V_{crit} = critical velocity (m/s)

V_{norm} = normal velocity (m/s)

The depth is calculated from the velocity and the known flow rate using the bisection method already described and from this value the wave speed is found. The calculation can then proceed in the normal way as the program has a compatible flow velocity and wave speed. Two metres is suitable for the test rig at Brunel but could be changed to suit circumstances found elsewhere.

A more exact solution to the problem would be to replace the equations for linear interpolation with those of a curve such as the

gradually varied flow surface profile but the computational difficulties are great, particularly in terms of the small time-step size which results from the necessary reduction of the pipe calculation sections. The results would in any case be similar to the results obtained using the approximation described above. The alternative entry boundary condition is set up at the first time step and subsequently allowed to propagate down the pipe during the following time steps.

6.4 Subcritical Depth At Entry

The second alternative entry boundary condition explored was that of subcritical depth at entry. The depth at the entrance to the laboratory test pipe was measured for a range of steady-state flow conditions and the relationship between the flow rate and the depth of water in the pipe at the entrance determined (Figure 6.6). Also shown is the relationship between the calculated critical depth and the measured subcritical depth. The curve of subcritical depth against flow rate is input to the program as a set of data points then examined at each time interval and the appropriate depth at the entrance to the pipe taken depending upon the input flow rate. The velocity is found given continuity and the following equation,

$$V = V_{sub} - (V_{sub} - V_{norm})\, L^{0.5} \qquad (6.3)$$

with $0 < L < 1.0$

and where V_{sub} = subcritical flow velocity (m/s),which is applied to find the velocity at each of the nodes for the next two metres downstream. The velocity is assumed to vary between a subcritical value dependent upon the depth and discharge at the pipe entrance and normal velocity which is achieved two metres further down the pipe.

6.5 Results Using the Alternative Entry Boundary Conditions

Both of the suggested alternative boundary conditions assume that supercritical flow exists downstream. This assumption is true for the majority of flows within building drainage pipe networks but if subcritical flow does exist then the boundary conditions can still be used. As the cross-sectional area of flow downstream of the pipe entry increases then the velocity decreases until it matches the velocity of the subcritical flow.

Figure 6.7 shows the observed results from Figure 6.2 and the predicted results recomputed using the critical depth instead of the normal depth entry boundary condition. Figure 6.8 shows the observed results from Figure 6.3 with the predicted results recomputed in the same way. These two examples show that the critical depth entry boundary condition does improve the prediction of the depth profiles at the first two tapping points. Figure 6.9 illustrates the predicted and observed depths shown in Figure 6.4 recalculated with the original boundary condition replaced with subcritical flow depth while Figure 6.10 shows the results from Figure 6.1 again with the subcritical entry boundary condition for the predicted depth profiles. These two examples of the effect of using subcritical depth at entry demonstrate that this boundary condition provides an accurate prediction of the depth profiles at the first two tapping points.

Generally the changed entry conditions allow a more accurate prediction of the depth profiles at the first two tapping points. Critical depth at entry is less appropriate to the Brunel test rig due to the vertical velocity component in the water as it reaches the horizontal glass drainage pipe. The effect of the changed boundary condition gradually dies away downstream with a transition length of

about two metres. The experimental verification of the accuracy of these alternative entry boundary conditions suggests that they most accurately reflect conditions remote from high energy inputs, such as vertical stack to drain connections, and that another entry boundary condition is necessary to model high energy situations.

6.6 Energy Entry Boundary Condition

The entry boundary conditions described above are used when the wave profile is generated using the pressure vessel and arrives at the head of the pipe via the vertical riser. If the drop-valve cistern is used to produce a high energy wave then these entry boundary conditions are not suitable and a further alternative must be found. High energy waves are most likely to occur at vertical stack to drain connections and in other similar situations. The flush from the cistern is delivered to the head of the pipe through a small bore plastic tube with an internal diameter of about 43mm; this can be modelled by assuming the tube flows full-bore and then determining the energy of the flow in terms of the water jet velocity (Swaffield, 1981) (Figure 6.11).

The specific energy of the flow at entry is described thus,

$$E = \frac{1}{2}\frac{u^2}{g} = \frac{Q^2}{2ga^2} \qquad (6.4)$$

where E = specific energy (m)

u = water jet velocity (m/s)

g = acceleration due to gravity (m/s^2)

Q = flow rate (m^3/s)

a = area of the delivery tube (m^2)

This entry energy is equated with the specific energy of the partially

filled pipe flow,

$$E = y_e + \frac{V^2}{2g} \qquad (6.5)$$

where y_e = depth of flow at entry to partially filled pipe (m)

V = mean velocity of flow at entry (m/s)

Using the equation of continuity it follows that,

$$E = y_e + \frac{Q^2}{2gA^2} \qquad (6.6)$$

where A = cross-sectional area of flow at pipe entry (m^2)

The flow area A is a function of the depth y_e and the inflow Q is known as a function of time. The flow depth at the entrance to the pipe may be calculated from the following equation,

$$y_e = \frac{Q^2}{2g}\left(\frac{1}{a^2} - \frac{1}{A^2}\right) \qquad (6.7)$$

This equation must be solved iteratively by selecting trial values of y_e in order to calculate the value of A and therefore satisfy the equivalence; thus the flow depth at the pipe entrance may be found at each time step.

6.6.1 Results

Comparisons made between the depth profiles observed at seven points along the experimental pipe and those calculated using the energy entry boundary suggest that this boundary condition is a more accurate method of simulating the entry of a high energy wave into the pipe. Figure 6.12 shows the results for a wave produced by the drop-valve cistern and entering the pipe set at a gradient of 1/100. The new entry condition produces a better prediction of the attenuation and velocity of the wave although there is a discrepancy in the middle section of the pipe in the timing of the passage of the wave front. It

was thought that the wave produced by the cistern might be rapidly varied instead of gradually varied and thus the computational methods used in the computer program would be inappropriate. The method for modelling rapidly varied (or steep fronted) waves is described below in Chapter Eleven but further investigation revealed that the wave generated by the drop-valve cistern could not be modelled using the equations for rapidly varied flow and that the gradually varied flow equations were in fact more applicable. A further improvement in the prediction was made by replacing Manning's expression with the Colebrook-White equation which is fully described in Chapter Eight.

6.7 Conclusions

Four different entry boundary conditions are presented which can be incorporated into the final program. Two of these are particularly suitable for modelling the flow conditions found within the laboratory rig used for experimentation and the other two entry boundary conditions are included to make the program more flexible and generally applicable. It is possible to incorporate any entry boundary condition into the program in order to model a particular pipe network. The subcritical entry model accurately reflects conditions in pipes remote from high energy inputs while the energy entry model simulates the effect of a vertical stack to horizontal pipe connection. The inclusion of a variety of entry boundary conditions gives greater flexibility to the computer program.

6.8 Wave Attenuation in Relation to Pipe Length

A study by Burberry (1978) of the attenuation of a surge wave (or flush) down a long pipe reported results obtained from tests

undertaken in a hydraulics laboratory partly to full scale and partly in the form of scale model tests. Figure 6.13 illustrates these results and the conclusion that the flush from a 9 l water closet is attenuated for most gradients by a factor of five in a distance of between ten and thirty metres. The family of lines is produced using the same inflow profile to the pipe and the same value of Manning's n, only the slope is varied. A simple relationship between the duration of flow of a surge and the distance the surge has travelled along the drain pipe is implicit in these results.

The computer model was used to attempt to replicate the results reported above. Figure 6.14 shows that it is reasonable to approximate the relationship between the duration of flow of the surge and the distance along the pipe by a straight line, though it may be seen that the flow attenuates more rapidly near the entrance to the pipe. A good approximation to the previously reported results is obtained at a gradient of 1/40, with a very similar rate of attenuation. However by simply changing the gradient of the pipe it is not possible to reproduce the family of lines represented by the three gradients. Significantly less attenuation of the flow rate is predicted by the computer program at gradients of 1/80 and 1/120 than is shown in the earlier results. Further analysis shows that the rate of attenuation is also very sensitive to quite small changes in Manning's n.

The results produced by Burberry cannot be adequately reproduced by the computer model developed to simulate flow attenuation in long drainage pipes. It is probably an over-simplification of a complex problem to suggest that the flush from a 9 l water closet is attenuated by a factor of five for most gradients over a distance of between ten and thirty metres since the rate of attentuation is very

much affected by the slope and roughness of the pipe. The computer model provides a very useful tool for predicting the action of unsteady flow profiles in a variety of circumstances, for example, the subsequent addition of inflow profiles downstream may be dealt with, which is a condition not capable of solution using a single attenuation factor. The computer analysis has also demonstrated that the relative depth of the wave to the base flow affects the attenuation which is another variable not taken into account by the attenuation factor approach.

7. Non-Dimensional Analysis

7.1 Introduction

A parametric study was carried out to obtain a more general view of the wave attenuation predicted by the computer program and to investigate the effect of altering certain variables. By converting the analysis to a non-dimensional form it is possible to study the effect of channel, wave and flow parameters on the subsidence of the wave as it travels down the pipe. Independent and systematic variation of each of these parameters allows their effect on the gradually varied unsteady flow to be more easily understood. Five governing factors are investigated: the Froude number of the initial uniform flow, two wave parameters and two channel parameters. A dimensionless form of each is used and varied over a wide range of values in order to study its effect on the attenuation of the wave.

Sridharan and Mohan Kumar (1981) reported a parametric study of flood wave propagation in rectangular and trapezoidal channels which restricted the flow to subcritical throughout the passage of the wave. The occurrence of subcritical flow in a drainage pipe is unusual and the results presented are not directly applicable to the problem of supercritical flow in partially filled circular drainage pipes. Mozayeny and Song (1969) reported a similar study but of a more restricted nature; a very limited range of wave amplitudes were considered and the greatest only formed a small fraction of the depth of initial uniform flow,which is in direct contrast to flow in a drainage pipe where large waves are superimposed on small base flows. Sakkas and Strelkoff (1976) made a dimensionless parametric study of unsteady flow for the dam-break problem; a parametric study of the effect of

channel shape on gradually varied flow profiles was reported by Lakshmana Rao and Sridharan (1971), and Chen and Wang (1969) reported a non-dimensional study of flow in infinitely wide channels. Further non-dimensional studies of unsteady flow include those by Vallentine (1967), Silvio (1969) and Minton and Sobey (1973).

Other methods have also been used to explain the behaviour of waves in open channels. Ponce and Simons (1977) used linear stability theory to investigate the propagation characteristics of various types of waves including the dynamic wave model. Ponce (1982) went on to clarify the nature of wave attenuation in open channels and investigated the physical mechanisms involved. Menendez and Norscini (1982), also using linear stability theory, presented results which allowed a rough determination of the characteristics of a wave to be made from the Froude number of the flow and the dimensionless wave number.

The non-dimensional study described below investigates the attenuation of gradually varied flow in small diameter circular pipes with supercritical flow throughout the passage of the wave.

7.2 The Governing Parameters

The parameters governing the attenuation of a gradually varied flow profile in a circular drainage pipe are the Froude number of the initial uniform flow, the non-dimensional wave duration, the non-dimensional wave amplitude, the slope of the pipe and the non-dimensional pipe diameter. Each of these parameters is varied independently of the others to allow their effect on the subsidence of the wave to be studied. The method of characteristics using a regular rectangular grid is used to solve the unsteady flow equations as

described in Chapter Four. The flow is initially steady with a constant depth y and all the dimensionless parameters, including the non-dimensional distance, are defined using this value.

7.2.1 Froude Number

The Froude number describes the régime of the initial steady base flow (i.e. whether it is super- or subcritical), for this study all the values used are supercritical for the reasons outlined above. Values of Froude number between 1.1 and 1.7 are taken.

$$Fr = \frac{V}{\sqrt{g\frac{A}{T}}} \qquad (7.1)$$

where Fr = Froude number

V = velocity of the initial flow (m/s)

g = acceleration due to gravity (m/s^2)

A = cross-sectional area of initial uniform flow (m^2)

T = surface width of initial uniform flow (m)

7.2.2 Non-Dimensional Wave Duration

The duration of the wave is the time in seconds of the base of the triangular hydrograph input at the start of the pipe, the non-dimensional wave duration (T_w) is defined as follows (Figure 7.1),

$$T_w = \frac{t_w S_o V}{Y} \qquad (7.2)$$

where t_w = actual wave duration (s)

S_o = slope of the pipe

7.2.3 Non-Dimensional Wave Amplitude

The wave amplitude (a) is the depth of flow at the point of maximum discharge on the inlet hydrograph (Figure 7.1); the non-dimensional wave amplitude (A_w) is defined as follows,

$$A_w = \frac{a}{y} \tag{7.3}$$

where a = actual wave amplitude (m).

7.2.4 Pipe Slope

This is a dimensionless parameter.

7.2.5 Non-Dimensional Pipe Diameter

This is the second parameter describing the characteristics of the channel and is defined with reference to the depth of the initial uniform flow (y),

$$D_p = \frac{D}{y} \tag{7.4}$$

where D = actual pipe diameter (m).

7.2.6 Other Parameters

The effect of each of these parameters on the attenuation of the wave is shown by demonstrating the subsidence of the relative depth (Y) with the non-dimensional distance (X). The relative depth is the local wave amplitude normalised with respect to the initial wave amplitude at X = 0 and is defined thus,

$$Y(X) = \frac{y_{max}(X) - y}{y_{max}(0) - y} \tag{7.5}$$

where $y_{max}(X)$ = maximum depth at distance X (m)

$y_{max}(0)$ = maximum depth at X = 0(m)

The non-dimensional distance is defined as follows,

$$X = \frac{xS_o}{y} \qquad (7.6)$$

where x = actual distance along pipe (m)

Two other parameters are also of interest in analysing the results, the length scale and the time scale. The length scale (l) is defined thus,

$$l = \frac{y}{S_o} \qquad (7.7)$$

The time scale (t) is defined as follows,

$$t = \frac{l}{V} \qquad (7.8)$$

Manning's formula may be stated as,

$$V = \frac{R^{2/3}S_o^{1/2}}{n} \qquad (7.9)$$

where n = Manning's roughness coefficient

R = hydraulic radius (m)

7.3 Results

Each of the five non-dimensional parameters was systematically varied whilst the others were held constant and the resulting effect on the subsidence of the wave with distance was determined. The dimensionless parameters were held constant with the following values throughout the analysis:

Froude number	= 1.5
Non-dimensional wave duration	= 1
Non-dimensional wave amplitude	= 3
Slope of the pipe	= 0.01
Non-dimensional pipe diameter	= 6

7.3.1 Effect of the Froude Number

Figure 7.2 shows the variation of relative depth with non-dimensional distance along the pipe for Froude numbers between 1.1 and 1.7; the values of the other dimensionless parameters are as above. The subsidence of the wave is greatest for the lowest Froude number,which is explained as follows. Given an initial uniform flow depth and pipe slope,

$$n \alpha \frac{1}{Fr} \qquad (7.10)$$

(from the definition of the Froude number and Manning's formula) The length scale l is constant and the time scale t is also inversely proportional to the Froude number so that an increase in Fr indicates a decrease in both channel roughness and time scale. However, calculations have shown that a reduced wave duration results in a greater subsidence of the wave (Figure 7.3) so it is the greater influence of the channel roughness which is producing lower subsidence for the higher Froude numbers. Sridharan and Mohan Kumar (1981) also observed the overwhelming influence of channel roughness when considering subcritical flows with Froude numbers between 0.1 and 0.7.

Mozayeny and Song (1969) found that the relative depth decayed exponentially with distance but only considered channels with a dimensionless length X of about 0.35. No constant exponent could be found to describe the decay of relative depth shown in Figure 7.2 (and in all subsequent similar figures) due to the greater non-dimensional distance considered.

7.3.2 Effect of Wave Duration

Figure 7.3 shows that as the duration of the wave increases the

subsidence is less at any given distance X; dimensionless wave durations from 0.5 to 2.0 are considered in the analysis. The rate of attenuation is greater for waves of shorter duration, particularly in the initial reaches of the pipe and it appears that as the volume of the wave decreases the subsidence rate increases.

7.3.3 Effect of Wave Amplitude

As the non-dimensional amplitude of the wave increases so does the subsidence of the wave with distance (Figure 7.4); dimensionless wave amplitudes of between 2 and 5 are presented. The relative depth at X = 10 is 21% and 28% of the initial wave amplitude for A_W = 5 and 2 respectively.

7.3.4 Effect of Pipe Diameter

Calculations have shown that for a constant Froude number Manning's n increases as D increases. This is difficult to demonstrate since for a circular channel,

$$n = \frac{A^{1/6}\ T^{1/2}\ S_o^{1/2}}{Fr\ g^{1/2}\ P^{2/3}} \qquad (7.11)$$

where P = wetted perimeter (m)

Therefore,

$$n\ \alpha\ \frac{A^{1/6}\ T^{1/2}}{P^{2/3}} \qquad (7.12)$$

which is a complex function of the pipe diameter. In order to maintain the non-dimensionality of the analysis it is therefore necessary for the value of Manning's n to increase as the pipe diameter increases. In spite of this the subsidence rate is still greatest for narrow channels (Figure 7.5),which indicates that the diameter of the pipe has a very significant effect on the rate of subsidence.

7.3.5. Effect of Pipe Slope

From Manning's formula

$$n \alpha S^{1/2} \qquad (7.13)$$

therefore as the slope increases so does Manning's n for a fixed base flow (as used in this study to define the other non-dimensional parameters). Figure 7.6 shows that as the slope of the pipe becomes steeper so the subsidence of the wave is greater. However, as the slope steepens so the roughness increases in order to maintain the non-dimensionality at different gradients, but the effect of the slope overwhelms this increase in Manning's n thus indicating the very significant effect of pipe slope on the rate of subsidence.

7.4 Conclusions

The non-dimensional analysis of unsteady flow in partially filled circular pipes allows a number of conclusions to be drawn.

(i) There is considerable attenuation of the wave depth in a channel of circular cross-section over a dimensionless distance of 10.

(ii) Greater subsidence occurs for lower initial uniform flow Froude numbers.

(iii) The initial duration of the wave has a pronounced effect, with significantly greater subsidence for lower values of T_w.

(iv) Increased wave amplitude increases the wave attenuation.

(v) The pipe diameter is particularly significant for narrow pipes; as the diameter increases the change in the rate of subsidence decreases.

(vi) Steeper slopes produce greater subsidence at any given non-dimensional distance.

8. Hydraulic Pipe Roughness

8.1 Introduction

The hydraulic roughness of a pipe or channel is dependent upon the flow conditions and it is possible for a pipe to be hydraulically smooth even when the surface is apparently rough. A pipe is said to be hydraulically smooth when the surface projections are so deeply embedded within the boundary layer, or laminar sublayer, that they exert no influence over the flow. If a channel or pipe is already hydraulically smooth then no amount of additional smoothing of the pipe surface will increase the flow, at lower Reynolds numbers the laminar sublayer thickens and is then capable of burying greater roughness projections (Powell, 1949). As the Reynolds number, which is an inverse measure of the effect of viscosity, increases then the thickness of the laminar sublayer decreases and the surface roughness ceases to be deeply embedded within the boundary layer, this is known as the transitional stage. Finally the projections break through the laminar sublayer, the flow becomes fully rough and the resistance of the pipe is then independent of the Reynolds number (Figure 8.1).

Surfaces such as glass, UPVC, cast iron etc. are regarded as being moderately smooth and produce flows which are in the transitional zone between hydraulically smooth and fully rough flow for the range of Reynolds numbers to be expected in small, circular open channels. With a flow velocity of 1.0 m/s the Reynolds number is 6,625 in a 100mm diameter channel which falls midway between the expected values of 500 to 12,500 for transitional flow (Chow, 1959).

8.2 Manning's Equation

Manning's equation is based upon the empirical relationship,

$$C = \frac{R^{1/6}}{n} \qquad (8.1)$$

where C = Chézy coefficient

R = hydraulic radius (m)

n = Manning's coefficient of surface roughness

By using the Chézy equation,

$$V = C\sqrt{RS_o} \qquad (8.2)$$

where V = flow velocity (m/s)

S_o = channel slope

Manning's equation is more usually written as,

$$V = \frac{R^{2/3}S_o^{1/2}}{n} \qquad (8.3)$$

8.3 Colebrook-White Equation

The Colebrook-White equation for pipeflow (Colebrook, 1939) is based on empirical observations and may be written,

$$\frac{1}{\sqrt{f}} = -2\log_{10}\left(\frac{k}{14.83R} + \frac{2.52}{R_e\sqrt{f}}\right) \qquad (8.4)$$

where f = Darcy resistance coefficient

k = roughness coefficient (m)

R_e = Reynolds number (characteristic length equal to the hydraulic radius)

The Colebrook-White equation for full bore pipe flow may be developed from the general equation by taking the hydraulic radius R to be equal to D/4 where D is the pipe diameter in metres.

The Reynolds number represents the effect of viscosity and is expressed thus,

$$R_e = \frac{4QR}{A\nu} \qquad (8.5)$$

where Q = discharge (m^3/s)

A = cross-sectional area of flow (m^2)

ν = kinematic viscosity of water (m^2/s)

It is important to use the correct characteristic length for the Reynold's number, here it is the hydraulic radius of flow. Open channel flow is laminar if the Reynolds number R_e is less than about 500 and turbulent if R_e is greater than about 12,500, the transitional zone occurs between these two extremes.

The Chézy equation (defined in the last section) was developed for large open channels, however the effect of cross-sectional channel shape on the Chézy coefficient has been shown to be limited (Report, 1963) and it may be used for channels which are hydraulically moderately smooth (Henderson, 1966). The Chézy coefficient can also be expressed in terms of the Darcy resistance coefficient,

$$C = \sqrt{\frac{8g}{f}} \qquad (8.6)$$

From these equations the following expression may be derived,

$$Q = \sqrt{32gRS_o}\, A \log_{10}\left(\frac{k}{14.83R} + \frac{2.52\,\nu}{R\sqrt{128gRS_o}}\right) \qquad (8.7)$$

8.4 Experimental Investigation

Laboratory experiments were carried out using the laboratory test apparatus to investigate the stability of Manning's n. A constant steady flow was discharged into the glass pipe which was set at a known gradient and the depth of flow measured at a point midway along the pipe where the flow régime was undisturbed by entry or exit conditions. This was repeated for the same discharge at five different

gradients and the value of Manning's n for each gradient calculated, the results of this experiment are shown in Figure 8.2. These tests clearly show that Manning's n varies with gradient although the discharges in the pipe remained constant. Similar tests were then carried out at a fixed gradient and with a variable discharge; the results of these tests (Figure 8.3) show that Manning's n also varies with discharge which confirms the findings of Camp (1946), Amein and Fang (1970) and others.

The results shown in Figure 8.2 are for 100mm diameter cast-iron pipe; the value of Manning's n varies from about 0.008 to 0.01 which is not significantly different from the values of Manning's n found for 100mm diameter glass pipe in similar tests. It is felt that the values of Manning's n for the cast-iron pipe are too low and not representative of the true hydraulic roughness of the surface.

Manning's coefficient was originally derived for large open channels of rectangular cross-section with fully rough flow and although it is frequently used in sewer network models (Yen and Sevuk, 1975, Mays and Tung, 1978 and Akan and Yen, 1981) the results reported here led to serious doubts about the validity of using Manning's coefficient for fairly small bore partially filled pipeflow.

The question of friction factors in open channels was studied extensively by a committee of the American Society of Civil Engineers (Report, 1963) who found the Colebrook-White equation to be more reliable than the Manning equation with a constant value of n. For any given channel it was found that the roughness coefficient k (used in the Colebrook-White equation) was more likely to be constant than Manning's n. The Colebrook-White equation, unlike Manning's expression, is based on empirical studies of flow and is suitable for

partially filled pipeflow,providing the surface is hydraulically moderately smooth and the pipe diameter fairly small (i.e. less than about 1 m diameter) (Henderson, 1966). Figure 8.4 shows the change in Manning's n with discharge at two gradients with a fixed value of the roughness coefficient k (the depth for each discharge was found from the Colebrook-White equation and Manning's n then calculated using the known depth and discharge) and further demonstrates the variation of the Manning coefficient compared with the roughness coefficient k. Ackers (1958) concluded that the Colebrook-White equation with the hydraulic radius R equal to D/4 (where D is the pipe diameter) is the most suitable formula available for open channel flow although the value of k for an open channel should be greater than the value for the same material in pipes; however, since it is seldom known with a high degree of accuracy this correction may be ignored.

A number of sewer network models use the roughness coefficient k, including the Illinois Storm Sewer System Simulation Model (Sevuk, Yen and Patterson, 1973), a surcharging model for storm sewer systems developed by the Hydraulics Research Station, Wallingford,and applied to a small test catchment in Derby (Bettess, Pitfield and Price, 1978) and also for a design and simulation method for storm sewers (Price and Kidd, 1978).

8.5 The Roughness Coefficient k

The roughness coefficient k is a length parameter characteristic of the surface roughness and for fully rough flow is defined as the sand grain diameter for a sand-coated surface having the same value of f, the Darcy resistance coefficient, as the pipe under consideration. In the transition region between laminar and fully

rough flow the coefficient does not fully represent the roughness of the pipe material and ideally a length parameter is needed to describe the distribution of the surface projections. No practicable definition of roughness using both of these parameters has yet been offered and for the hydraulically moderately smooth surfaces under discussion additional consideration of a length parameter is probably unnecessary (Henderson, 1966).

Commenting on Nikuradse's equation for fully rough flow which may be expressed,

$$\frac{1}{\sqrt{f}} = 2 \log_{10}\left(\frac{12R}{k}\right) \qquad (8.8)$$

Henderson (1966) says that although it is not easy to determine accurate values of k this is not a problem since the logarithmic relationship in the equation means large errors in the value of k produce only small errors in the value of f. This observation also applies to Equation 8.6 so that slightly inaccurate values of k do not give rise to serious errors in the value of Q. The Transport and Road Research Laboratory Roadnote No.35 (1975) provides a comprehensive list of k values for a wide variety of materials and channel types including the pipe materials currently being used on the Brunel laboratory test rig. Glass is generally agreed to be hydraulically smooth and to have an effective roughness of zero, cast iron varies between about 0.1 and 0.3 mm and a value of 0.2 mm is used for the laboratory test pipe. Figure 8.5 gives values for some of the more commonly used drainage pipe materials.

8.6 Unsteady Flow Test Results

8.6.1 Wave Velocity

The computer program for the attenuation of flow through a single pipe was run using Manning's equation to calculate both the normal depth and the steady-state loss; the same data were then used to run the program with the Colebrook-White formula to determine the normal depth and steady-state loss. The results from these two computer simulations were then compared with results obtained from the laboratory rig. All three sets of data are shown in Figure 8.6,which shows the time when the maximum depth occurs along the pipe during the passage of a wave, Figure 8.7 is another illustration of these results with the pipe at a different gradient. Both of these examples show that the use of the Colebrook-White equation improves the prediction of the velocity of the wave peak along the pipe; this improvement is due to the constancy of the value of the roughness coefficient k with changing depth of flow. Any value of Manning's n used is only valid for one discharge and will therefore over- or under-estimate the loss as the wave travels along the pipe. The Colebrook-White equation allows the loss to be calculated for each node at each time step, thus significantly reducing the error in estimating the losses.

8.6.2 Maximum Depth

Figures 8.8 and 8.9 are examples at two different gradients of how the maximum depth of flow decreases as the wave attenuates along the pipe; the critical depth entry boundary is used for both these cases. The graphs show the results observed on the laboratory test rig and the two sets of predicted results, one calculated using Manning's equation and the other Colebrook-White. In both cases the

Colebrook-White equation provides a better prediction of the attenuation of the wave; occasionally the improvement is marginal but generally justifies the use of the roughness coefficient k in preference to Manning's n. Figure 8.10 shows the result of a wave from a drop-valve cistern attenuating along a cast-iron pipe; a k value of 0.2mm is used and this produces a significantly better result than Manning's equation. The Colebrook-White equation is far more satisfactory for the cast iron pipe than Manning's expression which is undoubtedly due to the stability of k over a wide range of discharge values.

8.7 Conclusion

The Colebrook-White equation and roughness coefficient k generally predict wave attenuation in both glass and cast iron pipes with greater accuracy than Manning's equation. The improvement is particularly noticeable in the prediction of the velocity of the wave peak along the pipe. The variation of Manning's coefficient with both depth and gradient, particularly for small-bore circular pipes,(i.e. less than about one metre diameter) highlights the utility of the Colebrook-White equation. It is clear therefore that for small bore partially filled pipeflow, which is in the transition region between laminar and fully rough flow,the Colebrook-White equation offers a more stable measure of pipe roughness than Manning's formula. The Colebrook-White expression is therefore used within the computer program to calculate both the normal depth and also the steady-state loss at each node in the space-time grid.

9. Pipe bends

9.1 Introduction

Building drainage networks may contain pipe bends and their effect on the propagation and attenuation of unsteady flow must be studied. If this type of pipe fitting has a significant effect on the passage of the flow profile then a suitable model must be included in the computer program. Pipe bends of 45 degrees and 90 degrees were investigated; bends greater than 90 degrees are unlikely to be used in building drainage systems.

9.2 Tests Performed

The laboratory rig was altered to incorporate either a 90 degree or a 45 degree bend by adding the 6m spur to the existing length of 100mm diameter glass pipe. The unsteady flow profile was produced either by the pressure vessel or by the drop-valve cistern,thus allowing two different wave types to be studied. Depths were measured at six points along the pipe length and the results processed by the Apple data logging system and then transferred to the Honeywell mainframe to be plotted and drawn.

Tests were carried out with the two bend types (90 degree and 45 degree), five pipe gradients (1/50, 1/80, 1/100, 1/150, 1/200) and two wave profiles (a shallow wave from the pressure vessel and a steep wave from the drop-valve cistern). The number of tests conducted was therefore twenty, excluding repetitions to ensure repeatibility. The effect of the two bend types on the attenuation of the gradually varied flow profile was studied by considering the velocity of the wave peak and the attenuation of the depth of flow after the bend section. The

velocity of the wave peak was found by plotting the time of maximum depth of flow against distance down the pipe. Before the tests were carried out it was expected that the effect of the bend would be a section of locally enhanced attenuation which would be seen as a change in both the velocity and depth of the wave peak.

9.3 Attenuation of Depth

Figure 9.1 illustrates the depth profiles at six points along a straight pipe with no bend; the gradient was 1/100 and the wave profile was produced from the pressure tank. Figure 9.2 is of the depth profiles at six points along the pipe with a 90 degree bend at 7.0m, Figure 9.3 is the depth profiles with a 45 degree bend at 6.9m. In both the latter cases the gradient was 1/100 and the wave was produced by the pressure vessel. There is some difficulty in interpreting these three figures since the tapping points are not in the same position for either the straight pipe or the two bend configurations. The tapping points along the pipe spur are not at the same distance from the pipe entrance as the tapping points along the original straight pipe, and since the length of the two junctions differs slightly the tapping points are not in exactly the same place for the 45 degree and 90 degree bends. The positions of the tapping points are marked on the relevant figures. In order to give more information downstream of the bend one of the tapping points was moved from the head of the pipe to a position after the bend. Despite the problem of comparibility between the three sets of results there is no obvious difference in the attenuated wave depth at the last few tapping points, it appears that neither the 90 degree nor the 45 degree bend exert any great influence over the depth of flow measured downstream of the bend. Figures 9.4,

9.5 and 9.6 are examples of the results obtained at a gradient of 1/200 and again no obvious difference between the depths of flow downstream of the bend and the depths measured at a similar position in the straight pipe can be found.

The results of the tests which were carried out at five gradients and with two different wave types were analysed but no obvious systematic variation in the attenuation of the waves downstream of the bend could be found and attributed to the presence of the bend.

9.4 Velocity of the Wave Peak

Figure 9.7 shows the time of maximum depth against distance along the pipe for a wave from the pressure vessel travelling along a pipe with no bend, Figure 9.8 and 9.9 shows the same wave travelling along pipes with bends of 90 and 45 degrees respectively. Results are shown for pipe gradients of 1/50, 1/100 and 1/150 and it should be noted that the origins of both axes for all three figures is not zero. No break in the slope of the curves in Figures 9.8 and 9.9 can be detected at or about the bend at 7.0m, which would indicate that the velocity of the wave peak is not noticeably affected by the presence of a 90 or 45 degree bend. The velocity of the wave peak is shown by the slope of the line and this remains reasonably constant for each pipe gradient with either a 90 or 45 degree bend or with no bend. There is no clear difference between the velocity of the wave for any one gradient with no bend, a 90 degree bend or a 45 degree bend.

Figures 9.10 and 9.11 show the velocity of a wave from a drop-valve cistern through a 90 and 45 degree bend for gradients of 1/50, 1/100 and 1/200. Again the velocity of the wave peak is not obviously affected by the presence of the bend.

The results from the tests carried out to study the velocity of the wave peak at various gradients and with two different bend configurations give no clear indication that the velocity of the wave is affected by the presence of a bend in the pipe.

9.5 Conclusions

The tests show that a 90 or 45 degree bend inserted into the 100mm diameter glass pipe has no noticeable effect on either the wave depth or wave velocity upstream or downstream of the bend section. Any disturbance is purely local and does not influence the propagation or attenuation of the wave profile; therefore it is not necessary to model the effect of the bend in the computer program.

This result is supported by the findings of other workers modelling unsteady flow in partially full pipe networks. The Wallingford Storm Sewer Package which was developed at the Hydraulics Research Station, Wallingford,is a sophisticated hydrologic model but no special account is taken of bends as their influence was found to be unimportant.

10. Review of Junction Modelling

10.1 Introduction

Junctions are important elements in the building drainage network and the method used to model them in the computer program requires considerable attention. If the method is not carefully selected to closely approximate the actual conditions at the junction then the errors which occur may abrogate the effect of using complex methods of solution for the unsteady flow equations. The problem of adequately modelling junctions is complex due to the backwater effect in both the main and branch channels and the energy loss which occurs across the junction. It is further complicated by the use of the equations for unsteady flow which provide an excellent method of predicting flow attenuation in single pipes but can become very complex at boundaries (Sevuk and Yen, 1973). Even modelling the movement of steady flows through junctions is not straight-forward due to the numerous variables involved (e.g. the shape and slope of the channel, the angle of the junction,etc.).

Early work in the field concentrated on investigating the effect of junctions on steady flows and reached conclusions about the nature of flow upstream, downstream and within the junction. Later the same equations were used to route unsteady flows through junctions and alternative methods were also explored. This chapter reviews the work of other authors in the field and summarises their conclusions which are of relevance when considering the effect of junctions within the building drainage network on the attenuation of waves under unsteady flow conditions.

10.2 Junction Models

A number of studies of both steady and unsteady flow through channel junctions have been made which use different approaches to the problem of modelling the effect of the junction upon the flow profile.

10.2.1 The Momentum Formulation

Taylor (1944) carried out one of the earlier investigations into the problems of combining flows based upon the following assumptions,

(i) the flow is parallel to the channel walls.

(ii) ordinary wall friction is negligible compared with the other forces involved.

(iii) the depths in the main and branch channels are equal immediately upstream of the junction.

(iv) the flow is from the upstream and branch pipe into the downstream pipe.

(v) the upstream and downstream pipes lie in a straight line.

Neglecting the weight of water in the control volume ABCDE (Figure 10.1), the net force F acting on the control volume is given by,

$$F = \rho g \bar{y}_1 A_1 + \rho g \bar{y}_2 A_2 \cos\theta - \rho g \bar{y}_3 A_3 - U \qquad (10.1)$$

where ρ = density of water (kg/m^3)

g = acceleration due to gravity (m/s^2)

A_i = cross-sectional area of flow in pipe i (m^2)

$\bar{y}_i$ = depth to centroid of flow area A_i (m)

θ = angle between the main and branch channels (degrees)

U = reaction force ($kg/m/s^2$)

The rate of change of momentum ΔM (Figure 10.1) is given by,

$$\Delta M = Q_3 \rho V_3 - Q_1 \rho V_1 - Q_2 \rho V_2 \cos\theta \qquad (10.2)$$

where Q_i = discharge in pipe i (m^3/s)

V_i = velocity of flow in pipe i (m/s)

By inspection it is seen that the reaction force U is equal to the component of the hydrostatic pressure force acting upon the wall marked CD in Figure 10.1. If the simplification is made that the depth everywhere in the triangle CDE is equal to the depth at D, then the reaction force U is given by,

$$U = \rho g \bar{y}_4 A_4 \cos(90-\theta) \qquad (10.3)$$

where the subscript 4 refers to the area CD.

From the principle that the force acting upon a fluid system is equal to the rate of change of momentum, Equations 10.1 and 10.2 may be equated,

$$A_1\left(g\bar{y}_1 + \frac{Q_1^2}{A_1^2}\right) = A_3\left(g\bar{y}_3 + \frac{Q_3^2}{A_3^2}\right) - A_2\left(g\bar{y}_2 + \frac{Q_2^2}{A_2^2}\right)\cos\theta$$

$$-g\bar{y}_4 A_4 \cos(90-\theta) \qquad (10.4)$$

Taylor then introduced a dimensionless form of the equation and compared experimental results with those obtained from the theory outlined above; the conclusions reached can be summarised as follows,

(i) the agreement between the theoretical and experimental results supported the initial assumptions outlined above.

(ii) the experimental data showed that the depths in the main and branch channels upstream of the junction have nearly the same value.

(iii) boundary friction may be considered negligible.

Investigation of a branch angle of 135 degrees revealed that the velocity distribution below the junction is greatly distorted and

the assumption that the flow remains parallel to the walls is violated; it is unlikely that this model can be applied to junctions with an angle greater than 90 degrees because the infringement of this assumption means there is a lack of agreement between experimental and theoretical data.

Although Taylor's work was not an exhaustive study of all the possible combinations of channel widths, junction angles, directions of flow, etc., it does highlight the importance of the problem and the many limitations on the theory of combining flows at junctions. This study of steady flow through junctions forms the basis for much of the subsequent work described in the next section.

10.2.2 Applications of the Momentum Formulation

Joliffe (1981, 1982) has made a study of combining flows using the equation produced by Taylor (Equation 10.4) for a branch angle of 90 degrees, Equation 10.4 then reduces to the following,

$$A_1\left(g\bar{y}_1 + \frac{Q_1^2}{A_1^2}\right) = A_3\left(g\bar{y}_3 + \frac{Q_3^2}{A_3^2}\right) \qquad (10.5)$$

Joliffe used this equation to predict the relationship between flow depths at the pipe junction and then verified the model by experimental observation. The assumption that the flow is parallel to the pipe walls was found to be incorrect; upstream of the junction the flow was basically parallel to the pipe walls but downstream of the junction an oblique hydraulic jump formed which distorted the stream lines. Joliffe used the presence of the oblique hydraulic jump to justify one further assumption, that the flow depth y_3 (downstream of the junction) corresponds to the critical flow at that location. A close examination of the flow depths upstream and downstream of the

junction reveals that they may be independent of one another and separated by a section of critical flow. The results predicted using Equation 10.5 correspond well to experimental results obtained in the laboratory. Joliffe also applied the model, which was derived for steady flow, to the unsteady flow case and simulated the passage of an unsteady flow profile through a pipe junction.

Radojkevic and Maksimovic (1977) investigated the flow conditions found at the junctions of circular conduits during flood periods in storm sewer systems. The mathematical method used was the momentum model proposed by Taylor rather than the point junction formulation (discussed below), which was not felt to be suitable. Experimental evidence supported the use of the momentum model.

Soliman (1977) studied the confluence of two rivers and the subsequent rise in water level in both the main and branch channels. The river cross-sections were assumed to be rectangular and very wide; more importantly the flow was subcritical in all its stages. Again the computer model was based upon the work by Taylor and verified by scale model tests in the laboratory; this work is of less relevance since the channel is rectangular rather than circular in shape. Hu (1967) used the momentum formulation to model lateral inflows into the main pipe of a soil drainage system and concluded that as a result of momentum conservation the upstream depth at a junction with an inflow will always be greater than the downstream depth.

Kanda and Kitada (1977) presented a model for unsteady flows at junctions caused by artificial control of flood discharges in urban rivers, again based upon the momentum formulation as proposed by Taylor. Kanda and Kitada also rejected the point junction formulation, which assumes the water level just upstream of a junction to be equal

to that just downstream of a junction,because it is unsuitable in a situation where the velocity head is not negligible compared to the depth of water. The momentum equation is incorporated into the four-point implicit method used to model unsteady flow profiles in single river channels and the results of this combined model compare well with experimental results from a long rectangular channel.

10.2.3 Presentation of Results

There is an interesting diversity in the presentation of experimental results amongst the authors using Taylor's momentum formulation for junctions in open channel flow, whether in conduits or rivers.

Taylor himself introduces a dimensionless version of the momentum junction formulation using the factors n_q, the ratio of the branch discharge to the downstream discharge, n_y, the ratio of the depth of flow above the junction to the depth of flow below the junction and k_2 which is the ratio of the velocity head to the depth in the branch channel. The relationship between these factors is shown graphically in Figure 10.2 for a branch pipe angle of 45 degrees. Problems occur with this method of presenting results when the depth ratio exceeds that shown in Figure 10.2 as the curve has a point of reflection and the value of k_2 begins to drop,which is not in accord with the original dimensionless version of the momentum junction formulation.

Joliffe (1981, 1982) found that after numerous attempts to fit experimental data to Taylor's theory it was most useful to relate the energy loss at the junction to the Froude number of the flow in the branch pipe instead of to the velocity head. Joliffe (1982)

shows 26 methods of presenting the experimental data, some of which are satisfactory and some unsatisfactory, and finally chose to show the ratio of upstream depth to downstream critical depth as a function of the branch Froude number and discharge ratio (Figure 10.3). The curves described by the experimental data are then found to be of the form,

$$\frac{y_u}{y_{cd}} = aFr_b^{-b} \qquad (10.6)$$

where y_u = upstream depth (m)

y_{cd} = downstream critical depth (m)

Fr_b = Froude number in the branch pipe

a,b = coefficients described by two further equations

Carballada et al.(1981) present results for both a 45 and a 90 degree junction; they found the flow at the junction exit to be subcritical in all cases and therefore relate their findings upstream to flow conditions downstream by plotting the ratio of upstream depth to downstream depth against the Froude number of the downstream flow for various discharge ratios. Joliffe took the flow depth downstream to be critical (with, therefore, a Froude number of unity) so this method presents an alternative approach to the interpretation of experimental data. Carballada et al.also plotted the depth ratio against the ratio of branch discharge to downstream discharge for various Froude numbers but were less successful in fitting their experimental data.

Soliman (1977) plotted the ratio of upstream depth to downstream depth against the ratio of the discharge per unit width in the main upstream channel to the discharge per unit width downstream for various Froude numbers of the downstream flow. No experimental data are presented to support the theoretical results.

Radojkovic and Maksimovic (1977) use the momentum formulation for flow through a junction and plot the Froude number in the branch channel against the Froude number in the main channel downstream of the junction for a number of values of Froude number of flow in the main channel upstream of the junction. Results from a physical model correspond reasonably well to the theoretical predictions.

Although the momentum formulation for flow through junctions has been widely used since Taylor's original investigation of steady flow through junctions there is a considerable division of opinion as to the best method of presenting both experimental and theoretical results. The diversity of methods described in this section reflects the resourceful way in which many authors have approached the problem of verifying the accuracy of the momentum formulation for junctions and also throws doubt on the usefulness of the model.

10.2.4 Other Junction Models

Other methods have been suggested for modelling the confluence of two (or more) channels, usually based at least in part upon the continuity equation,

$$Q_3 = Q_1 + Q_2 \qquad (10.7)$$

This method has the advantage of simplicity and is therefore particularly useful in numerical models dealing with large open-channel networks. However,the method also suffers from a number of serious disadvantages including the neglect of the backwater effect upstream of the junction and the implicit assumption that the flow within the junction is steady. An extension of this procedure is used for routing floods through the Minneapolis - St. Paul storm sewer model (Sevuk and Yen, 1973) where a drop is assumed at the end of each of the two

upstream channels with critical flow at the lip and the flow cascading into the junction where the downstream discharge is given by Equation 10.7. This method has the same limitations as the simpler case previously described.

The point type-junction (Sevuk and Yen) assumes the depth of water immediately upstream of the junction to be equal to the depth of water immediately downstream of the junction; the backwater effect is partially accounted for but the flow within the junction is still considered to be steady (since the junction is in fact only a point). This method is particularly suitable for open channels with predominantly subcritical flows; Yen and Akan (1976) assume that the water surface at the junction is continuous in their model to route unsteady flow through dendritic channels using a four-point implicit finite-difference scheme. The method has been widely used (Baltzer and Lai, 1968, Sevuk et al, 1973, Shubinski and Roesner, 1973 and Quinn and Wylie, 1972) although the computations involved are not simple due to the presence of six unknowns (the discharge and depth in all three pipes).

Fox (1976) recommends a point-type junction by assuming that the water depth at the junction is equal in all the branches and that the inflow to the junction is equal to the outflow from it. The method of modelling junctions described by Fox is only adequate for flows with a very low Froude number, for flows with a higher Froude number it is necessary to include local losses and kinetic energy losses. Having assumed the depths in all branches to be equal,it follows that the wave celerity must also be the same for all branches. Therefore,

$$Y_1 = Y_2 = Y_3 \qquad (10.8)$$

and

$$c_1 = c_2 = c_3 \tag{10.9}$$

where y_i = depth of flow in pipe i (m)

c_i = wave celerity in pipe i (m/s)

The characteristic equation is then formed and solved for the wavespeed in each channel by using a form of the continuity equation; the depth and velocity in each of the channels can then also be calculated.

Another approximation which may be used is the reservoir-type junction,where the junction is assumed to have a relatively large storage capacity and to behave like a reservoir (Sevuk and Yen). The continuity equation becomes,

$$Q_1 + Q_2 = Q_3 + \frac{ds}{dt} \tag{10.10}$$

where $\frac{ds}{dt}$ = rate of change of storage within the junction.

Since the junction is assumed to behave like a reservoir the depth at the exit to the junction is equal to the specific energy of the flow,

$$Y_1 = Y_2 = Y_3 + \frac{V_3^2}{2g} \tag{10.11}$$

For junctions with a large cross-sectional area as in the Illinois Storm Sewer System Simulation Model (Sevuk, Yen and Patterson, 1973), this method is better than the point-type junction as it accounts for the backwater effect upstream of the junction and assumes unsteady flow through the junction itself.

Another method of evaluating the effect of a junction is by consideration of the energy-loss coefficient; this method does account for the rate of change of storage within the junction but not for the change of storage of energy within the junction.

Townsend and Prins (1978) consider the design of efficient storm sewer junctions by modelling the loss of energy between the

upstream and downstream sides of the junction and then combining the energy-loss coefficient for different junction geometries. This method allows junction efficiency to be measured quantitatively so different junction geometries can be easily compared.

Pinkayan (1972) used the method of characteristics to solve the unsteady flow equations in storm drainage systems with an energy loss coefficient to model the movement of the unsteady flow profile through junctions. This approximation for solving the unsteady flow equations at the junction does not give good results due to the backwater effect from the junction along the main drain which is not taken into consideration in the model.

Lin and Soong (1979) evaluated the energy loss at the junction of a rectangular open channel and a rectangular side channel experimentally and then divided the loss into two components. The first is the boundary friction loss which is found using a precalibrated average value of Manning's n (although this has been shown to vary with discharge by a number of authors including those contributing to the American Society of Civil Engineers Report (1963)) and then deducted from the total energy loss to give the turbulent mixing loss. The boundary friction loss and the turbulent mixing loss are shown to be of the same order of magnitude indicating that neither element can be ignored in assessing the effect of a junction in open channel flow. Lin and Soong also note that the branch inflow has a significant effect on the flow profile in the main channel both upstream and downstream of the junction and acknowledge that this backwater effect may "pose a problem for some junction flows in open channels".

Marsalek (1981) shows that energy losses at sewer junctions

with a free water surface are considerably less than the losses experienced at junctions in pressurised sewer systems. Since recent practice has been to design sewer systems which are allowed to surcharge to a limited extent before damage occurs an accurate assessment of the losses at surcharged junctions is obviously essential. Considerable savings on the cost of sewer networks can be made by providing an adequate method of calculating energy loss at a junction within the computer program used at the design stage.

10.3 Conclusions

The following conclusions may be drawn from this literature review which are relevant when considering the effect of junctions within building drainage networks.

(i) The depths of flow in the main and branch channels are equal immediately upstream of the junction.

(ii) Downstream of the junction the flow passes through a section of critical flow before returning to supercritical flow.

(iii) As a result of the conservation of momentum the depth upstream of the junction will always be greater than that downstream.

(iv) Many junction models are inaccurate because they do not take the effect of the backwater profile into account.

(v) Ordinary wall friction is negligible compared with the other forces involved.

(vi) Flow is parallel to the channel walls immediately upstream of the junction.

(vii) Applying models to junctions with angles greater than 90 degrees is not possible as the velocity distribution within the flow is greatly distorted.

(viii) Justifying the use of the momentum formulation is difficult using experimental data.

11. The Junction Model

11.1 Introduction

Accurate simulation of junction conditions is an essential part of any partially filled pipe network model and is of particular importance in building drainage networks due to the relatively small pipe bore and the short runs between boundaries such as junctions, entries and exits. Any junction model which does not reflect with some accuracy the true physical conditions within the pipe network will nullify the effect of using complex equations to route the unsteady flow through the straight pipe sections.

11.2 Steady Flow

11.2.1 Test Programme

The first stage in developing a junction model was to investigate the effect of steady flow through a junction. This was done by altering the original laboratory rig to allow a junction to be incorporated by joining a spur to the main 14m length of 100mm diameter glass pipe. A 45 degree glass junction and a 90 degree glass junction were tested by changing the angle between the moveable spur and the main channel. The gradient of the two pipes was altered synchronously so the branch and main pipe remained at the same slope. For the steady flow tests the upper ends of both the main and branch pipe were fed through the system of pumps and rotameters described in Chapter Five which allowed wide variation in the ratio between the two discharges. The flow depth was measured about two diameters upstream of the junction in the main and branch pipes and the same distance downstream of the junction. The Apple logging system was not used as chart

recorders were more suitable for measuring steady flows.

Tests were carried out with the two junction geometries (45 and 90 degrees) at slopes of 1/50, 1/80, 1/100, 1/150 and 1/200 for a variety of discharge ratios. The discharge ratio QR is defined as the ratio of the upstream discharge to the downstream discharge and therefore defines the relative discharge into the main and branch pipes. Discharge ratios of 0.0, 0.2, 0.4, 0.6 and 0.8 were used with upstream main channel flows in the range 5.0 1/min to 60 1/min,giving branch flows in the range 3.3 1/min to 80 1/min. Twenty-three tests were carried out at each of the five gradients.

11.2.2 Steady Flow Test Results

The results of the steady-state flow tests for junctions of 45 and 90 degrees show that the depth upstream of the junction is the same in both the main and branch channels. Figure 11.1 shows the scatter of observations about the line of exact agreement for a 45 degree junction and Figure 11.2 shows similar results for a junction angle of 90 degrees. Figure 11.1 has a correlation coefficient of 0.94 and Figure 11.2 has a correlation coefficient of 0.98. These results support Taylor's original assumption, Chapter Ten, that the depths in the main and branch channels are equal immediately upstream of the junction and also confirm similar findings reported by Joliffe (1982).

Examination of the depth just upstream of the junction in both the main and branch pipes at all slopes revealed that the depth was a function of the discharge ratio, QR, and was virtually unaffected by the pipe slope. To demonstrate this the standard deviation from the mean depth was found for all tests using a particular combination of flows in the main and branch pipes (at whatever gradient). For the

90 degree junction this gave a standard deviation from the mean of 0.92mm with an average coefficient of variation of 8.5% and for the 45 degree junction a standard deviation from the mean of 1.98mm with an average coefficient of variation of 7.5%. These small values for the average coefficient of variation demonstrate that the depth was little affected by the slope of the pipe. The steady-state tests also showed that the flow just upstream of the junction in both the main and branch pipes was subcritical for all slopes and discharge ratios.

Although the slope did not appear to affect the depth of flow just upstream of the junction it did cause the length of the backwater profile upstream of the junction in both the main and branch pipes to alter which could influence the passage of a wave through the junction.

Observations just downstream of the junction showed that an oblique hydraulic jump formed when the subcritical flow within the junction returned to supercritical flow in the downstream pipe, the downstream boundary of the junction can therefore be defined as a section of critical flow.

11.2.3 Conclusions

The following conclusions were drawn from the results of the steady flow tests through 45 and 90 degree junctions.

(i) The depth immediately upstream of the junction was the same in the main and branch channels.

(ii) This depth was a function of the combination of flows entering the junction and was not dependent on the slope of the pipe.

(iii) The pipe slope did affect the length of the backwater profile and therefore presumably influenced the movement of a wave through the junction.

(iv) The downstream junction boundary was formed by a section of critical flow.

(v) The flow immediately upstream of the junction was subcritical for all pipe slopes and discharge ratios tested.

These conclusions, based upon a number of steady-state flow tests, form the basis for the model of the junction described below. The tests were not exhaustive but cover the range of conditions likely to be encountered in building drainage networks or any other small bore pipe network flowing partially full within the range of gradients tested.

11.3 The Junction Model

The conclusions reached in the previous section and in the previous chapter allow the outlines of a model for junctions to be developed. First it is necessary to consider the flow pattern surrounding the junction and analyse the hydraulic régime associated with each section of flow, both upstream and downstream of the confluence. The model which follows is based upon the premise that the majority of flow régimes within building drainage networks are supercritical.

Firstly consider the flow which is sufficiently far upstream to be unaffected by the presence of the junction, here the flow is supercritical and at normal depth. Immediately upstream of the junction the flow is subcritical with a backwater profile whose length is affected by the slope of the pipe. The flow régime therefore changes from supercritical to subcritical upstream of the confluence, this transformation can only be achieved by the presence of a hydraulic

jump which dissipates some of the energy of the supercritical flow in order to convert it to subcritical flow. Observations of flow within the test pipe show that a hydraulic jump does form upstream of the junction in both the main and branch channels. The position of the jump within the pipe is a function of three factors; firstly the depth at the junction (which is in itself a function of the combined flows in the main and branch channels), secondly the upper sequent depth of the hydraulic jump (which is a function of the normal depth and flow velocity) and thirdly the slope of the pipe. The depth immediately upstream of the junction is the same in both the main and branch channels but the position of the hydraulic jump may be different since it is also dependent upon the slope of the pipe and the upper sequent depth. The depth at the junction is a function of the combined flow in the main and branch pipes and is independent of the slope of either pipe. At the junction the flows combine and pass through a section of critical flow before continuing as a supercritical flow in the downstream pipe.

To summarise, supercritical flow upstream of the confluence in both the main and branch channels passes through a hydraulic jump and is transformed into subcritical flow which reaches a maximum depth just upstream of the junction. Here the flows combine, pass through a section of critical flow and continue as a supercritical flow in the downstream pipe (Figure 11.3).

11.4 Steep-Fronted Waves

11.4.1 Definition of a Steep-Fronted Wave

The numerical solution presented previously for the attenuation of waves in long drainage pipes is based upon the equations for

gradually varied unsteady flow. The analysis is only accurate while the flow remains gradually varied; any abrupt change in the curvature of the stream lines and the flow ceases to be gradually varied and becomes rapidly varied. The analysis previously described is no longer valid and a different solution to the problem is required.

The region of rapidly varying flow has been variously described as a steep-fronted wave, a travelling surge, a bore or a moving hydraulic jump; for reasons of clarity the term "steep-fronted wave" will be used here. Certain hydraulic conditions must be fulfilled for a steep-fronted wave to exist; the definition of the steep-fronted wave is that "the relative Froude number change across the surge must be such that the two relative Froude numbers span the value of unity" (Fox, 1977). If the relative Froude numbers are both less than or greater than unity then no steep-fronted wave can be generated. Figure 11.4a illustrates the theoretical, though physically impossible profile of a steep-fronted wave forming with the critical depth falling between the two sequent depths of the hydraulic jump. The anomaly can only be resolved by the occurrence of an abrupt discontinuity (Figure 11.4b) which forms the steep-fronted wave.

Figure 11.5 illustrates the four possible types of steep-fronted wave caused by increases or decreases in flow either upstream or downstream. Owing to the nature of the situation under consideration the conditions of principal interest are those shown in Figures 11.5a and 11.5b where a rapidly varied negative wave moves both up and down the pipe. The passage of an unsteady flow profile through the hydraulic jump which separates the supercritical normal flow from the subcritical flow nearer the junction causes the previously stationary hydraulic jump to move and become what is defined here as a steep-fronted wave.

11.4.2 Review of Previous Work

The problem of simulating the movement of steep-fronted waves in open channels has been considered by a number of authors, though very little interest has been shown in the particular problems of partially filled pipe flow. Many authors recognise that gradually varied flow theory is not theoretically applicable to the rapidly varied flow at a steep wave front; however,very few attempts have been made to use the equations of continuity and force to model the rapidly varied phase of the flow régime. A theoretical discussion of the equations used to model a steep-fronted wave is given by several authors, including Abbott (1979), Cunge, Holly and Verwey (1980), Fox (1977) and Henderson (1966).

Martin and DeFazio (1969) investigated the applicability of gradually varied flow theory to rapidly varying waves and found that "many rapidly varied wave forms can be simulated to a fair degree of accuracy by simply using the differential equations of gradually varied flow". However,experimental work conducted by Mitchell (1967) and Ackers and Harrison (1964) was used to provide data for simulation and discrepancies were found which were attributed to the extremely rapid change in discharge at the upstream end of the pipe; apparently the technique used could not deal with the very rapid change in flow which is experienced in partially filled pipes.

Martin and Zovne (1976) point out that although the large vertical accelerations at a steep-fronted wave are certainly not modelled by any gradually varied flow solution, it is also true that the one-dimensional equations of continuity and force only provide a gross representation of the equations at the discontinuity. Just as the gradually varied flow equations only provide an approximate

solution to rapidly varied problems,so the one-dimensional equations of continuity and force only approximate the conditions at a steep-fronted wave; for instance,it is assumed to have a vertical face but in reality the face is always sloping (since there cannot be an abrupt change in velocity). Martin and Zovne conclude that the nature of the problem and the type of solution required should be considered before attempting complex simulations of the movement of steep-fronted waves; an adequate solution to an engineering problem can often be found without recourse to the complex techniques necessary to model rapidly varied flow.

Chaudhry and Contractor (1973) present an implicit method of modelling unsteady flows with steep-fronted waves in open channels which ignores the one-dimensional equations of continuity and force and uses the equations of gradually varied flow; it is therefore unnecessary to detect the inception of a steep-fronted wave or to keep track of its subsequent movement. The results appear to be acceptable and the authors also remark that an objective method should be devised for differentiating between gradually varied and rapidly varied flows; this is particularly important if flows both sides of the discontinuity are subcritical but with a relative Froude number which spans the value of unity as may be the case if a small wave moves over a deep baseflow.

The time and location of the steep-fronted wave as it first forms were found by Terzidis and Strelkoff (1970) as a function of the initial Froude number and the shape of the inflow hydrograph; this method assumes that the absolute value of the Froude number either side of the discontinuity spans the value of unity,which does not allow for the occasion in which subcritical flow is present on both sides of the wavefront. Terzidis and Strelkoff also found that the equations of

gradually varied flow gave results which compared favourably with those obtained from the two explicit schemes presented, both of which included the continuity and force equations to model the movement of the steep-fronted wave. The techniques used in the two explicit schemes to model the steep-fronted wave were not suitable for incorporation into the method of characteristics.

The equations of continuity and force are only an approximation and cannot provide an accurate simulation of rapidly varying waves; however, they do produce better results than the gradually varied flow equations when applied to rapidly varying situations. Authors attempt to use the gradually varied flow equations whenever possible even if the results lose accuracy due to the difficulties involved in applying the equations of continuity and force. This method could not be used to model the flow régime upstream of the junction as a transition from supercritical to subcritical flow must take place. One of the major problems is predicting the inception of the wave, but in the situation considered here this is not a problem as the discontinuity exists as a hydraulic jump before it begins to move.

11.4.3 Modelling the Steep-Fronted Wave

Consider the steep-fronted wave in Figure 11.6, by applying a velocity V_w to the system the boundary at the free surface is brought to rest. The steep fronted wave can now be treated as a travelling hydraulic jump and applying continuity to sections 1 and 2,

$$(V_1 - V_w)A_1 = (V_2 - V_w)A_2 \qquad (11.1)$$

where V_i = velocity of flow at section i (m/s)

V_w = velocity of the steep-fronted wave (m/s)

A_i = cross-sectional area of flow (m^2)

i = cross-section subscript

Applying the force equations to sections 1 and 2,

$$\rho g A_1 \bar{y}_1 - \rho g A_2 \bar{y}_2 = \rho A_2 (V_2 - V_w)^2 - \rho A_1 (V_1 - V_w)^2 \qquad (11.2)$$

where ρ = density of water (kg/m^3)

g = acceleration due to gravity (m/s^2)

$\bar{y}_i$ = depth to centroid of section i (m)

By substituting for V_2 from Equation 11.1 in Equation 11.2 an expression for the velocity of the wave can be derived,

$$V_w = V_1 - \sqrt{\frac{g A_2 (A_1 \bar{y}_1 - A_2 \bar{y}_2)}{A_1 ((A_1 - A_2))}} \qquad (11.3)$$

This equation can be solved for any regular cross-section and can therefore be used to analyse steep-fronted waves in partially filled pipes.

The definition of the steep-fronted wave is that the relative Froude number across the discontinuity must span the value of unity; the absolute Froude number must therefore be less than unity (subcritical flow) on one side of the wavefront and either greater or less than unity (sub- or supercritical flow) on the other side of the wavefront. The situation of greatest interest here is that of supercritical flow upstream of the jump and subcritical flow downstream of the jump. This solution assumes that the wavefront is vertical and that two depths of flow occur simultaneously at the discontinuity; this is physically inaccurate but not of great importance when considering the overall accuracy of the method.

11.5 Programming the Junction Model

The model used to describe the flow régime surrounding a

junction is illustrated in Figure 11.7.

The method of characteristics solution requires that the flow depth and velocity are known in the pipes upstream of the junction and in the downstream pipe before the unsteady calculation can begin. The steady base-flow depth and velocity are calculated using the Colebrook-White equation so that the normal depth in each pipe upstream of the confluence is known; this flow is generally supercritical in building drainage pipes.

The depth just upstream of the junction is a function of the combined flows into the junction; Figure 11.8 shows the relationship between depth and discharge for junctions of 45 and 90,degrees which is of the form,

$$Q_t = aY^b \qquad (11.4)$$

where Q_t = combined flow in branch and main pipe (m^3/s)

Y = depth just upstream of the junction in both pipes (m)

a,b = empirical coefficients

The empirical equation formed is used to find the depth above the junction given the combined flows in the main and branch pipes. The results of similar steady-state flow tests can be used to produce corresponding equations for any type of junction.

The upstream supercritical flow and the downstream subcritical flow imply the presence of a hydraulic jump between the two flow régimes. The exact position of this jump is dependent upon the pipe slope, pipe roughness, flow rate and the difference in depth of flow between the junction and the upper sequent depth of the hydraulic jump, which is the alternative subcritical depth for the flow on the downstream side of the jump

The sequent depth of the hydraulic jump in both the main and

branch pipes may be calculated using the momentum equation for a stationary jump.

The depth and velocity of the flow upstream of the jump are known from the normal depth calculation; continuity is assumed and the depth and velocity of flow downstream of the jump are calculated using the following equation,

$$A_1 g\bar{y}_1 + \frac{Q^2}{A_1} = A_2 g\bar{y}_2 + \frac{Q^2}{A_2} \qquad (11.5)$$

where Q = flow rate (m^3/s).

The position of the hydraulic jump in the pipe is found by calculating the backwater profile between the jump and the junction. This gradually varied flow profile is found by integrating the equation of motion using a numerical technique which is suitable for solution by computer. The following expression is solved using Simpson's Rule,

$$\Delta L = \int_{y_o}^{y_1} \frac{1 - V^2T/gA}{S_o - S_f}\, dy \qquad (11.6)$$

where y = depth of flow (m)

T = surface width of flow (m)

S_o = pipe slope

S_f = slope of the energy grade line

The length ΔL is that which gives a change in depth of dy, where $dy = y_1 - y_o$ and initially y_o is set to the depth at the junction and y_1 is a small fraction of the difference between the upper depth of the hydraulic jump and the junction depth. Summation of the values of ΔL until the upper hydraulic jump depth is reached allows the position of the jump to be found.

The slope of the energy grade line is given by the Chézy equation for open-channel flow,

$$S_f = \frac{V^2}{R} \sqrt{\frac{f}{8g}} \qquad (11.7)$$

where R = hydraulic radius (m)

f = Darcy resistance coefficient found from the Colebrook-White equation.

The flow passes through a section of critical depth downstream of the junction before resuming normal supercritical depth and velocity. The critical depth value is that appropriate to the combined flow from the supply pipes,

$$Q_t = \Sigma (Q_L) \qquad (11.8)$$

where Q_L = local flow rate in each pipe at the junction boundary (m^3/s),

and critical depth is given by,

$$V = \sqrt{\frac{gA}{T}} \qquad (11.9)$$

The critical depth entry boundary condition is fully described in Chapter Six.

The initial steady-state flow conditions in the pipe are thus set up in preparation for the unsteady flow computation to begin.

11.5.1 Passage of the Wave

During the passage of the unsteady wave the hydraulic jump cannot be assumed to remain stationary and must be allowed to acquire a velocity independent of the flow in the pipe and move either upstream or downstream within the pipes which supply the junction. The hydraulic jump must now be treated as a moving boundary within the computational domain defined by the space-time grid. The hydraulic jump is now a steep-fronted wave and is brought to rest by superimposing a reverse wave speed on the system (Figure 11.9).

In order to determine the wave speed and the flow conditions both upstream and downstream of the steep-fronted wave, five equations are required since there are five unknown variables (the velocity of the steep-fronted wave and the depth and velocity both upstream and downstream of the wave).

(i) the equation of continuity applied across the wave,

$$(V_1 - V_w)A_1 = (V_2 - V_w)A_2 \qquad (11.10)$$

(ii) the force equation applied across the wave,

$$\rho g A_1 \bar{y}_1 - \rho g A_2 \bar{y}_2 = \rho A(V_w - V_1)(V_1 - V_2) \qquad (11.11)$$

These two equations are applicable across the wave because they are suitable for rapidly varying flow. The final three equations only apply to the flow either side of the wave front.

(iii) the forward (C^+) characteristic P'R associated with the upstream supercritical flow (Figure 11.9),

$$V_{p'} - V_R + \frac{g}{c_R}(y_{p'} - y_R) + g(S_R - S_o)\,\Delta t = 0 \qquad (11.12)$$

where $V_{p'}$ = calculated velocity at P' at time t + Δt (m/s)

V_R = interpolated velocity at R at time t (m/s)

c_R = interpolated velocity at R at time t (m/s)

$y_{p'}$ = calculated depth at P' at time t + Δt (m)

y_R = interpolated depth at R at time t (m)

S_R = interpolated slope of energy grade line at R at time t

S_o = pipe slope

t = time step (s)

(iv) the backward (C^-) characteristic P'Z also associated with the upstream supercritical flow,

$$V_{p'} - V_Z - \frac{g}{c_Z}(y_{p'} - y_Z) + g(S_Z - S_o)\,\Delta t = 0 \qquad (11.13)$$

where V_Z = interpolated velocity at Z at time t (m/s)

c_Z = interpolated wave speed at Z at time t (m/s)

y_Z = interpolated depth at Z at time t (m)

S_Z = interpolated slope of energy grade line at Z at time t

(v) the backward (C^-) characteristic P'S associated with downstream subcritical flow,

$$V_{p'} - V_S - \frac{g}{c_S}(y_{p'} - y_S) + g(S_S - S_o)\,\Delta t = 0 \qquad (11.14)$$

where V_S = interpolated velocity at S at time t (m/s)

c_S = interpolated wavespeed at S at time t (m/s)

y_S = interpolated depth at S at time t (m)

S_S = interpolated slope of energy grade line at S at time t

Solution of these five equations at each time step allows the method of characteristics to predict the movement of the steep-fronted wave and also the flow depths and velocities on either side of the wave front.

11.5.2 Revised Method

The method described in the previous section was used to model the movement of the hydraulic jump. However, it was found that two problems arose, firstly the surface profile downstream of the jump collapsed over time and secondly the hydraulic jump acquired a positive velocity during the passage of steady flows.

These problems were addressed by considering Equations 4.11 and 4.13 which may be written,

$$V_p = V_R - \frac{g}{c_R}(y_p - y_R) - g(S_R - S_o)\,\Delta t \qquad (11.15)$$

and

$$V_p = V_S + \frac{g}{c_S}(y_p - y_S) - g(S_S - S_o)\,\Delta t \qquad (11.16)$$

These are combined to give an equation for y_p

$$(V_S - V_R) + g\,y_p\left(\frac{1}{c_S} + \frac{1}{c_R}\right) - g\left(\frac{y_R}{c_R} + \frac{y_S}{c_S}\right) + g\,(S_R - S_o)\,\Delta t = 0 \qquad (11.17)$$

For steady uniform flow the following relationships are true;

$y_s = y_R$, $c_s = c_R$, $V_s = V_R$ and $S_s = S_R$ and therefore from Equation 11.17 it can be seen that $y_p = y_R = y_s$. This means that for steady uniform flow the calculation using the method of characteristics will remain stable as it proceeds through time.

Equation 11.17 may be rewritten for a channel of unit width in terms of y_s and y_R by substituting for V and S in terms of depth and discharge. Therefore,

$$Q\left(\frac{1}{y_S} - \frac{1}{y_R}\right) + g\,y_p\left(\frac{1}{c_S} + \frac{1}{c_R}\right) - g\left(\frac{y_R}{c_R} + \frac{y_S}{c_S}\right) + gQ^2n^2\left(\left[\frac{(1+2y)^{1.33}}{y^{3.33}}\right]_R - \left[\frac{(1+2y)^{1.33}}{y^{3.33}}\right]_S\right)\Delta t = 0 \qquad (11.18)$$

Figure 11.10 shows a section of the backwater profile between the hydraulic jump and the junction showing the position of the interpolated points R and S and the value of the depth at these two points. Linear interpolation between points A and C and points B and C produces values for depth at points R and S which are lower than the actual values. When substituted into Equation 11.18 this leads to an underestimate of the value of y_p at the next time step. In order to obtain a value for V_p the value of y_p is substituted into either Equation 11.15 or 11.16 which will cause inaccuracy in V_p as well.

The overall effect of this interpolation error is to produce a very small increase in the discharge and a very small decrease in the depth of flow.

This gradually increasing discharge and decreasing depth of a steady backwater profile has been noted previously (Fox, 1983), but, particularly for subcritical flows, it has always been disregarded, although it can lead to discharges increasing by 10% at the end of a long backwater profile. When the equations for rapidly varied flow are used in the conventional sense, that is with a steep front caused by a wave of water moving down the channel, then this problem is of little importance since the approaching steep wave overwhelms the accumulating error in the backwater profile.

In the case considered here it is necessary for the hydraulic jump (or steep-fronted wave) to remain absolutely stationary until the wave arrives from the head of the pipe and then to move with a negative velocity until the crest of the wave has passed. If the discharge downstream of the jump is allowed to creep up, then the velocity of the jump will never remain at zero and it will slowly travel towards the junction even with steady flow. In addition to this steady shortening of the length of the backwater profile the depth will also begin to drop even though the boundaries of the profile are fixed.

In order to prevent the collapse of the steady flow backwater profile, correction coefficients (C1 and C2) are used in Equations 4.11 and 4.13. These are calculated by taking the initial values of depth and velocity at each node downstream of the hydraulic jump, calculated from the integral Equation 11.6, and substituting them into the following equations,

$$C1 = \frac{V_R - V_C - g/c_R(y_C - y_R)}{g(S_s - S_o)\,\Delta t} \qquad (11.19)$$

$$C2 = \frac{V_S - V_C - g/c_S(y_C - y_S)}{g(S_s - S_o)\,\Delta t} \qquad (11.20)$$

These values are then used at each subsequent time step to maintain the profile until the wave arrives. During the passage of the wave the presence of the correction coefficients does not significantly change the depth values calculated,since the loss term is very small compared to the depths involved. In order to model the storage effect of jump movement,the jump is treated as a movable boundary between two separate pipes. The correction coefficients C1 and C2 ensure that the velocity of the hydraulic jump remains zero until the arrival of the wave. Thus at all times the upstream depth and velocity values may be calculated in the usual way using the equations for supercritical flow. The downstream sequent depth of the hydraulic jump is calculated using the momentum equation (Equation 11.5) and the velocity of the hydraulic jump over the next time-step can then be calculated using Equation 11.10, applied to the depth and velocity immediately upstream and at a point one distance step downstream of the current jump position (Figure 11.11).

The magnitude of the jump velocity must lie between the velocity defining the path of the positive characteristic in the supercritical flow upstream of the jump and that defining the path of the negative characteristic in the subcritical flow downstream of the jump (Cunge, Holly and Verwey, 1980 and Fox, 1977). Therefore (Figure 11.11),

$$(V - c)_{downstream} < V_w < (V + c)_{upstream}$$

If the calculated jump velocity falls outside of these limits then it is assigned a maximum value equal to the limit (the sign of V_w is

self-regulating in the inequality stated).

This method ensures that the jump velocity will remain at zero during the passage of steady flows and that when a wave arrives the jump will move in the appropriate direction, based on Equation 11.3, until the crest or trough of the wave has passed and then it will move back towards its steady state position. The movement of the jump is essential as it ensures that information about the flow conditions downstream of the jump can pass upstream. The effect of backflow occurring in one pipe when a wave is travelling down the other pipe is modelled by a decreasing flow rate and an increasing depth downstream of the jump resulting in a negative jump velocity.

11.6 Unsteady Flow

11.6.1 Test Programme

The final stage in the development of the junction model was to compare the depths of flow measured on the laboratory rig with results obtained from the computer program. The laboratory rig which was set up for the steady flow tests was also used for the unsteady flow tests. Two types of wave input were used, the first generated by the pressure tank and the second by a cistern; these two input devices are described in Section 5.5. The flow depth was measured at six points, two of these points were upstream of the junction in both the main and branch pipes and two were downstream of the junction. The exact position of the tapping points is shown in Figure 11.12. The Apple logging system was used to simultaneously record the depth of flow at each of the six points over a period of about 15.0 seconds.

Tests were carried out with two junction geometries (45 and 90 degrees) at slopes of 1/50, 1/80, 1/100, 1/150 and 1/200. Five

combinations of wave type were tested; these were a pressure tank wave in either the main or branch pipes, a pressure tank wave in both pipes, a wave generated by the cistern in the main pipe or a cistern wave in the main pipe with a pressure tank wave in the branch pipe. A small base flow was provided in both the main and branch pipes in all cases. Twenty tests were carried out (Figure 11.13) covering a variety of slope, junction and input combinations.

11.6.2 Unsteady Flow Test Results

11.6.2.1 The Effect of Backflow

During the passage of a wave through the junction backflow is caused in the branch containing only steady flow. The backflow causes a rise in depth accompanied by a change in velocity which propagates upstream through the subcritical flow until it attenuates and dies away. If the stationary steep-fronted wave is met whilst the backflow still has a velocity then the steep-fronted wave will begin to move upstream and lengthen the section of subcritical flow. Thus the effect of the backflow is dependent upon the magnitude of the wave travelling through the junction.

Figure 11.14 shows the effect of a simulated wave,generated by the pressure tank,travelling along one of the pipes and passing through a 45 degree junction. Figure 11.14a shows the depth and velocity of flow in the branch pipe just upstream of the junction. The depth increases as the backflow enters the pipe and the velocity decreases as the flow begins to reverse and move upstream. Figure 11.14b shows the wave just as it enters the junction, both the depth and velocity increase and then decrease with the flow rate.

Figure 11.14c shows the position and velocity of the

steep-fronted wave (or hydraulic jump) in the branch pipe, the backflow just begins to cause the jump to move upstream. Figure 11.14d shows the position and velocity of the steep-fronted wave in the main pipe, the wave acquires a negative velocity as the flow rate increases and then a positive velocity once the maximum flow rate has passed. The wave velocity reverts to zero when the steady baseflow has re-established itself.

Figure 11.15 illustrates the effect of a simulated cistern generated wave in the main pipe and a wave from the pressure tank in the branch pipe. The branch pipe is shorter than the main pipe so the depth and velocity begin to increase together in the branch pipe (Figure 11.15a) before the effect of the larger disturbance in the main pipe causes the velocity to reverse and backflow to occur. The steep-fronted wave in the branch pipe begins to move in a negative direction as the unsteady flow passes and then in the positive direction as the flow rate decreases. The backflow then causes the velocity of the steep-fronted wave to oscillate before it approaches zero as steady flow re-asserts itself. The movement of the steep-fronted wave in the main pipe is similar to that in Figure 11.14 as no backflow is experienced.

Figure 11.16 shows the simulated effect of a wave,generated by the cistern,travelling down the main pipe. The effect is similar to that seen in Figure 11.14 but the backflow is stronger so the steep-fronted wave in the branch pipe acquires a negative velocity which reaches the minimum limit described previously before tending back to zero and then becoming slightly positive.

The technique used to model junctions in the computer program clearly allows backflow to take place over a variable region of

subcritical flow whose length is dependent upon the magnitude of the disturbance causing the backflow. If the flow régime in any of the pipes meeting at the junction is subcritical throughout the length of the pipe then backflow can be modelled using the same technique.

11.6.2.2 Experimental Verification

The computer program incorporating the junction model was used to predict the depth versus time profiles at each of the six tapping points along the pipe during the passage of a wave in either the main or branch pipes or in both pipes. These profiles were then compared to those obtained from the laboratory rig in order to assess the accuracy of the junction model. Six examples are described which cover a range of gradients, junction type and input profiles in order to demonstrate the validity of the proposed junction model.

Two general points can be made before these examples are examined in more detail. Firstly, it was felt from observations that the pressure transducers had a tendency to exaggerate the steepness of the leading edge of the wave and secondly, that there is an occasional loss of data from the laboratory rig at some tapping points due to vibration of the test rig caused by parallel use of the pipe support system by other researchers.

Figure 11.17 shows a wave from the pressure tank in the main pipe passing through a 45 degree junction with the pipes at a gradient of 1/150. Figures 11.18 and 11.19 show a wave from the pressure tank in the branch pipe; Figure 11.18 shows the pipe system at a gradient of 1/80 with a 45 degree junction and Figure 11.19 illustrates a gradient of 1/100 with a 90 degree junction geometry. These three examples demonstrate that the computer model can simulate the passage of a wave

through the system with a high degree of accuracy. Both the timing and attenuation of the wave are modelled and it should be noted that the backflow in the pipe without the unsteady flow is also simulated (e.g. tapping 2 in Figure 11.18).

Figure 11.20 shows a wave from the pressure tank travelling down both the main and the branch pipes and meeting at the junction. The junction angle was 45 degrees and the pipes were set at a gradient of 1/150. The branch pipe is 1.6m shorter than the main pipe so the branch wave arrives at the junction first. The wave in the main pipe is then augmented by the backflow from the branch (tapping 2), this in turn causes backflow in the branch pipe giving a double maximum at tapping 4. The wave then travels past tapping 5 and is still accurately modelled as it passes tapping 6.

Figure 11.21 shows a wave generated by the cistern travelling down the main pipe, the pipe system is at a gradient of 1/150 with a 45 degree junction. The wave is very steep (rising to 5 l/s in 0.25s) and the computer model does not simulate the passage of the wave as well as for shallower waves. At tapping 6 the predicted wave is too low and lags the observed wave by about 1.5s. It should also be noted that at tapping 3 the observed backflow has extended further up the branch pipe than predicted by the computer program. These two problems are due to the exceptional steepness of the wave produced by a cistern emptying directly into the head of the pipe. It is unlikely that any input into a building drainage system would exceed a rise of 1 l/s over 0.5s and the program is well able to treat waves of this type.

Figure 11.22 illustrates the result of a wave from the cistern travelling down the main pipe and a wave generated by the pressure tank moving down the branch pipe (the observed data for tapping 3 is partly

missing due to a pressure transducer malfunction). The pipe system is set at a slope of 1/80 with a junction geometry of 90 degrees. The predicted results lag behind the observed data at tapping 6 by about 1s, although the depth is well modelled.

Generally the comparison between the observed and predicted depth data at the six tapping points is good, the exception being the very steep wave generated by the cistern. The effect of backflow in the pipe without the wave is well modelled, as is the interaction between waves arriving at different times at the junction.

11.6.3 Conclusion

The junction is an important element in the building drainage system and a satisfactory method of analysing its effect is essential to the formulation of any simulation program. The model described in this chapter adequately simulates the passage of a wave through a junction and its inclusion in the computer program will allow networks containing one or more junctions to be modelled. The interaction of waves arriving from different parts of the system can then be simulated and the effect of backflow represented.

12. The Multi-Storey Building Drainage Network Model

12.1 Ordering the Drainage Network

A building drainage system may consist of a large number of sanitary appliances served by a complex network of pipes. The problem then arises of ordering the unsteady flow calculations in such a way that flows can be accumulated at junctions at each time-step,thus allowing backflow to occur and the calculation to proceed downstream through the network. The system is always a tree-shaped network of pipes connecting sanitary appliances which contains no loops and serves a single drainage area operating entirely by gravity. The network also has only one final collection point (the sink node) (Argaman, Shamir and Spivak, 1973).

A number of authors have suggested methods of ordering the drainage network; the technique described by Berthouex, Wagner and Scully (1974) and proposed by Argaman, Shamir and Spivak is employed here as it will accept an arbitrary list of junction (node) and pipe numbers and translate this into an ordered system. Imaginary lines called drainage (or isonodal) lines are used to describe the physical arrangement of the network; these lines are defined such that they pass through nodes that are separated from the sink node by the same number of pipe sections (links) (Mays, 1978). Figure 12.1 shows an example of a network with the drainage lines illustrated; these are constructed by starting at the outlet and proceeding upstream and are numbered in the same way.

A tree of N nodes is completely connected by N-1 links; the number of drainage lines for the network will be between (N-1)/k and N-k where k is the number of upstream dead-end nodes in the system, k

therefore represents the number of sanitary appliances. The number of the sink node must be specified in advance and it is then assigned to drainage line number one. Other drainage lines will pass through nodes connected to the sink node by the same number of links. The direction of flow is determined by the value of the drainage line and is independent of the number used to identify the node (Berthouex, Wagner and Scully). This technique is also used by Mays and Wenzel (1976) and Mays, Wenzel and Liebman (1976).

The node incidence matrix for the network is constructed simply from a list of pipes,with each pipe carrying the number of the two nodes it connects (Figure 12.2). A cross in the matrix indicates that a pipe exists between two nodes, e.g.,pipe E connects nodes 4 and 6. The column headed Pn shows the number of pipes connected to each node, values of Pn are found by counting the crosses in each row. Nodes with sanitary appliances would have Pn = 1, the sink node also has Pn = 1 but must be labelled as the sink node in the input list.

Row β is all zeros to begin with and i is given the sink node number. A counter α is set to 2. The following steps are then carried out;

1. Record the value of Pn_i
2. Search row i to identify the pipe in column j connected to node i
3. Search column j to identify the upstream node and assign $DL_i = \alpha$
4. Set $\beta_i = 1$ to show the pipe has been connected
5. Repeat 3, 4 and 5 for $(Pn_i - 1)$ times
6. Locate new node i by searching column DL for α
7. If $Pn_i = 1$ the node is an upstream dead-end and has no

connecting pipe, if $Pn_i > 1$ then search row i for column j which has a cross and $\beta_i = 0$

8. For the pipe found in step 7 search column j to find the upstream node, assign $DL_i = \alpha + 1$ and $\beta_i = 1$

9. Repeat 7 and 8 ($Pn_i - 2$) times to identify all nodes on drainage line $\alpha + 1$

10. If all values in column DL are non-zero the solution is complete, if not then set $\alpha = \alpha + 1$ and return to step 6.

The node at the head of each pipe has now been assigned a drainage line number and the unsteady flow calculation may proceed by starting with the pipes with the highest drainage line number and working towards the sink node at each time-step.

12.2 Vertical Stack

12.2.1 Introduction

The drainage network model developed so far would typically represent one floor of a multi-storey building. In order to extend the model to provide a complete analysis of building drainage systems in whole buildings, it is necessary to link the network on each floor using a model for the vertical stack. Flow in the stack is normally annular with the water layer thickness dependent on total flowrate and on stack length until terminal velocity is reached. A suitable boundary condition for flow entry from the stack to the lowest level drain in the system is also necessary.

12.2.2 Annular Flow Thickness

The force balance equation for a length ΔL (Figure 12.3) of the fully developed annular flow in a vertical may be expressed thus

(Pink, 1973),

$$\pi D \tau_o \Delta L = \rho \pi D t \Delta L g \qquad (12.1)$$

where D = pipe diameter (m)

τ_o = wall shear stress (N/m^2)

ρ = fluid density (kg/m^3)

t = annular thickness (m)

g = acceleration due to gravity (m/s^2)

Under steady flow conditions it follows that,

$$\tau_o = \rho t g \qquad (12.2)$$

The Colebrook-White equation for full bore pipe flow (Equation 8.4) may be written,

$$\frac{1}{\sqrt{f}} = -2 \log_{10} \left(\frac{k}{3.7D} + \frac{2.52}{R_e \sqrt{f}} \right) \qquad (12.3)$$

where f = Darcy resistance coefficient

k = roughness coefficient (m)

R_e = Reynolds number (characteristic length equal to the pipe diameter)

Under full pipe flow conditions,

$$f = \frac{8 \tau_o}{\rho V^2} \qquad (12.4)$$

It has already been noted that for partially full pipe flow the diameter may be replaced by 4R where R is the hydraulic radius in metres.

The Reynolds number is expressed,

$$R_e = \frac{4RV}{\nu} \qquad (12.5)$$

Equation 12.3 may now be rewritten as,

$$\sqrt{\frac{\rho V^2}{8 \tau_o}} = -2 \log_{10} \left(\frac{k}{14.8R} + \frac{2.52 \nu}{4RV} \sqrt{\frac{\rho V^2}{8 \tau_o}} \right) \qquad (12.6)$$

For annular flow it has been shown that

$$\tau_o = \rho t g$$

and also

$$R = \frac{\pi D t}{\pi D} = t \qquad (12.7)$$

if $t << D$ as is the case here. The flow rate Q may be expressed as,

$$Q = \pi D t V \qquad (12.8)$$

Equation 12.6 may now be written,

$$\frac{Q}{4\pi\ Dt}\sqrt{\frac{1}{2gt}} = -\log_{10}\left(\frac{k}{14.8t} + \frac{0.314\nu}{t}\sqrt{\frac{1}{2gt}}\right) \qquad (12.9)$$

This equation can be solved iteratively to give t for a given Q and hence the annular velocity V.

The expressions above strictly only apply to fully developed flow and previous work has shown that the vertical stack length required to meet this condition is often less than 3m, i.e. less than one storey height.

12.2.3 Unsteady Stack Flow

The input profile to the stack is generated by applying the network program to a single storey of the building. The profile may then be treated as a finite number of time steps with the flow varying linearly within each time step (Figure 12.4).

Using the known flow rate, the stack properties and the distance to the next input level Hs the annular thickness for each point A to F can be calculated from Equation 12.9. The terminal velocity V_t can then be found from,

$$V_t = \frac{Q}{\pi D t} \qquad (12.10)$$

and used to find the arrival time of the flow particles A to F on the

inflow profile at the next entry point in the stack (Figure 12.4).

Wise (1973) reports that flow within a stack will reach terminal velocity within 5 to 10m of entering the stack. A factor based on a distance of 7.5m is used to include in the arrival time an allowance for the distance required to attain terminal velocity. The flow velocity V_e between floors in the stack is expressed thus,

$$V_e = ZV_t \qquad (12.11)$$

where $Z = H_s/7.5$ if $H_s < 7.5m$

$Z = 1.0$ if $H_s > 7.5m$

Generally the translation of a point I at time T on the inflow hydrograph may be written as,

$$T_{I'} = T_I + H/V_e \qquad (12.12)$$

Three possible cases may arise,

(i) Constant inflow; e.g. AB on Figure 12.4. Since the terminal velocities at A and B will be the same it is clear that $T_A - T_B = T_{A'} - T_{B'}$ and the mean flow $Q_{A'B'}$ will be equal to Q_{AB}.

(ii) Increasing inflow; e.g. BC. The terminal velocity at C will exceed that at B, therefore $T_B - T_C < T_{B'} - T_{C'}$. The mean flow $Q_{B'C'}$ is expressed thus,

$$Q_{B'C'} = 1/2(Q_B + Q_C)\frac{(T_B - T_C)}{(T_{B'} - T_{C'})} \qquad (12.13)$$

The wavefront steepens as it arrives at the lower level (Figure 12.4).

(iii) Decreasing inflow; e.g. DE. The same technique is used except that as the terminal velocity at D exceeds that at E the profile will be extended (Figure 12.4).

The translated flow profile may then be added to the inflow at the lower level; this process is repeated for each storey until the

base of the stack is reached.

12.2.4 Entry Boundary at the Base of the Stack

Summation of the translated inflow profiles gives a flow profile at the entry to the drain at the base of the stack. The entry energy E to the drain may be expressed as,

$$E = \frac{KV_e^2}{2g} \qquad (12.14)$$

where K is a loss coefficient representing the loss of energy at the base of the stack. Swaffield and Galowin (1983) suggest a value of 0.5 and this has been used to link the energy at the base of the stack to the depth y and velocity V at pipe entry. Therefore,

$$\frac{KV_e^2}{2g} = y + \frac{V^2}{2g} \qquad (12.15)$$

Experimental work is required to determine more accurate values of K, the loss coefficient at the base of the stack.

12.3 The Complete Model

The model for flow in a stack is used to complete the multi-storey building drainage network model by providing the link between the drainage systems on each floor of the building. It is now possible to simulate the flow through a complex system containing networks on a number of levels which drain to a single stack which in turn may discharge into either a single pipe or another network. The computer program for the complete building drainage system is known as BRUNET.

Figure 12.5 illustrates the results from a hypothetical system comprising four levels of flow (including the pipe draining the stack). The third floor is drained by a single pipe laid at a gradient

of 1/50, the second floor by a network at a gradient of 1/100 and the first floor by a network laid at a sufficiently shallow gradient to ensure the flow is subcritical. The input profile at the head of each upstream pipe in the network represents the flow from either a w.c. or a wash-hand basin, baths or showers can easily be represented by changing the shape of the profile.

Figure 12.5 also shows the effect of the flows combining at junctions and attenuating as they move through the network. The flow rate into the stack at the exit to the network on each floor is shown by a graph of discharge versus time. These profiles are then routed down the stack and result in the illustrated input to the drainage network at the lowest level. This flow is routed through a single pipe and the outflow at the exit from the complete drainage system is shown.

This example illustrates some of the network types which can be included into the drainage model, such as single pipes or networks which either flow supercritically or subcritically. It is also possible to include pipe systems with gradients, pipe diameters or roughness coefficients which vary between the pipes in the network. Any type of junction may be incorporated into the model assuming suitable tests have been conducted to find the empirical equation linking depth just upstream of the junction to the combined flow rate through the junction. Any type of sanitary appliance may also be linked to the system if the profile as the discharge enters the drain is known or can be found.

12.4 Conclusion

The program BRUNET uses the time-dependent equations defining unsteady flow to simulate the attenuation of multiple inflow profiles

moving through a multi-storey building drainage network system. The boundary equation at the head of each network may be varied so that sanitary appliances such as w.c.s, baths, basins, sinks,etc.,can be modelled using their characteristic flow profiles. The parameters describing each pipe, such as slope, roughness coefficient, diameter, etc., may be independently varied for every pipe in the system. Two specific types of junction are modelled in BRUNET by using empirical equations linking the depth upstream of the junction to the combined flow rate into the junction; similar equations can be found for any type of junction which requires modelling. The flow at the exit to the network on each floor of the building is routed down a vertical stack and the resulting discharge versus time profile at the base of the stack is used as an input to the network section of the program to simulate the flow at the lowest level in the system. The final result is a profile of the flow as it leaves the building drainage system.

13. Conclusion and Further Work

The attenuation of unsteady flow profiles in building drainage systems must be fully considered if water conservation proposals involving changes in flush volume or reduced pipe diameter are not to lead to solid deposition and subsequent blockage of drainage systems. Empirical methods of studying attenuation are limited in their application and there is a need for a time dependent numerical model which can accommodate random inflows to the system with variable boundary conditions at the entry and exit, the model must also be able to simulate both subcritical and supercritical flow when this becomes necessary. The method of characteristics was chosen for the numerical model because it has been proven for network analysis by other authors, is particularly suitable for simulating the supercritical flow régime and is also able to deal with variable boundary conditions at both the entry and exit to the system.

Full-scale flow tests were undertaken to validate the end boundary conditions used in the final program and the level of agreement reached for the range of wave durations and peak amplitudes likely in a building drainage network was sufficiently good to justify the development of a network program incorporating the various subsections previously validated. The final model of the building drainage system was completed using a representation of flow in a vertical stack based on work published elsewhere.

The program BRUNET is capable of modelling multi-storey drainage systems with multiple flow inputs and varied boundary and junction types. BRUNET is restricted to level invert junctions and requires the steady-flow depth characteristics of each type of junction

within the system. The program can be used to output depth or flow rate through time at any point in the system and could therefore be used by a designer to evaluate the performance of new systems. The program could also be used to determine the effects of water conservation legislation on system design or to calculate the load that could be carried by any particular pipe in the system.

The program BRUNET could be extended and improved by further work in a number of areas. A limited range of junction types have been incorporated so far and clearly there is a need for work on non-level invert junctions and on top entry junctions where no backflow occurs in the top entry branch. The model used for the vertical stack needs laboratory validation and it may also be possible to find a more accurate way of representing the steepening of the flow profile in the stack. It would also be useful to study manholes so that the flow from the building drainage system could be routed into a manhole after it left the building. Finally, the on-site validation of the whole model instead of the piecemeal validation of sections in the laboratory should be regarded as essential.

References

Abbott, M.B. — Computational Hydraulics. Pitman, London, 324 pages, 1979.

Abbott, M.B. and Verwey, A. — Four-point method of characteristics. J. Hyd. Div., A.S.C.E., 96, HY12, pp.2549-2564, 1970.

Ackers, P. — Urban drainage: the effects of sediment on performance and design criteria. Int. Conf. on Urban Storm Drainage, Southampton, April, 1978.

Ackers, P. and Harrison, A.J.M. — Attenuation of flood waves in part-full pipes. Proc., I.C.E., 28, pp.361-382, July 1964.

Adesanya, D.A. — An appraisal of self and locally induced siphonage. Unpublished PhD thesis, Brunel University, August, 1983.

Akan, A.O. and Yen, B.C. — Diffusion-wave flood routing in channel networks. J. Hyd. Div., A.S.C.E., 107, HY6, pp.719-732, 1981.

Amein, M. — Streamflow routing on computer by characteristics. Wat. Res. Res., 2(1), pp.123-130, 1966.

Amein, M. and Chu, H.L. — Implicit numerical modelling of unsteady flows. J. Hyd. Div., A.S.C.E., 101, HY6, pp.717-731, 1975.

Amein, M. and Fang, C.S. — Implicit flood routing in natural channels. J. Hyd. Div., A.S.C.E., 96, HY12, pp.2481-2500, 1970.

Argaman, Y., Shamir, U. and Spivak, E. — Design of optimal sewerage systems. J. Env. Eng. Div., A.S.C.E., 99, EE5, pp.703-716, 1973.

Baltzer, R.A. and Lai, C. — Computer simulation of unsteady flows in waterways. J. Hyd. Div., A.S.C.E., 94, HY4, pp.1083-1117, 1968.

Barnes, A.H. — Comparison of computed and observed flood-routing in a circular cross-section. Proc. Int. Hydrology Symposium, Vol. 1, pp.121-127, Fort Collins, Colorado, September 1967.

Berthouex, P.M., Wagner, G. and Scully, L.J.P. — Ordering sewer design calculations. J. Env. Eng. Div., A.S.C.E., 100, EE6, pp.1303-1307, 1974.

Bettess, R., Pitfield, R.A. and Price, R.K. — A surcharging model for storm sewer systems. Int. Conf. on Urban Storm Drainage, Southampton, April, 1978.

Burberry, P.J. Water economy and the hydraulic design of underground drainage. Proc., Seminar on Drainage Design, Brunel University, Uxbridge, Middx., May, 1978.

Burberry, P. and Griffiths, T. Demand and discharge pipe sizing for sanitary fittings. Basic calculations. The Architects Journal Information Library, 21-11-62, pp.1187-1191, 1962.

Camp, T.R. Design of sewers to facilitate flow. Sew. Works Journal, 18 (1), 1946.

Carballada, L., Ouach, T.T., Marche, C. and Remanesirthy, A.S. Modele de jonction des rivieres. Proc. 18th Congress I.A.H.R., New Delhi, 1981.

Chaudhry, Y.M. and Contractor, D.N. Application of the implicit method to surges in open channels. Wat. Res. Res., 9 (6), pp.1605-1612, 1973.

Chen, C. and Wang, C. Nondimensional gradually varied flow profiles. J. Hyd. Div., A.S.C.E., 95, HY5, pp.1671-1686, 1969.

Chow, V.T. Open-Channel Hydraulics. McGraw-Hill International, 680 pages, 1959.

Colebrook, C.F. — Turbulent flow in pipes with particular reference to the transition region between the smooth and rough pipe laws. Journal, I.C.E., 10, 1939.

Cooley, R.L. and Moin, S.A. — Finite element solution of the Saint-Venant equations. J. Hyd. Div., A.S.C.E., 102, HY6, pp.759-777, 1976.

Courant, R., Isaacson, E. and Rees, M. — On the solution of non-linear hyperbolic differential equations by finite differences. Comm. Pure and Applied Maths, 5, pp.243-255, 1952.

Courtney, R.G. — A multinominal analysis of water demand. Building and Environment, 11 (3), 1976.

Cunge, J.A., Holly F.M. and Verwey, A. — Practical Aspects of Computational River Hydraulics. Pitman, London, 420 pages, 1980.

Dawson, F.M. and Kalinske, A.A. — Hydraulics and pneumatics of plumbing systems. Engineering Studies Bulletin No. 10, University of Iowa, 1937.

Escoffier, F.F. and Boyd, M.B. — Stability aspects of flow in open channels. J. Hyd. Div., A.S.C.E., 88, HY6, pp.145-166, 1962.

Evans, E.P. The behaviour of a mathematical model of open channel flow. Proc. 17th Congress I.A.H.R., pp.173-180, Baden-Baden, W. Germany, 1977.

Fox, J.A. Hydraulic Analysis of Unsteady Flow in Pipe Networks. MacMillan, London, 216 pages, 1977.

Goldberg, D.E. and Wylie, E.B. Characteristics method using time - line interpolations. J. Hyd. Div., A.S.C.E., 109, HY5, pp.670-683, 1983.

Harris, G.S. Real time routing of flood hydrographs in storm sewers. J. Hyd. Div., A.S.C.E., 96, HY6, pp.1247-1260, 1970.

Hayward, A.T.J. Flowmeters: A Basic guide and Source Book for Users. John Wiley, New York, 197 pages, 1979.

Henderson, F.M. Open Channel Flow. MacMillan, New York, 522 pages, 1966.

Hu, W.W. Hydraulics of spatially varied pipe flow. J. Hyd. Div., A.S.C.E., 93, HY6, pp.281-296, 1967.

Hunter, R.B. Minimum requirements for plumbing. US Department of Commerce, Plumbing Code Committee Report, 1924.

Isaacson, E., Stoker, J.J. and Troesch, B.A. — Numerical solution of flow problems in rivers. J. Hyd. Div., A.S.C.E., 84, HY5, pp.1-18, 1958.

Joliffe, I.B. — Accurate pipe junction model for steady and unsteady flows. 2nd Int. Conf. on Urban Storm Drainage, pp.93-100, Urbana, Illinois, June, 1981.

Joliffe, I.B. — A study of open channel flow conditions at a pipe junction. Report WRE 82-2, Water Resources Engineering Group, University of Alberta, Edmonton, Canada, April, 1982.

Jones, S.B. — Choice of space and time steps in the Muskingham-Cunge flood routing method. Proc. I.C.E., 71 (2), pp.759-772, 1981.

Kanda, T. and Kitada, T. — An implicit method for unsteady flows with lateral inflows in urban rivers. Proc. 17th Congress I.A.H.R., pp.213-220, Baden-Baden, W. Germany, 1977.

Katys, G.P. — Continuous Measurement of Unsteady Flow. Pergamon Press, Oxford, 217 pages, 1964.

Keuning, D.H. — Application of the finite element method to open channel flow. J. Hyd. Div., A.S.C.E., 102, HY4, pp.459-468, 1976.

Koussis, A.D. Comparison of Muskingham method difference schemes. J. Hyd. Div., A.S.C.E., 106, HY5, pp.925-929, 1980.

Lakshmana Rao, N.S. and Sridharan, K. Effect of channel shape on gradually varied flow profiles. J. Hyd. Div., A.S.C.E., 97, HY1, pp.55-64, 1971.

Liggett, J.A. Mathematical flow determination in open channels. J. Eng. Mech. Div., A.S.C.E., 94, EM4, pp.947-963, 1968.

Lin, J.D. and Soong, H.K. Junction losses in open channel flow. Wat. Res. Res., 15 (2), pp.414-418, 1979.

Marsalek, J. Energy losses at straight flow-through sewer junctions. Research Report No.111, 29 pages, Environment Canada, 1981.

Martin, C.S. and De Fazio, F.G. Open channel surge simulation by digital computer. J. Hyd. Div., A.S.C.E., 95, HY6, pp.2049-2076, 1969.

Martin, C.S. and Zovne, J.J. Finite-difference simulation of bore propagation. J. Hyd. Div., A.S.C.E., 97, HY7, pp.993-1010, 1971.

Mays, L.W. — Sewer network scheme for digital computations. J. Env. Eng. Div., A.S.C.E., 104, EE3, pp.535-539, 1978.

Mays, L.W. and Tung, Y.K. — State variable model for sewer network flow routing. J. Env. Eng. Div., A.S.C.E., 104, EE1, pp.15-30, 1978.

Mays, L.W. and Wenzel, H.G. — Optimal design of multi-level branching sewer systems. Wat. Res. Res., 12 (5), pp.913-917, 1976.

Mays, L.W., Wenzel, H.G. and Liebman, J.C. — Model for layout and design of sewer systems. J. Water Resources Planning and Management Div., A.S.C.E., 102, WR2, pp.384-405, 1976.

Menendez, A.N. and Norscini, R. — Spectrum of shallow water waves, an analysis. J. Hyd. Div., A.S.C.E., 108, HY1, pp.75-94, 1982.

Minton, P. and Sobey, R.J. — Unified nondimensional formulation for open channel flow. J. Hyd. Div., A.S.C.E., 99, HY1, pp.1-12, 1973.

Mitchell, J.S. — Comparison of mathematical versus experimental flood wave attenuation in part-full pipes. Unpublished MSc. thesis, Colorado State University, Colorado, 1967.

Mozayeny, B. and Song, C.S. — Propagation of flood waves in open channels. J. Hyd. Div., A.S.C.E., 95, HY3, pp.877-892, 1969.

Murota, A., Kanda, T. and Eto, T. — Flood routing for urban river networks. Proc. Int. Symp. River Mech., 3, pp.339-350, Bangkok, January, 1973.

Pink, B.J. — Laboratory investigation of the discharge characteristics of sanitary appliances. Building Research Establishment Current Paper 37/73, December, 1973.

Pinkayan, S. — Routing storm water through a drainage system. J. Hyd. Div., A.S.C.E., 98, HY1, pp.123-135, 1972.

Ponce, V.M. — Nature of wave attenuation in open channel flow. J. Hyd. Div., A.S.C.E., 108, HY2, pp.257-261, 1982.

Ponce, V.M. and Simons, D.B. — Shallow wave propagation in open channel flow. J. Hyd. Div., A.S.C.E., 103, HY12, pp.1461-1476, 1977.

Ponce, V.M. and Yevjevich, V. — Muskingham-Cunge method with variable parameters. J. Hyd. Div., A.S.C.E., 104, HY12, pp.1663-1667, 1978.

Powell, R.W. — Resistance to flow in smooth channels. Trans. Am. Geophys. Union, 30, pp.875-889, 1949.

Price, R.K. — A mathematical model for river flows; I. theoretical development. Report INT127, Hydraulics Research Station, Wallingford, 1977.

Price, R.K. and Kidd, C.H.R. — A design and simulation method for storm sewers. Proc. Int. Conf. on Urban Storm Drainage, Southampton, 1978.

Price, R.K. and Samuels, P.G. — A computational hydraulic model for rivers. Proc. I.C.E., 69, pp.80-96, 1980.

Quinn, F.H. and Wylie, E.B. — Transient analysis of the Detroit river by the implicit method. Wat. Res. Res., 8 (6), pp.1461-1469, 1972.

Radojkovic, M. and Maksimovic, C. — Internal boundary conditions for free surface unsteady flow in expansions and junctions. Proc. 17th Congress I.A.H.R., pp.367-372, Baden-Baden, W. Germany, 1977.

Report — Friction factors in open channels. Task force on friction factors for the committee on hydromechanics of the hydraulics division. J. Hyd. Div., A.S.C.E., 89, HY2, pp.97-143, 1963.

Saint-Venant, A.J.C.B. — Elementary demonstration of the propagation formula for a wave or a translatory wave in a prismatic channel and remarks on the propagation of sound and light, on hydraulic jumps and also on the distinction between rivers and torrents. Comptes rendus des seances de l'Academie des Sciences, 71, pp.186-195, 1870.

Sakkas, J.G. and Strelkoff, T. — Dimensionless solution of dam-break flood waves. J. Hyd. Div., A.S.C.E., 102, HY2, pp.171-184, 1976.

Sevuk, A.S. and Yen, B.C. — A comparative study on flood routing computation. Proc. Int. Symp. River Mech, 3, pp.275-290, Bangkok, January 1973.

Sevuk, A.S. and Yen, B.C. — Comparison of four approaches in routing flood wave through junction. Proc. 15th Congress, I.A.H.R., 5, pp.169-172, September, 1973.

Sevuk, A.S., Yen, B.C. and Patterson, G.E. — Illinois storm sewer simulation model; user's manual.Research Report No. 73, Water Resources Centre, University of Illinois at Urbana-Champaign, 1973.

Shubinski, R.P. and Roesner, L.A. — Linked process routing models. Proc. Symp. Models for Urban Hydrology, American Geophysical Union, 1973.

Silvio, G.D. Flood wave modification along prismatic channels. J. Hyd. Div., A.S.C.E., 95, HY5, pp.1589-1614, 1969.

Sivaloganathan, K. Comparative study of characteristic methods for free surface flow computations. Proc. Int. Conf. Urban Storm Drainage, Southampton, 1978.

Sivaloganathan, K. Channel flow computations using characteristics. J. Hyd. Div., A.S.C.E., 105, HY7, pp.899-910, 1979.

Sivaloganathan, K. Accuracy of explicit methods of unsteady flow computations in channels. Proc., I.C.E., 69, pp.199-207, 1980.

Soliman, M.M. The hydrologic characteristics of river confluences. Proc. 3rd Int. Hydrology Symp. on Theoretical and Applied Hydrology, pp.663-669, Fort Collins, Colorado, 1977.

Sridharan, K. and Mohan Kumar, M.S. Parametric studies of flood wave propagation. J. Hyd. Div., A.S.C.E., 107, HY9, pp.1061-1076, 1981.

Strelkoff, T. Numerical solution of Saint-Venant equations. J. Hyd. Div., A.S.C.E., 96, HY1, pp.223-253, 1970.

Swaffield, J.A. Building drainage system research; past influences, current efforts and future objectives. Construction Papers, 1 (1), pp.45-62, 1980.

Swaffield J.A. Application of the method of characteristics to predict attenuation in unsteady partially filled pipe flow. NBSIR 82-2478 Report, US Department of Commerce, December, 1981.

Swaffield, J.A. and Galowin, L.S. A preliminary study of the vertical stack to horizontal drain entry condition as an extension to the modelling of unsteady partially filled pipe flow. NBSIR Progress Report, US Department of Commerce, September, 1983.

Taylor, E.H. Flow characteristics at rectangular open channel junctions. Trans. A.S.C.E., 109, pp.893-902, 1944.

Terzidis, G. and Strelkoff, T. Computation of open channel surges and shocks. J. Hyd. Div., A.S.C.E., 96, HY12, pp.2581-2610, 1970.

Townsend, R.D. and Prins, J.R. Performance of model storm sewer junctions. J. Hyd. Div., A.S.C.E., 104, HY1, pp.99-104, 1978.

Transport and Road Research Laboratory — A guide for engineers to the design of storm sewer systems. T.R.R.L. Roadnote No. 35, H.M.S.O., 1975.

Uujamhan, E.J.S. — Water conservation w.c. design: a study of the design parameters affecting w.c. performance. Unpublished PhD thesis, Brunel University, August 1981.

Vallentine, H.R. — Generalised profiles of gradually varied flow. J. Hyd. Div., A.S.C.E., 93, HY2, pp.17-24, 1967.

Webster, C.J.D. — An investigation of the use of water outlets in multi-storey flats. Building Services Engineer, 39 (1), 1972.

Weinmann, P.E. and Laurenson, E.M. — Approximate flood routing methods: a review. J. Hyd. Div., A.S.C.E., 105, HY12, pp.1521-1536, 1979.

Wise, A.F.E. — One pipe plumbing, some recent experience at the Building Research Station. Journal I.P.H.E., 51, 1952.

Wise, A.F.E. — Drainage services in buildings - a review of some fluid mechanics aspects of the subject. Building Research Establishment Current Paper 35/73, December, 1973.

Wise, A.F.E. — Water, Sanitary and Waste Services for Buildings. Batsford, London, 156 pages, 1979.

Wise, A.F.E. and Croft, J. — Investigation of single stack drainage for multi-storey flats. J. Royal Sanitary Inst., 74 (9), pp.797-826, 1954.

Wylie, E.B. — Unsteady free surface flow computations. J. Hyd. Div., A.S.C.E., 96, HY11, pp.2251-2541, 1970.

Wylie, E.B. and Streeter, V.L. — Fluid Transients. McGraw Hill, New York, 384 pages, 1978.

Wyly, R.S. — Investigation of the hydraulics of horizontal drains in plumbing systems. National Bureau of Standards, Monograph 86, December, 1964.

Yen, B.C. and Akan, A.O. — Flood-routing through river junctions. Rivers '76, A.S.C.E., 1, pp.212-231, 1976.

Yen, B.C. and Sevuk, A.S. — Design of storm sewer networks. J. Env. Eng. Div., A.S.C.E., 101, EE4, pp.535-553, 1975.

Zovne, J.J. and Martin, C.S. — Simulation of transient supercritical channel flow. J. Hyd. Div., A.S.C.E., 105, HY7, pp.859-876, 1979.

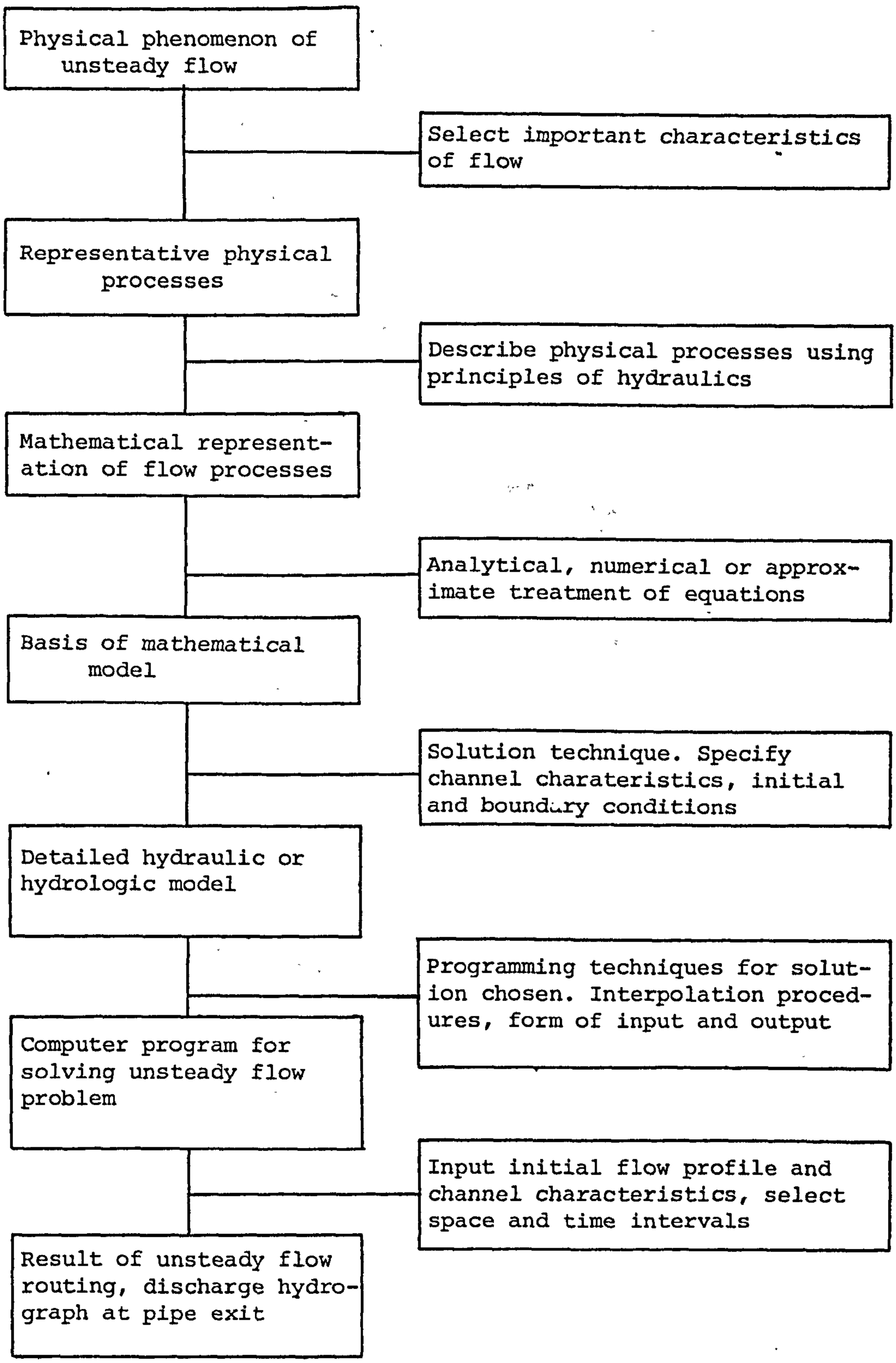

Figure 1.1 Development of model for unsteady flow computation

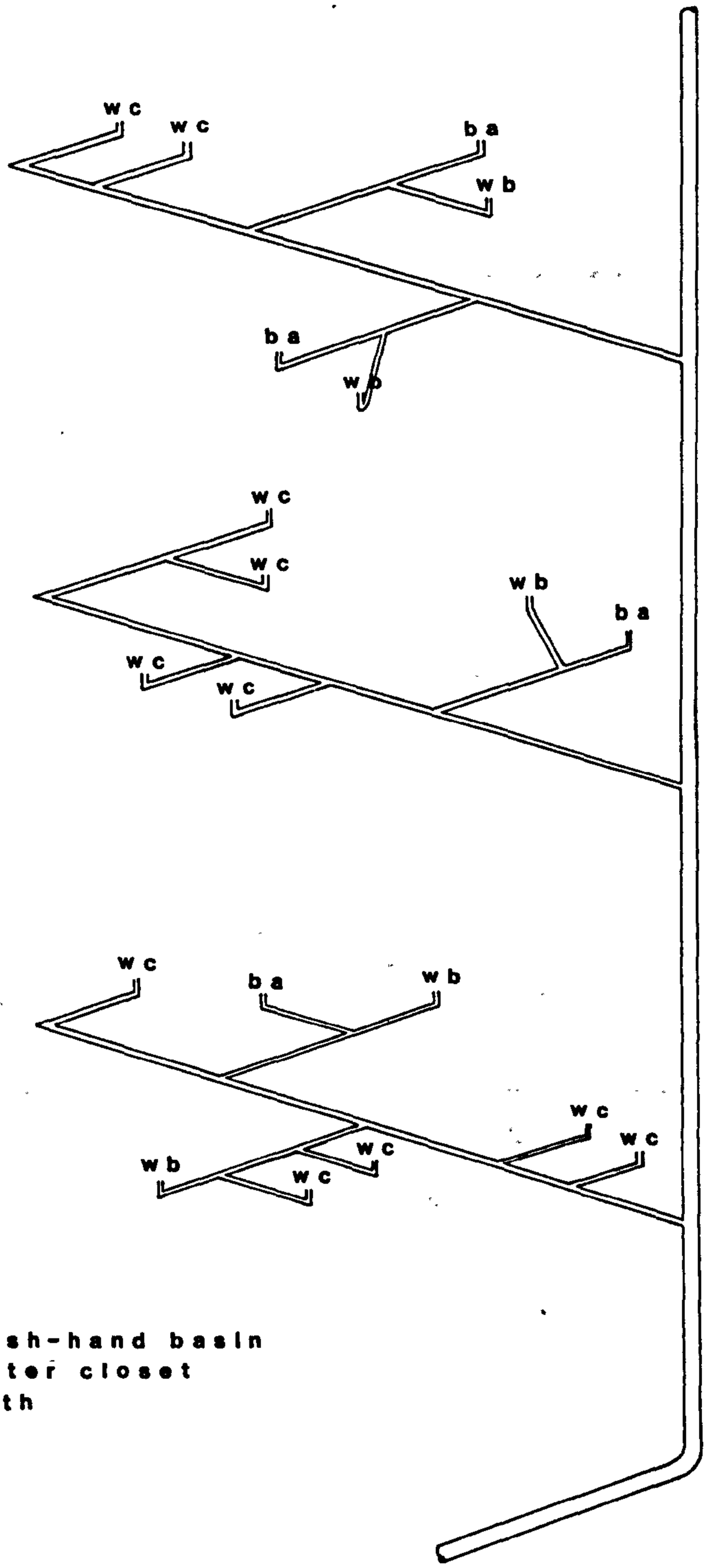

Figure 1.2 Building drainage system

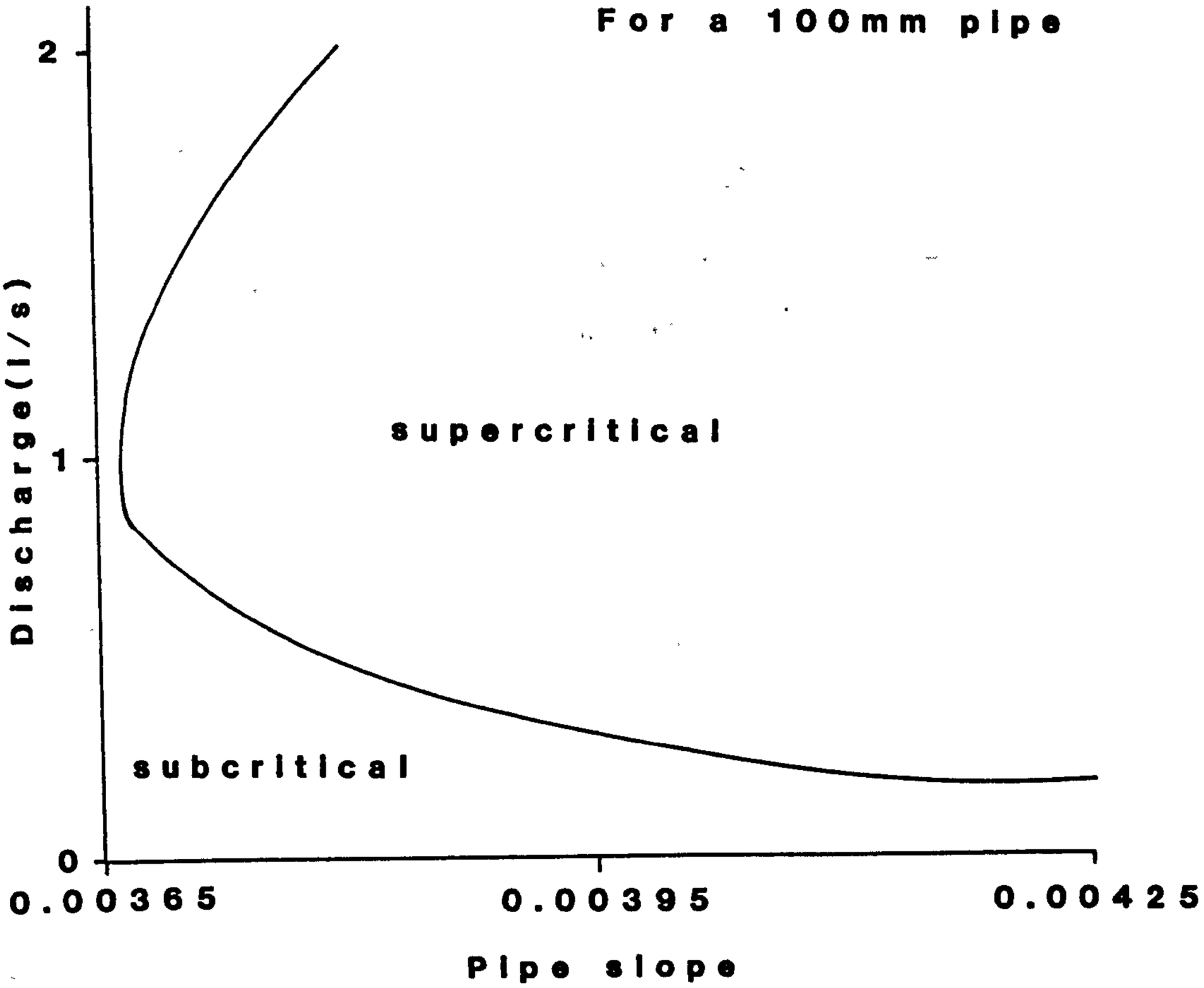

Figure 1.3 Variation of flow regime with pipe slope

(A) after Wise (1973)

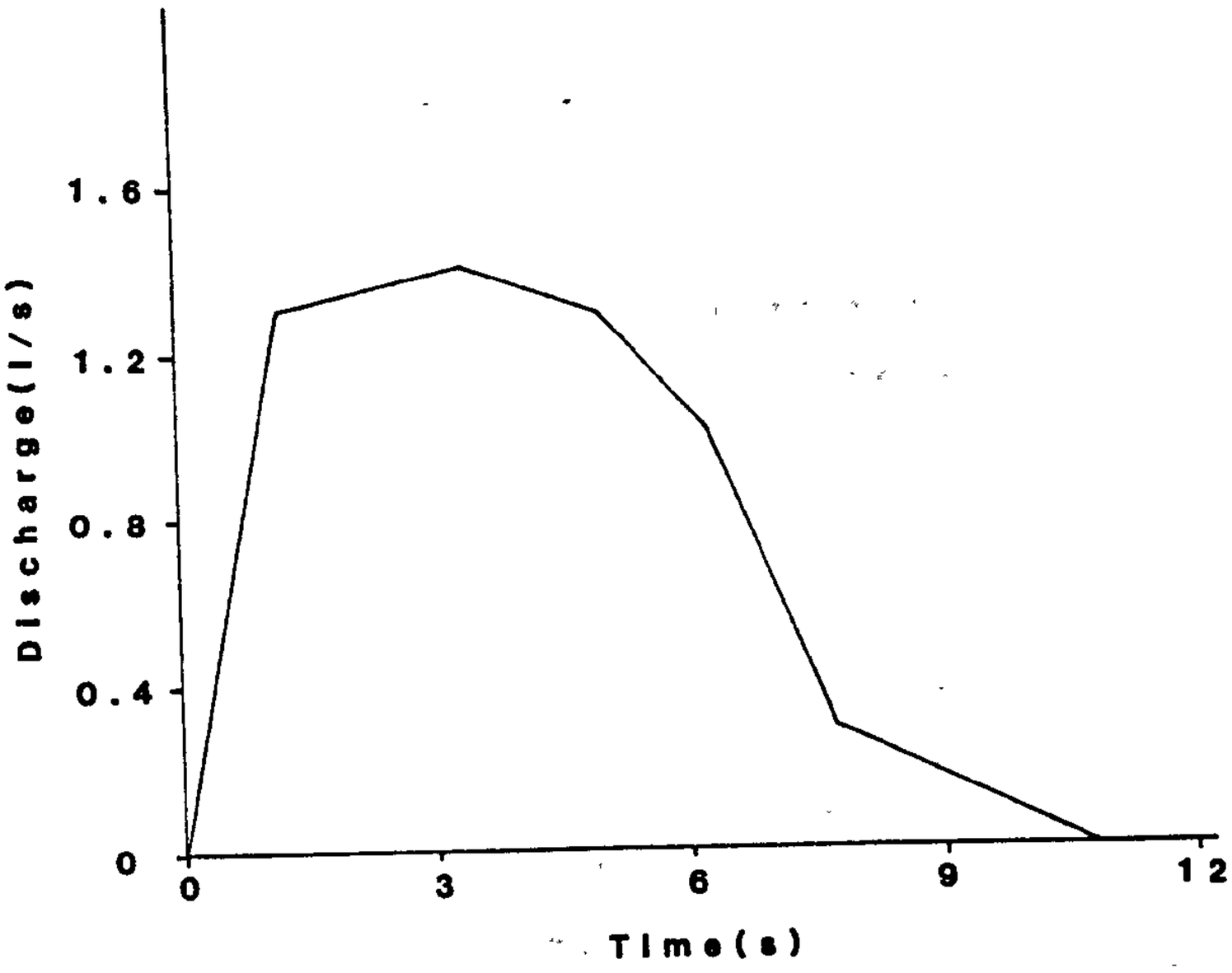

(B) after Uujamhan (1981)

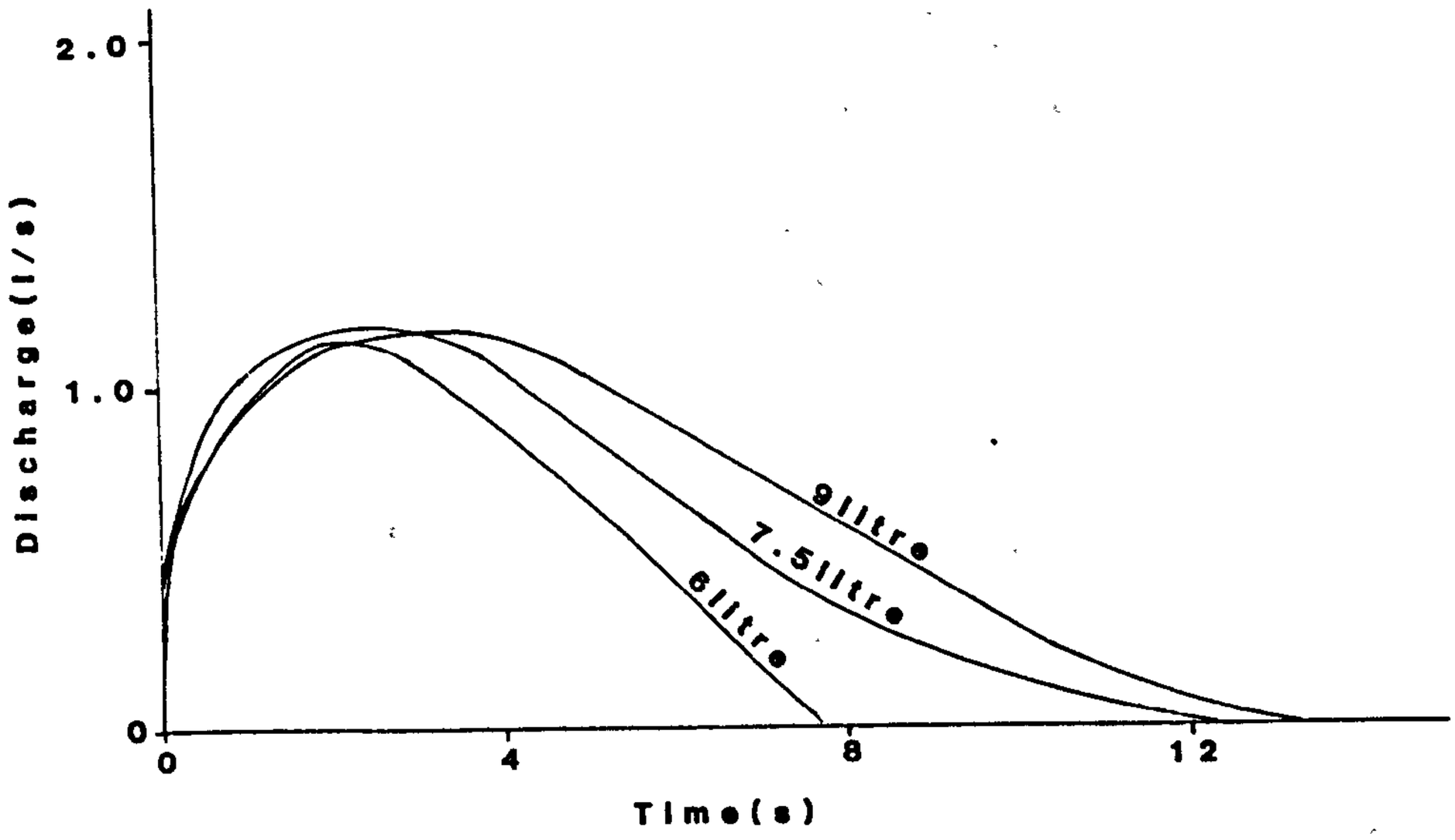

Figure 1.4 W.C. discharge characteristics

(a)

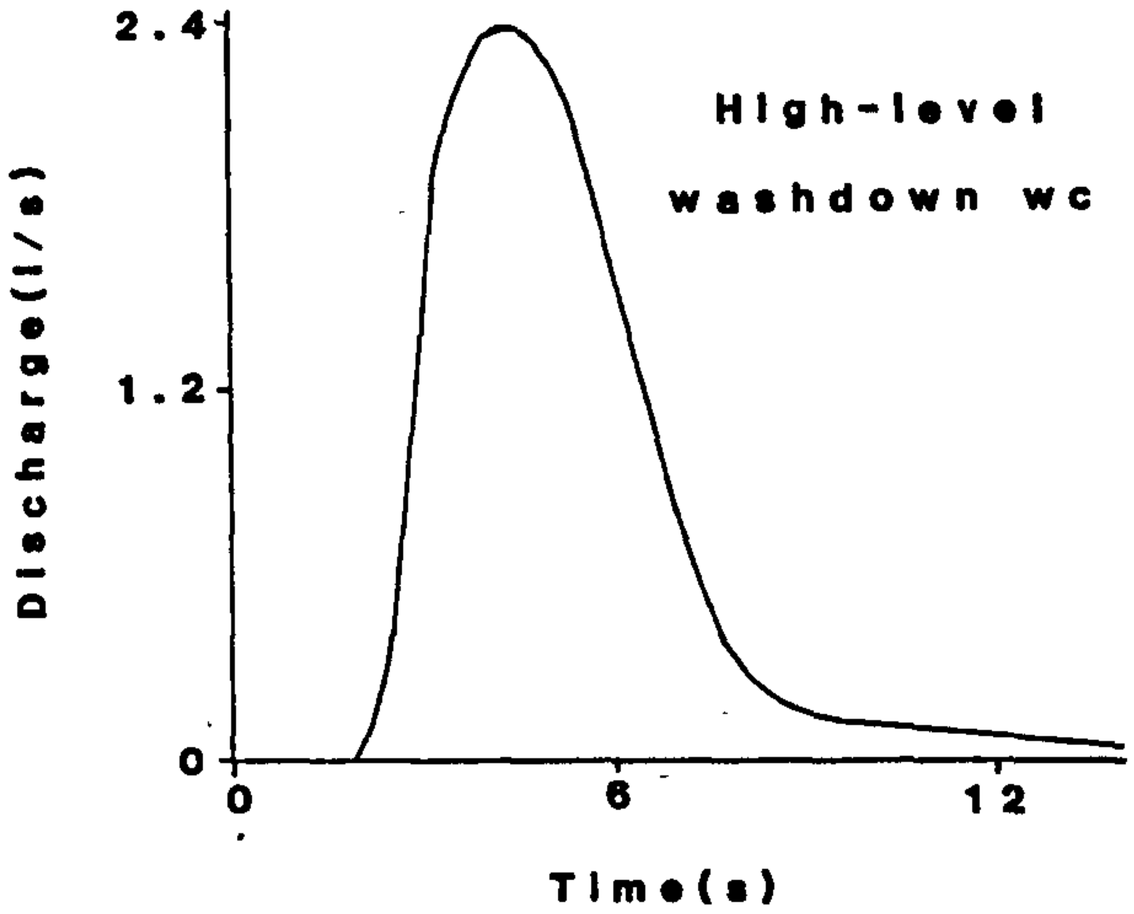

(b)

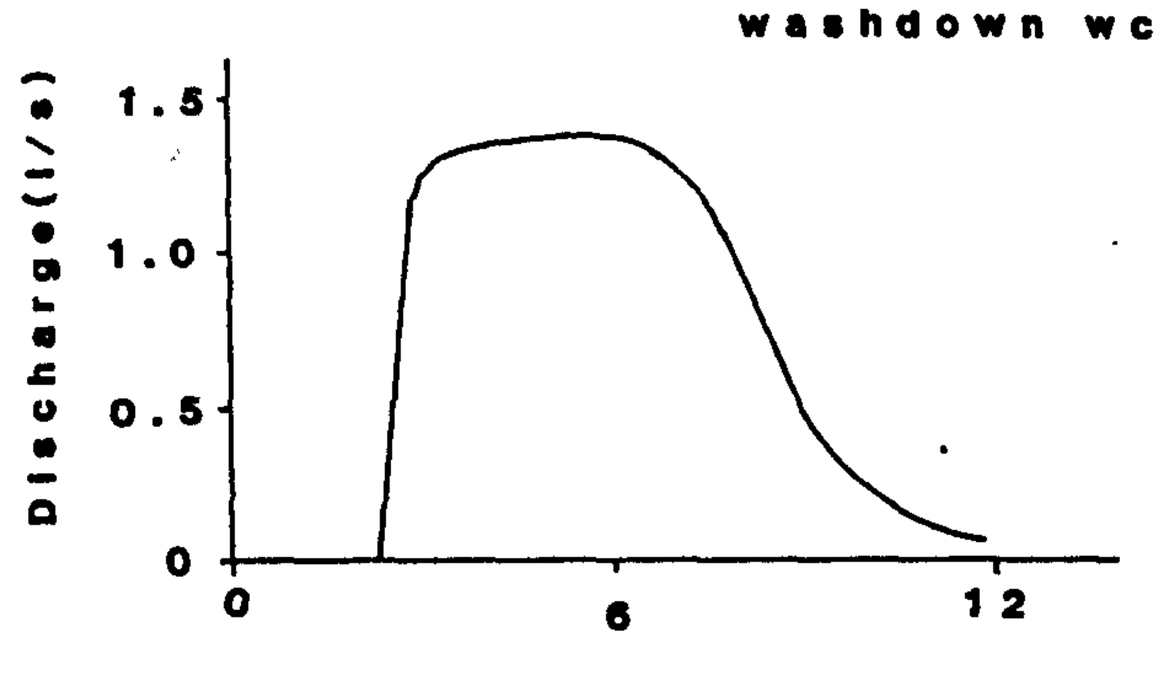

Figure 1.5 W.C. discharge characteristics (after Pink, 1973)

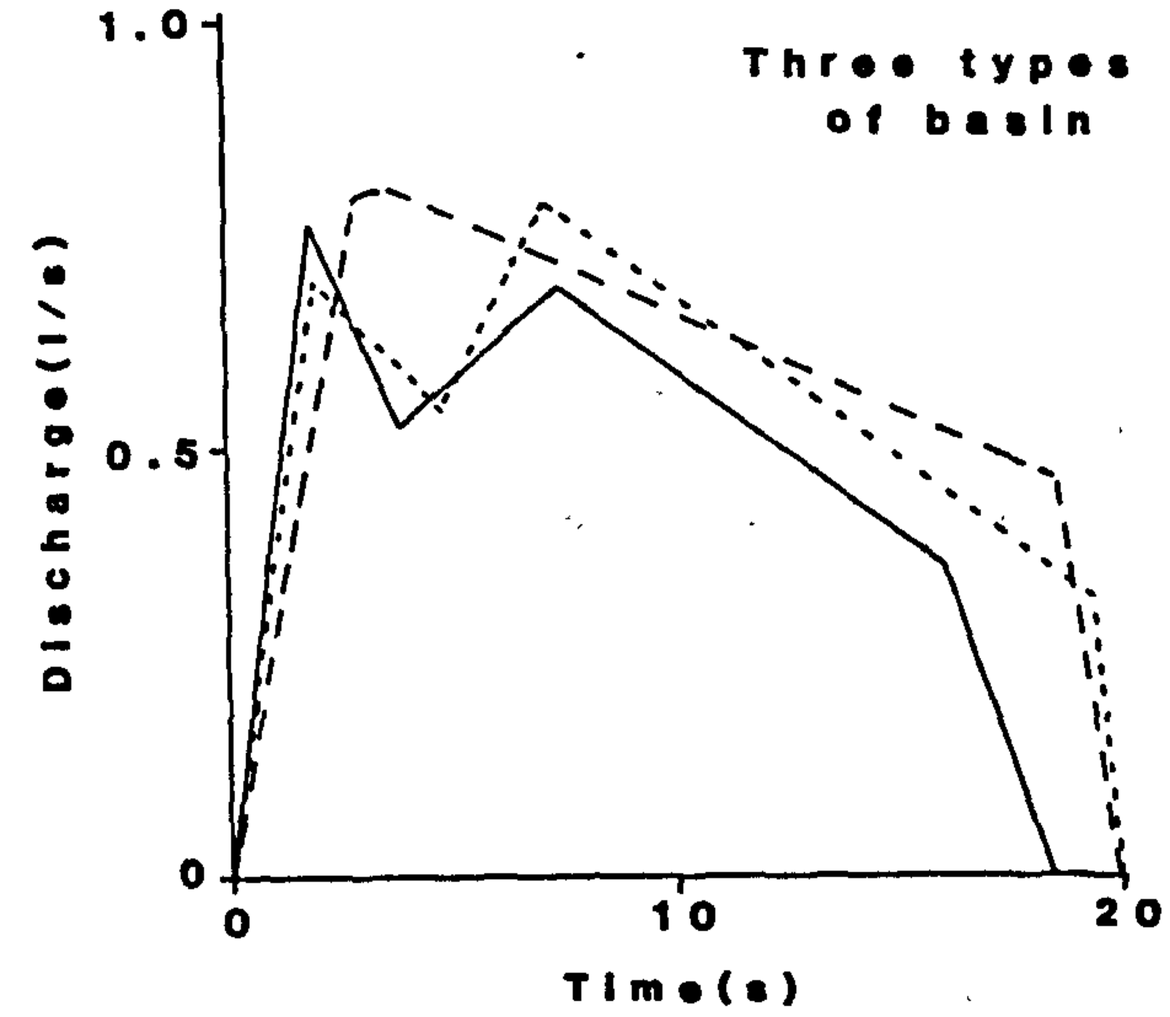

Figure 1.6 Wash-hand basin discharge characteristics (after Adesanya, 1983)

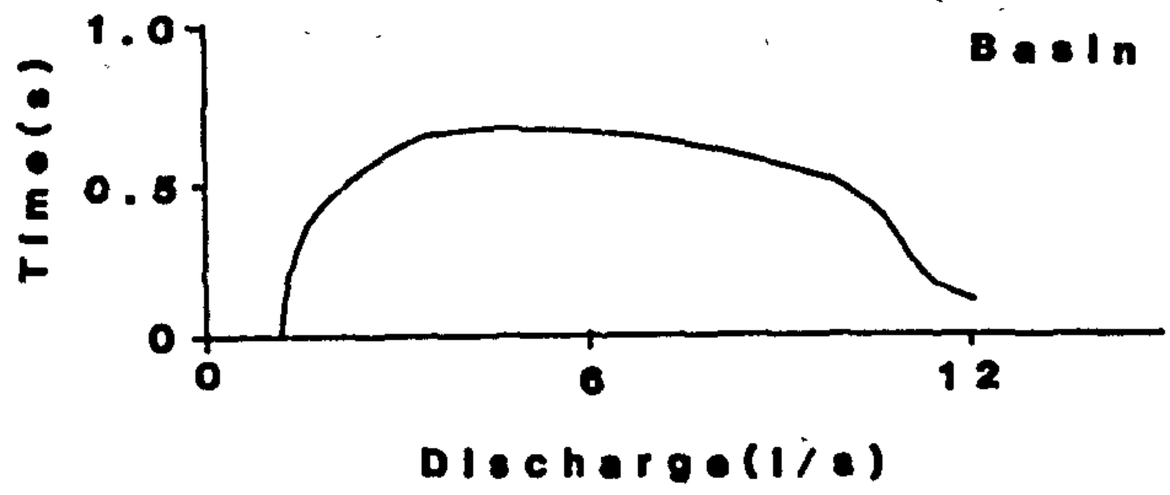

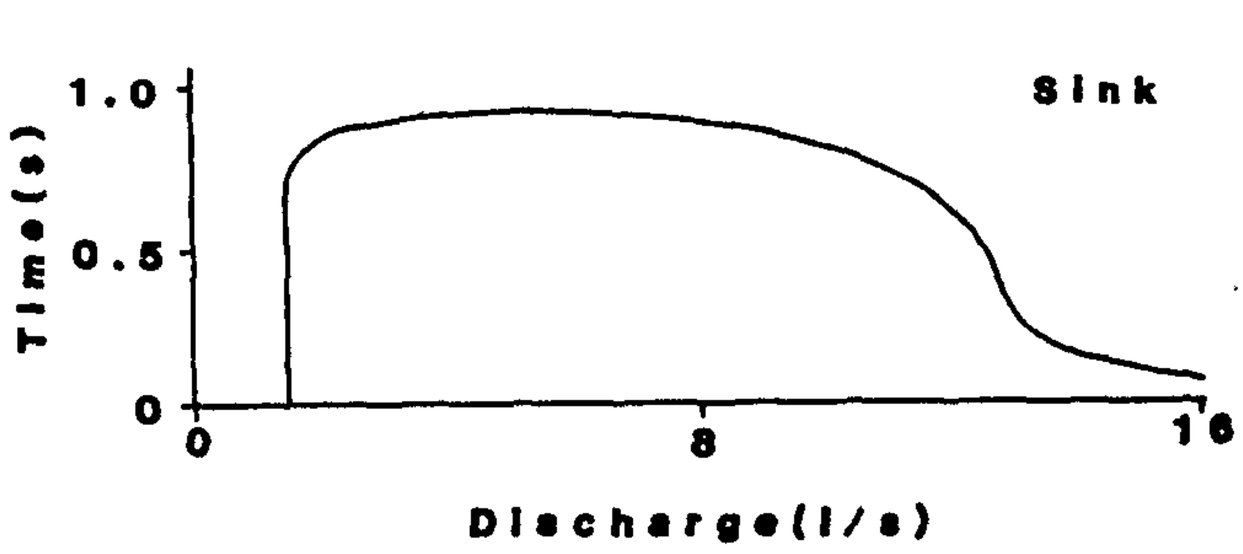

Figure 1.7 Basin discharge characteristics (after Pink, 1973)

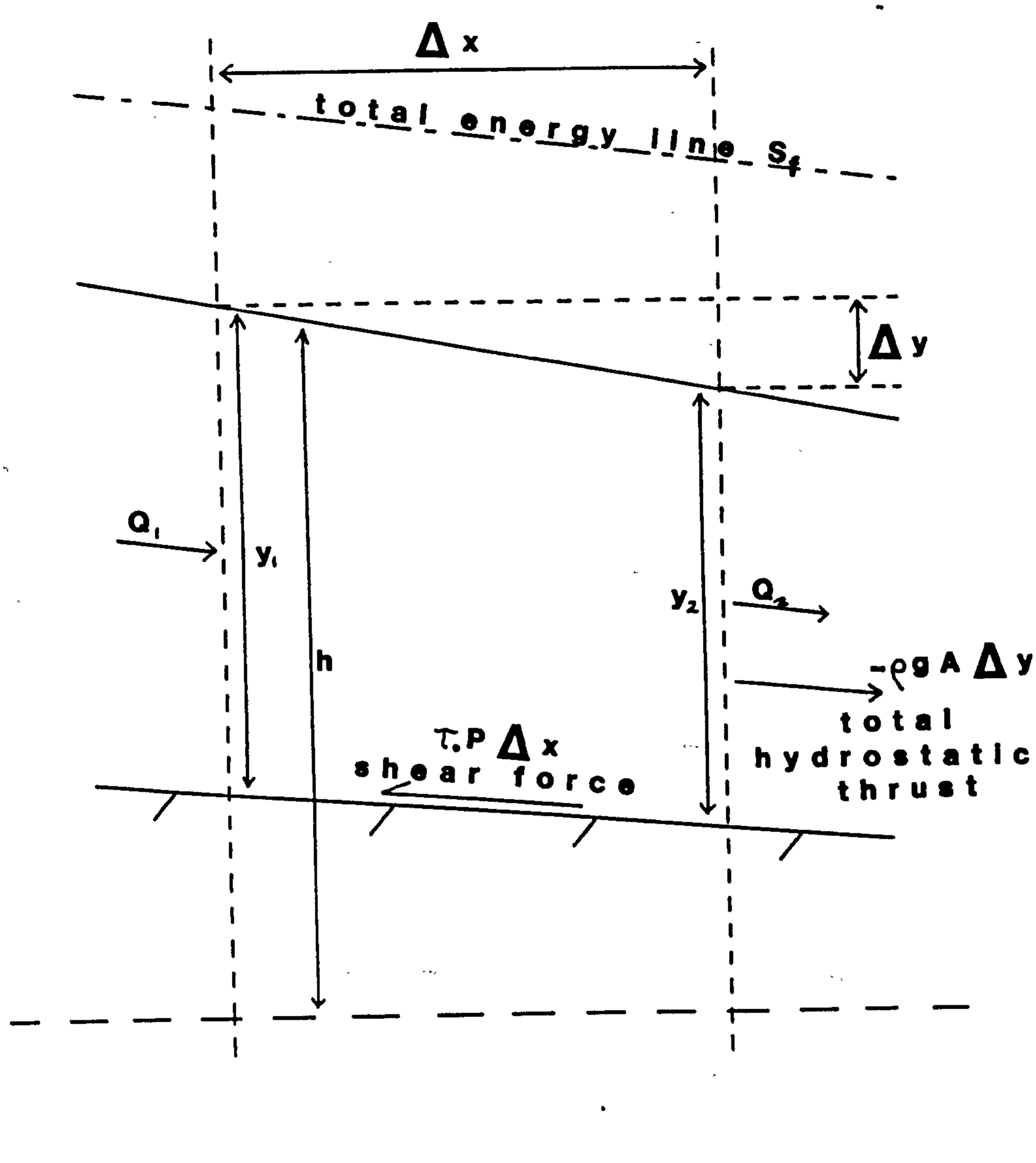

Figure 2.1 Definition sketch for unsteady flow

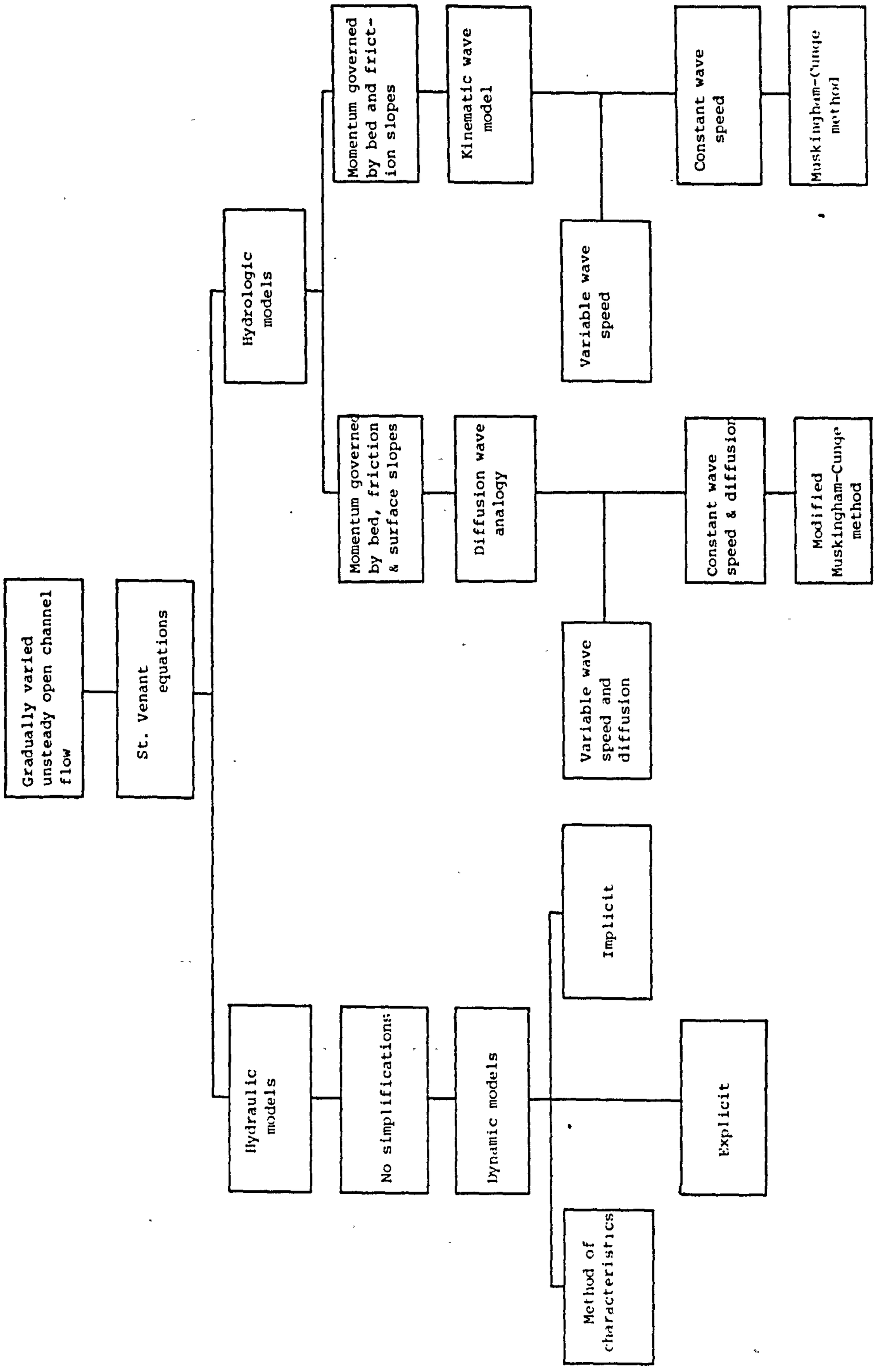

Figure 2.2 Techniques for solving the unsteady flow equations (after Jones, 1981)

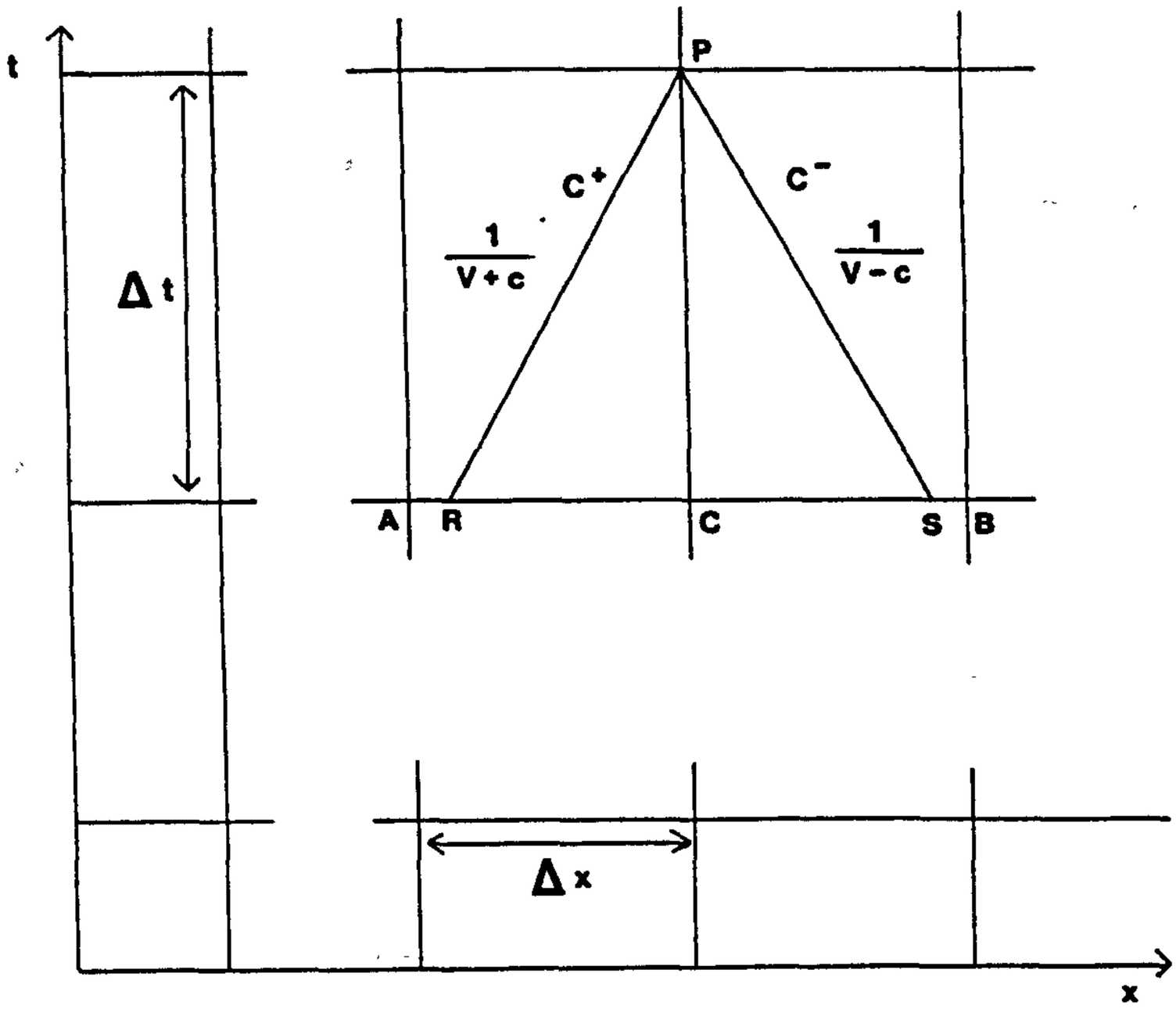

Figure 2.3 The rectangular grid for the method of characteristics

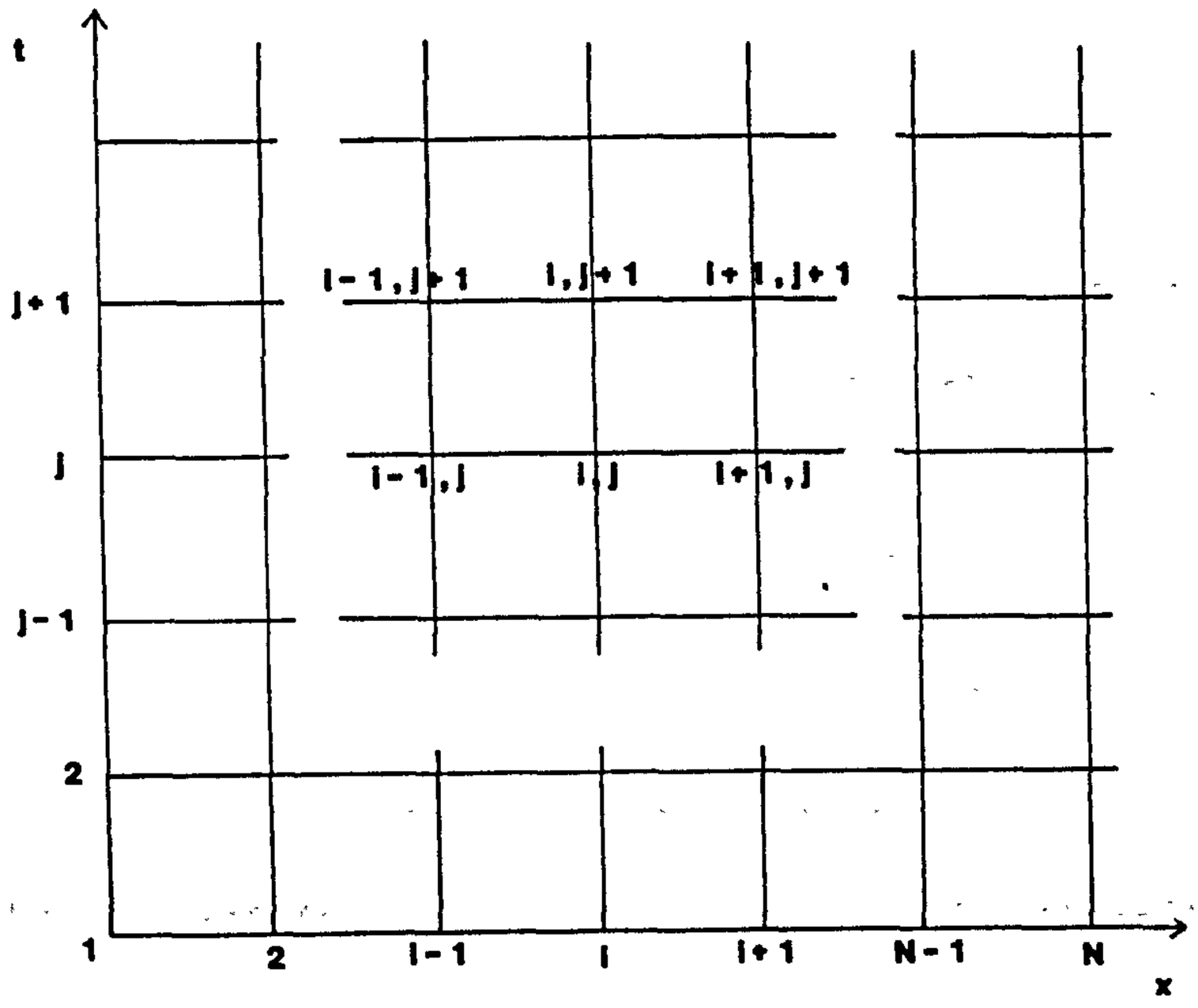

Figure 2.4 Computation grid for explicit and implicit schemes

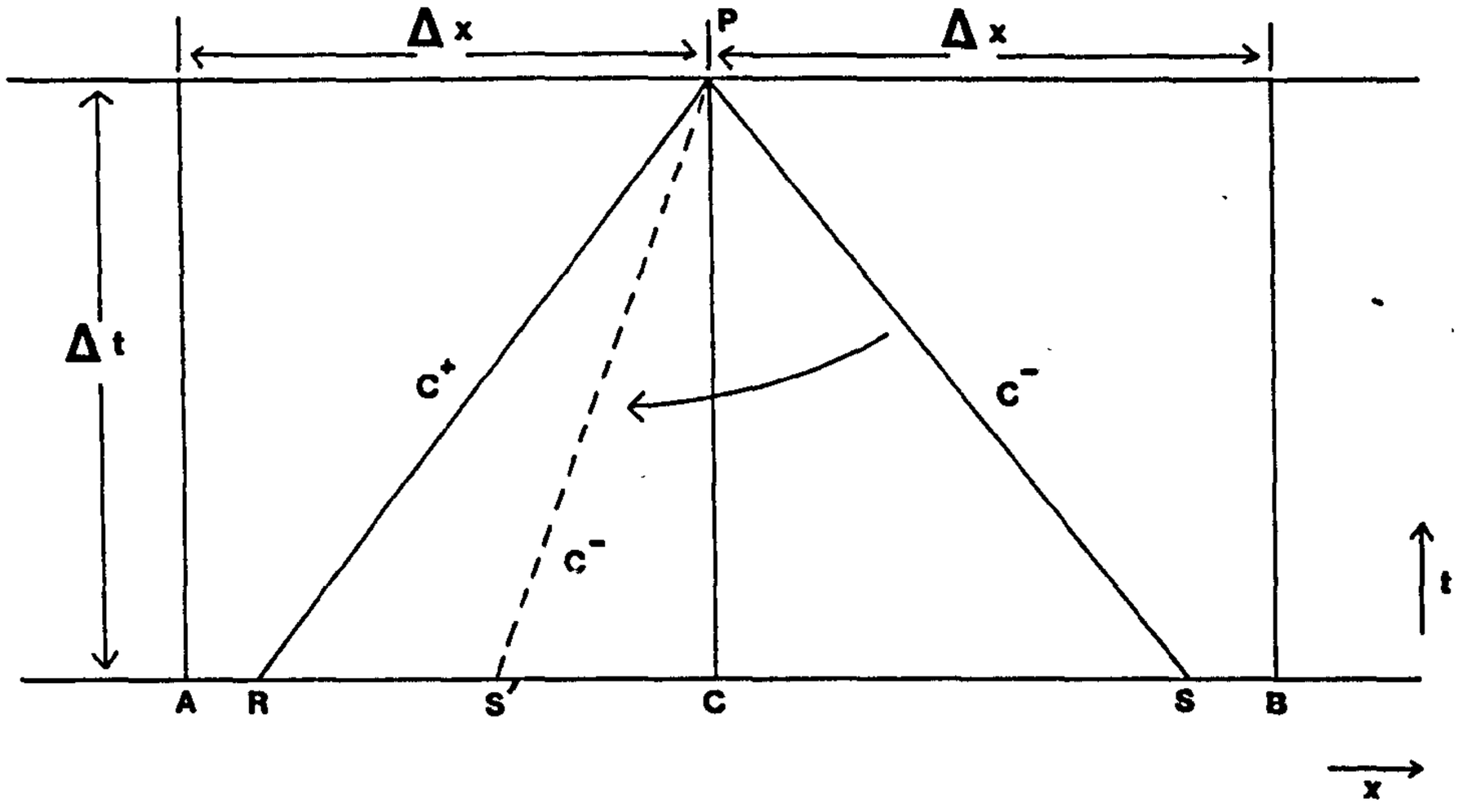

For subcritical flow(Froude number less than 1)

S lies in downstream section CB

For supercritical flow(Froude number greater than 1)

S′ lies in upstream section AC

Figure 4.1 The characteristic grid

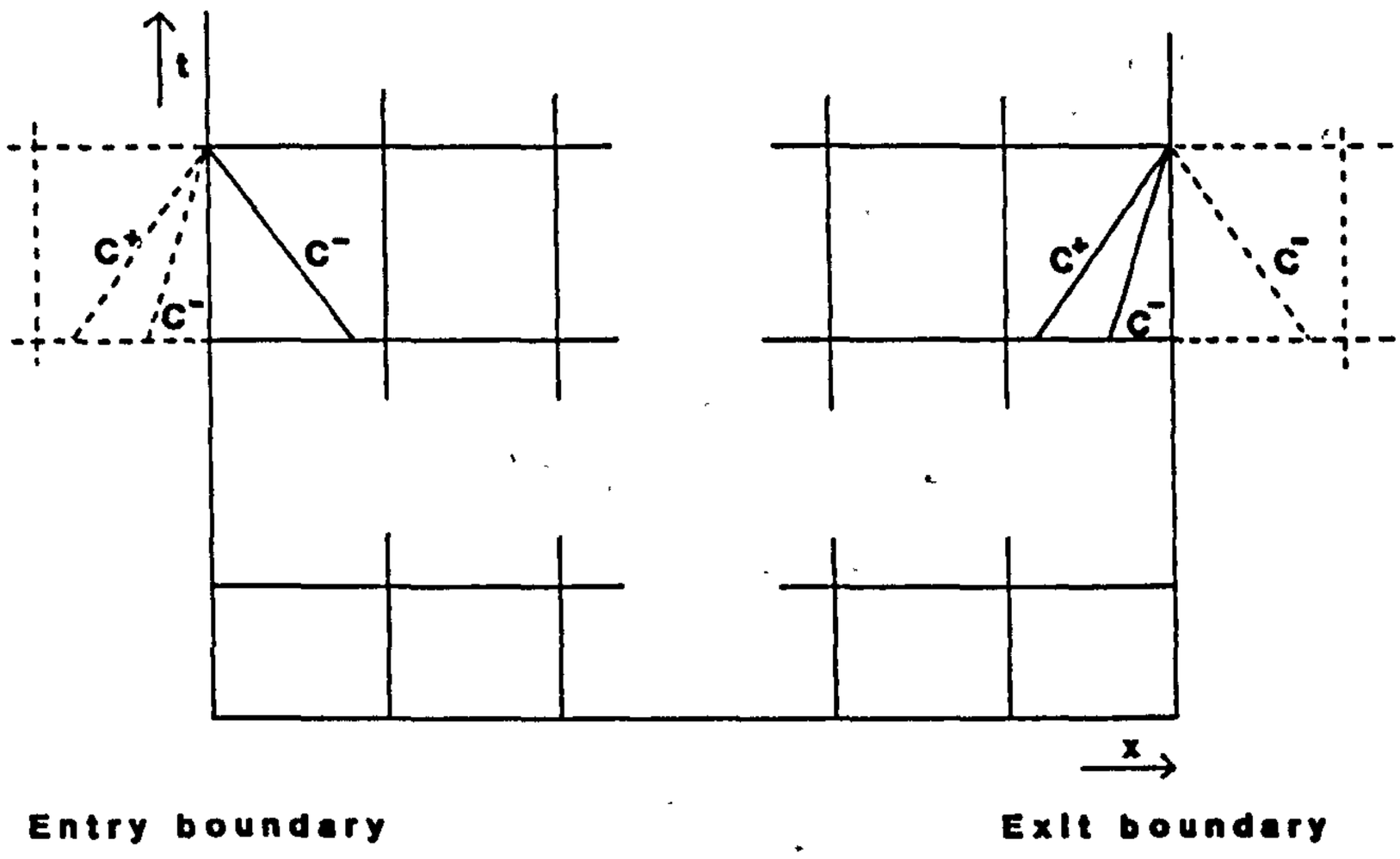

Figure 4.2 Subcritical and supercritical boundary conditions

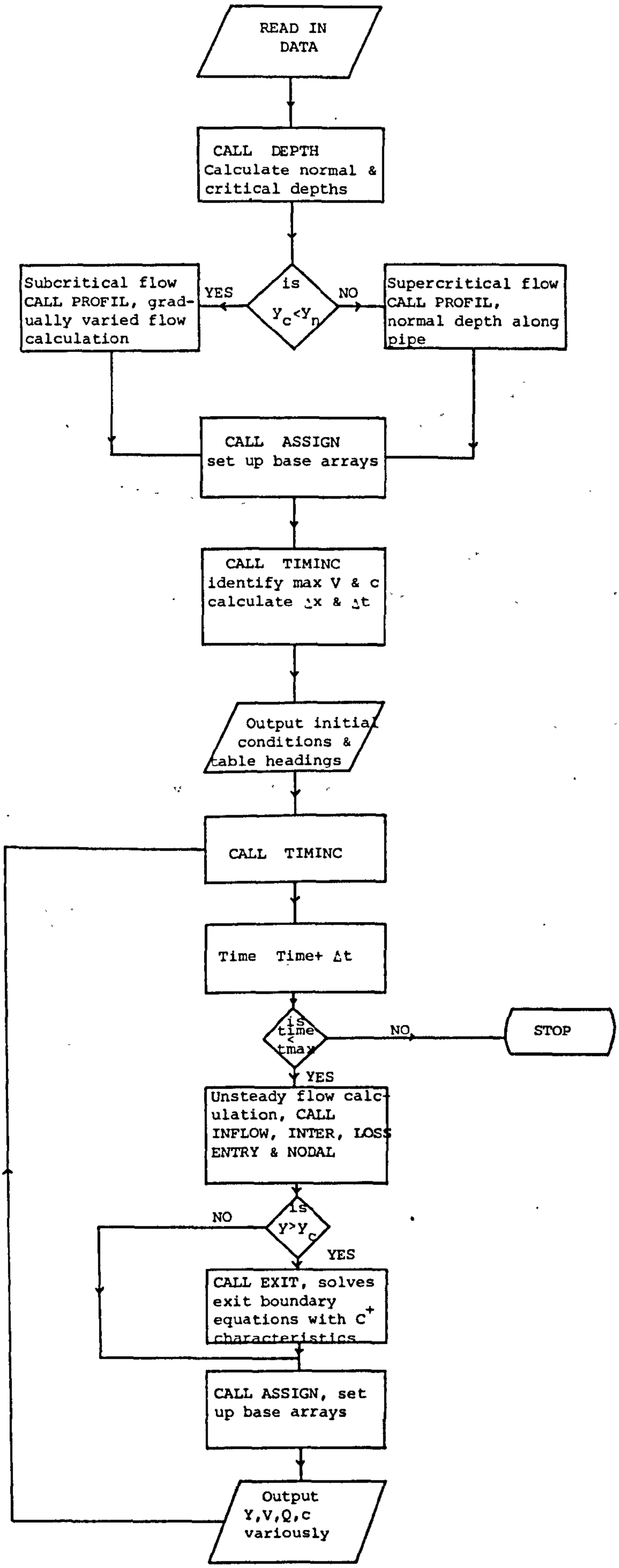

Figure 4.3 Flowchart for the single pipe program

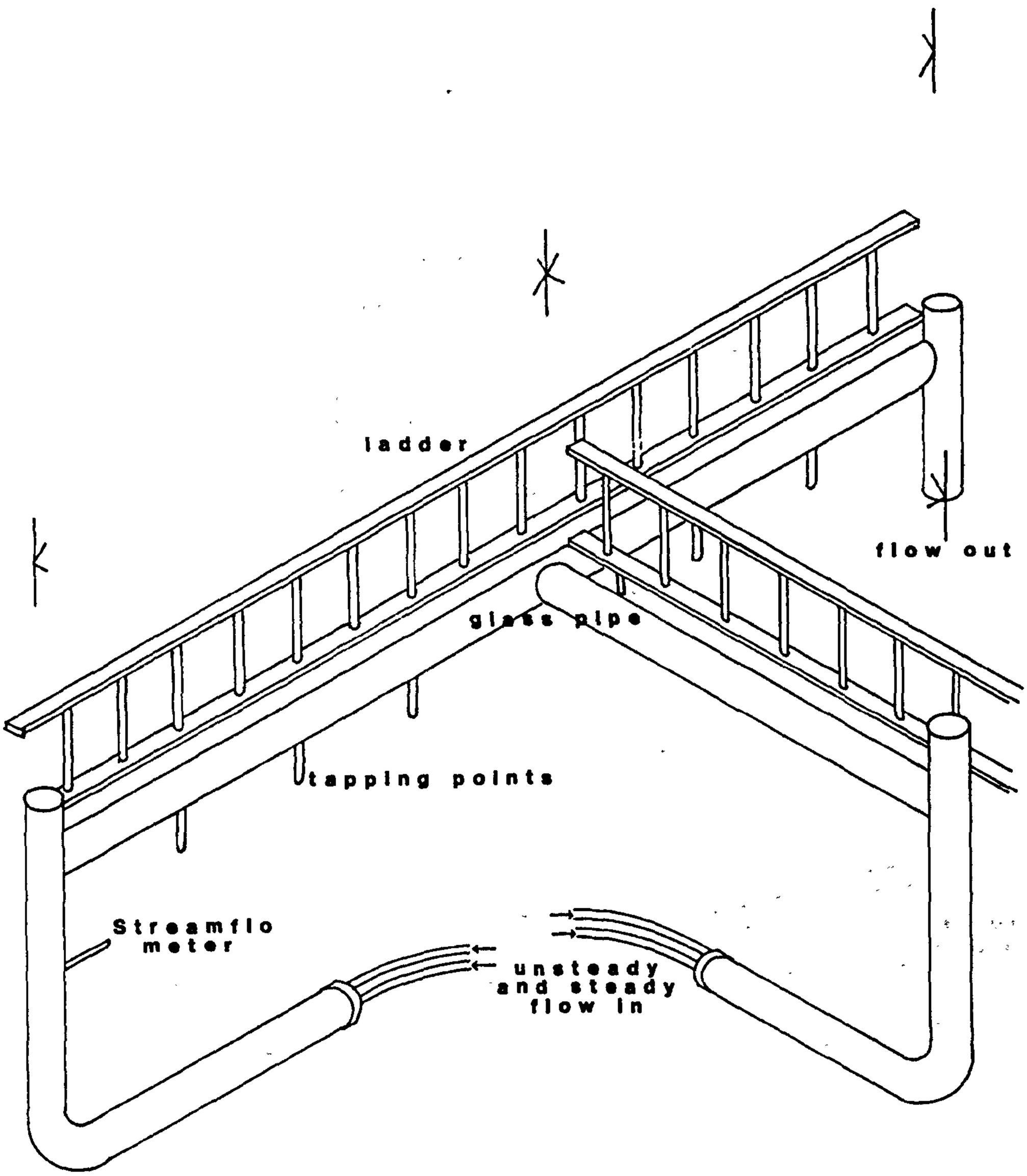

Figure 5.1 General layout of the test facility

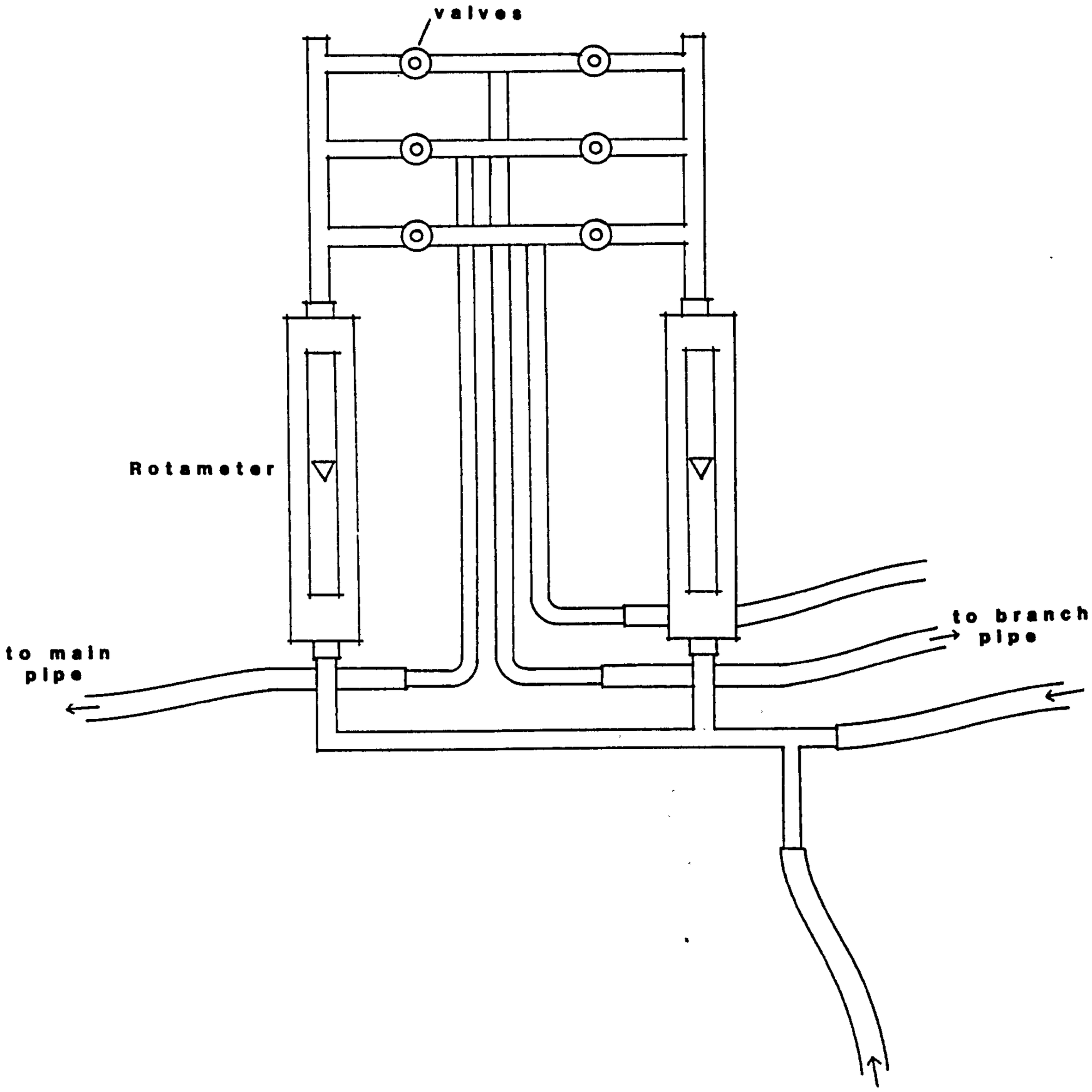

Figure 5.2 Steady flow supply system

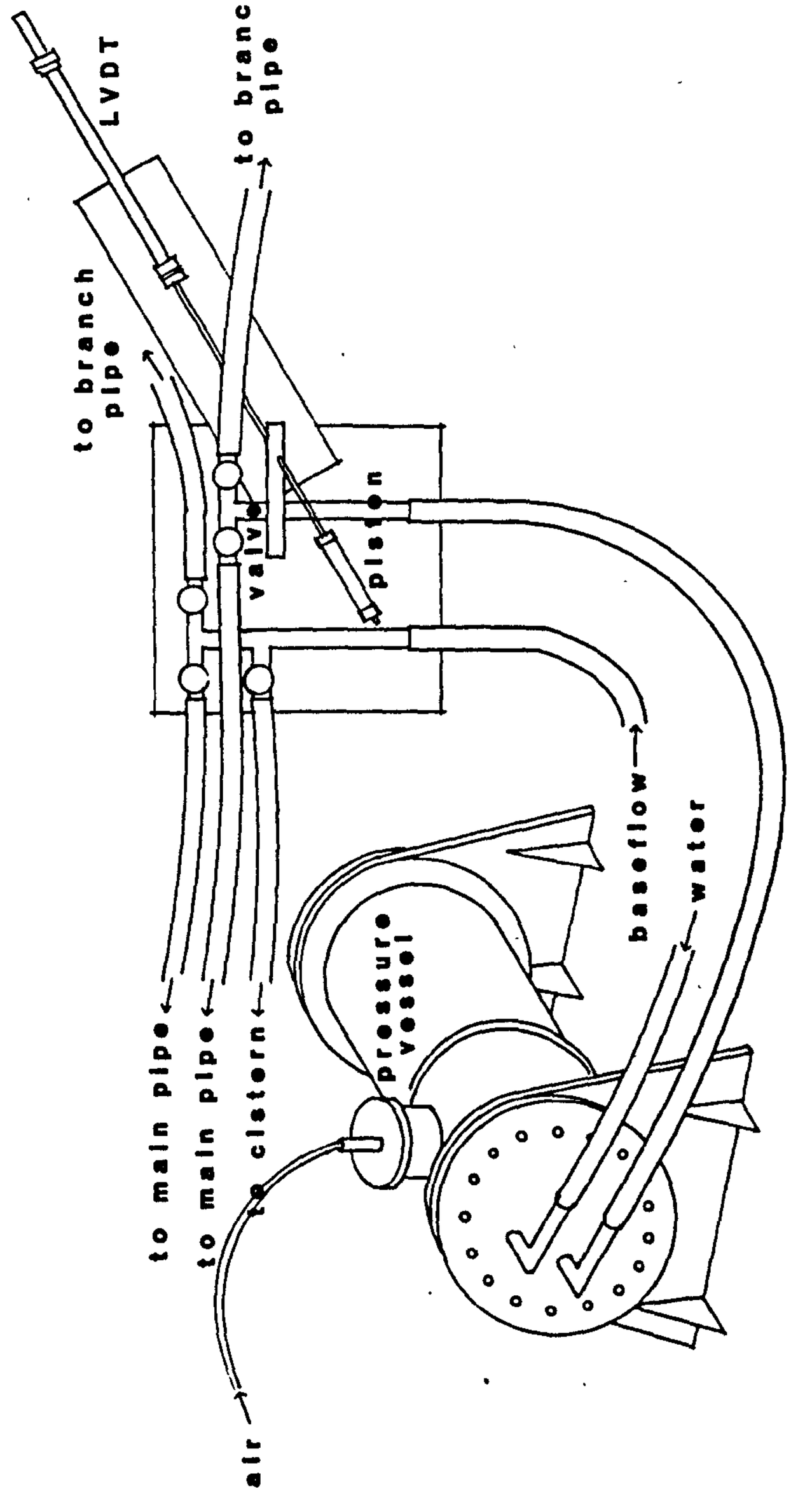

Figure 5.3 Unsteady flow supply system

Figure 5.4 Streamflo meter

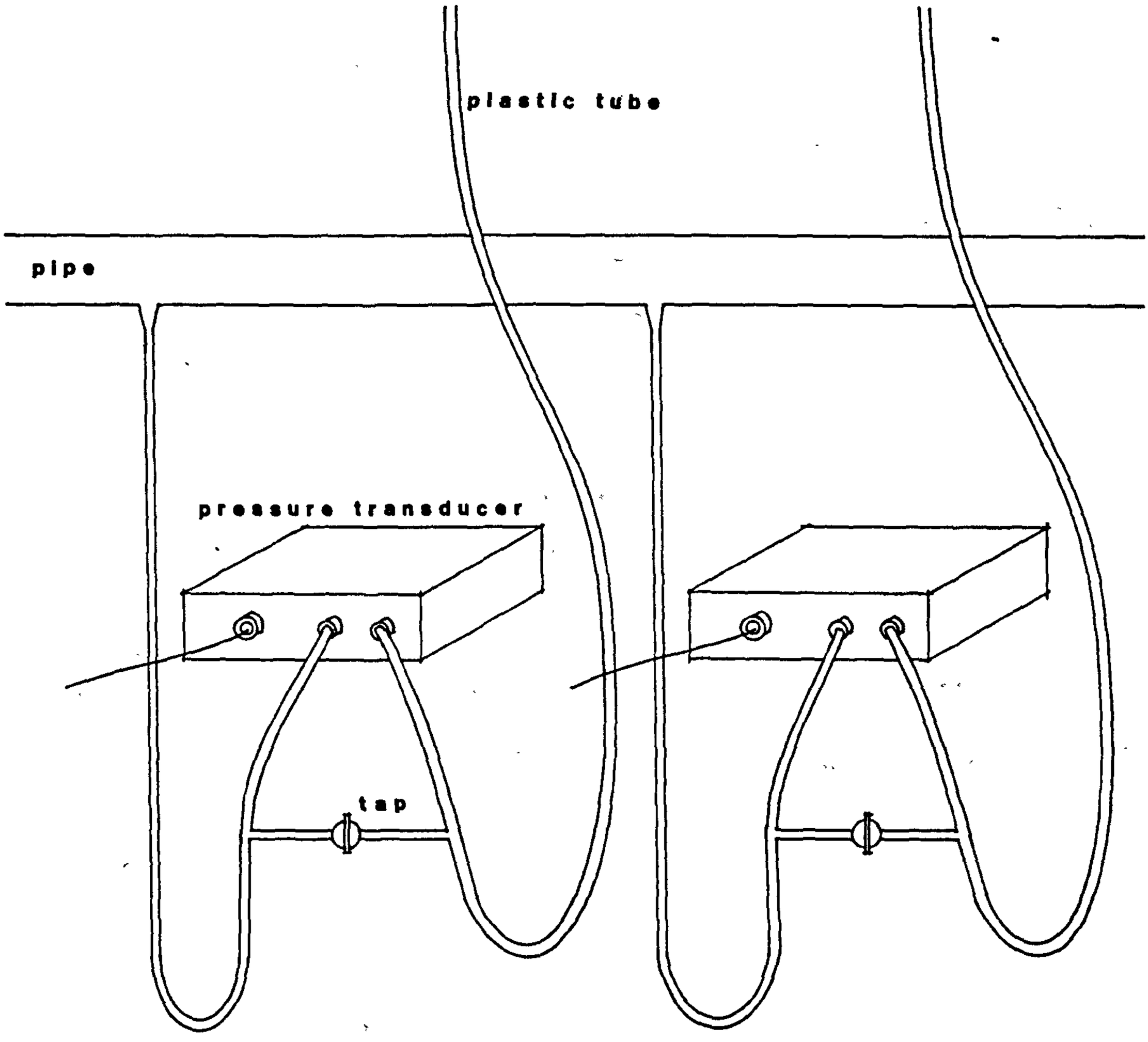

Figure 5.5 Pressure transducer system

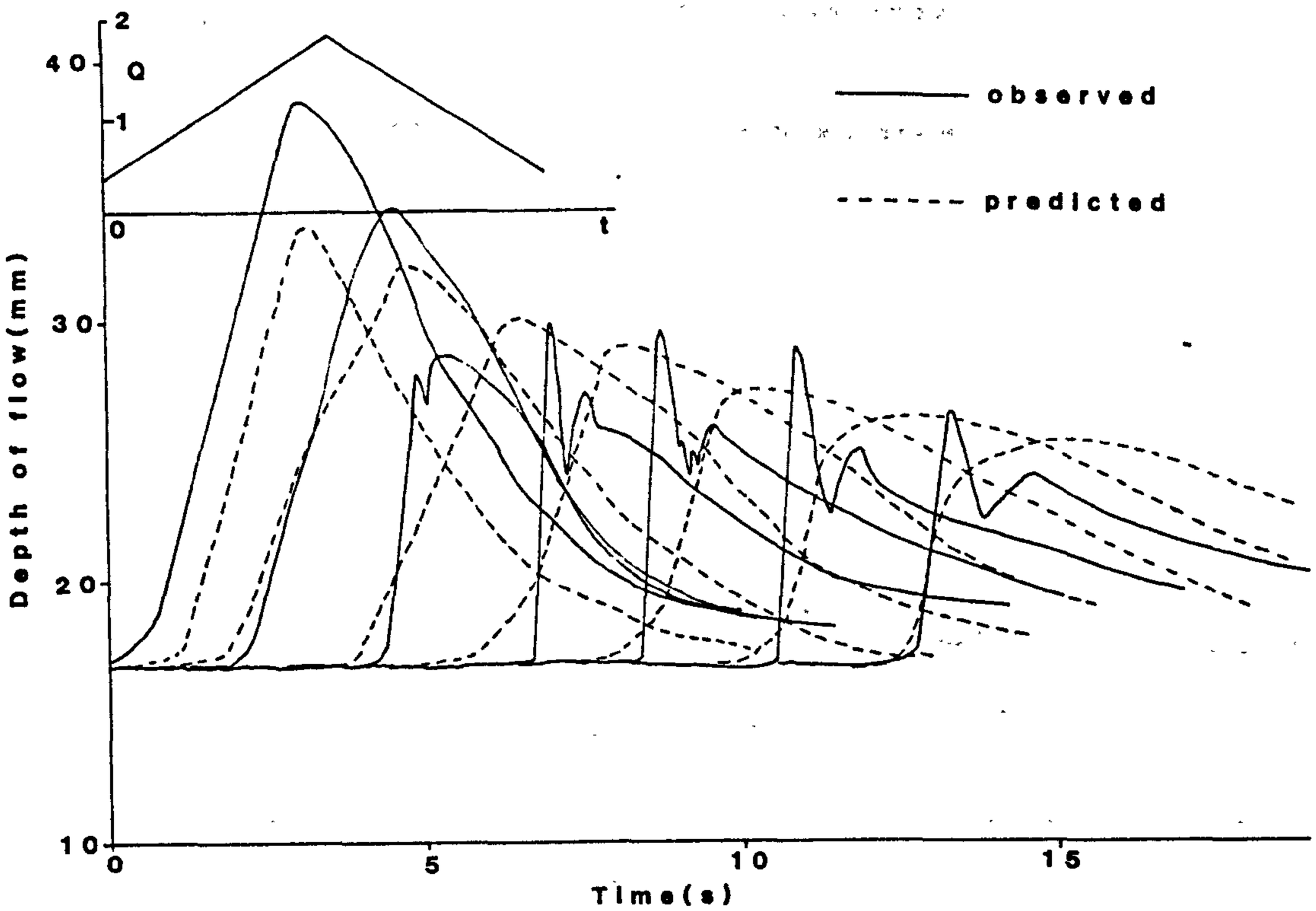

Figure 6.1 Comparison of observed and predicted depth profiles at a gradient of 1/100

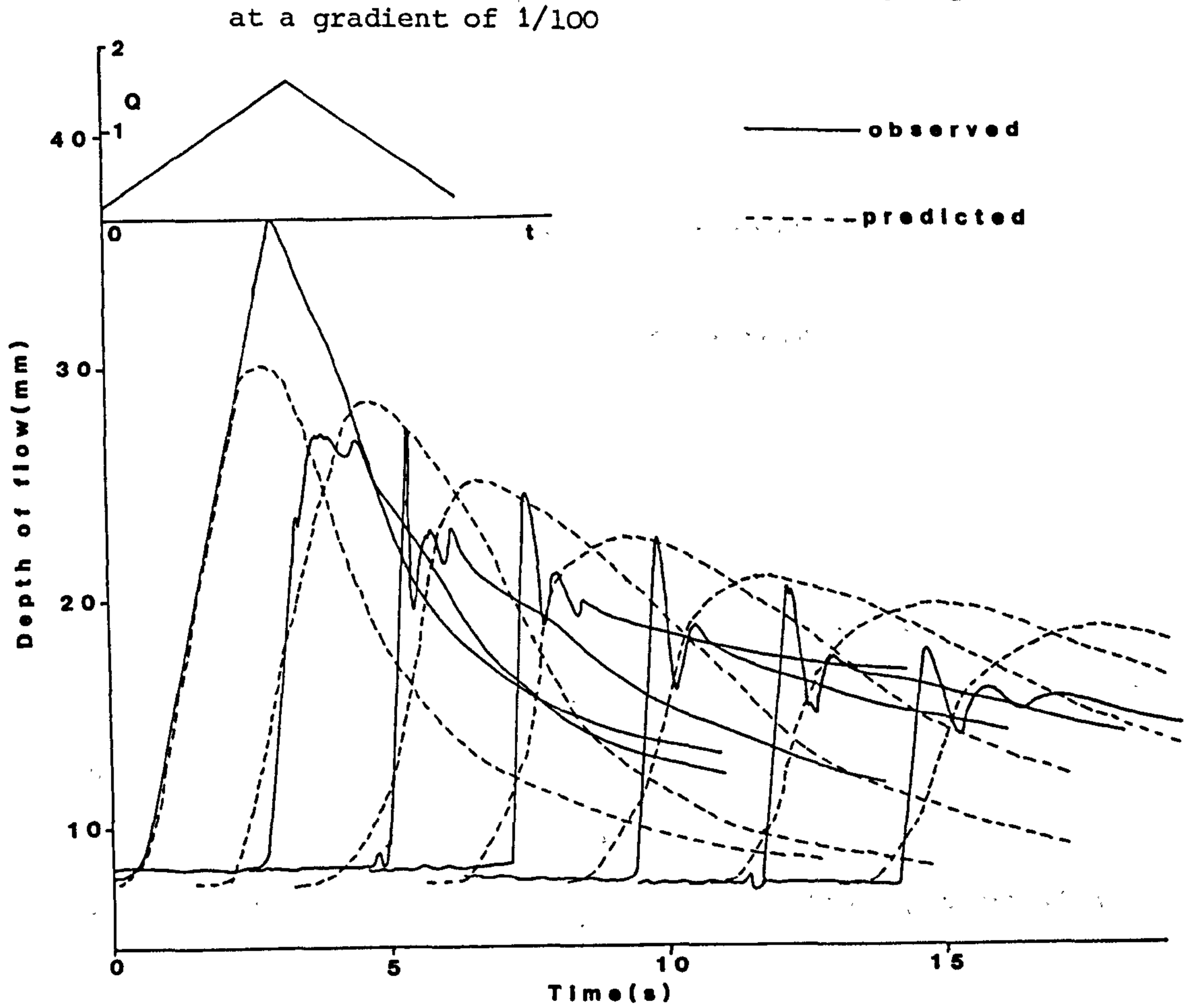

Figure 6.2 Comparison of observed and predicted depth profiles at a gradient of 1/100

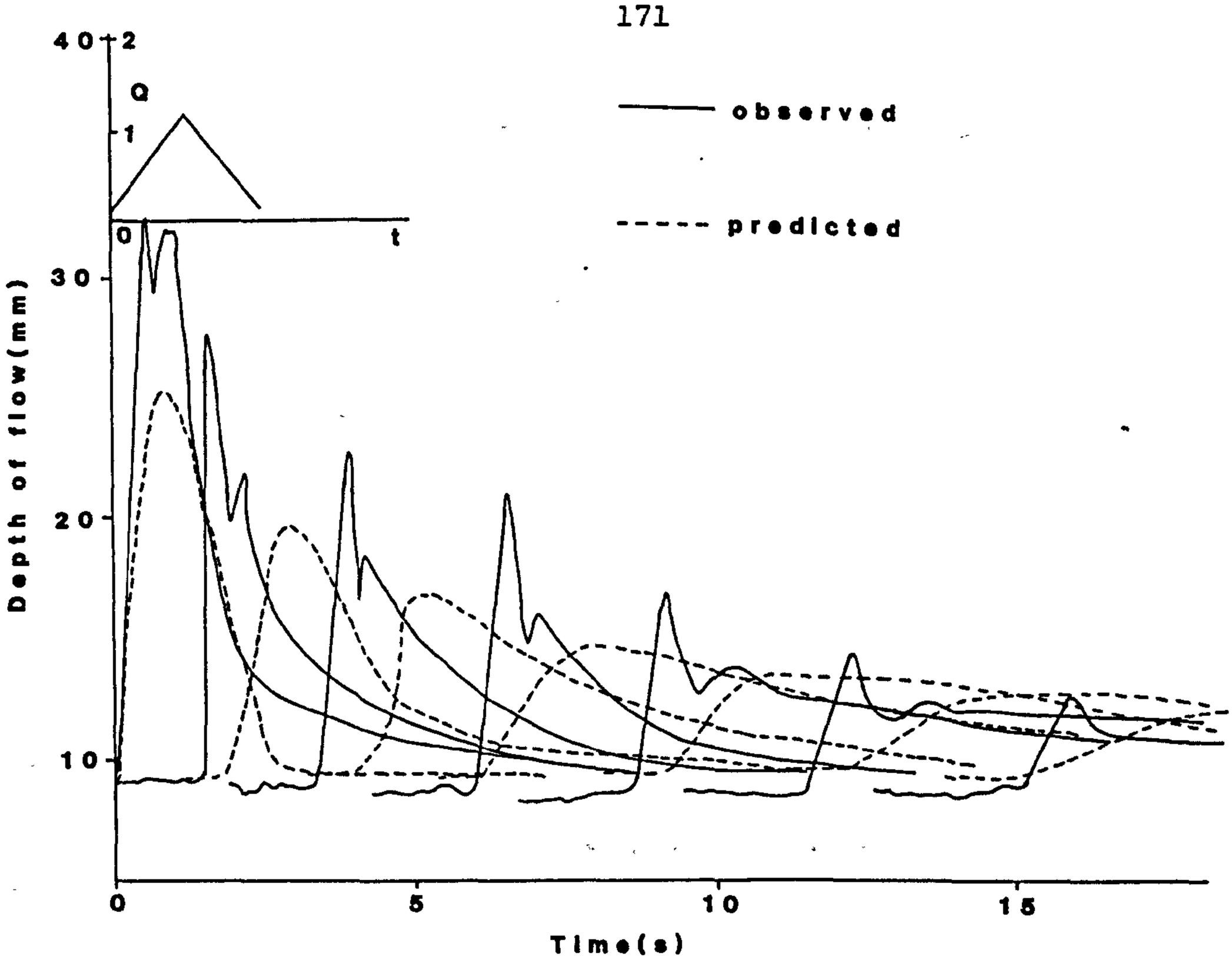

Figure 6.3 Comparison of observed and predicted depth profiles at a gradient of 1/150

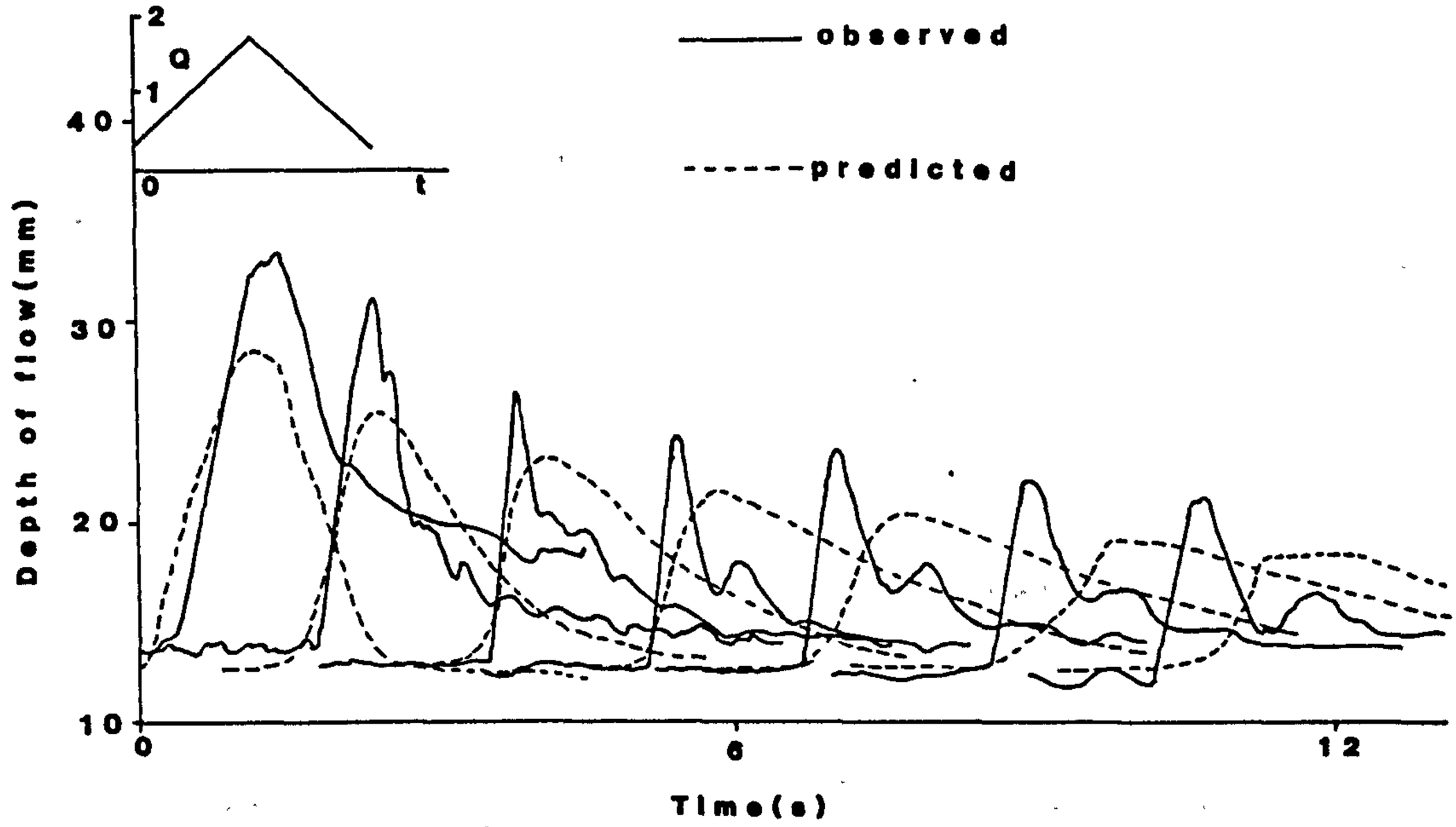

Figure 6.4 Comparison of observed and predicted depth profiles at a gradient of 1/60

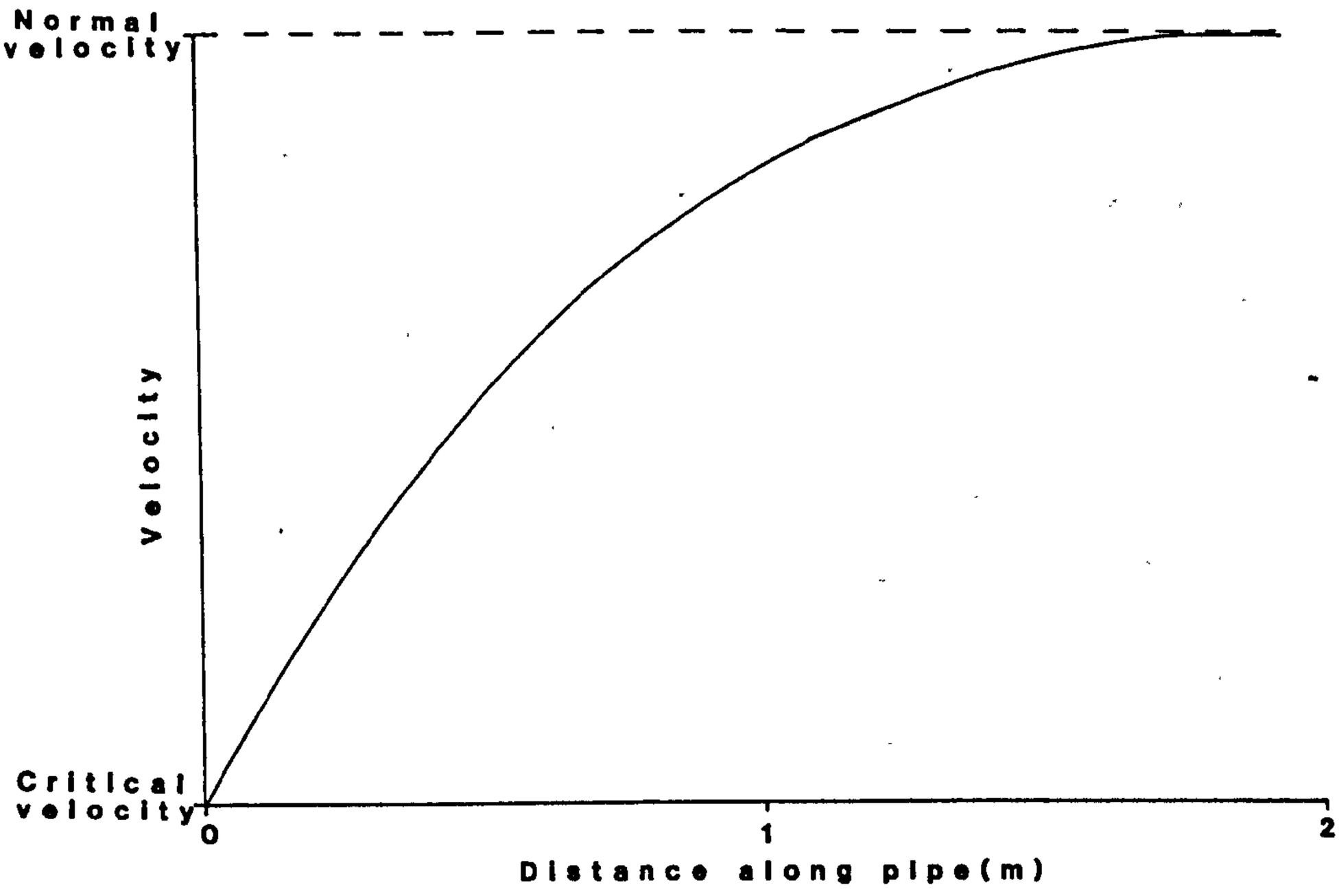

Figure 6.5 Velocity near the entry boundary

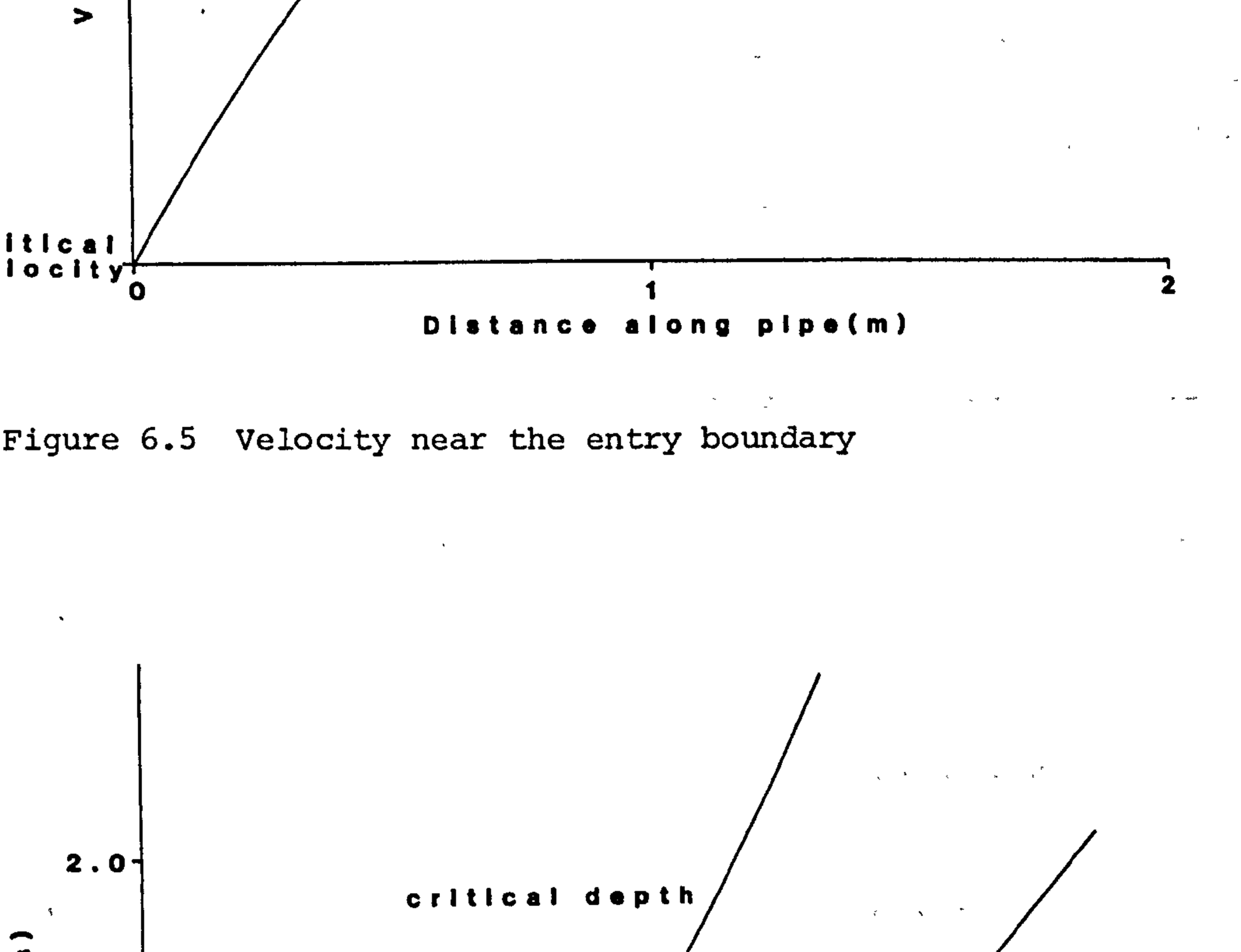

Figure 6.6 Observed depth and critical depth versus flow rate

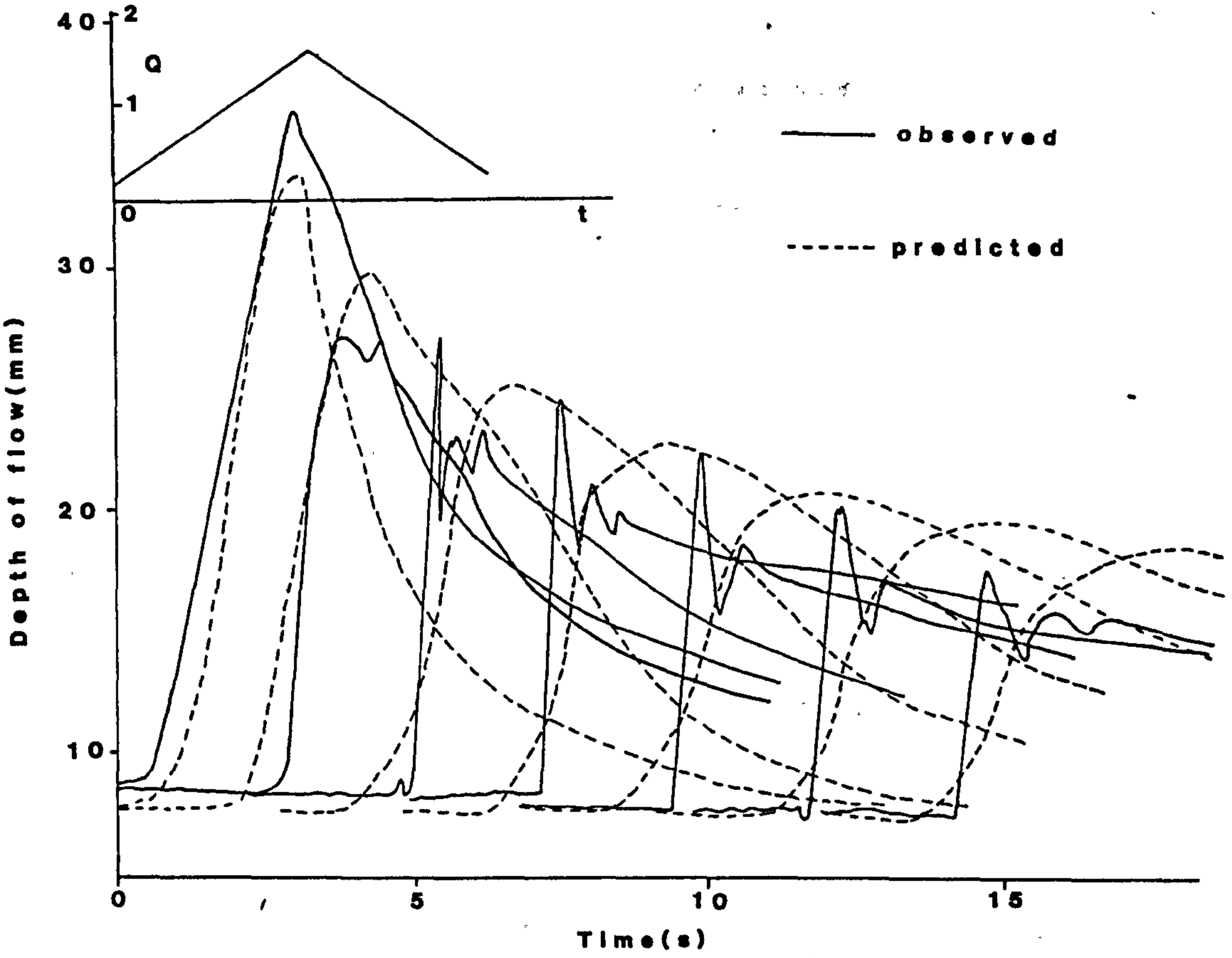

Figure 6.7 Comparison of observed and predicted depth profiles using critical depth at entry

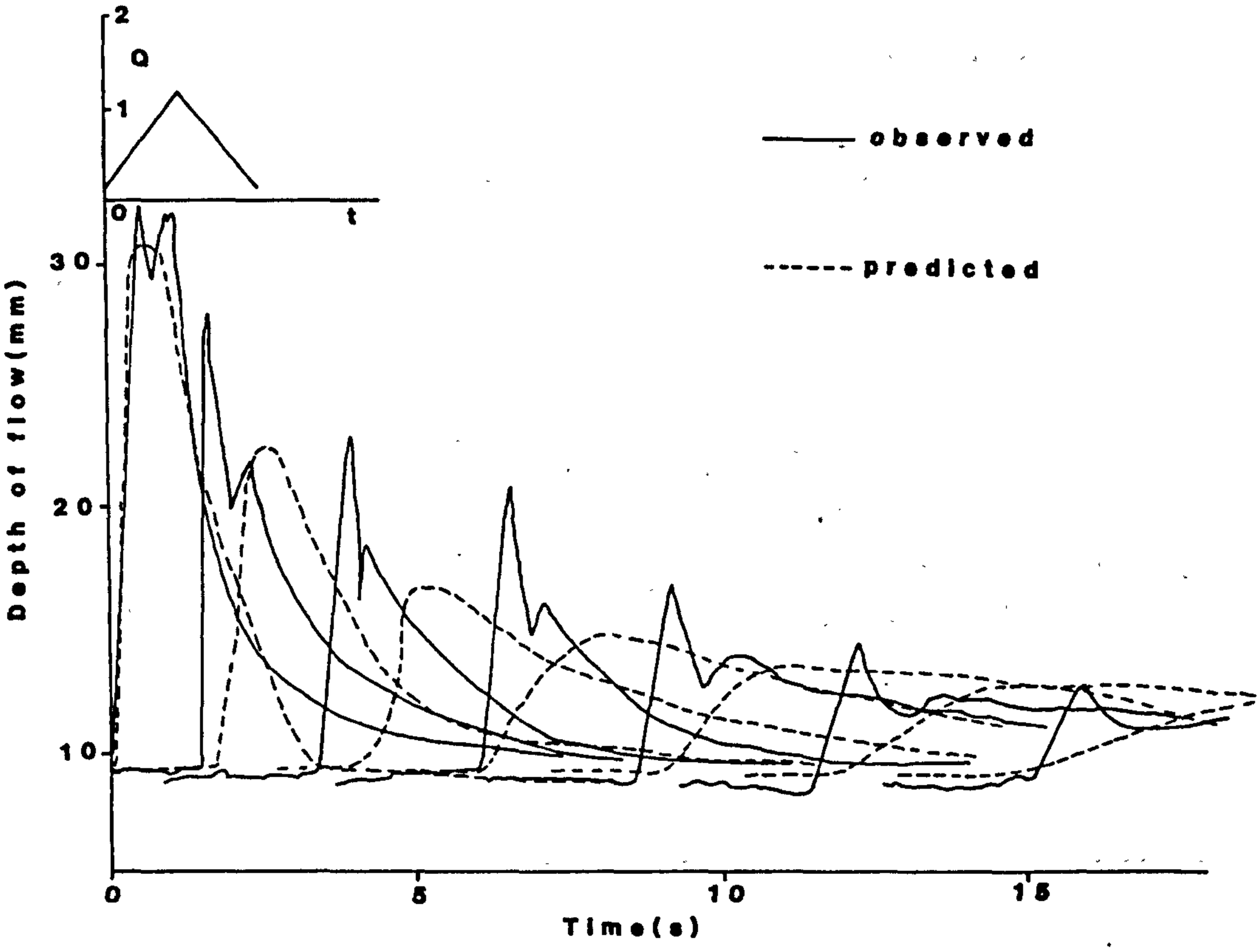

Figure 6.8 Comparison of observed and predicted depth profiles using critical depth at entry

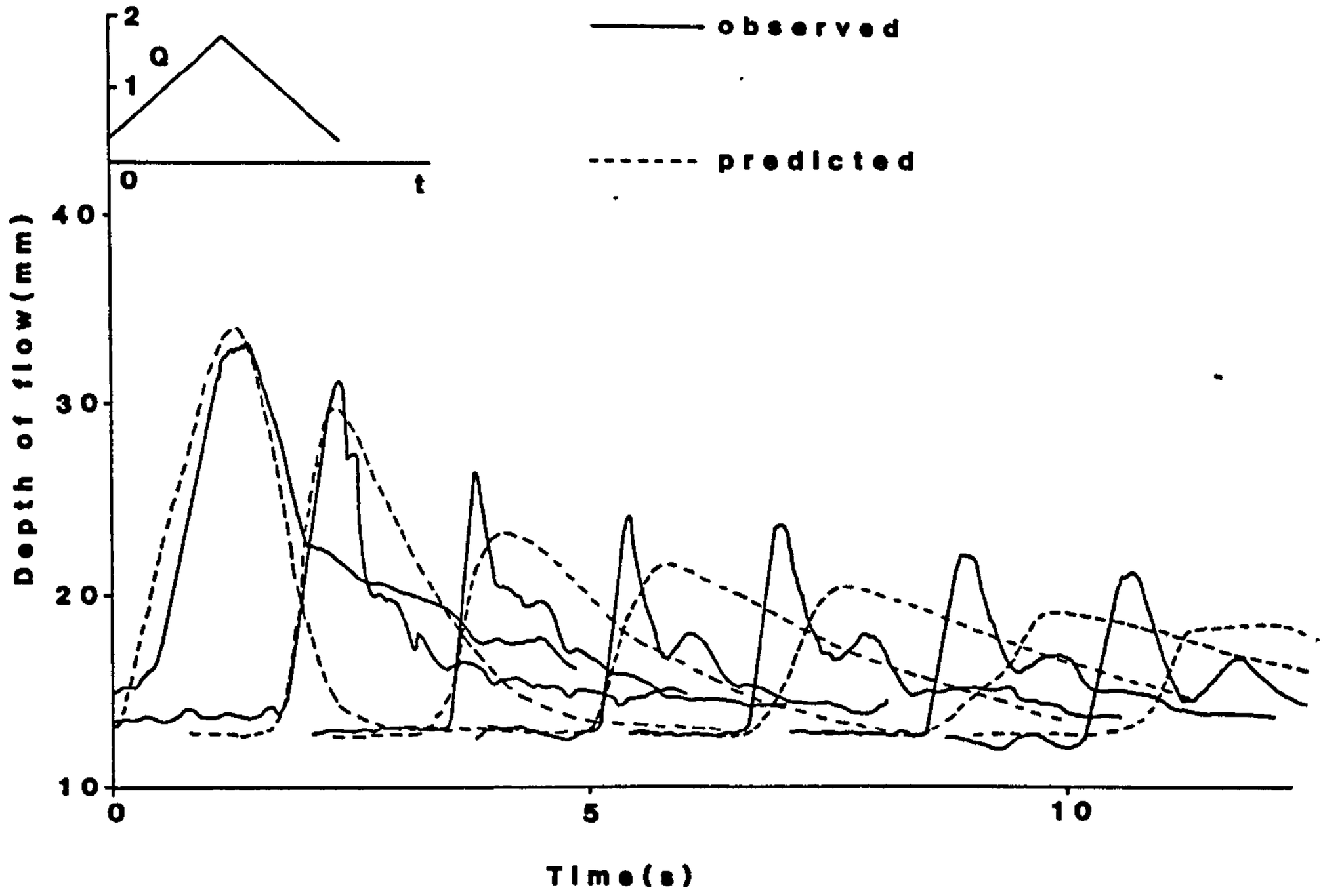

Figure 6.9 Comparison of observed and predicted depth profiles using subcritical depth at entry

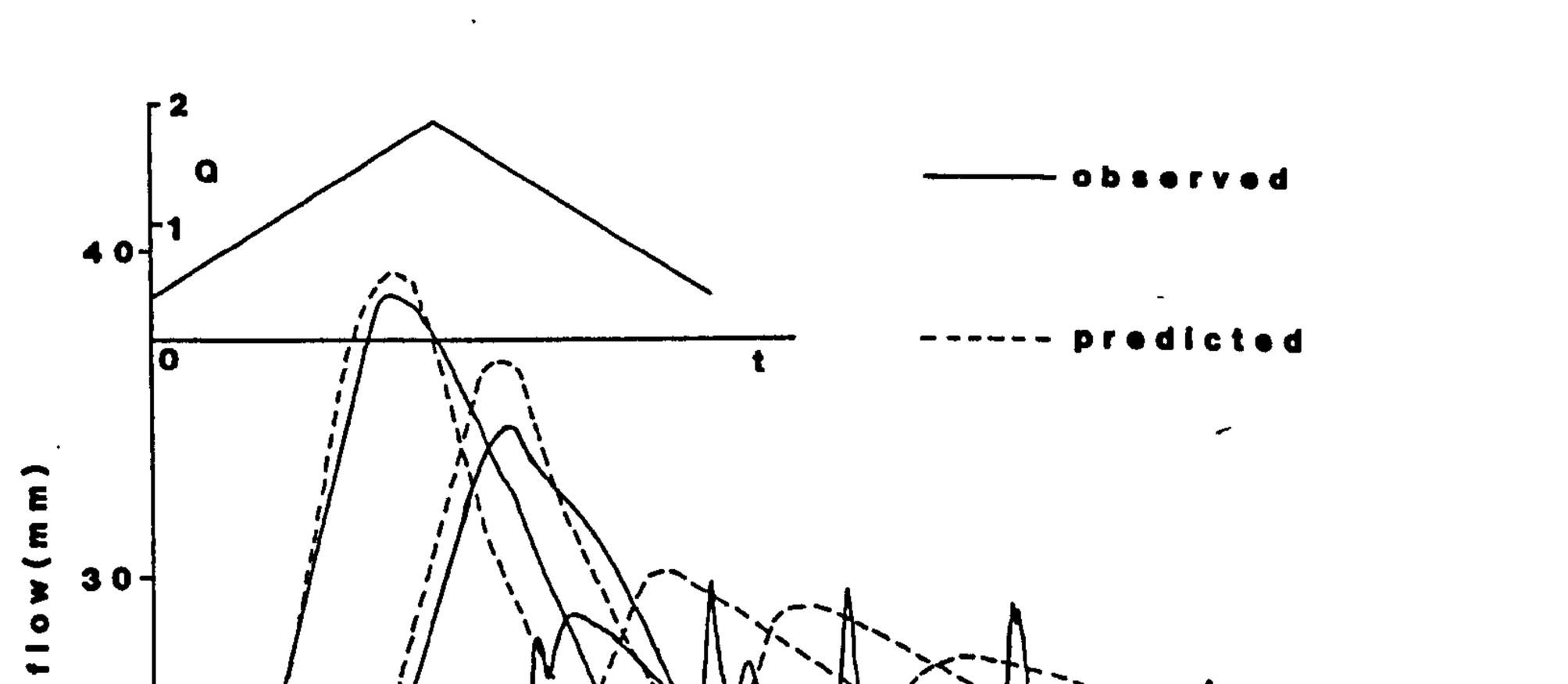

Figure 6.10 Comparison of observed and predicted depth profiles using subcritical depth at entry

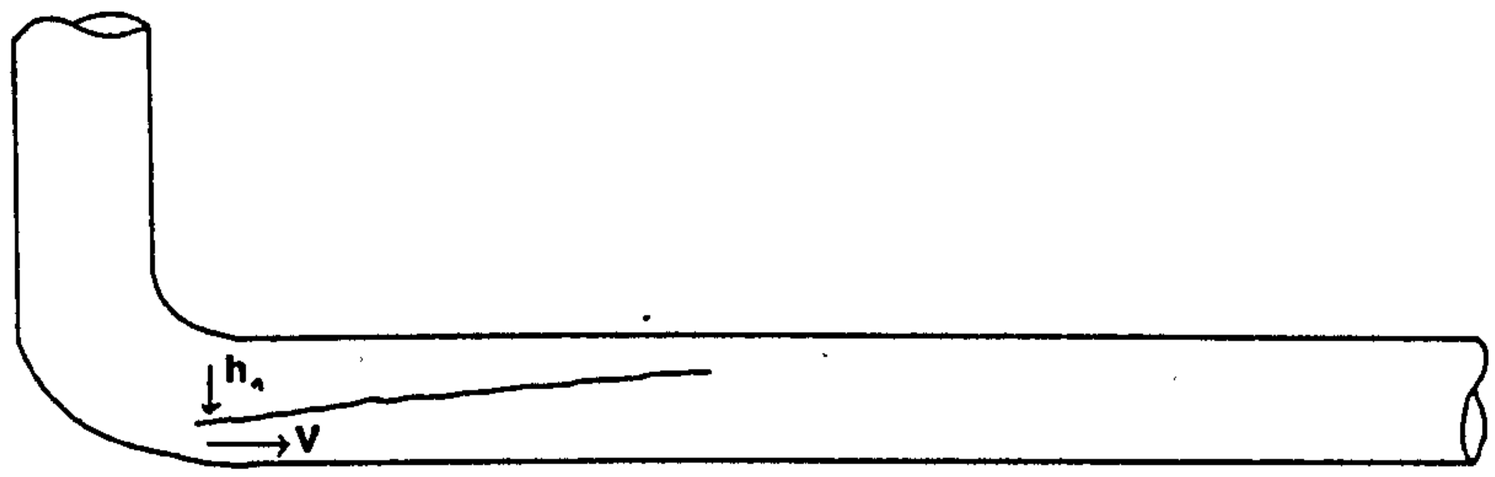

Figure 6.11 Alternative entry boundary condition

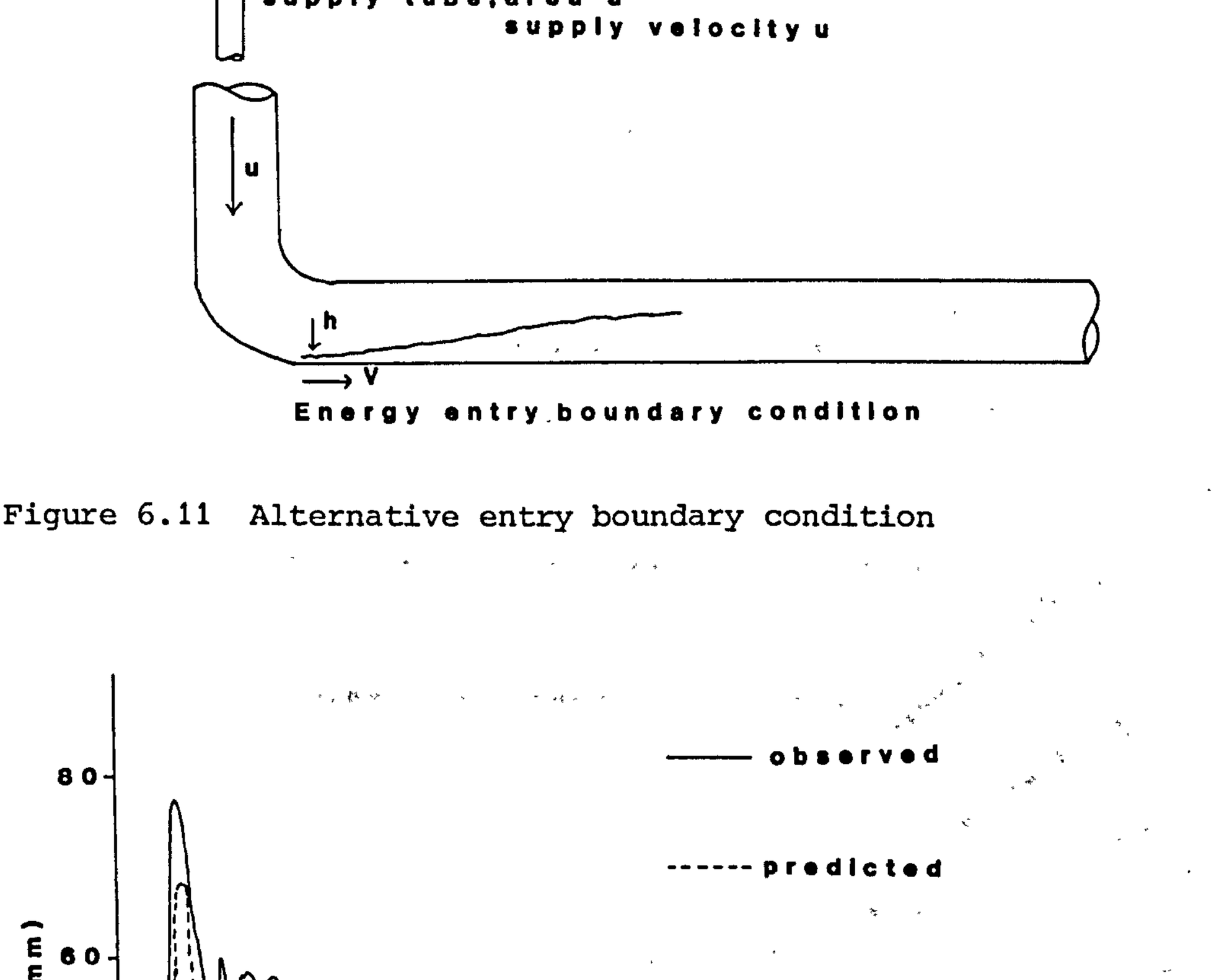

Figure 6.12 Comparison of observed and predicted depth profiles with the energy entry boundary condition

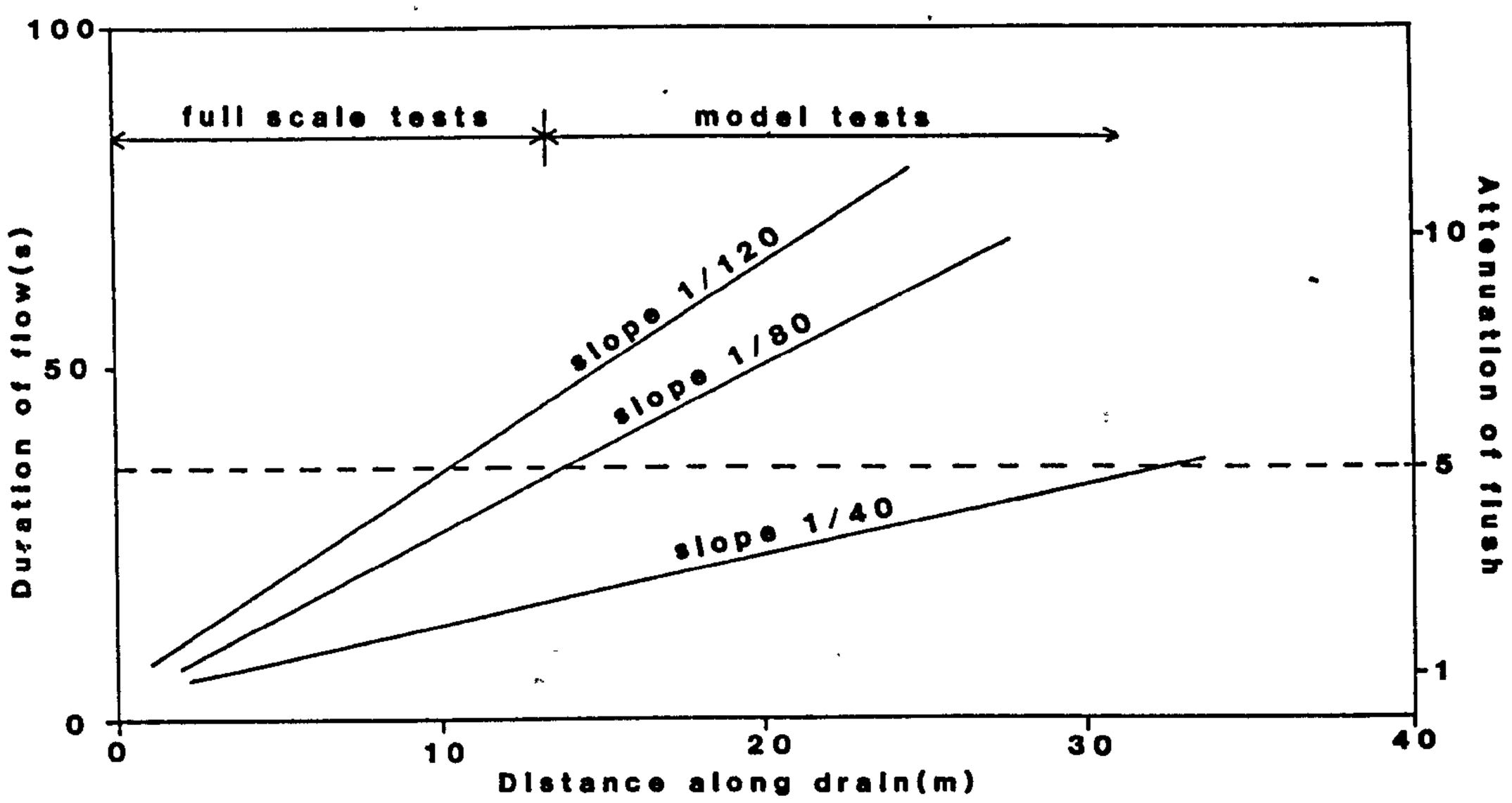

Figure 6.13 Study of the attenuation of flush in relation to length of pipe (after Burberry, 1978)

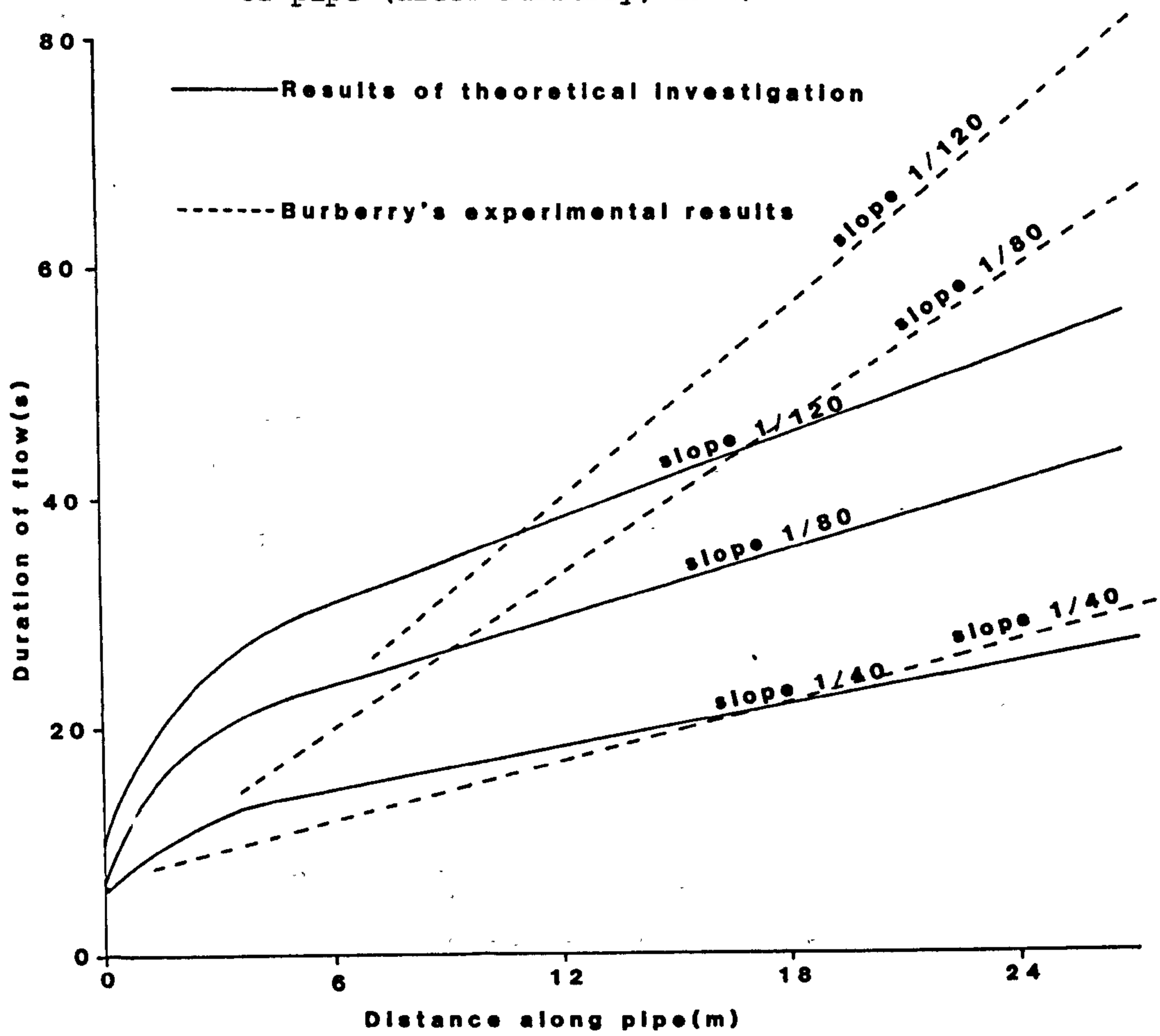

Figure 6.14 Theoretical investigation of the relationship between attenuation of flush and length of pipe

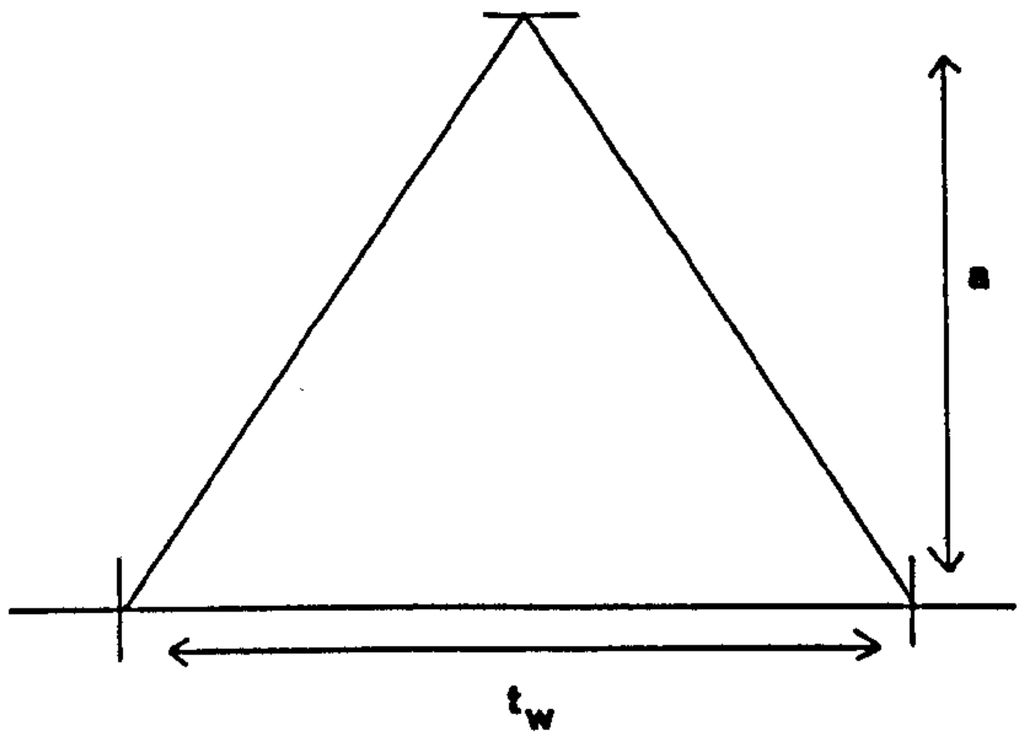

Figure 7.1 Definition of wave parameters

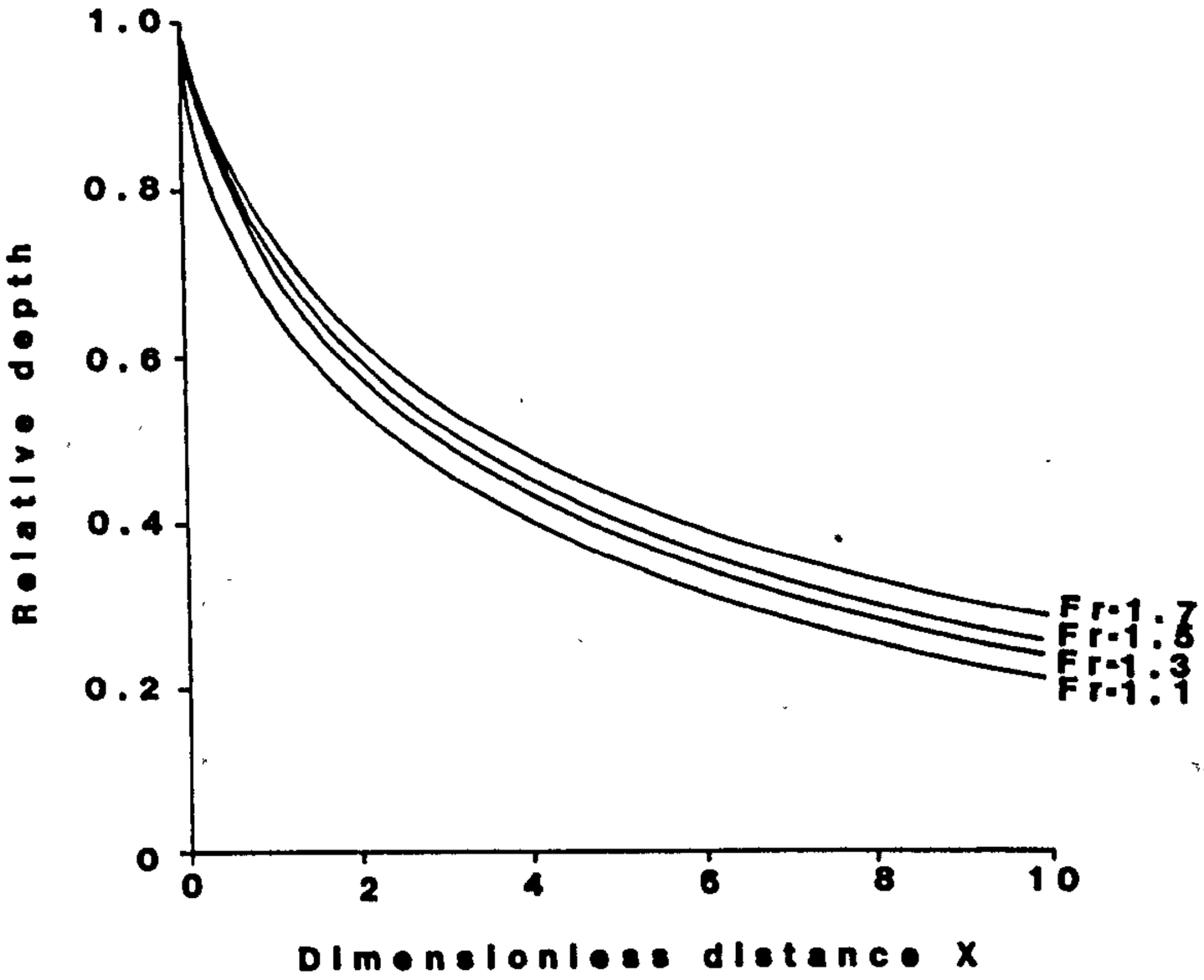

Figure 7.2 Effect of Froude number on wave attenuation

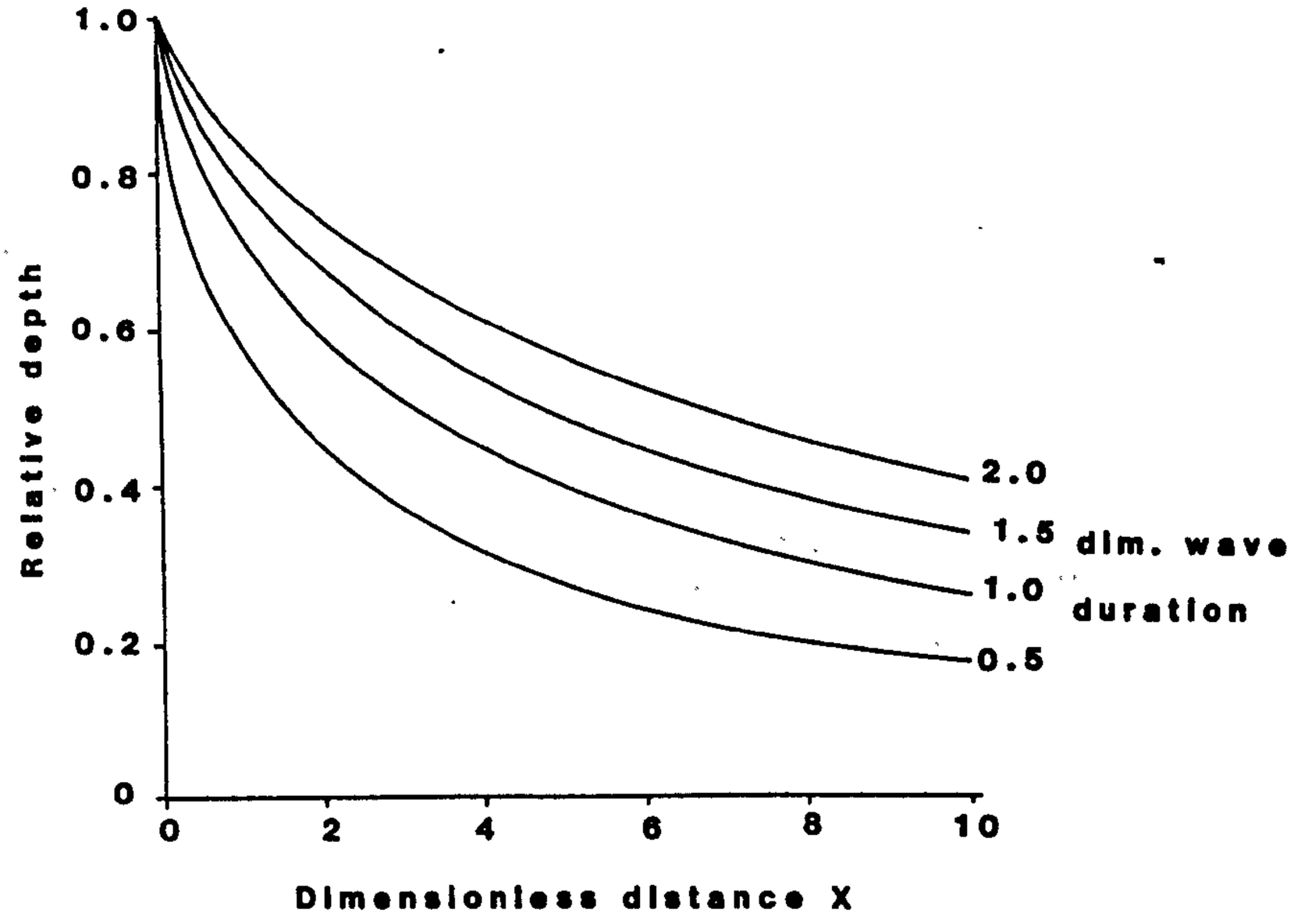

Figure 7.3 Effect of wave duration on wave attenuation

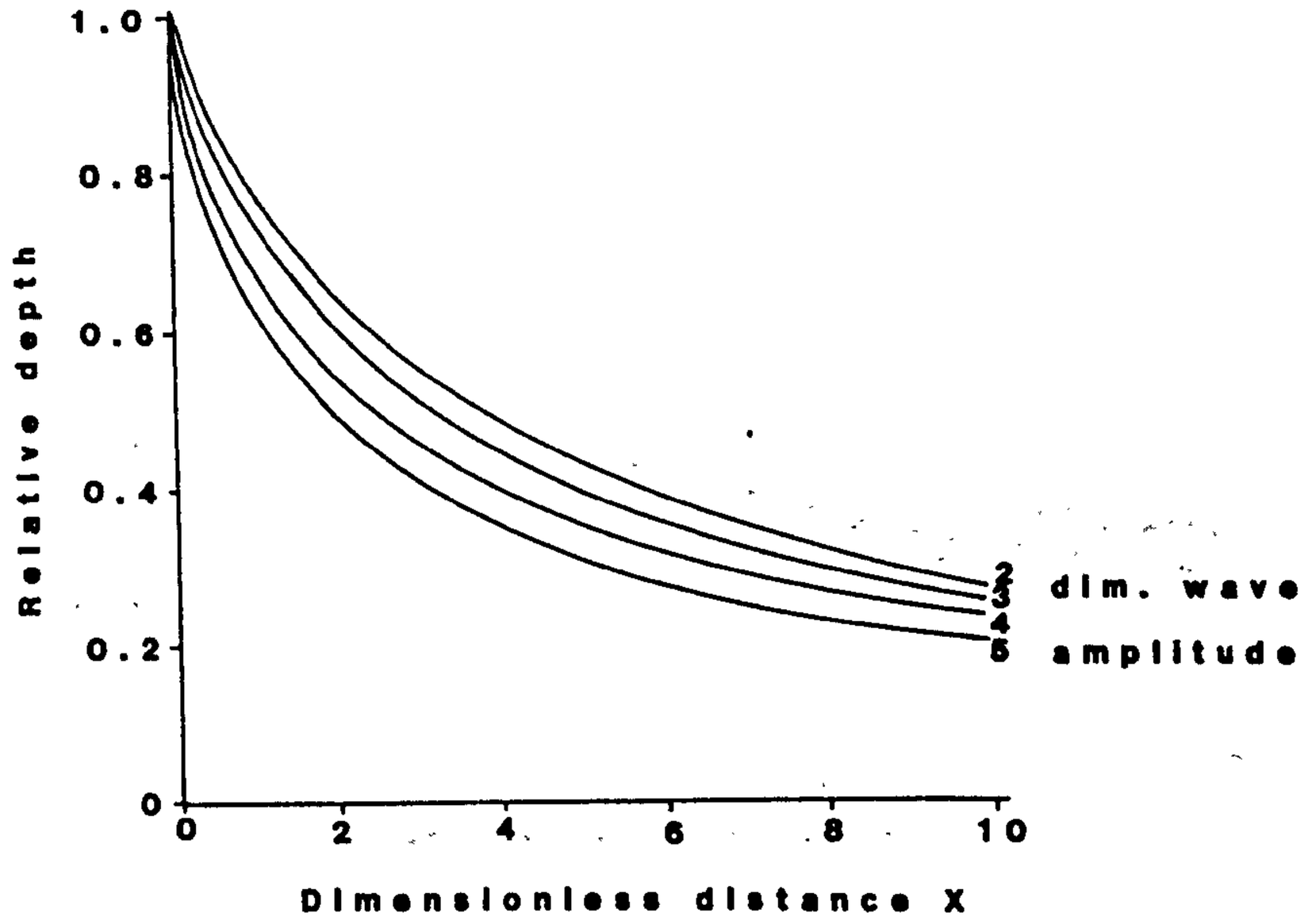

Figure 7.4 Effect of wave amplitude on wave attenuation

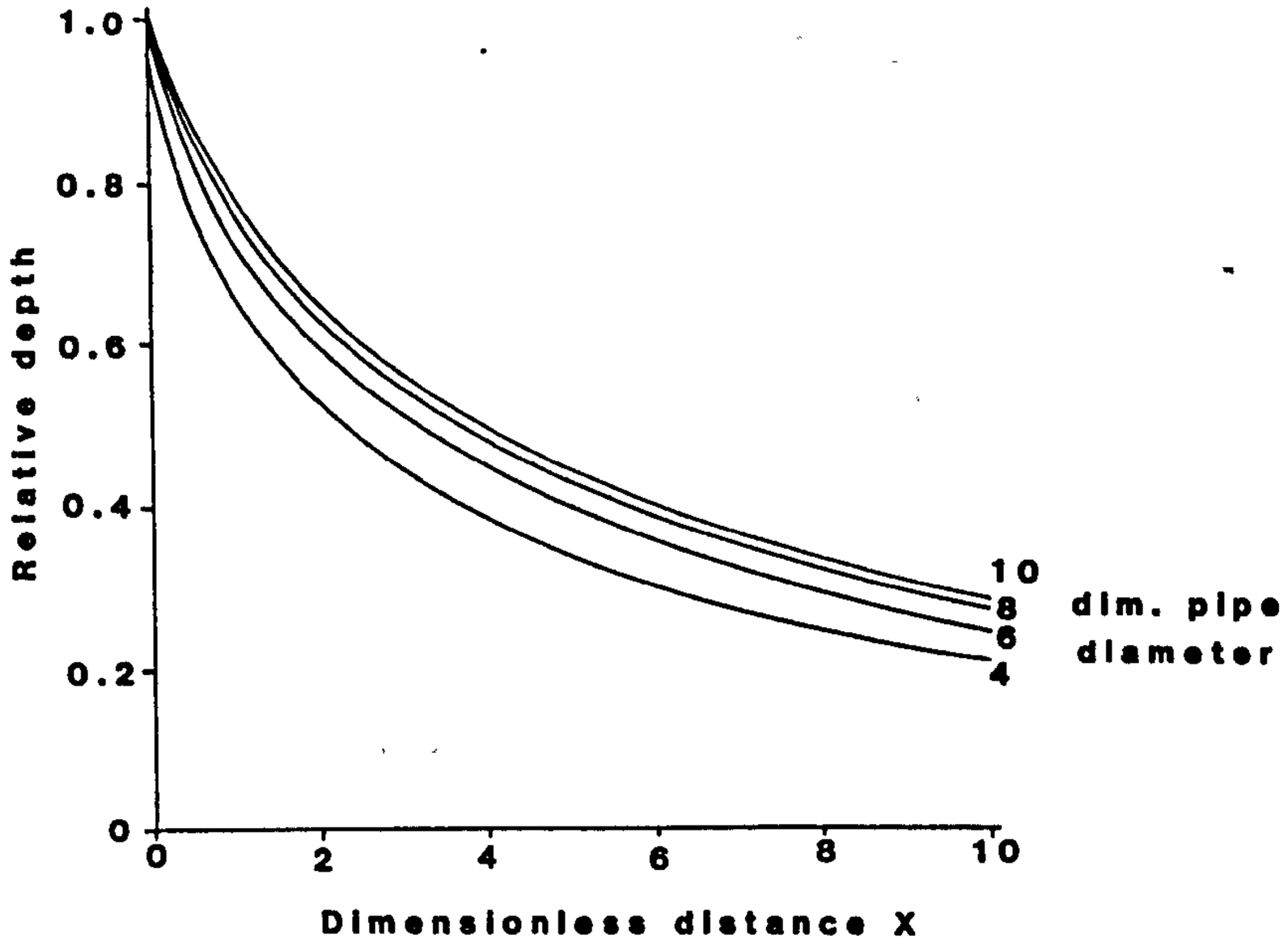

Figure 7.5 Effect of pipe diameter on wave attenuation

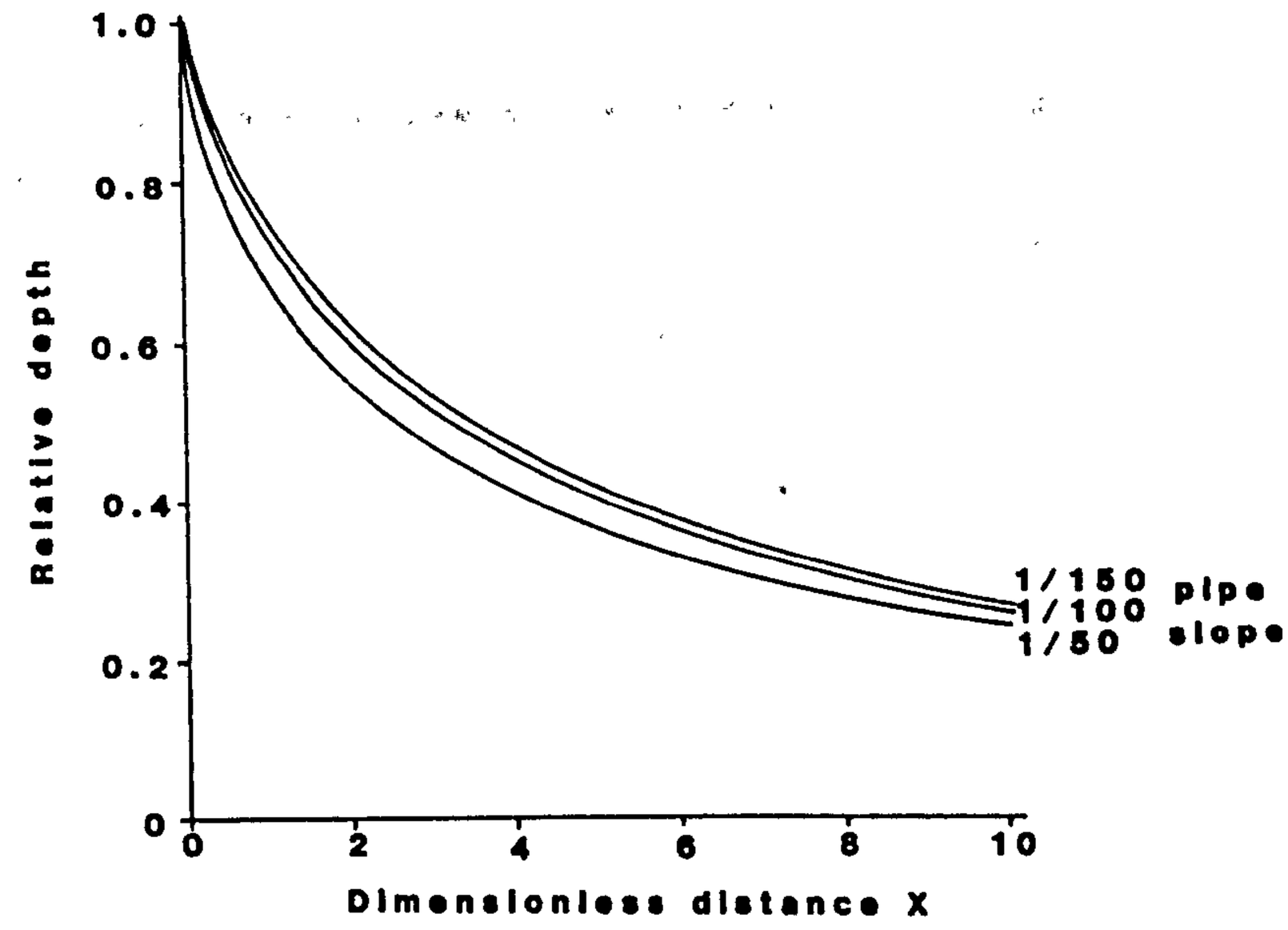

Figure 7.6 Effect of pipe slope on wave attenuation

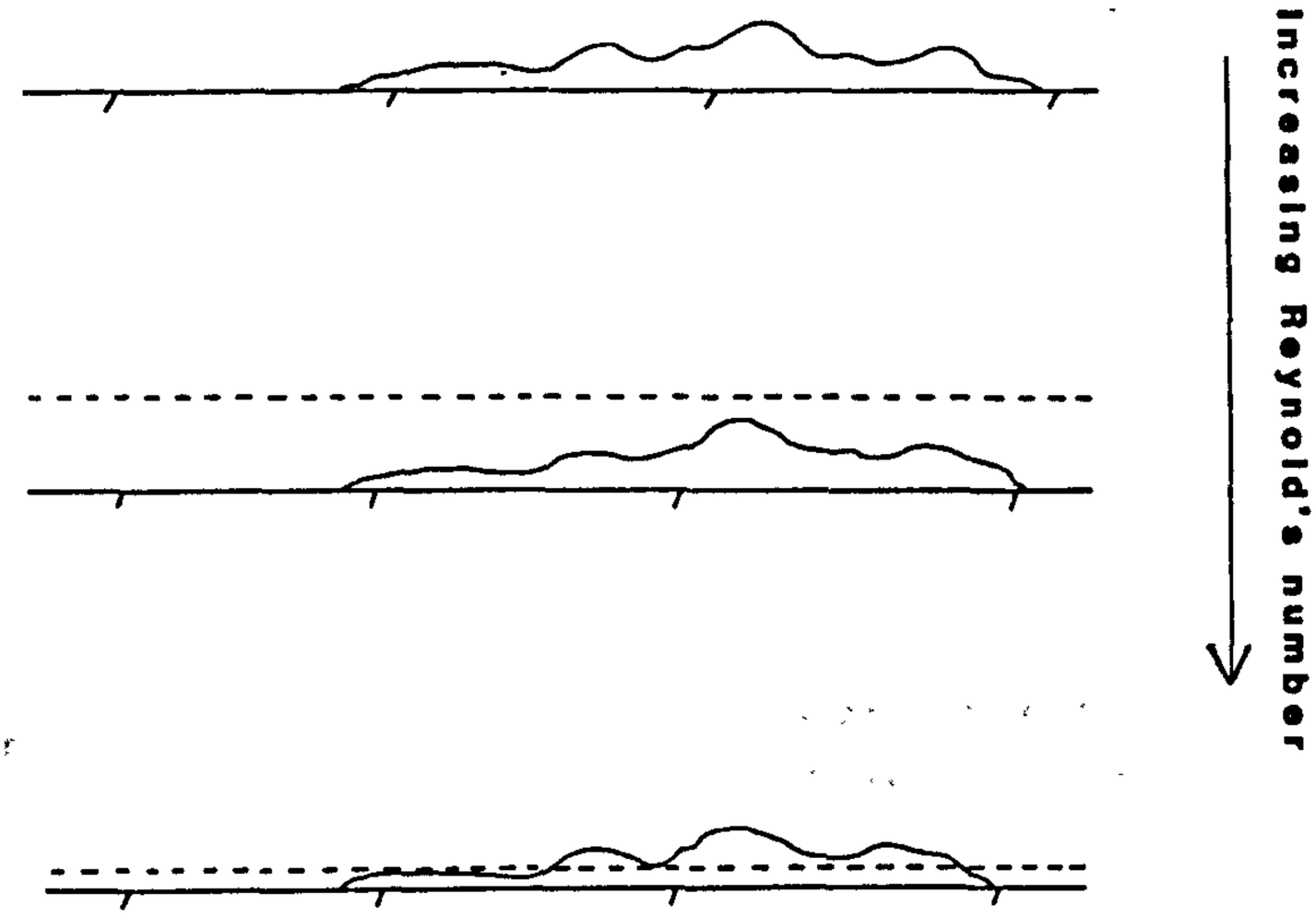

Figure 8.1 The effect of increasing Reynold's number

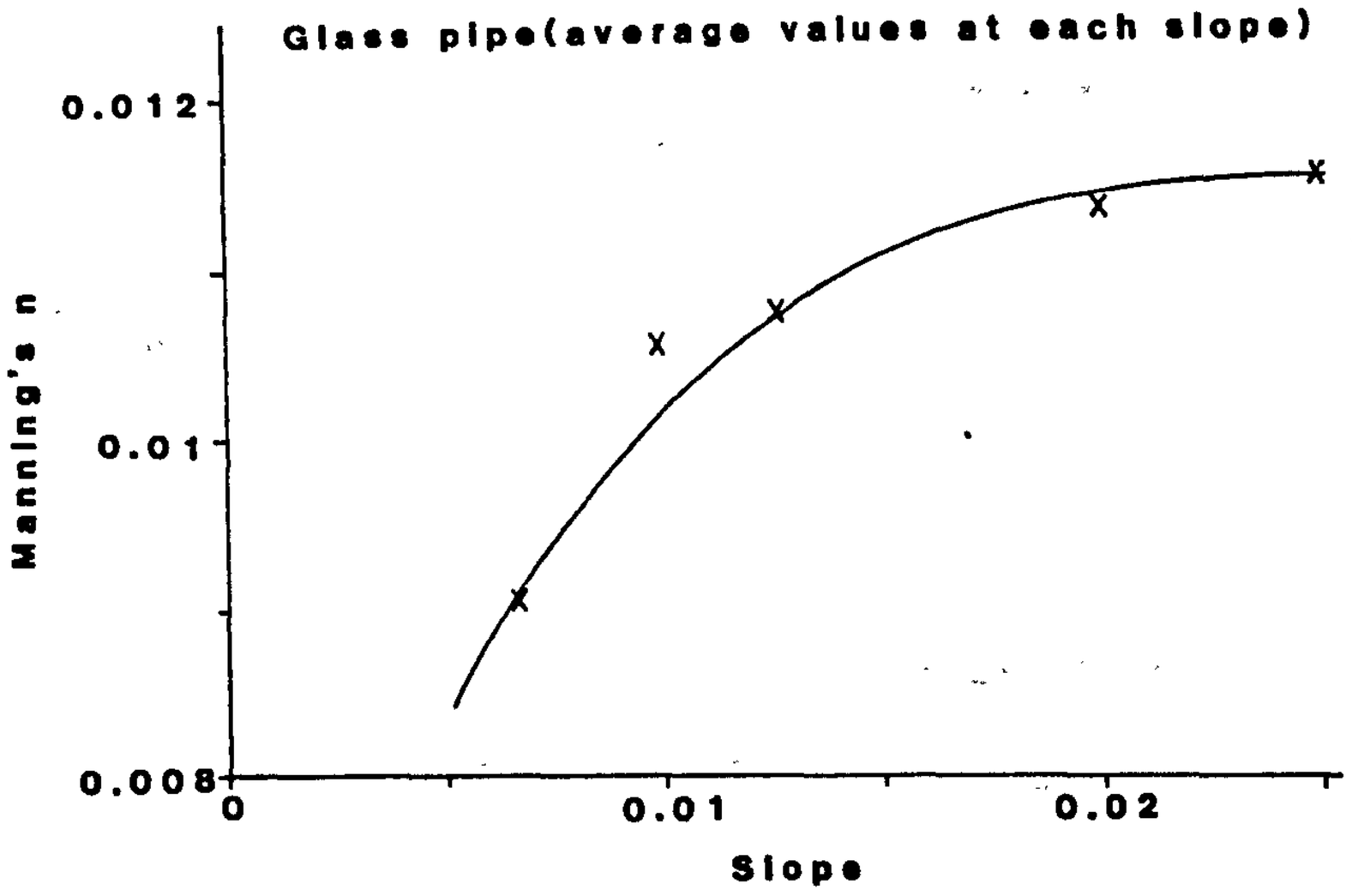

Figure 8.2 Variation of Manning's n with slope

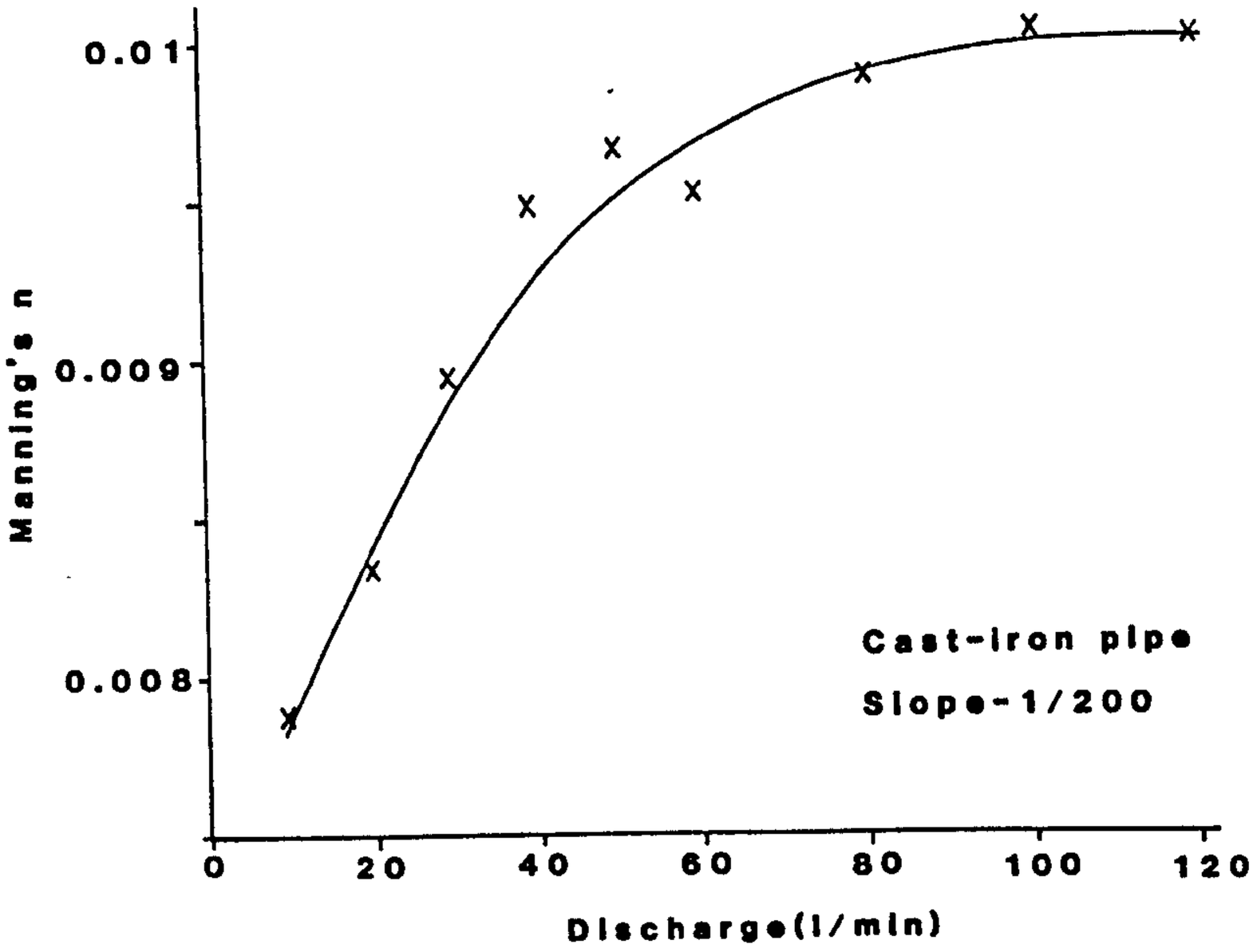

Figure 8.3 Variation of Manning's n with discharge

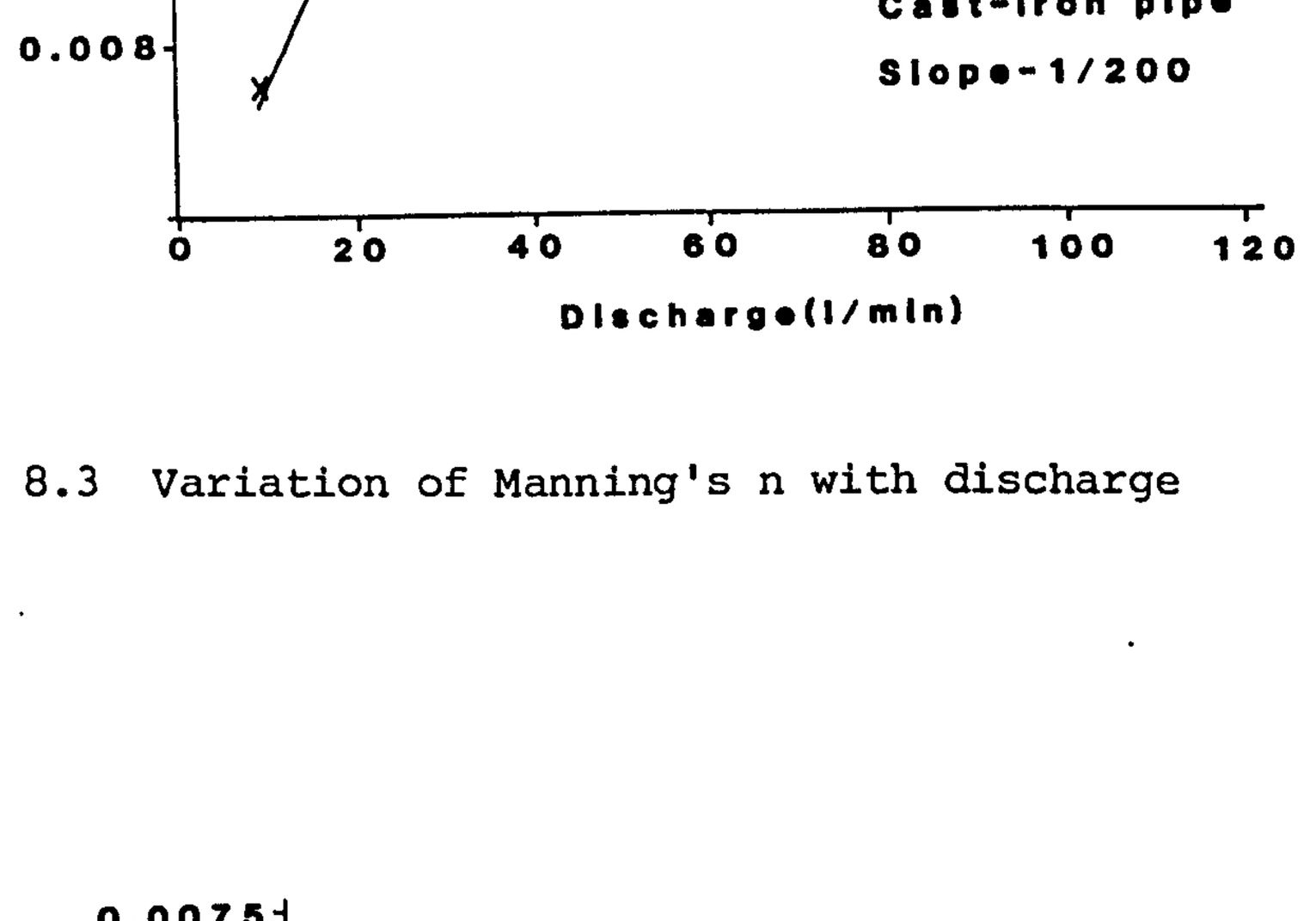

Figure 8.4 Variation of Manning's n with discharge for a fixed roughness value

Pipe material	k (mm)
Glass, perspex	0.0
U.P.V.C.	0.002
Coated cast-iron	0.1 - 0.3
Uncoated cast-iron	0.15 - 0.6
Glazed clay	0.15 - 0.6

Figure 8.5 k values for various pipe materials

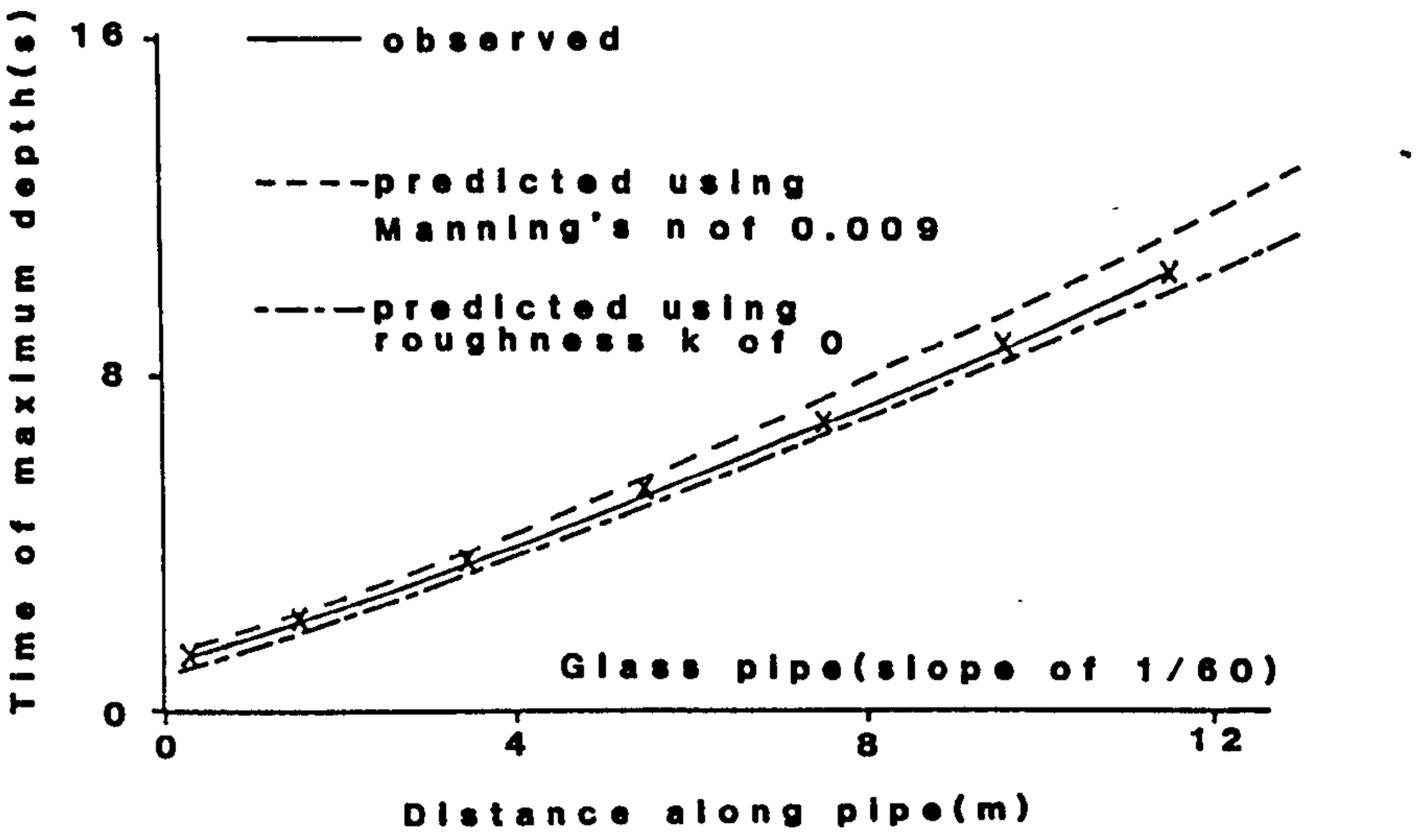

Figure 8.6 Time of maximum depth versus distance (gradient of 1/60)

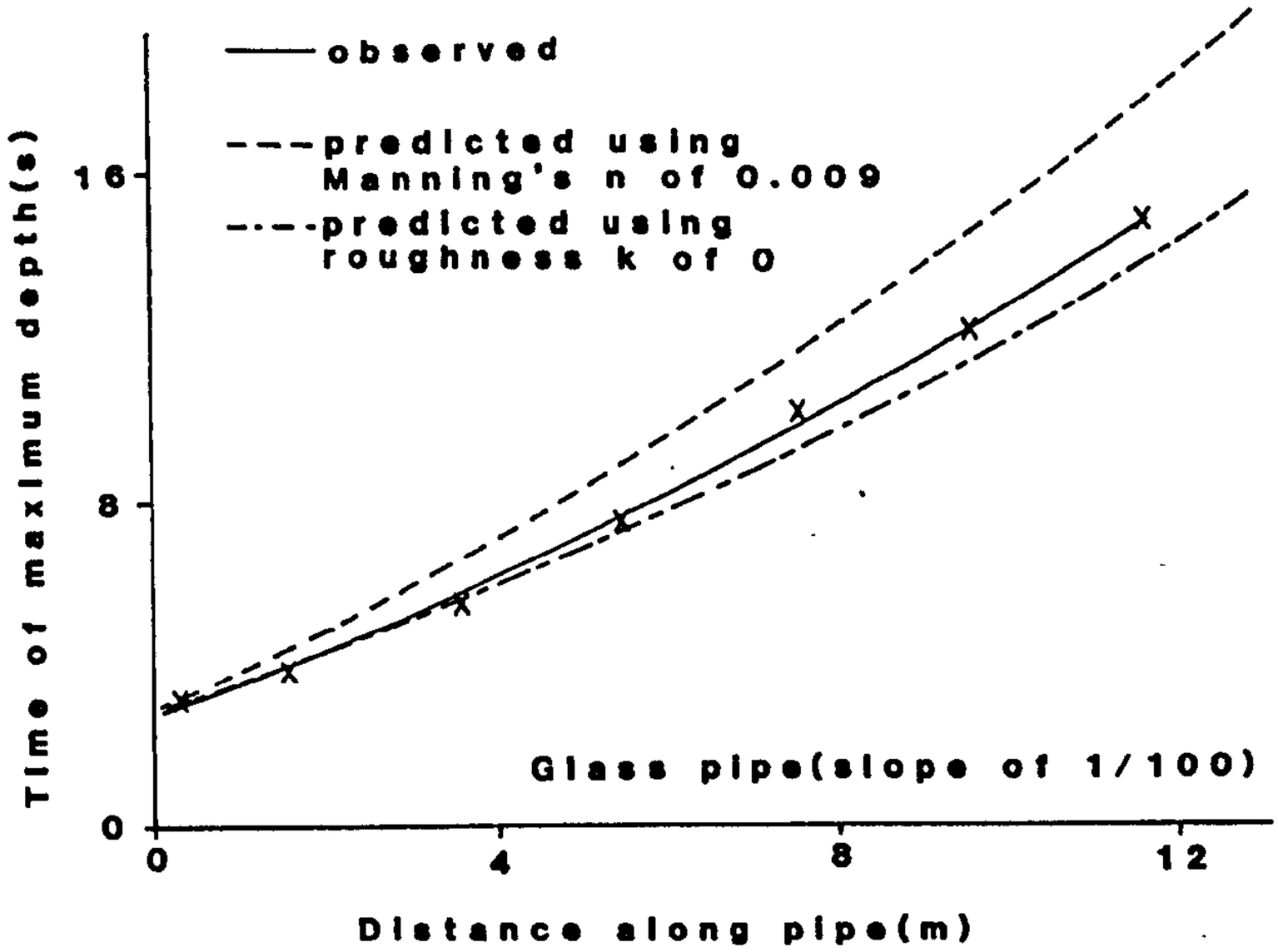

Figure 8.7 Time of maximum depth versus distance (gradient of 1/100)

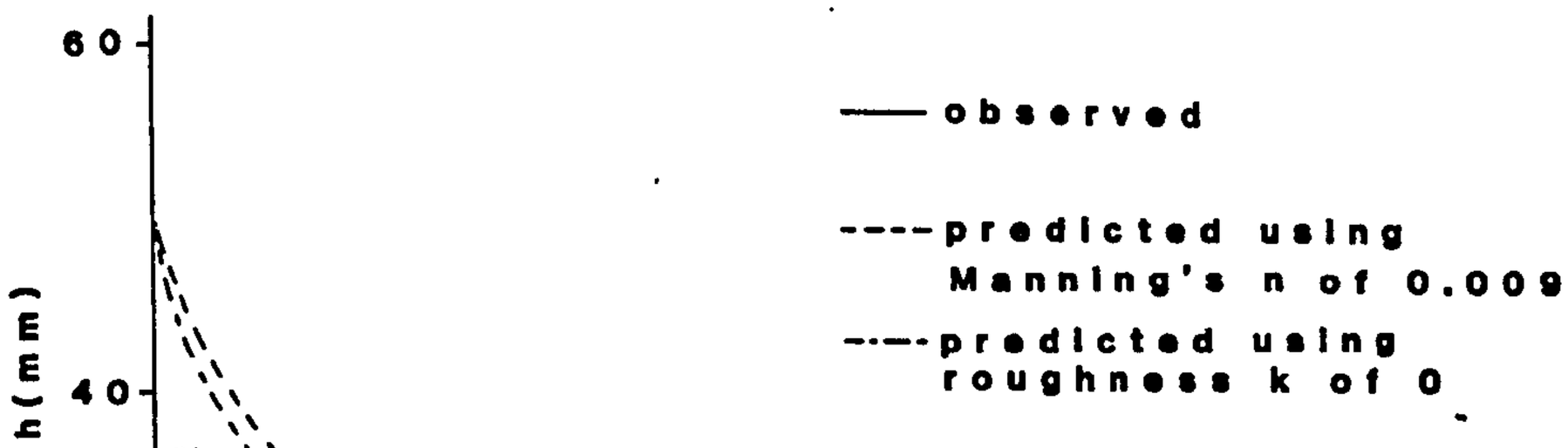

Figure 8.8 Maximum depth versus distance for glass pipe (gradient of 1/50)

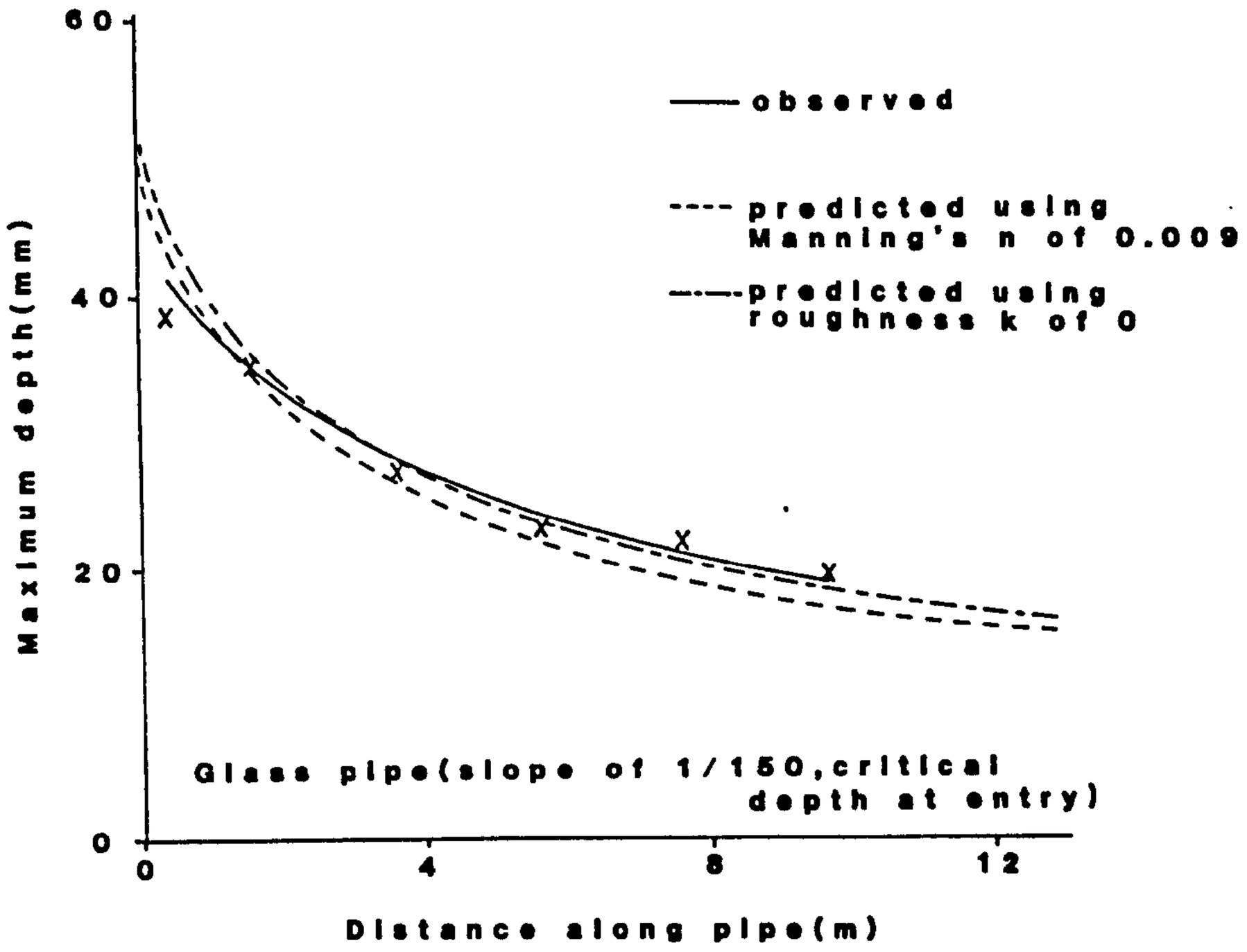

Figure 8.9 Maximum depth versus distance for glass pipe (gradient of 1/150)

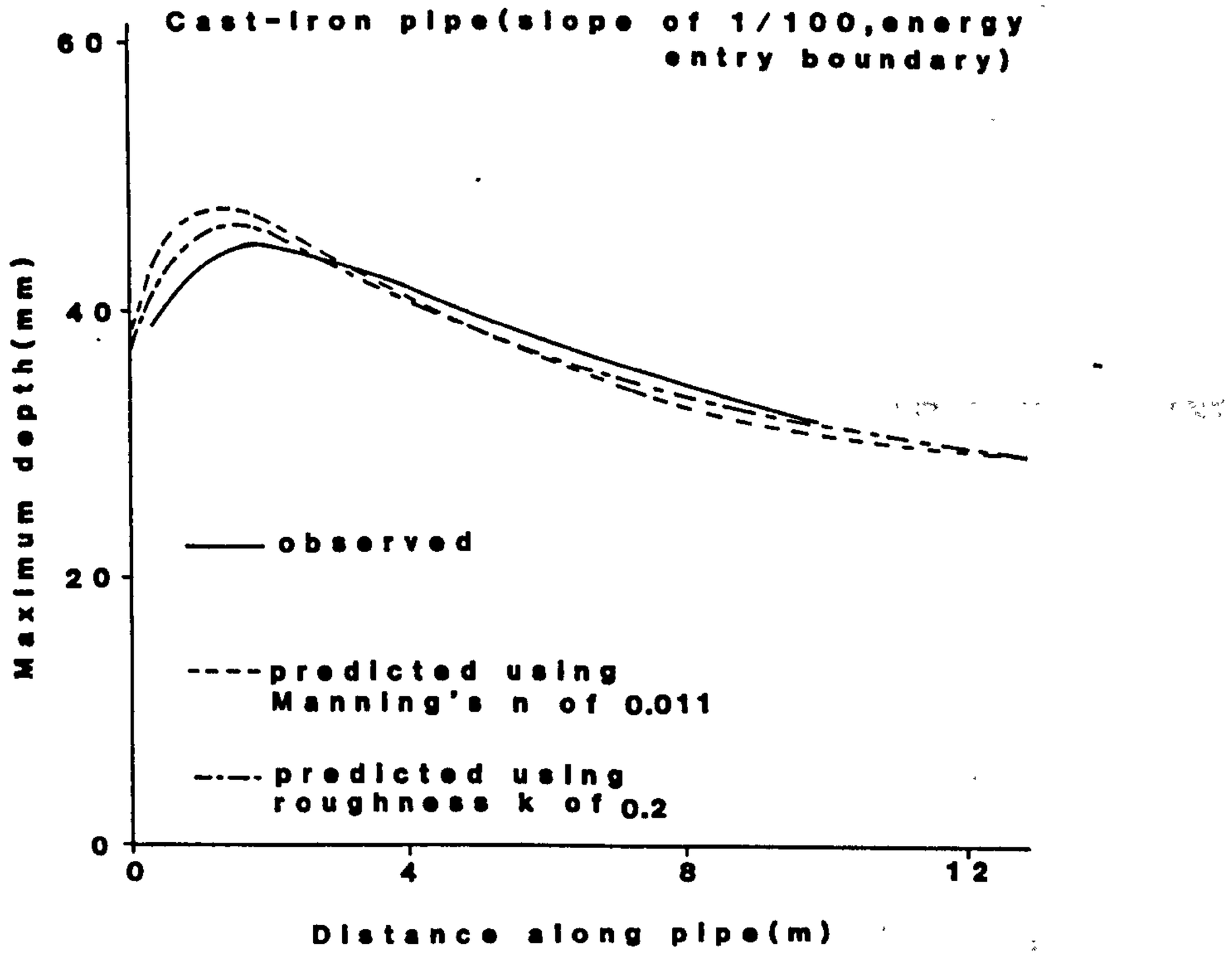

Figure 8.10 Maximum depth versus distance for cast-iron pipe (gradient of 1/100)

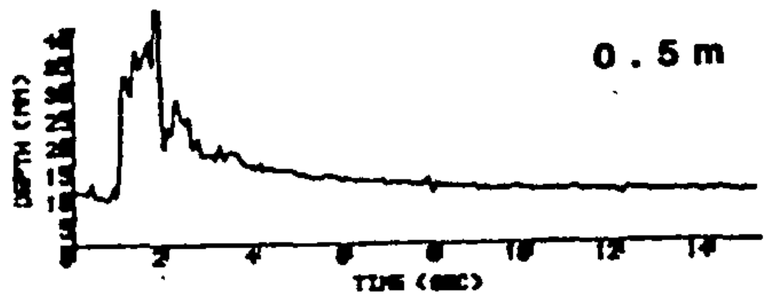

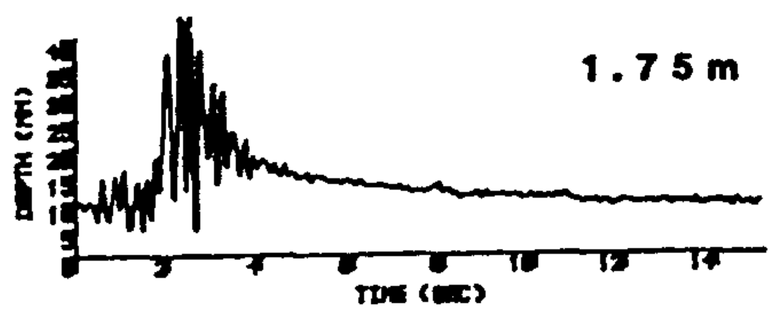

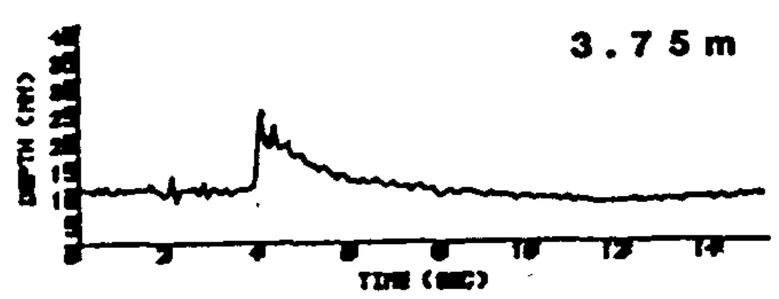

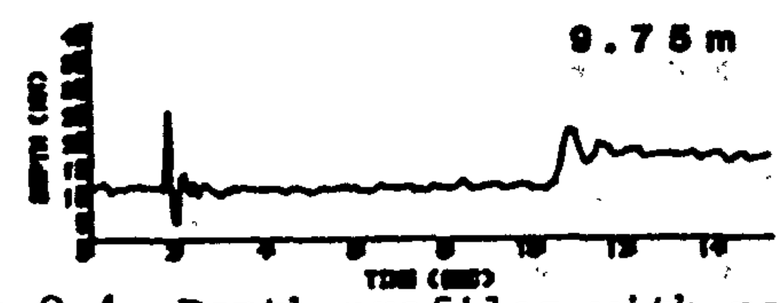

Figure 9.1 Depth profiles with no bend (gradient of 1/100)

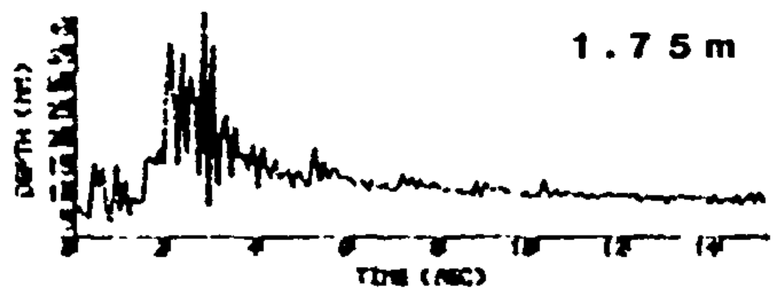

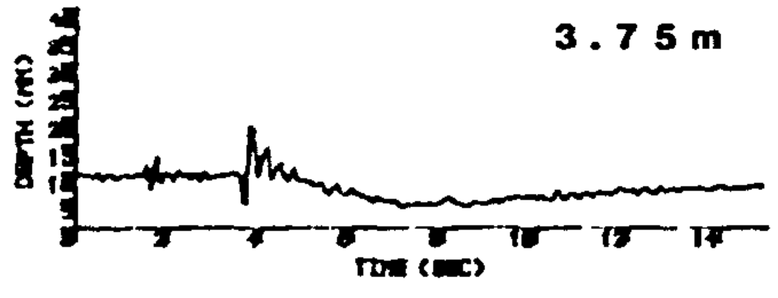

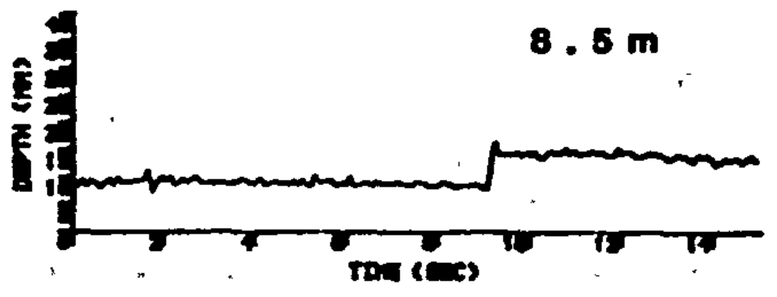

Figure 9.2 Depth profiles with a 90 degree bend (gradient of 1/100)

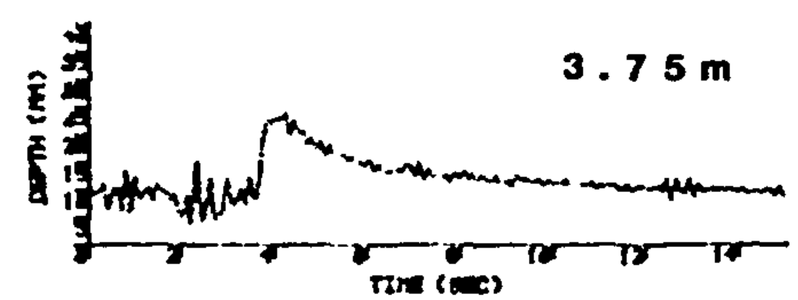

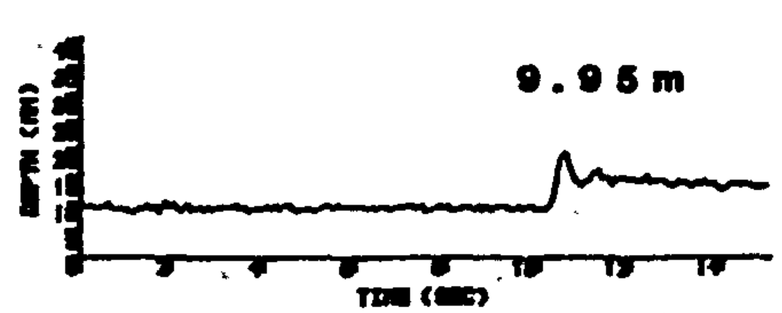

Figure 9.3 Depth profiles with a 45 degree bend (gradient of 1/100)

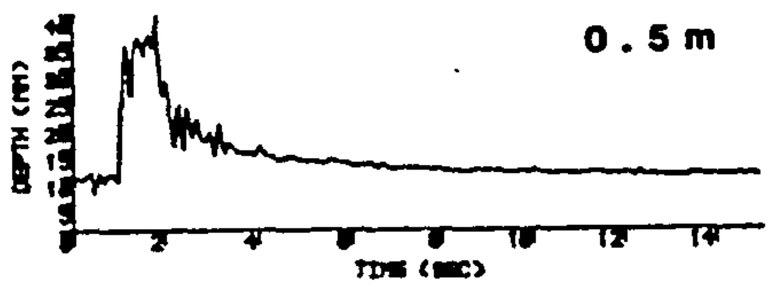

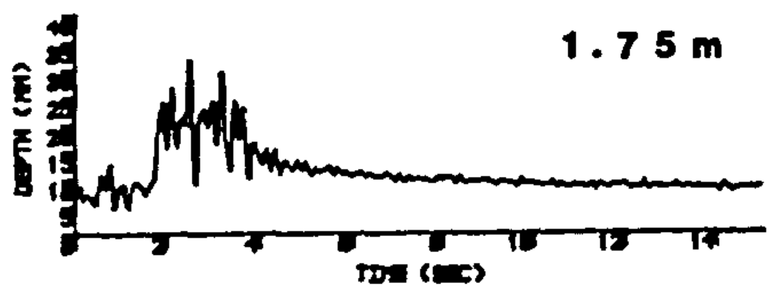

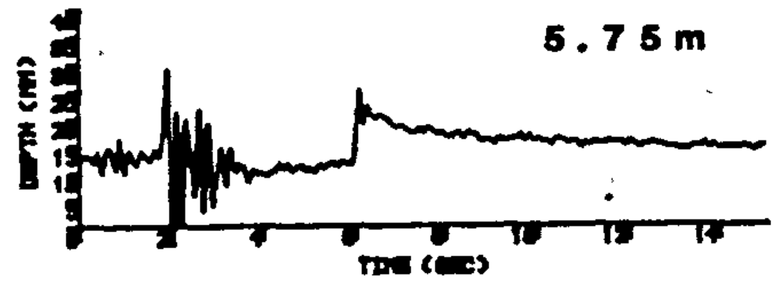

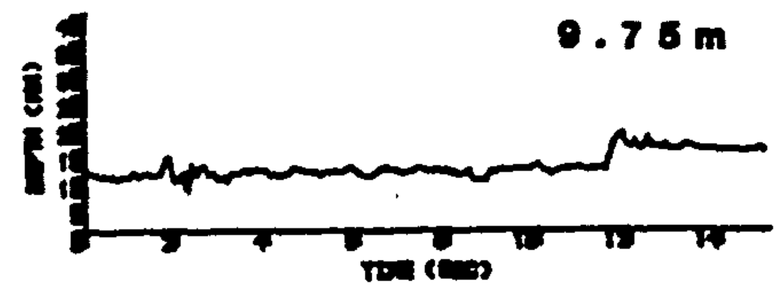

Figure 9.4 Depth profiles with no bend *(gradient of 1/200)*

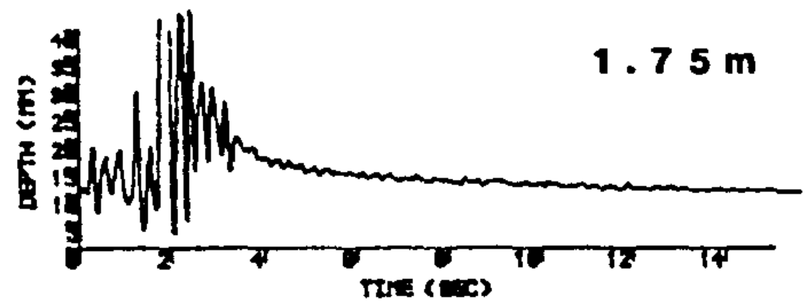

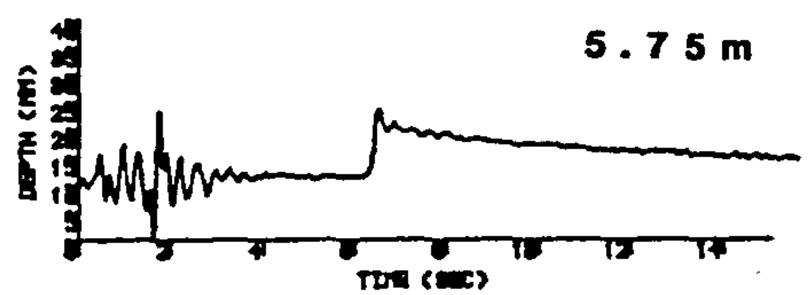

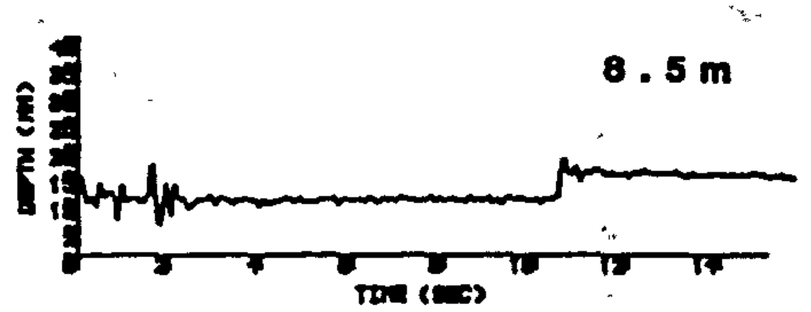

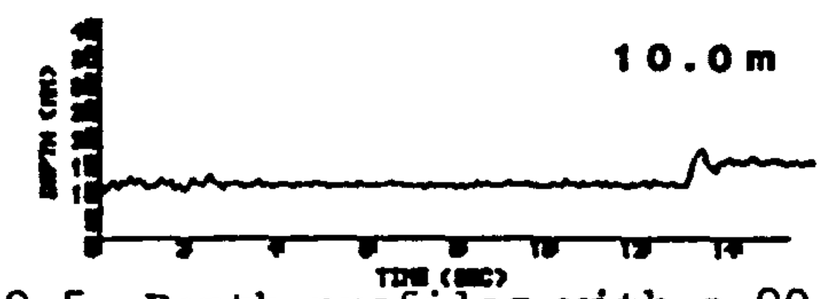

Figure 9.5 Depth profiles with a 90 degree bend (gradient of 1/200)

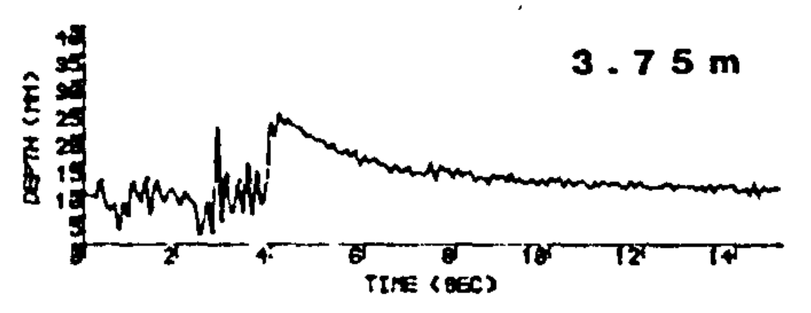

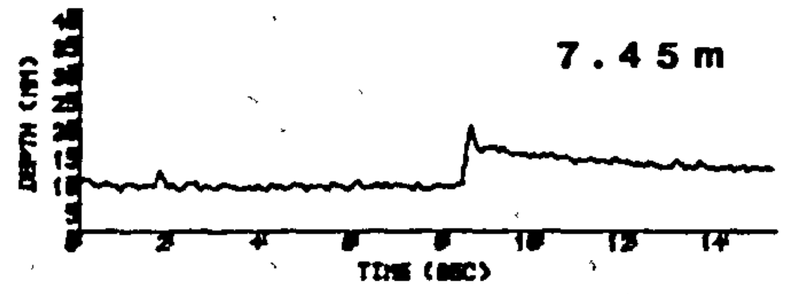

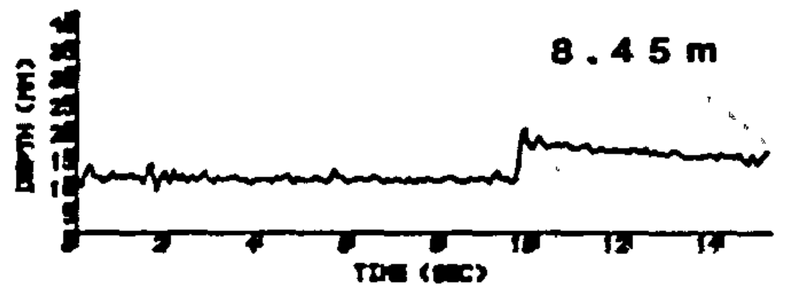

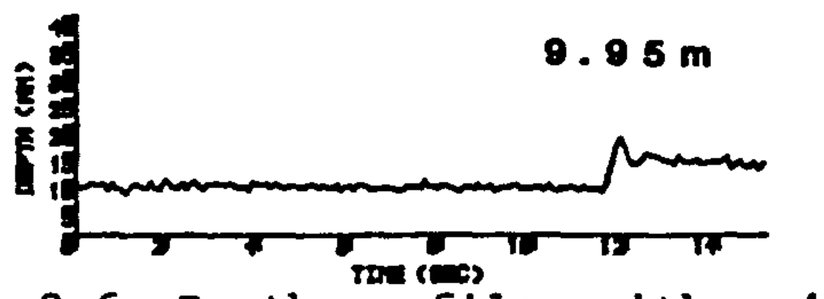

Figure 9.6 Depth profiles with a 45 degree bend (gradient of 1/200)

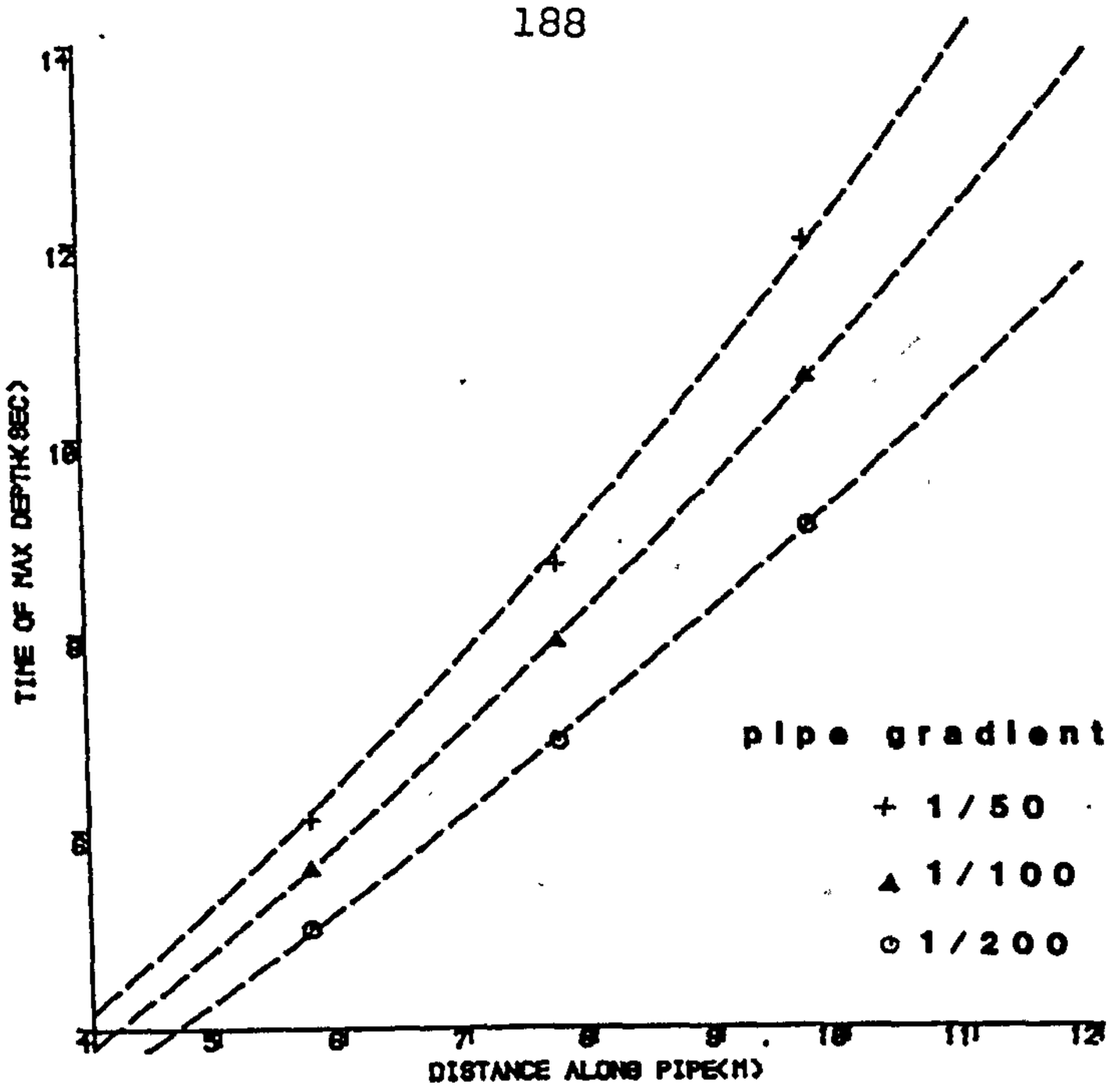

VELOCITY OF WAVE PEAK

Figure 9.7 Velocity of wave peak with no bend (shallow wave)

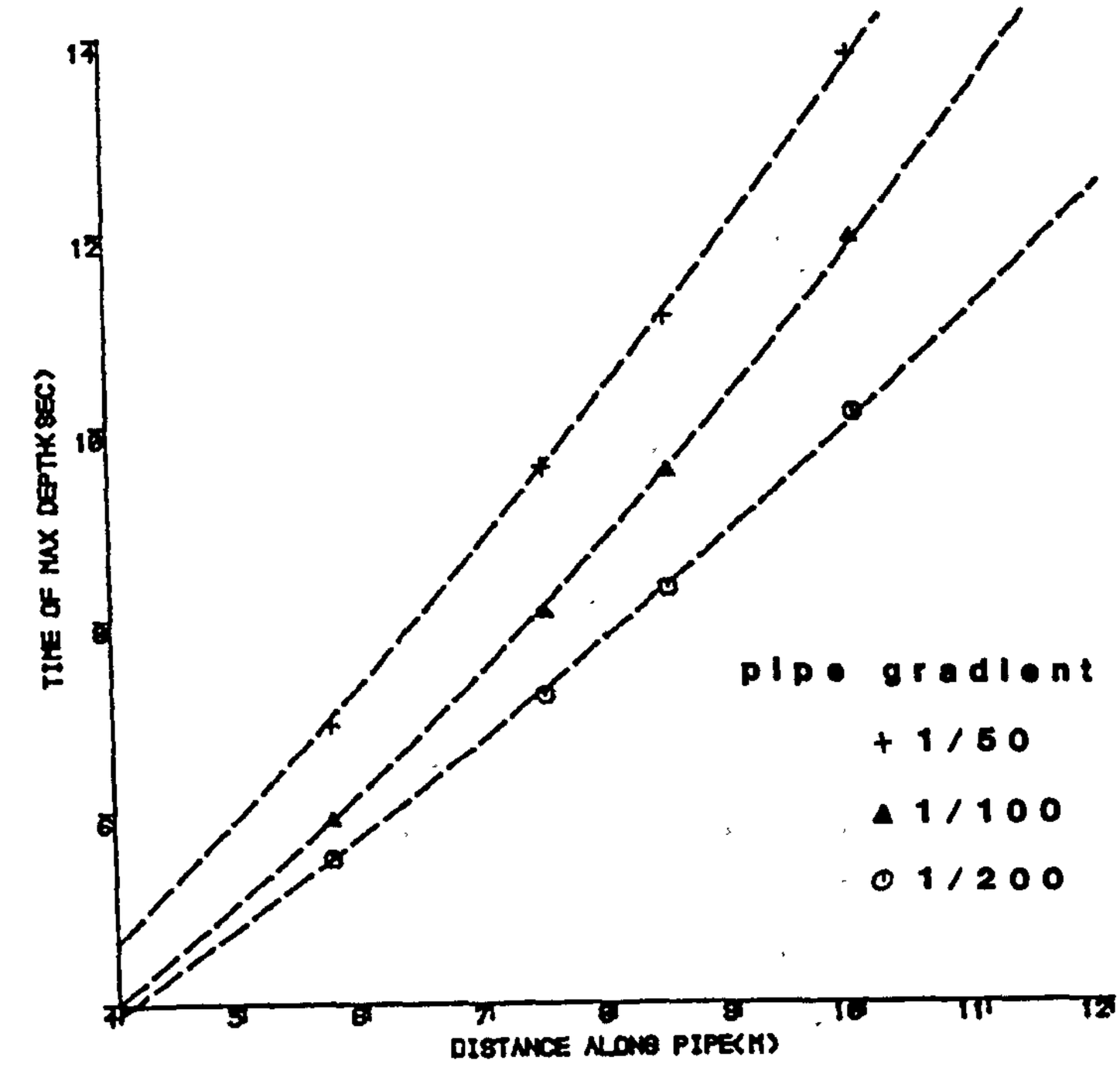

VELOCITY OF WAVE PEAK

Figure 9.8 Velocity of wave peak with a 90 degree bend (shallow wave)

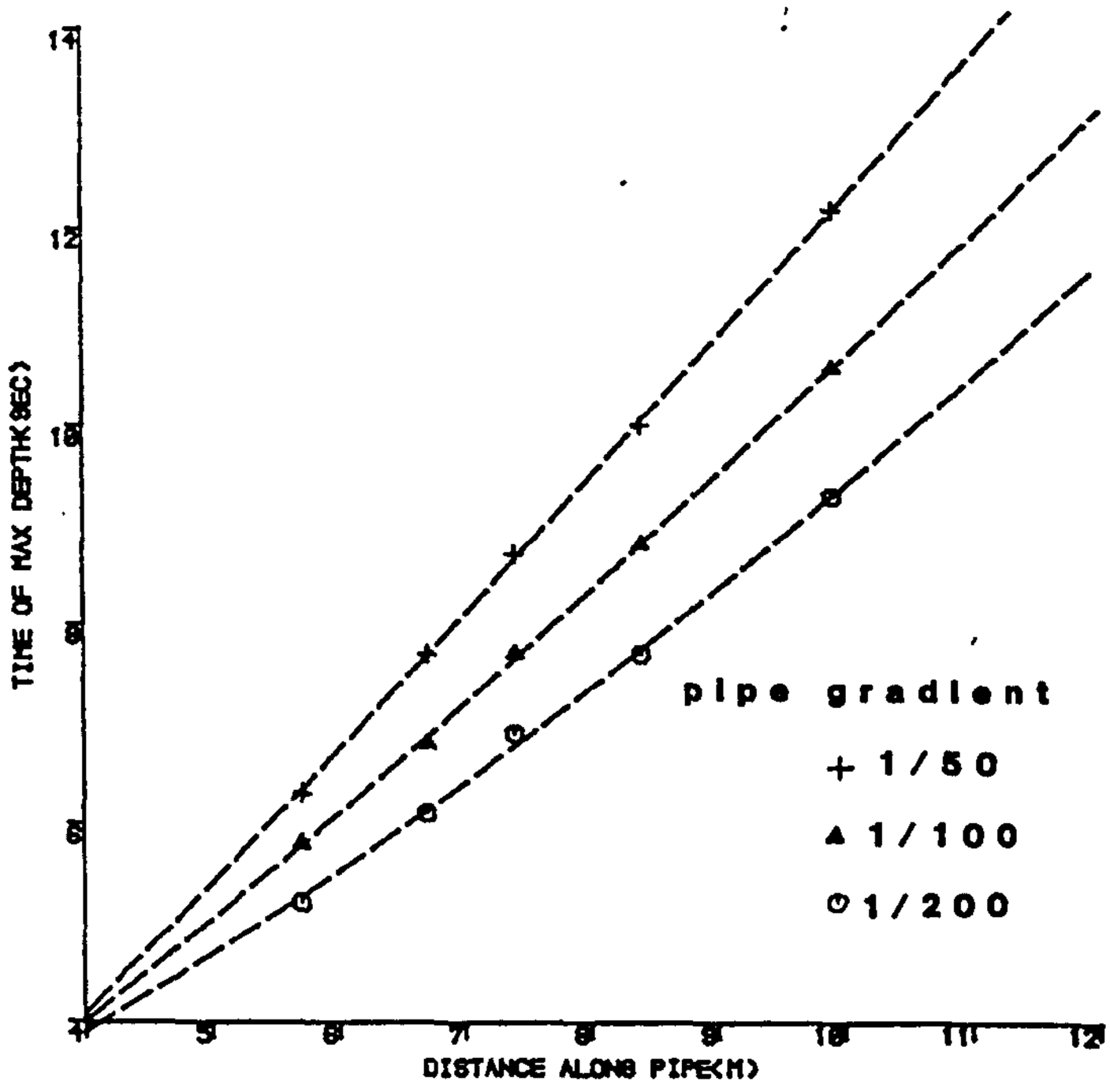

VELOCITY OF WAVE PEAK

Figure 9.9 Velocity of wave peak with a 45 degree bend (shallow wave)

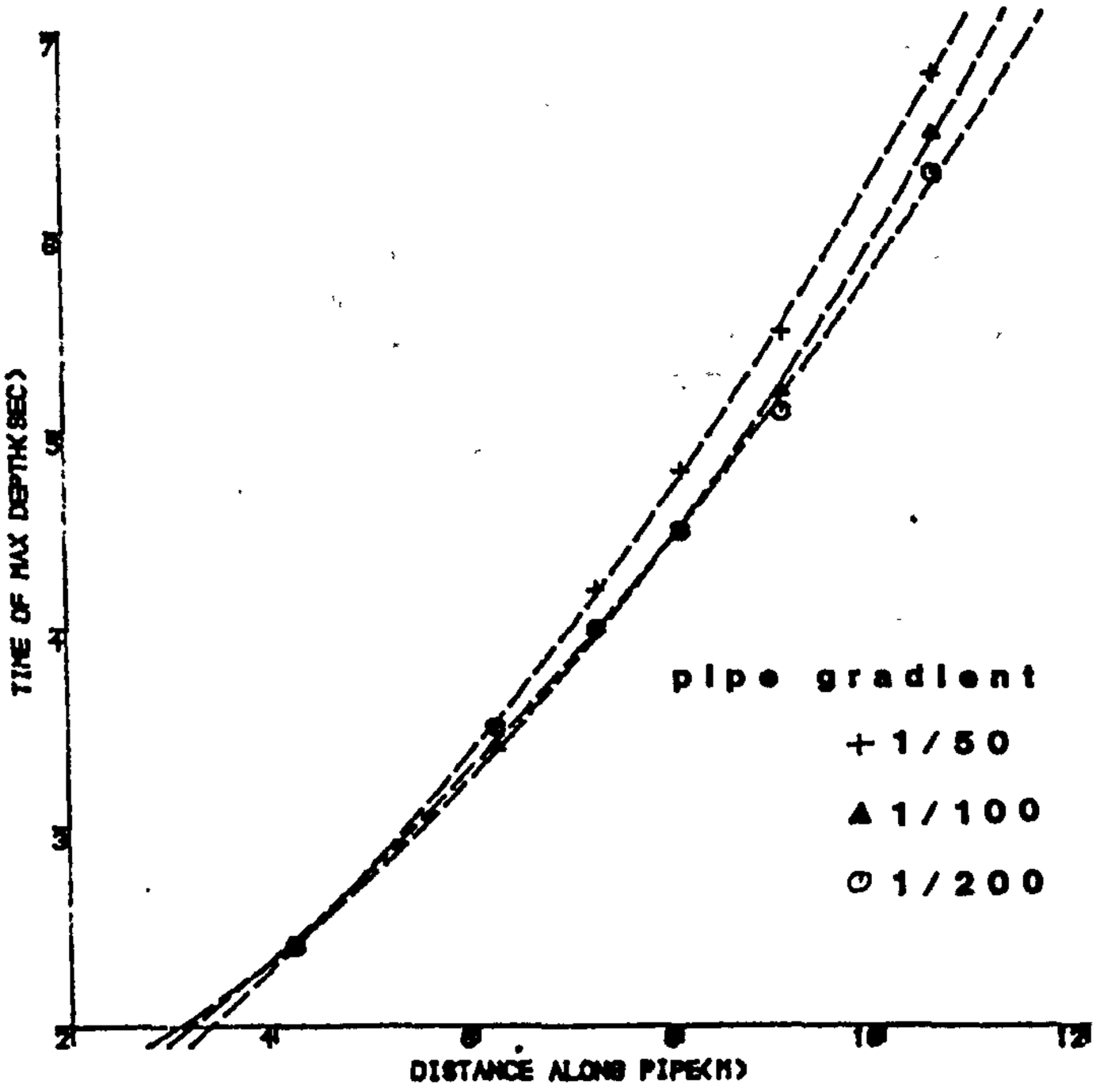

VELOCITY OF WAVE PEAK

Figure 9.10 Velocity of wave peak with a 90 degree bend (steep wave)

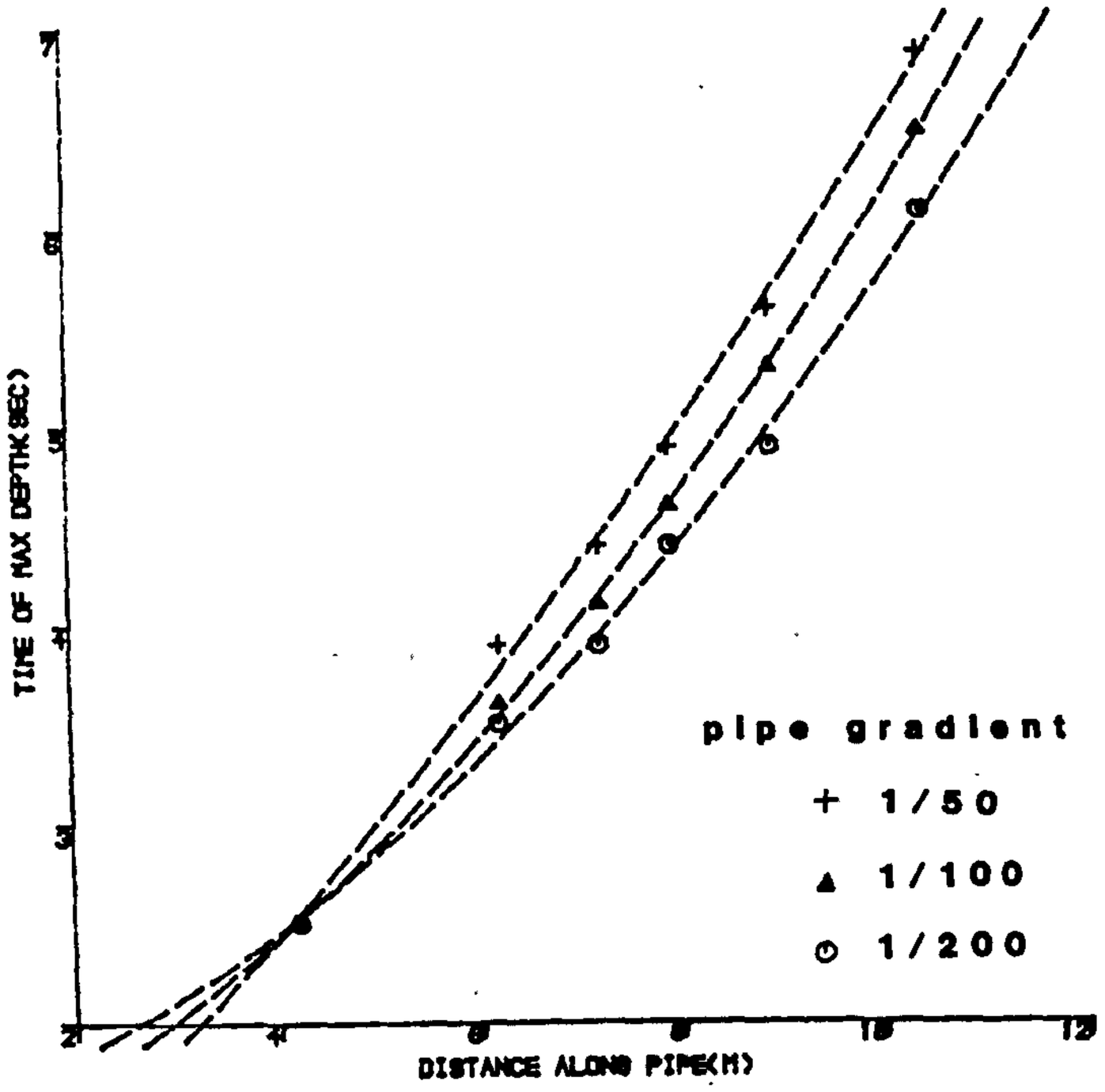

VELOCITY OF WAVE PEAK

Figure 9.11 Velocity of wave peak with a 45 degree bend (steep wave)

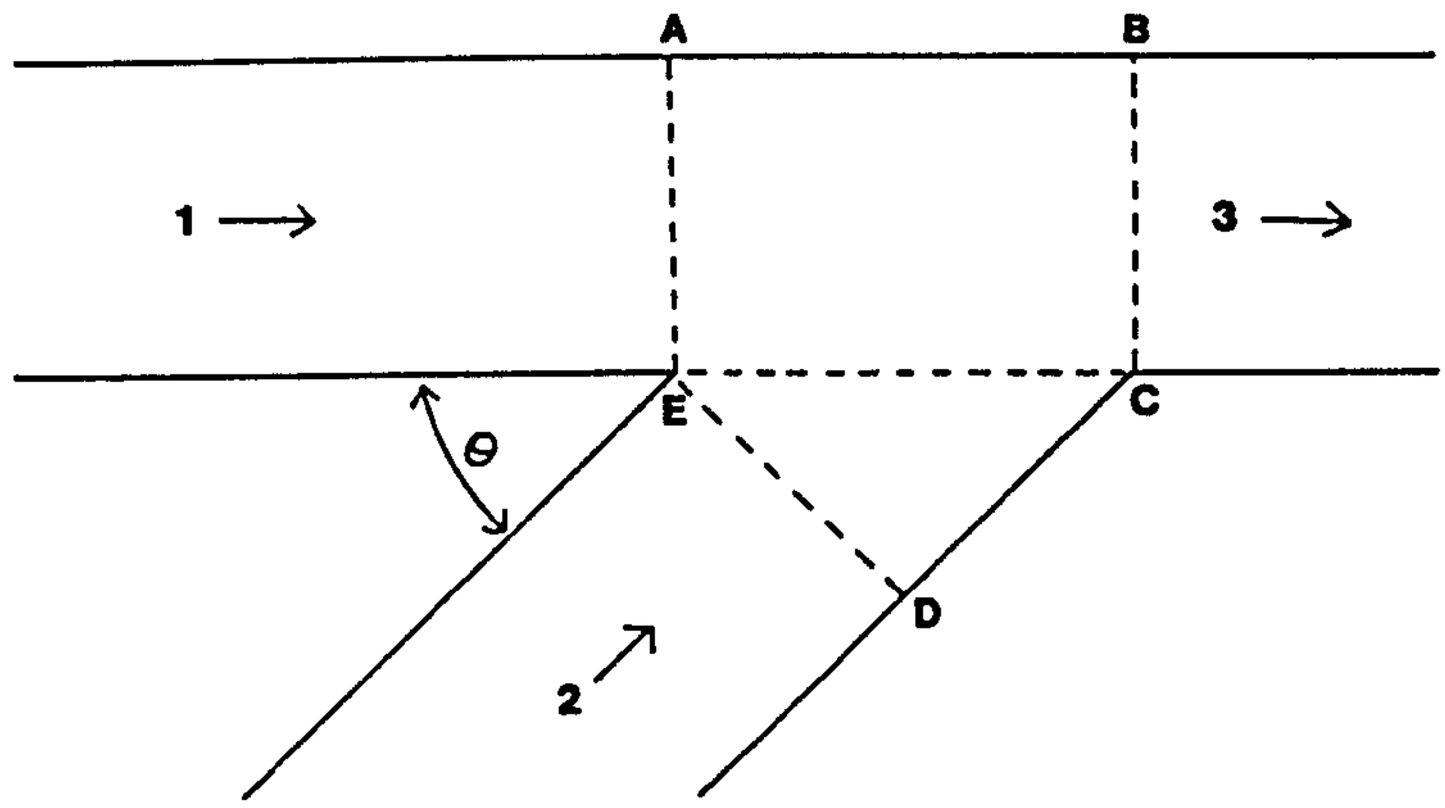

Figure 10.1 The geometry of the junction

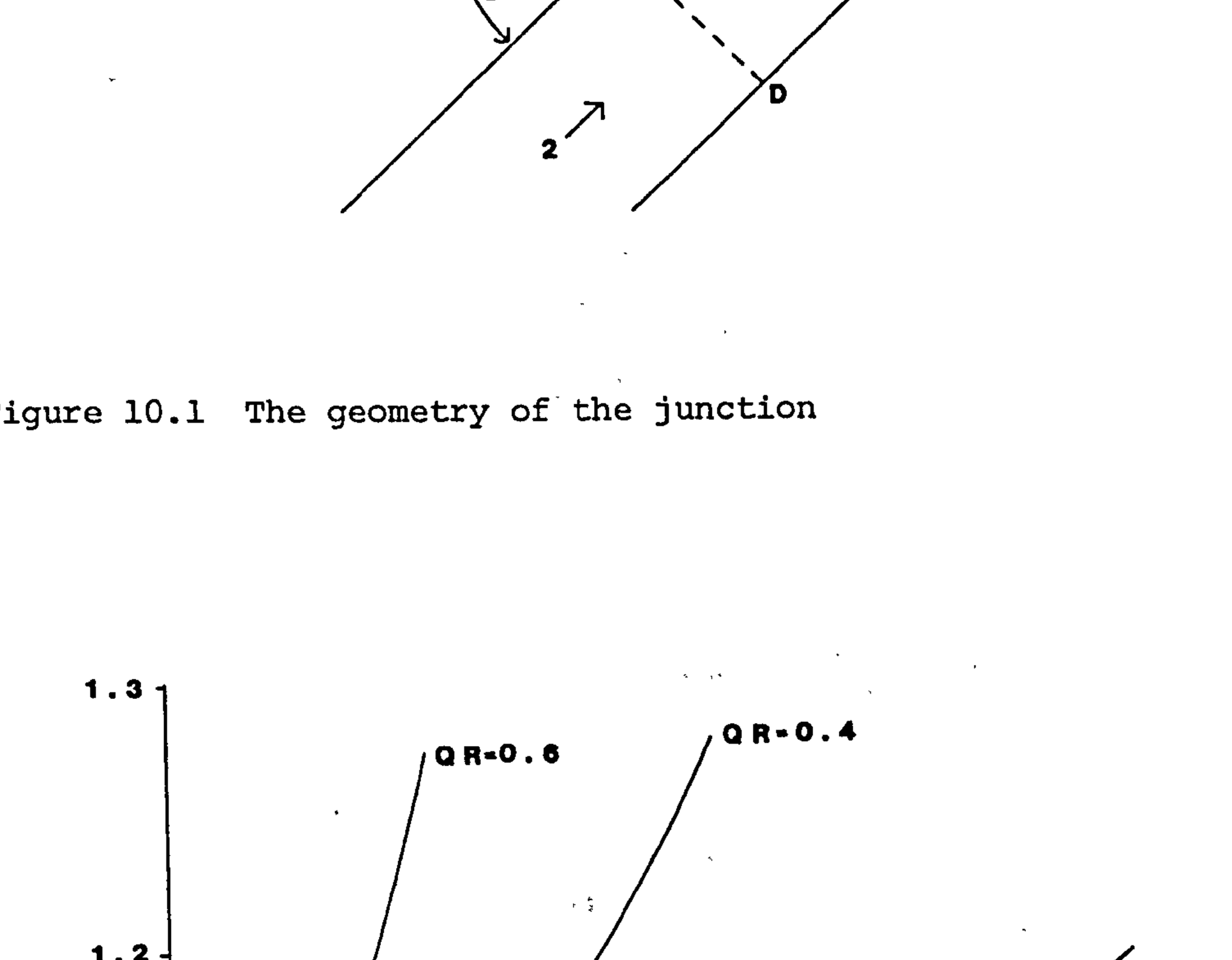

Figure 10.2 Intersection characteristics for combining flows (after Taylor, 1944)

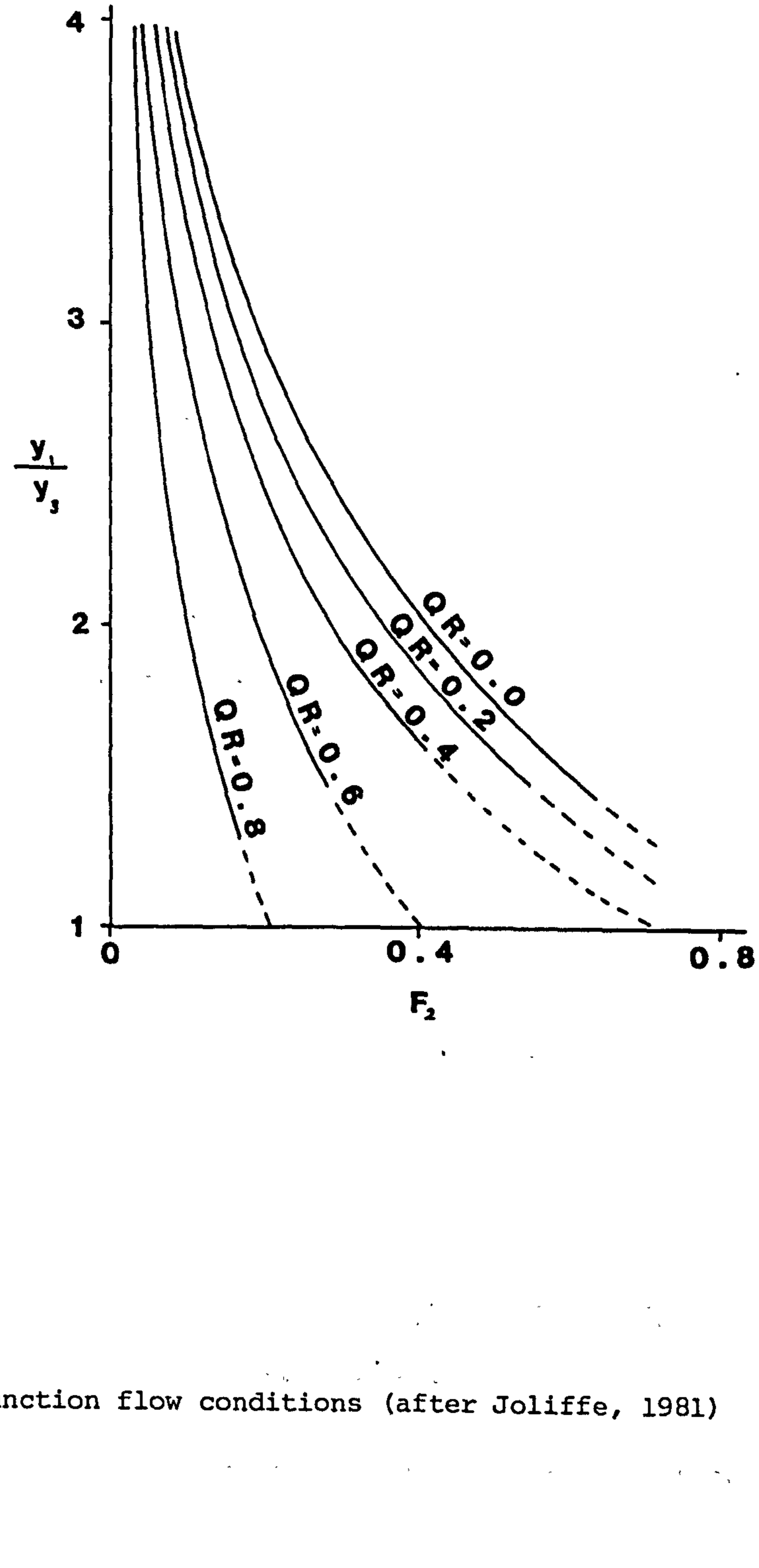

Figure 10.3 Junction flow conditions (after Joliffe, 1981)

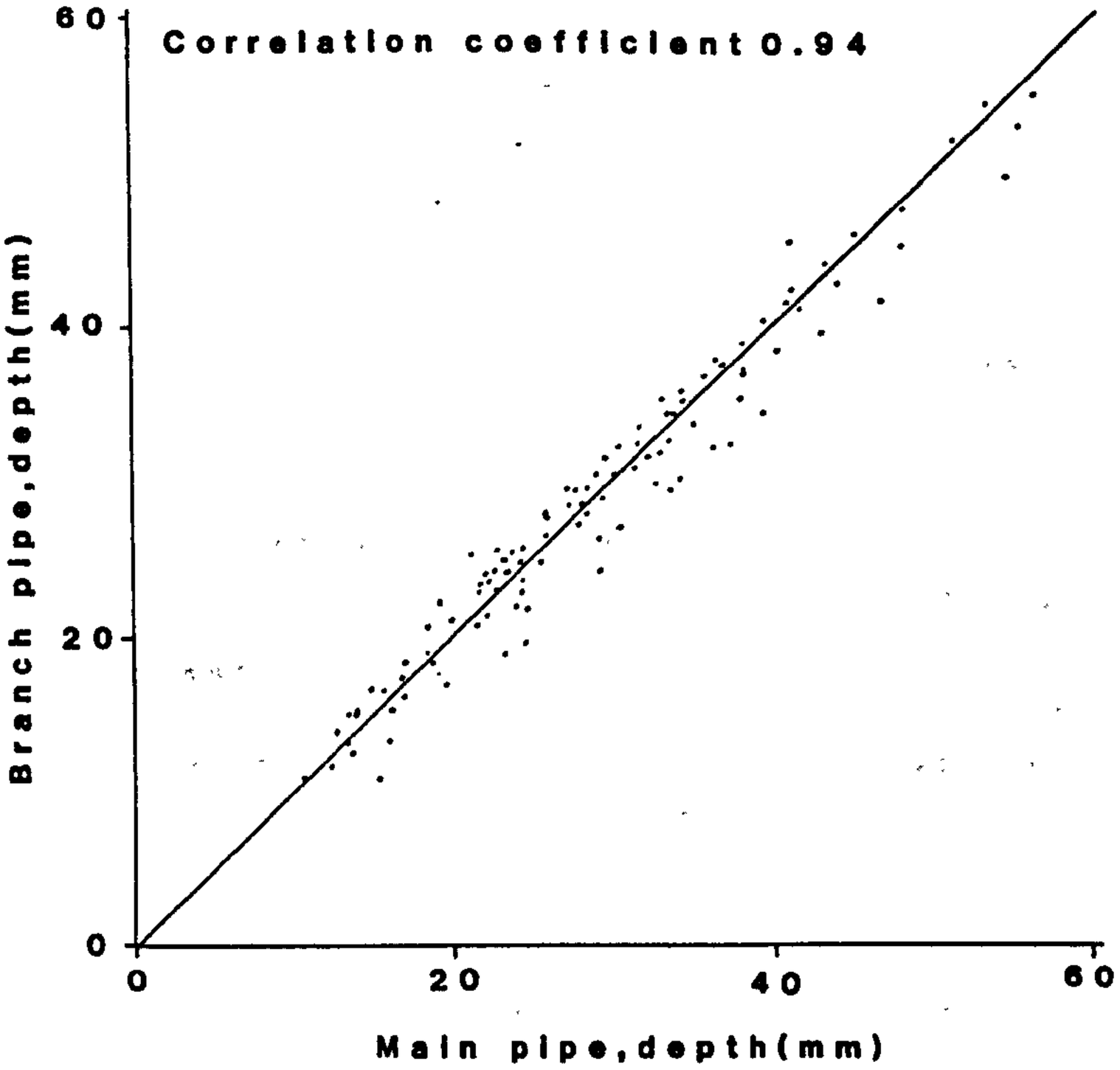

Figure 11.1 Flow depths upstream of the 45 degree junction

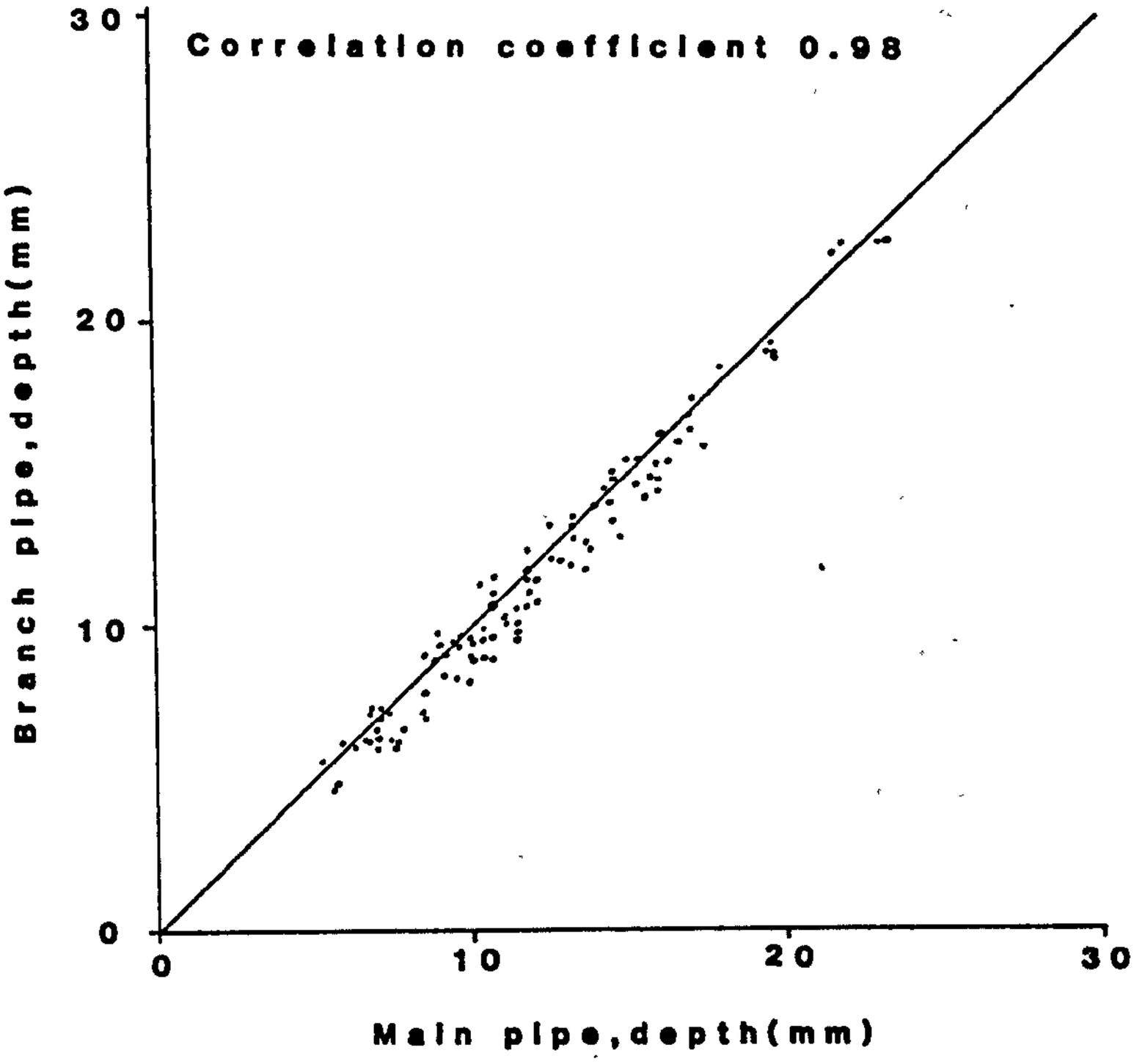

Figure 11.2 Flow depths upstream of the 90 degree junction

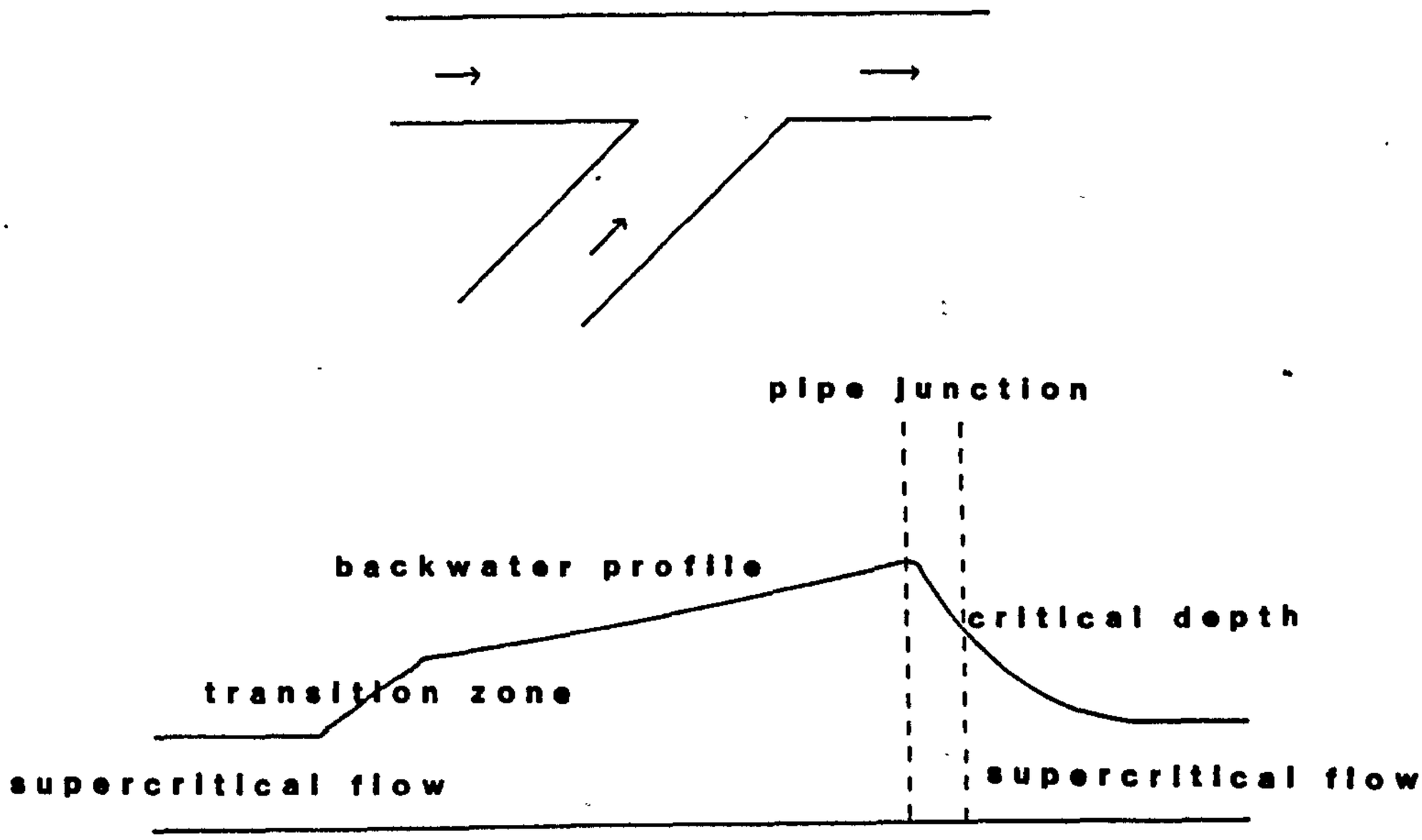

Figure 11.3 Flow regime in the region of the junction

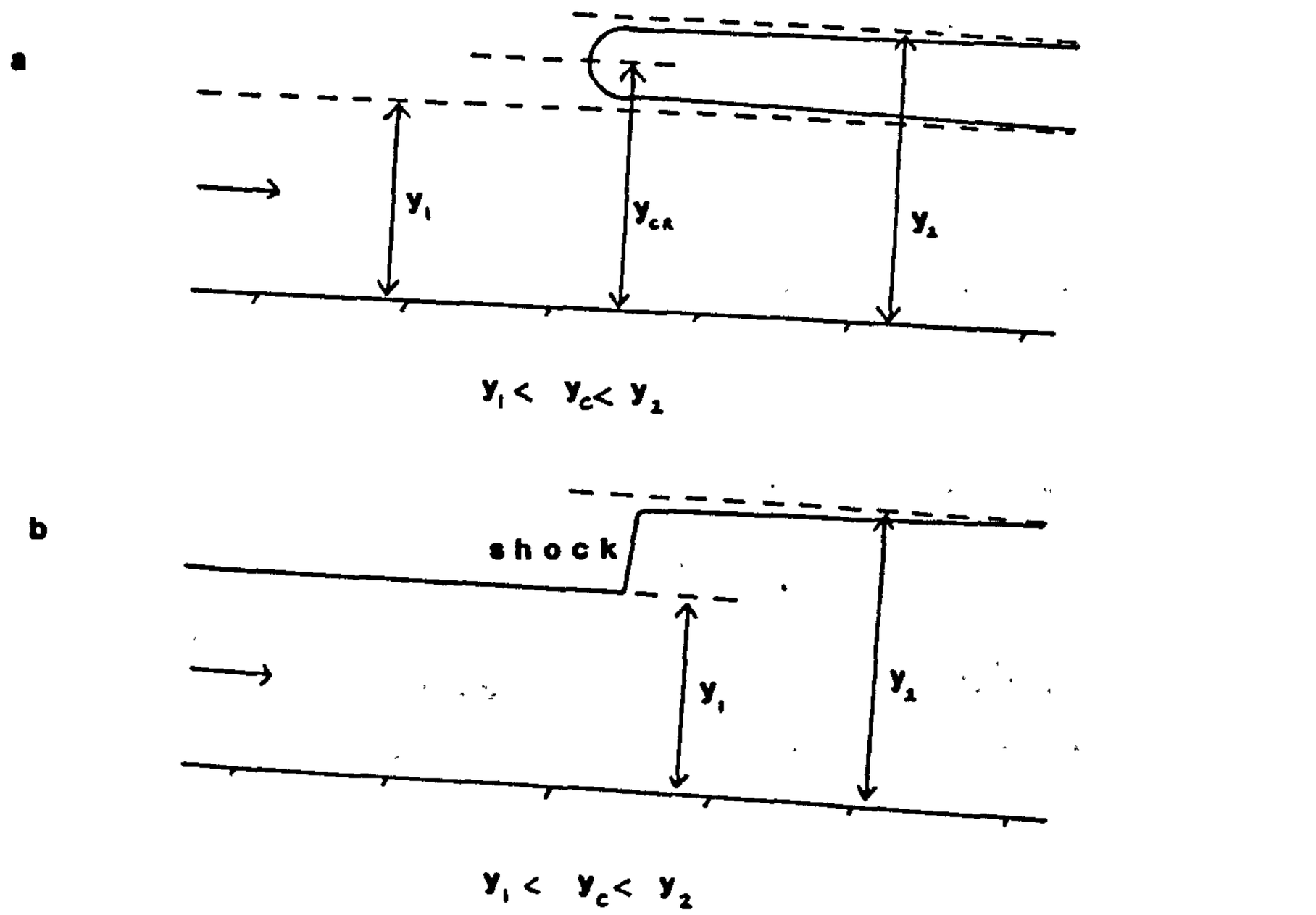

Figure 11.4 Profile of a steep-fronted wave

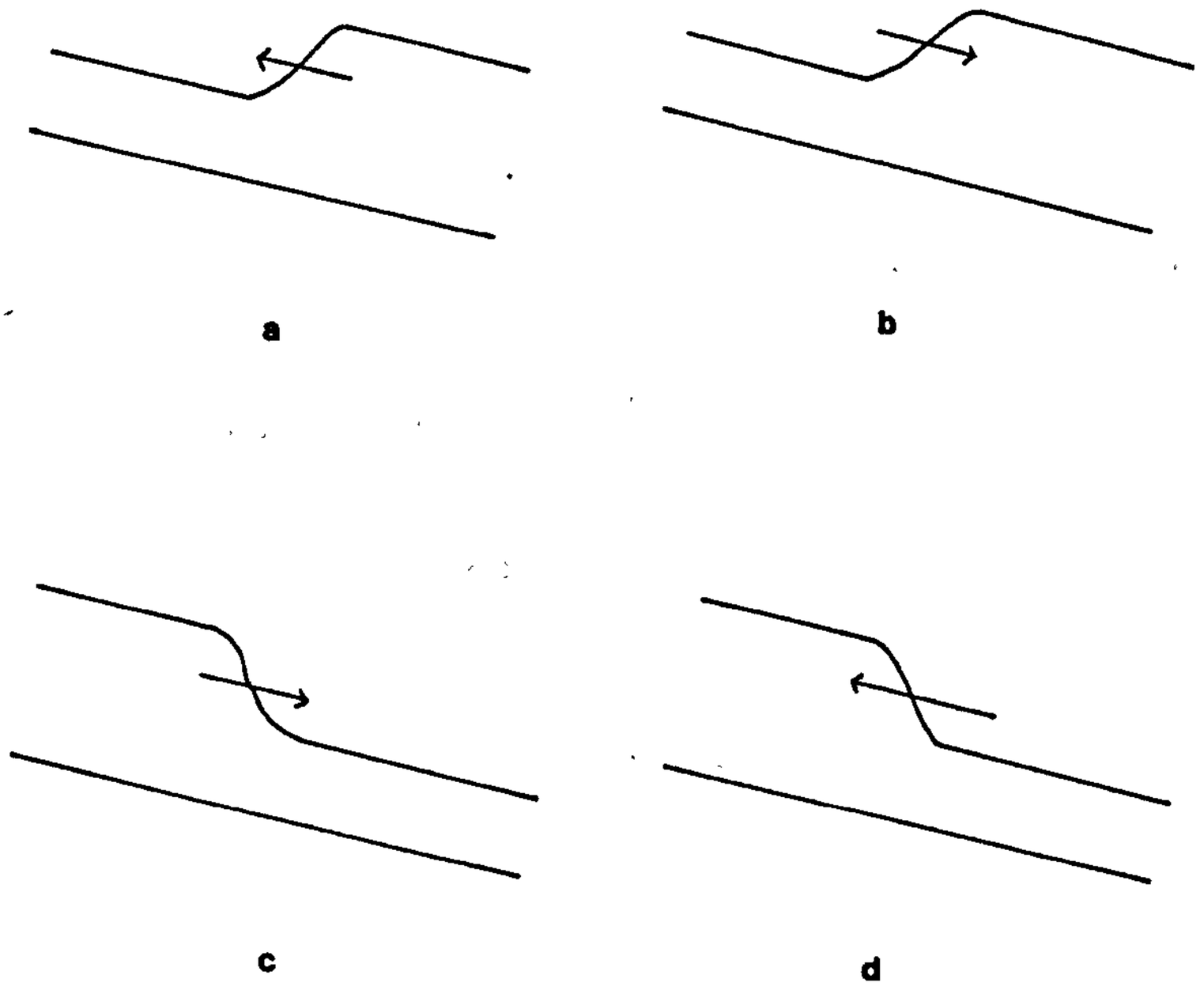

Figure 11.5 Four types of steep-fronted wave

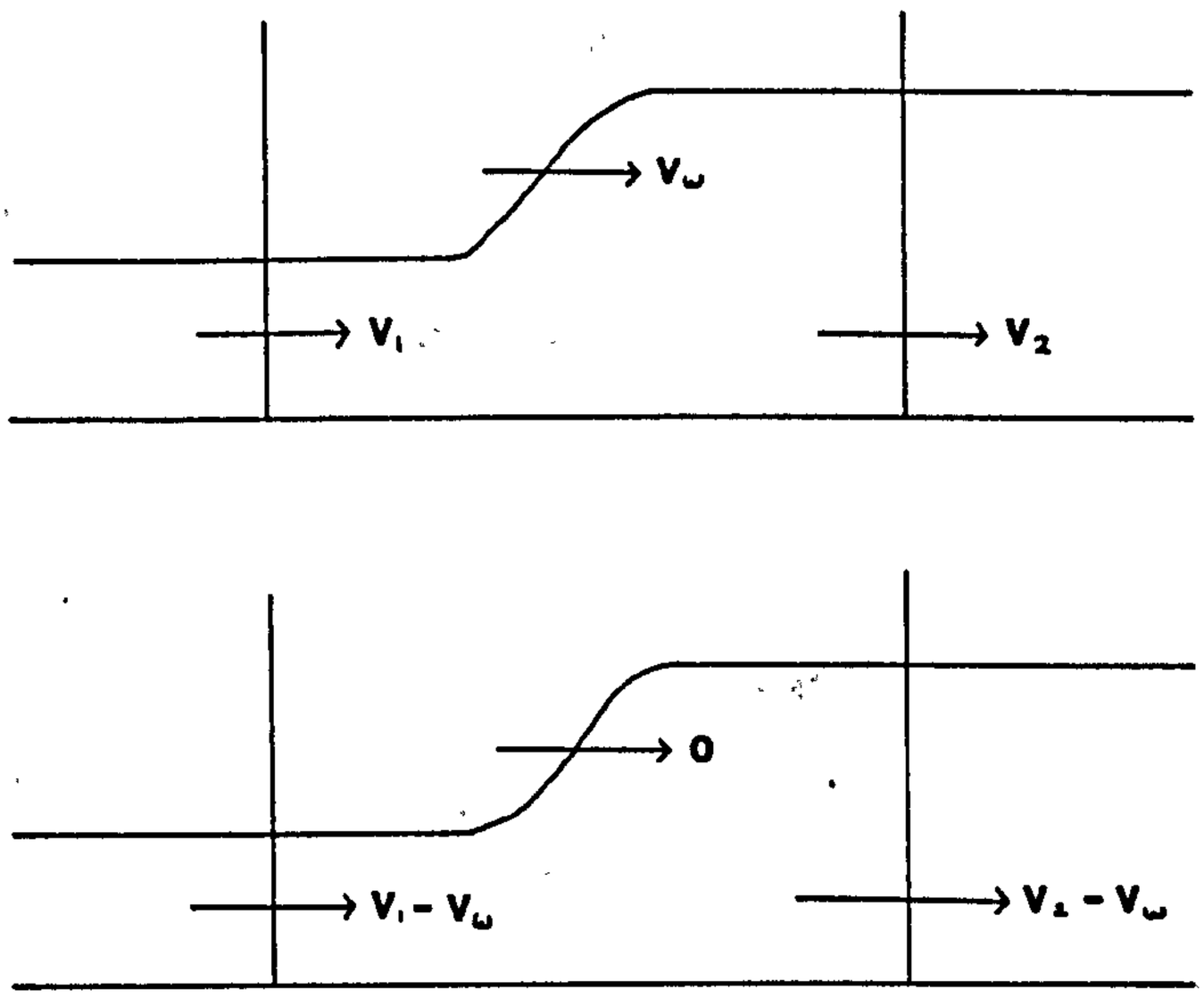

Figure 11.6 Relative wave velocity

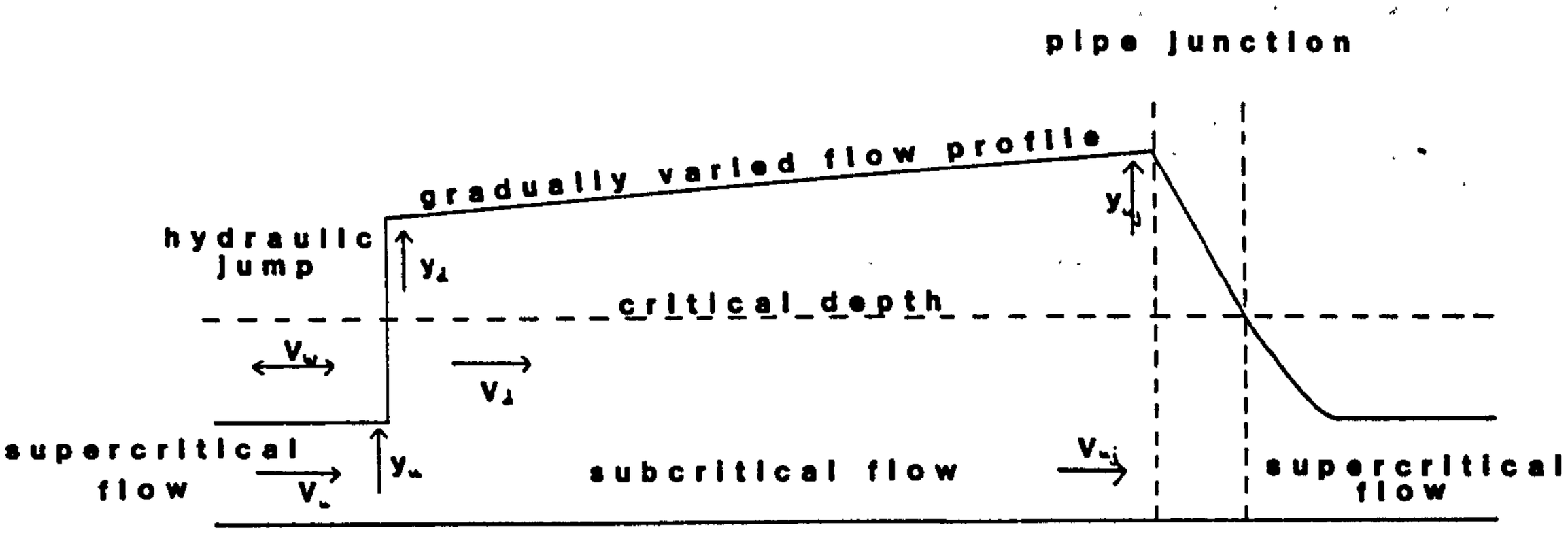

Figure 11.7 Junction model

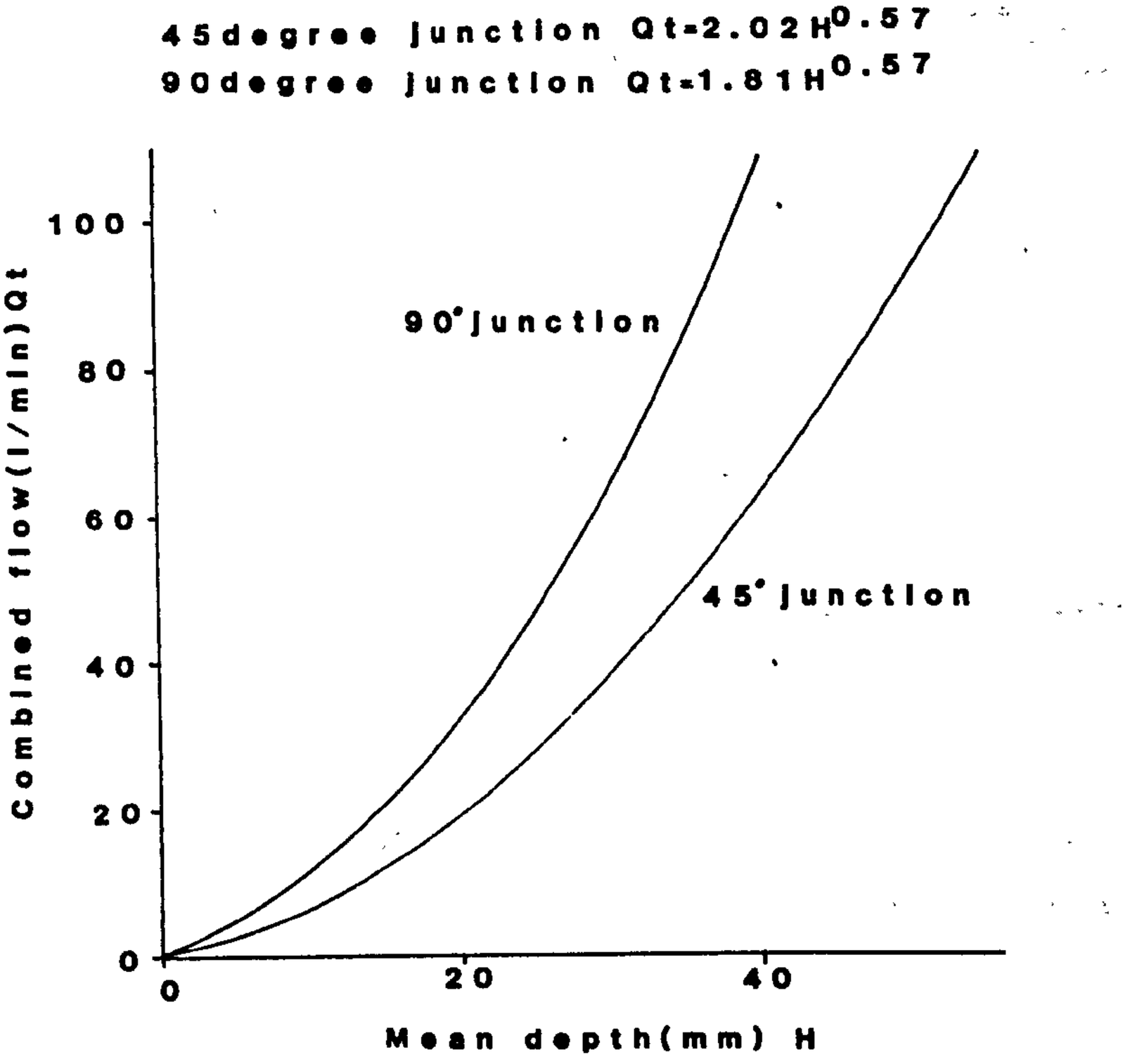

Figure 11.8 Depth just upstream of the junction versus the combined flow in the main and branch pipes

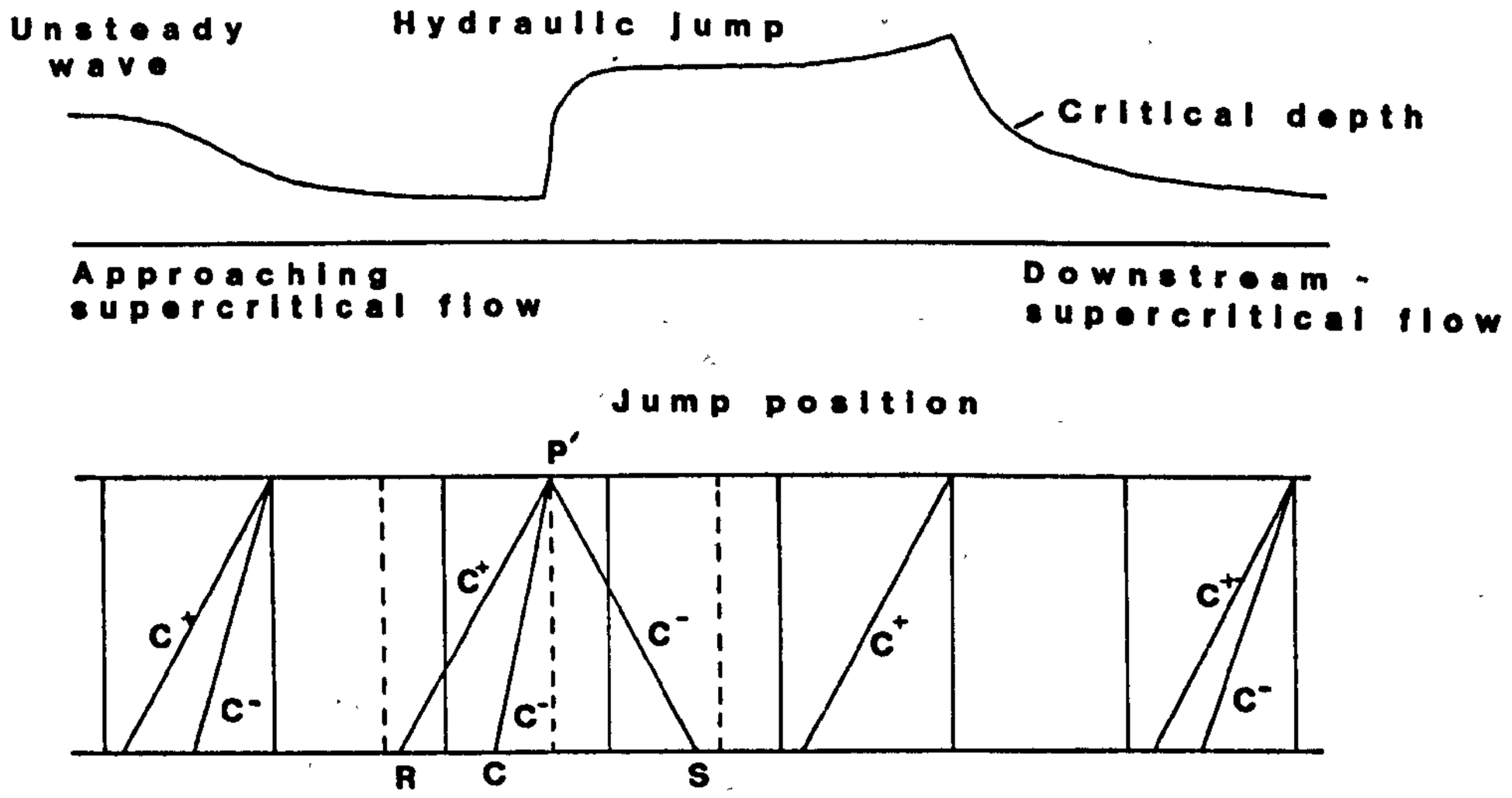

Figure 11.9 Summary of available characteristics in the junction region

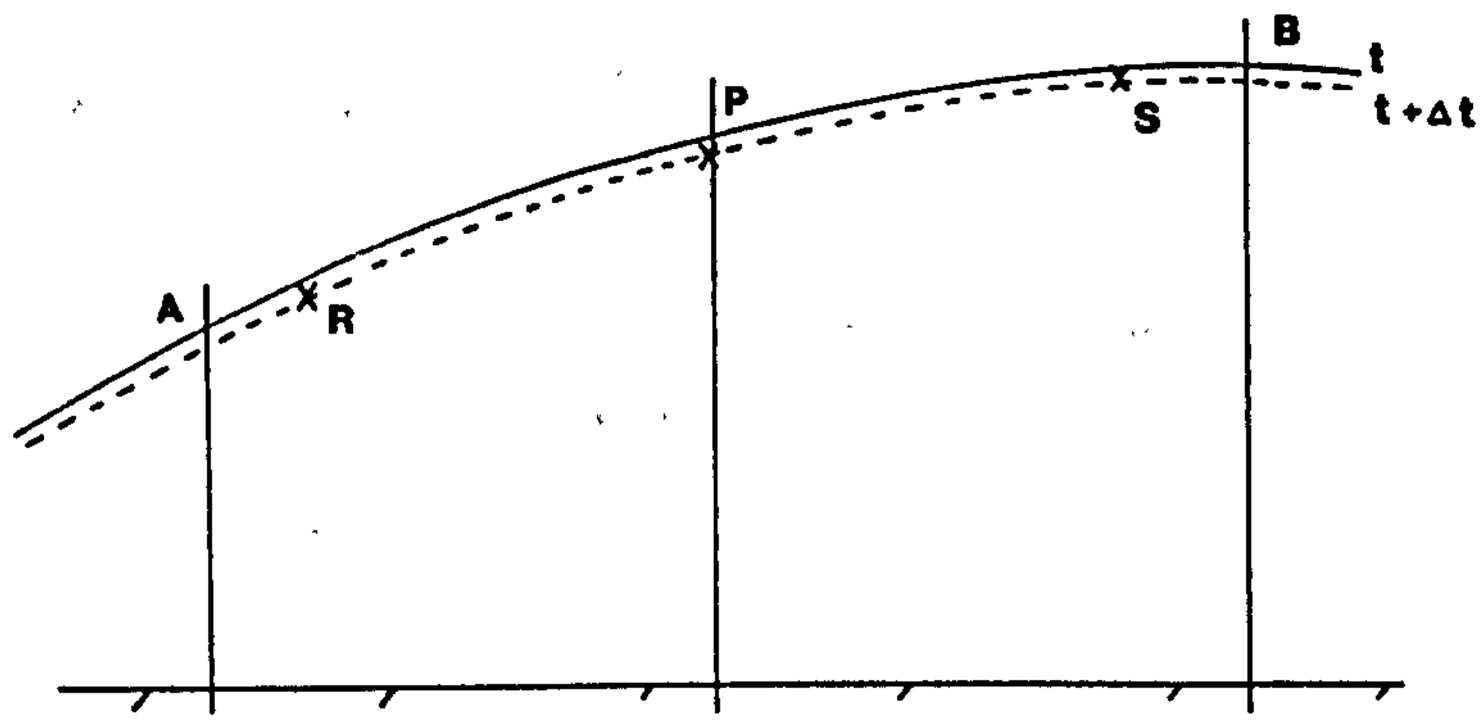

Figure 11.10 Interpolation error on the backwater profile

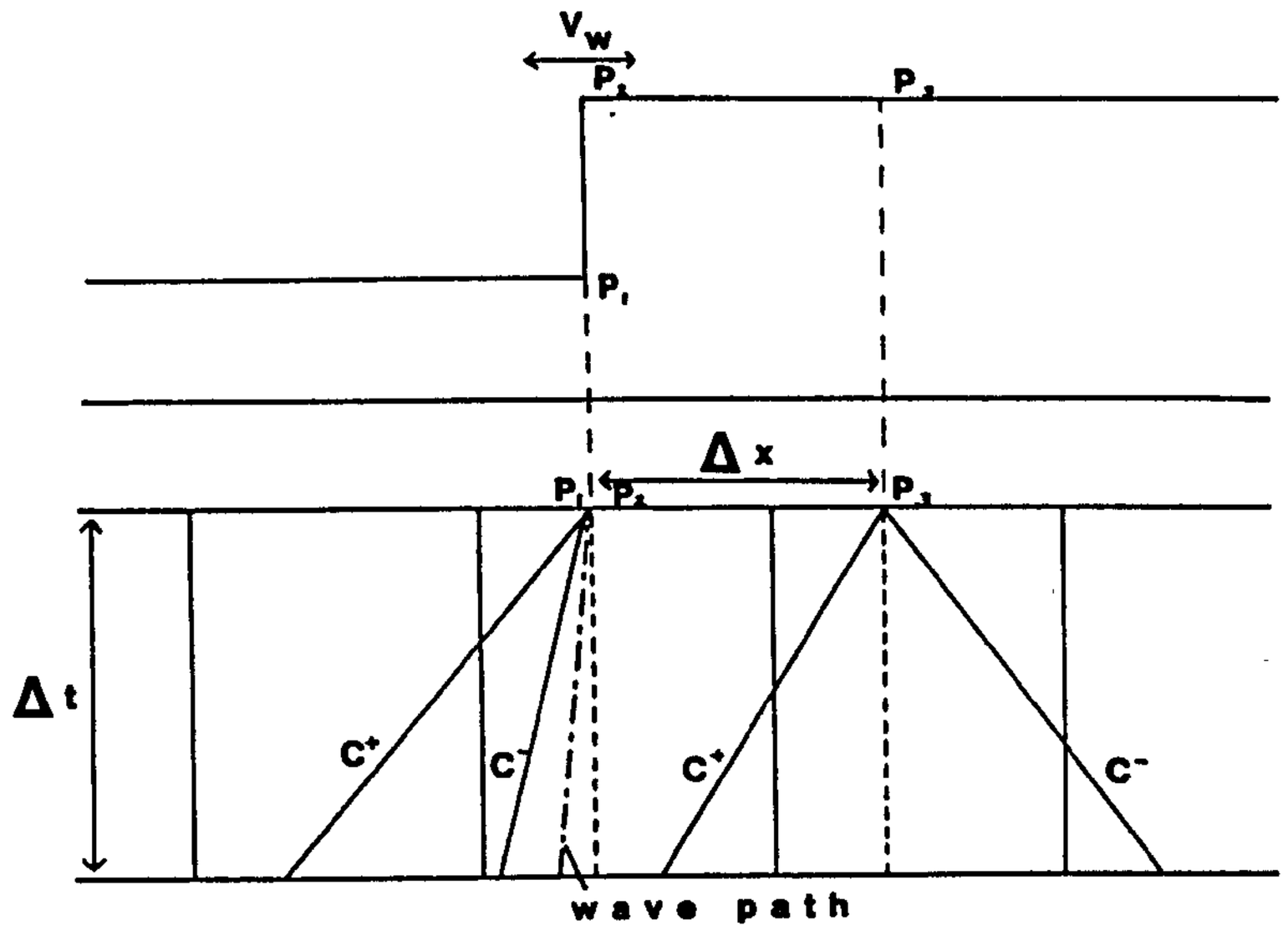

Figure 11.11 Revised jump model

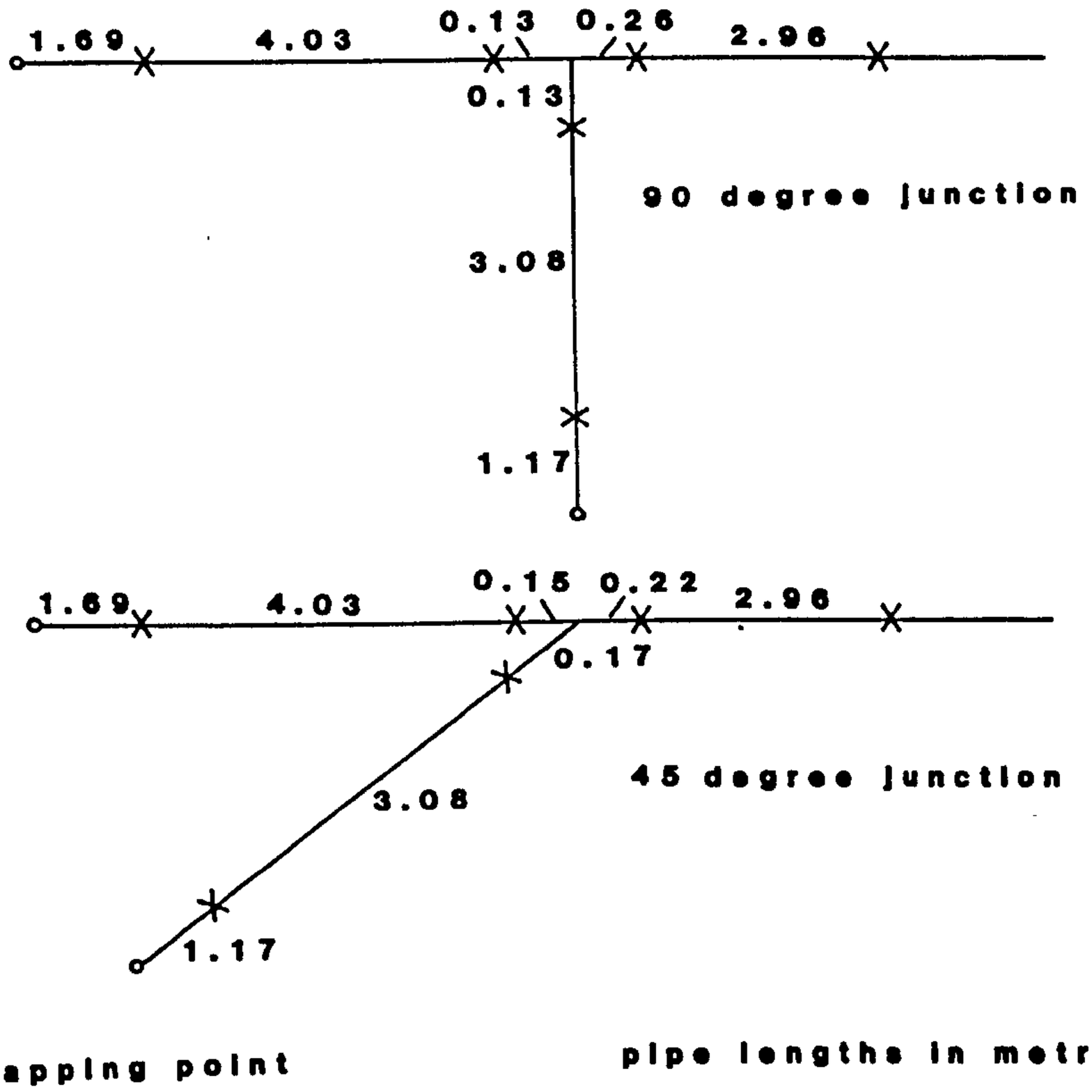

Figure 11.12 Position of the tapping points

Slope	Pressure wave in main	Pressure wave in branch	Pressure wave in both	Cistern wave in main	Cistern wave in main, pressure wave in branch
1/50	x	x	x		
1/80	o	o	o	x	x
1/100	x	x	x	o	o
1/150	o	o	o		
1/200				o x	o x

o 45 degree junction

x 90 degree junction

Figure 11.13 Unsteady flow tests

Figure 11.14 Backflow at the junction and movement of the steep-fronted wave (gradient of 1/150)

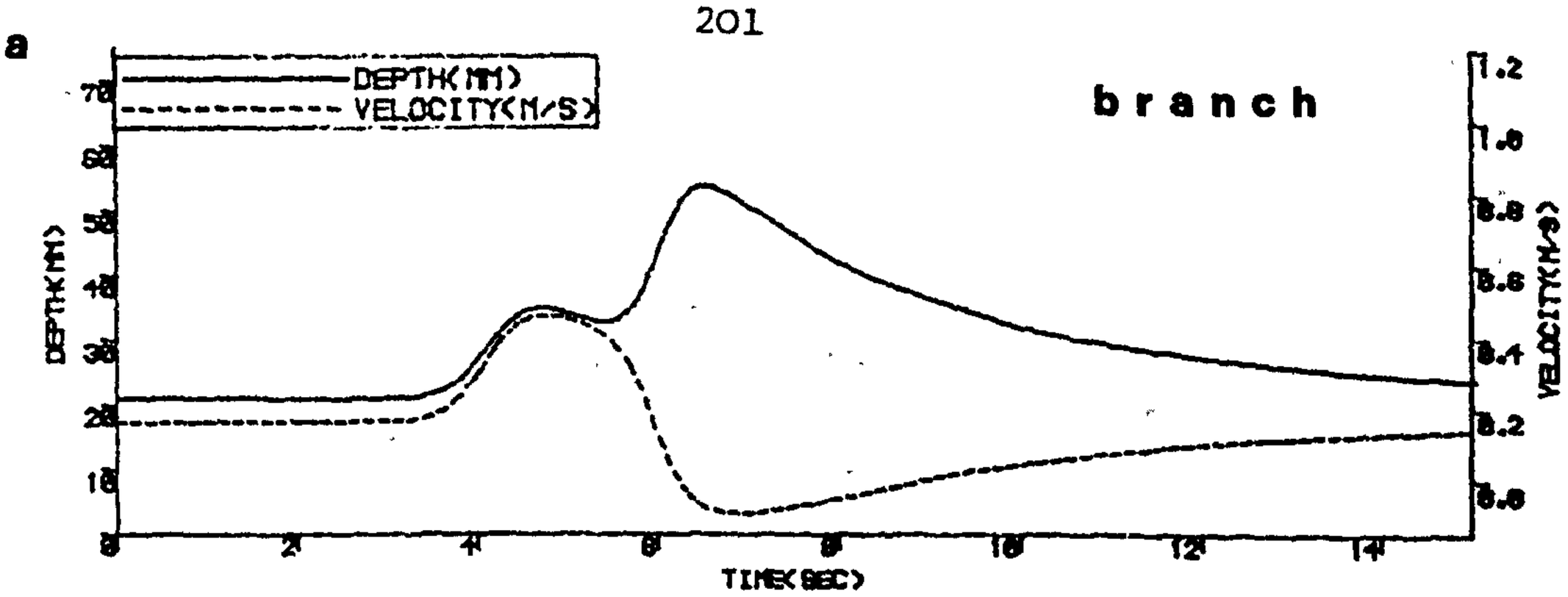

Figure 11.15 Backflow at the junction and movement of the steep-fronted wave (gradient of 1/100)

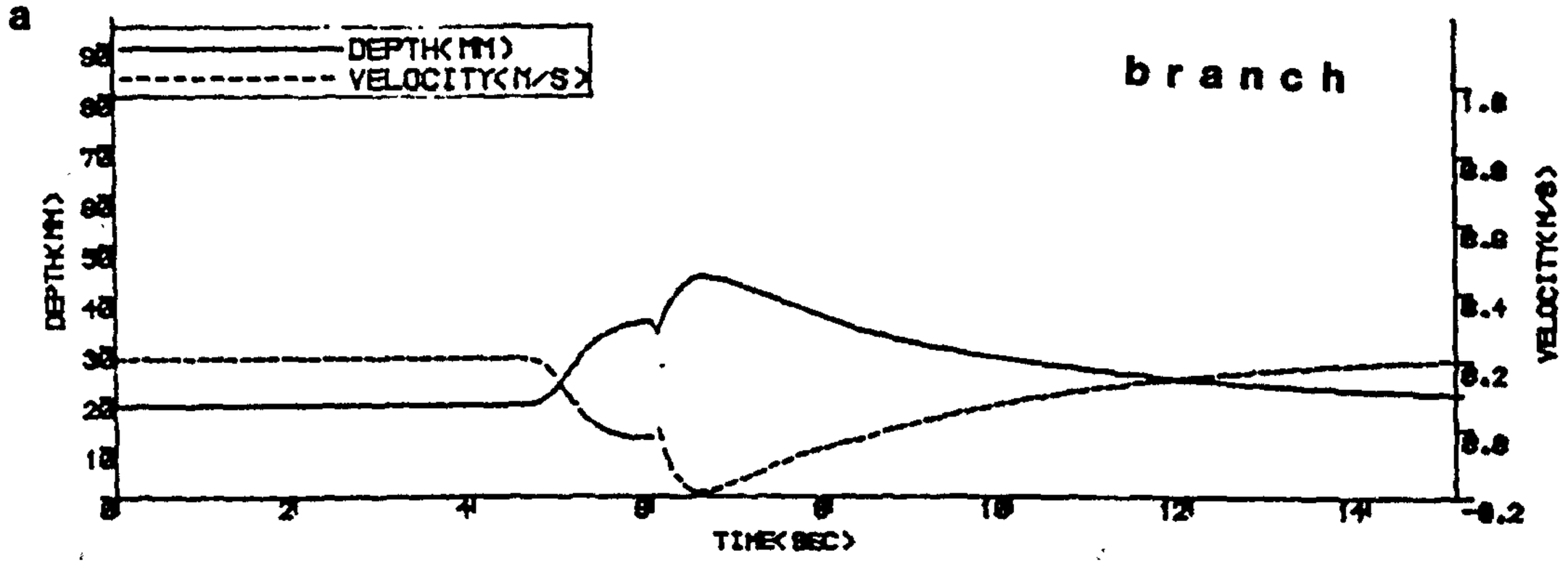

Figure 11.16 Backflow at the junction and movement of the steep-fronted wave (gradient of 1/80)

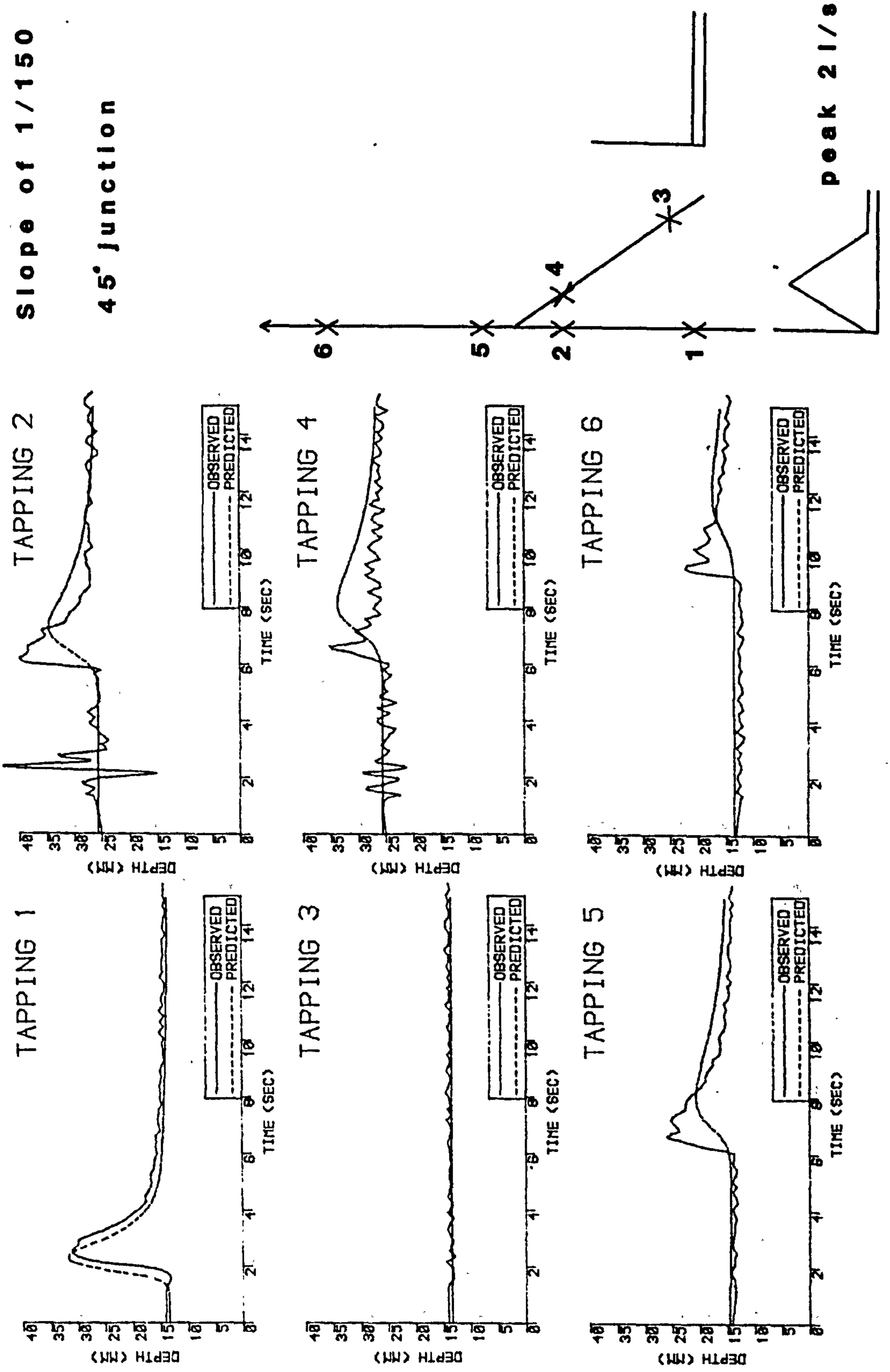

Figure 11.17 Attenuation of the wave through a junction (gradient of 1/150)

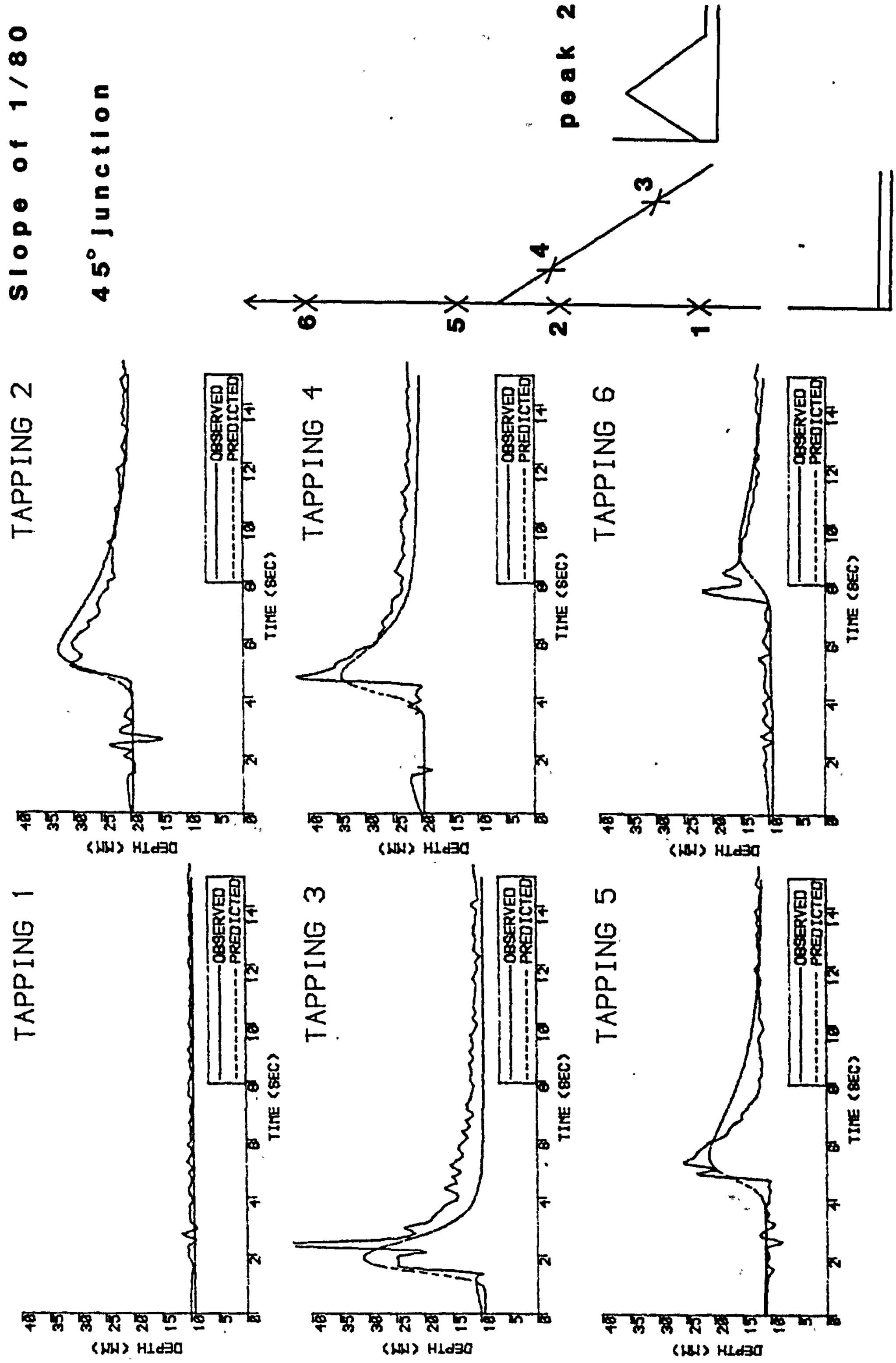

Figure 11.18 Attenuation of the wave through a junction (gradient of 1/80)

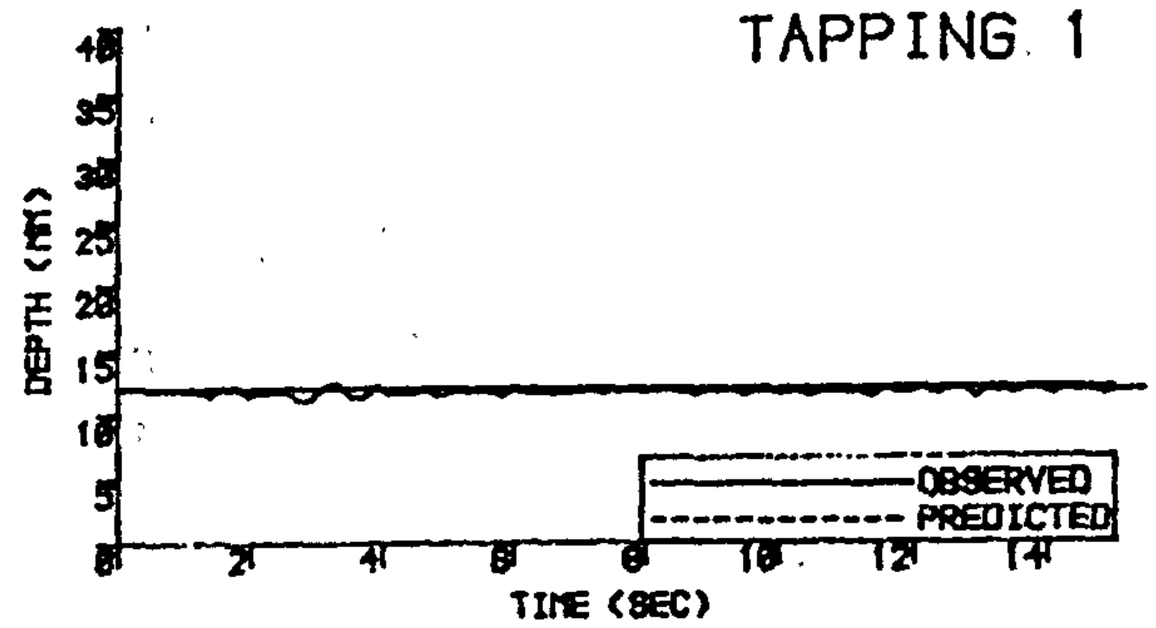

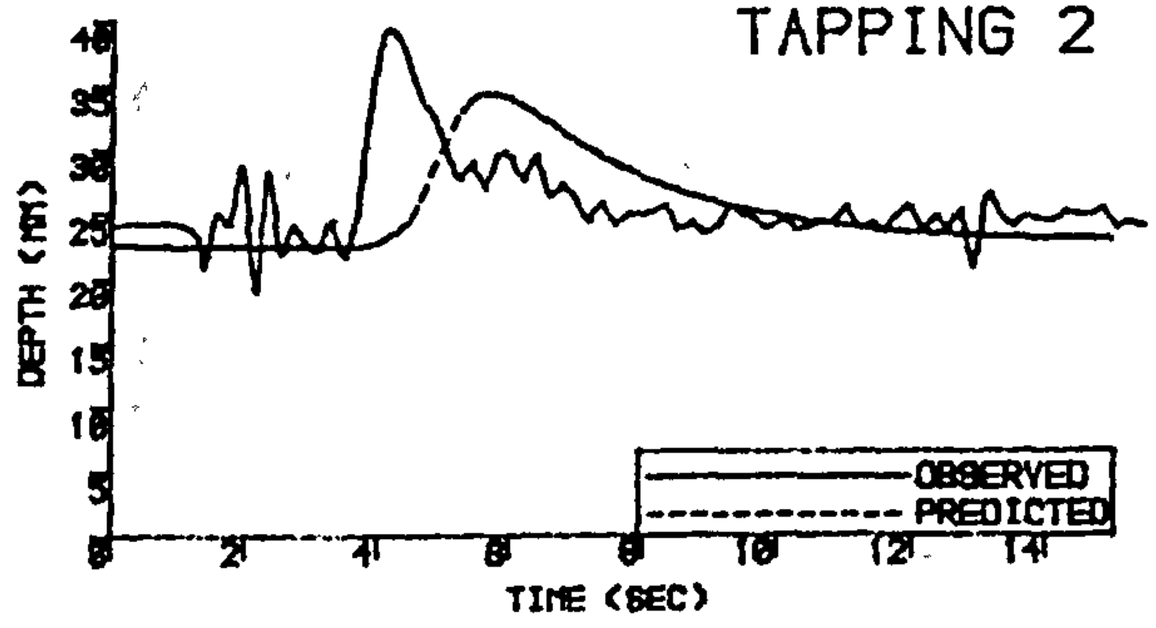

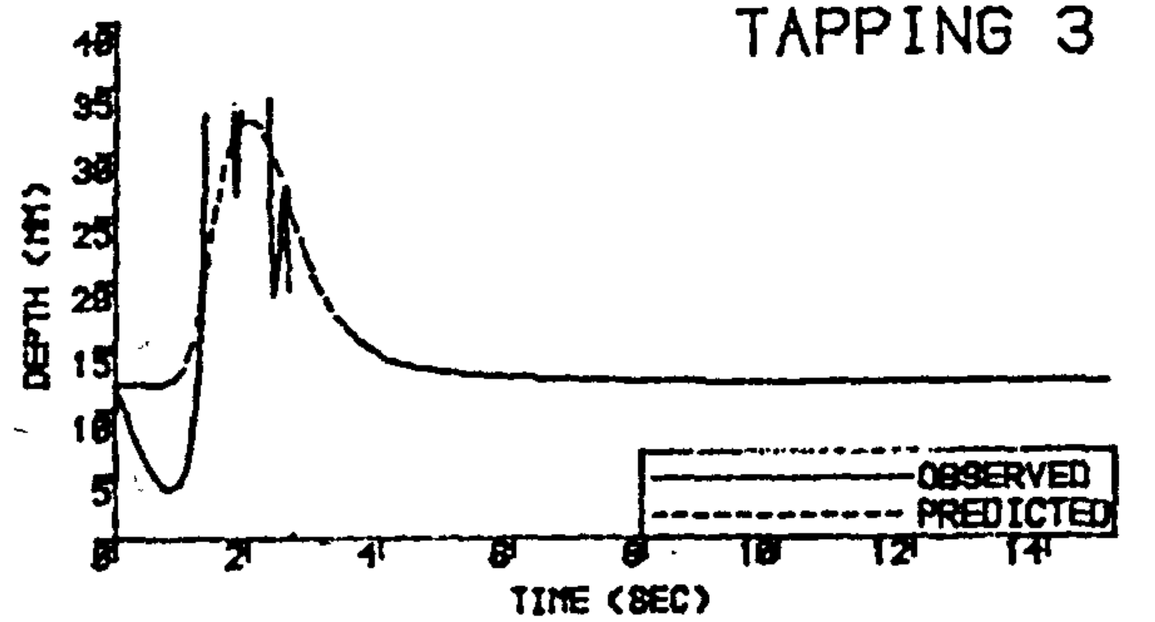

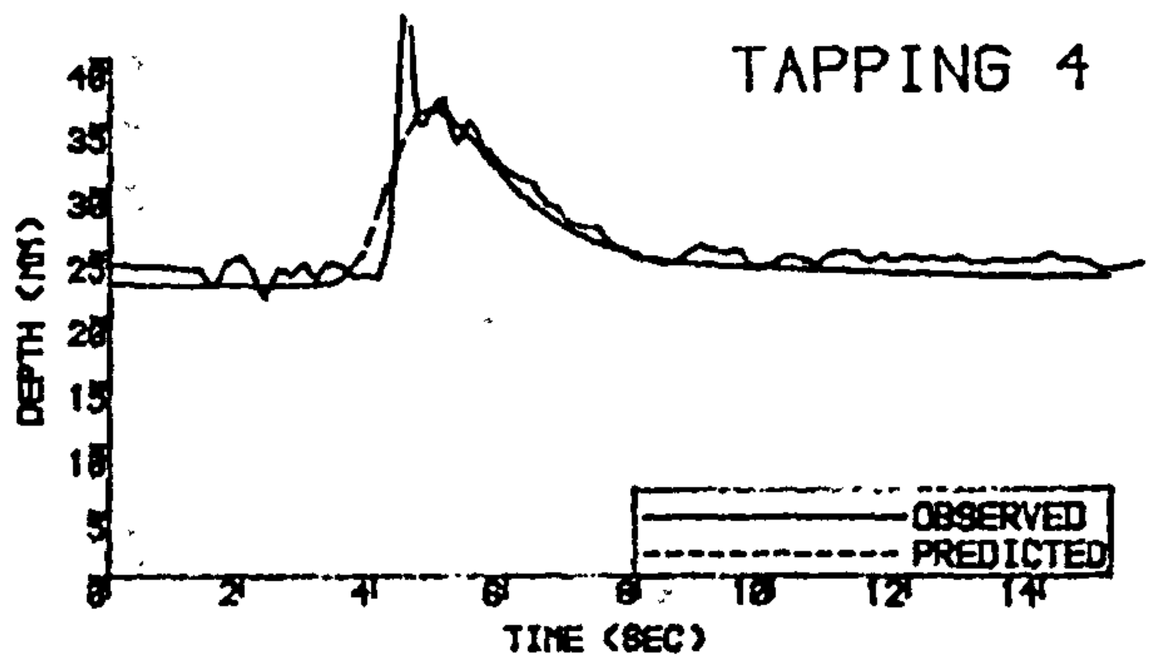

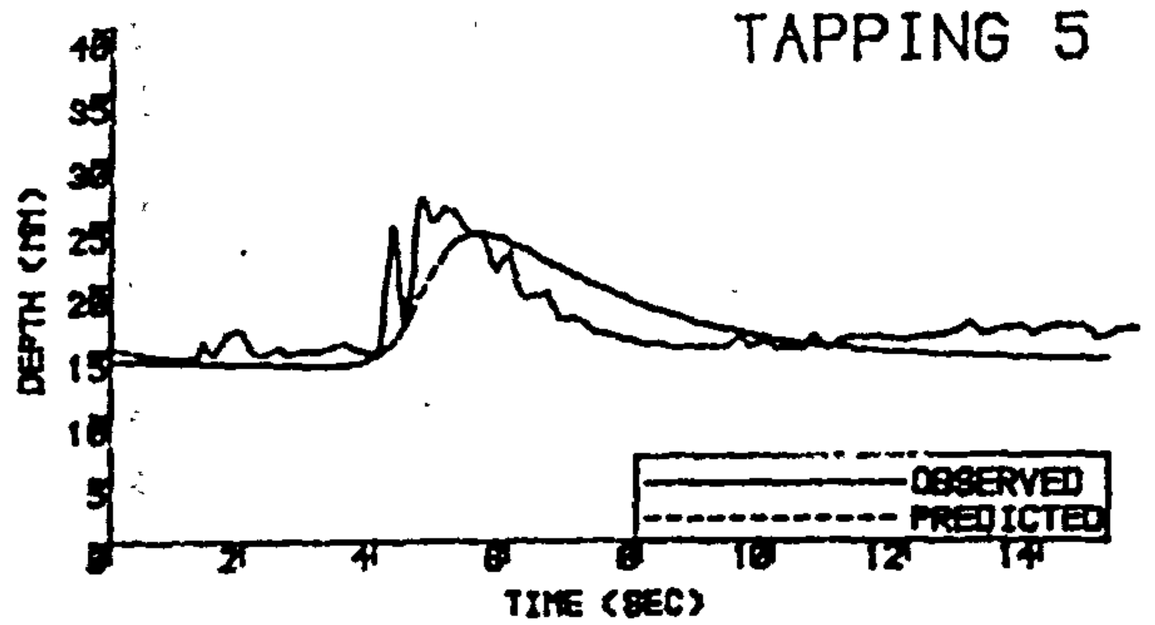

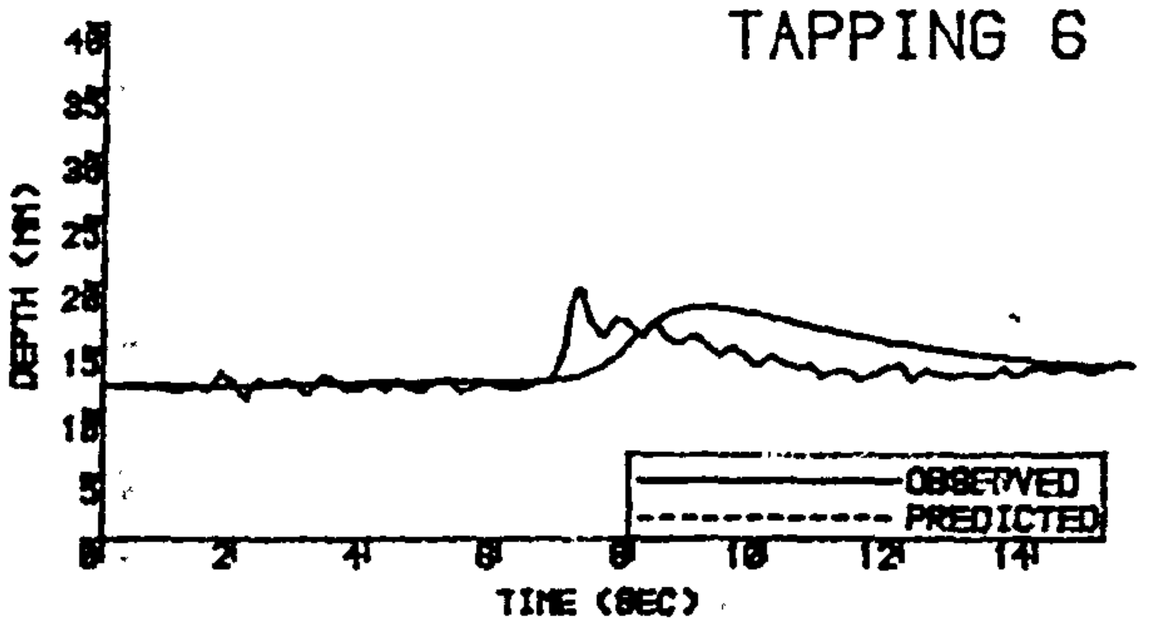

Slope of 1/100

90° junction

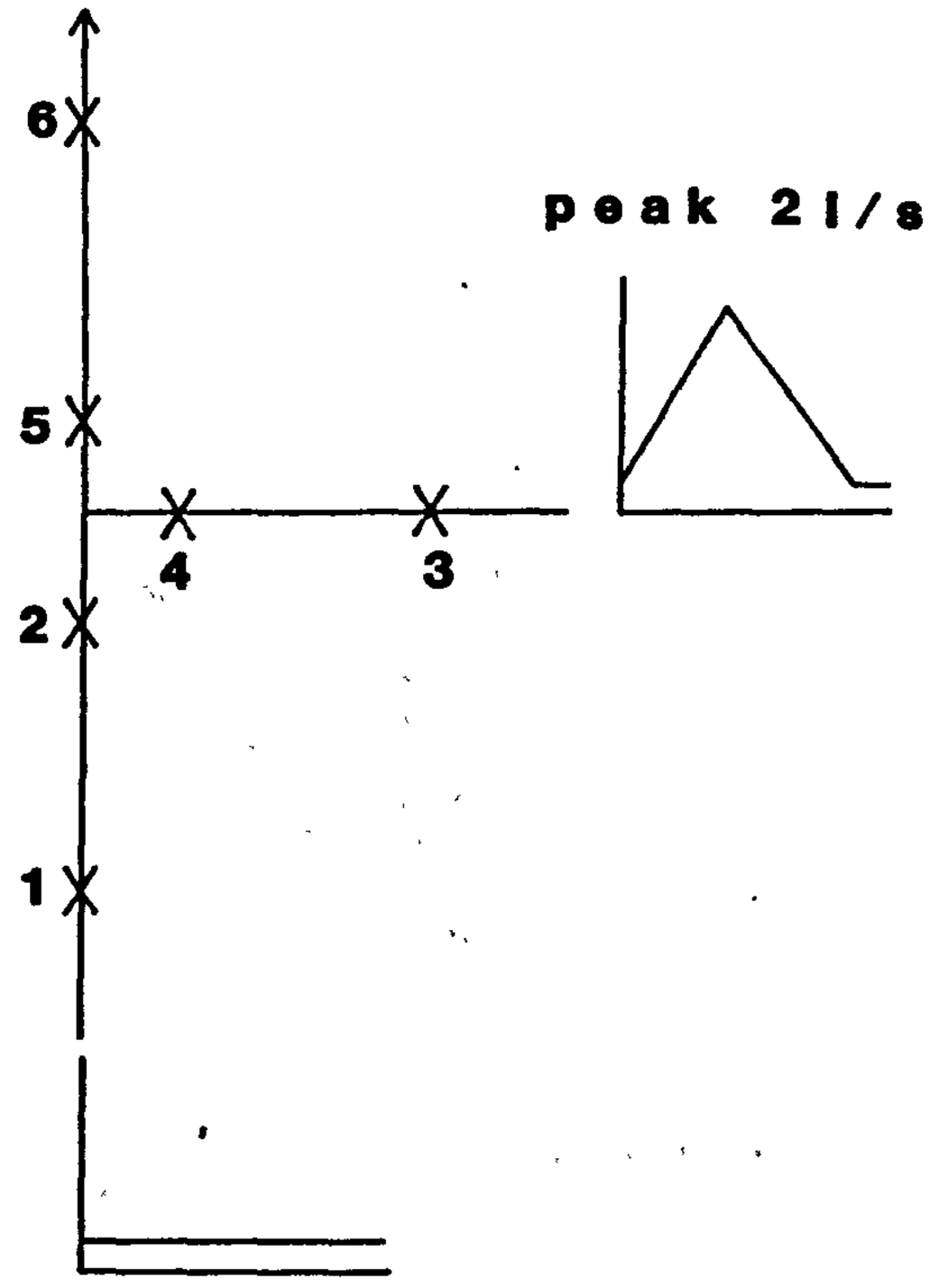

peak 2 l/s

Figure 11.19 Attenuation of the wave through a junction (gradient of 1/100)

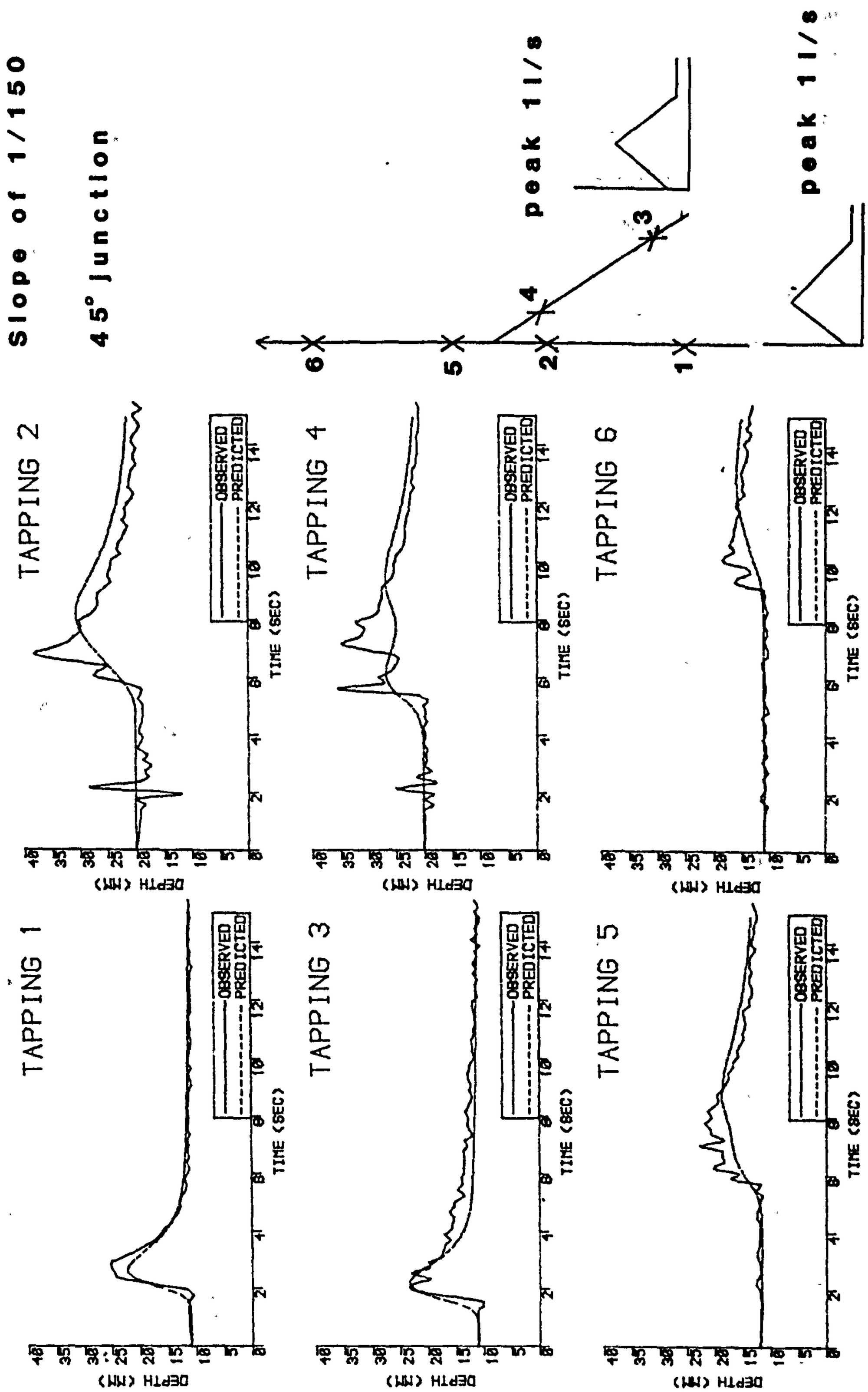

Figure 11.20 Attenuation of the wave through a junction (gradient of 1/150)

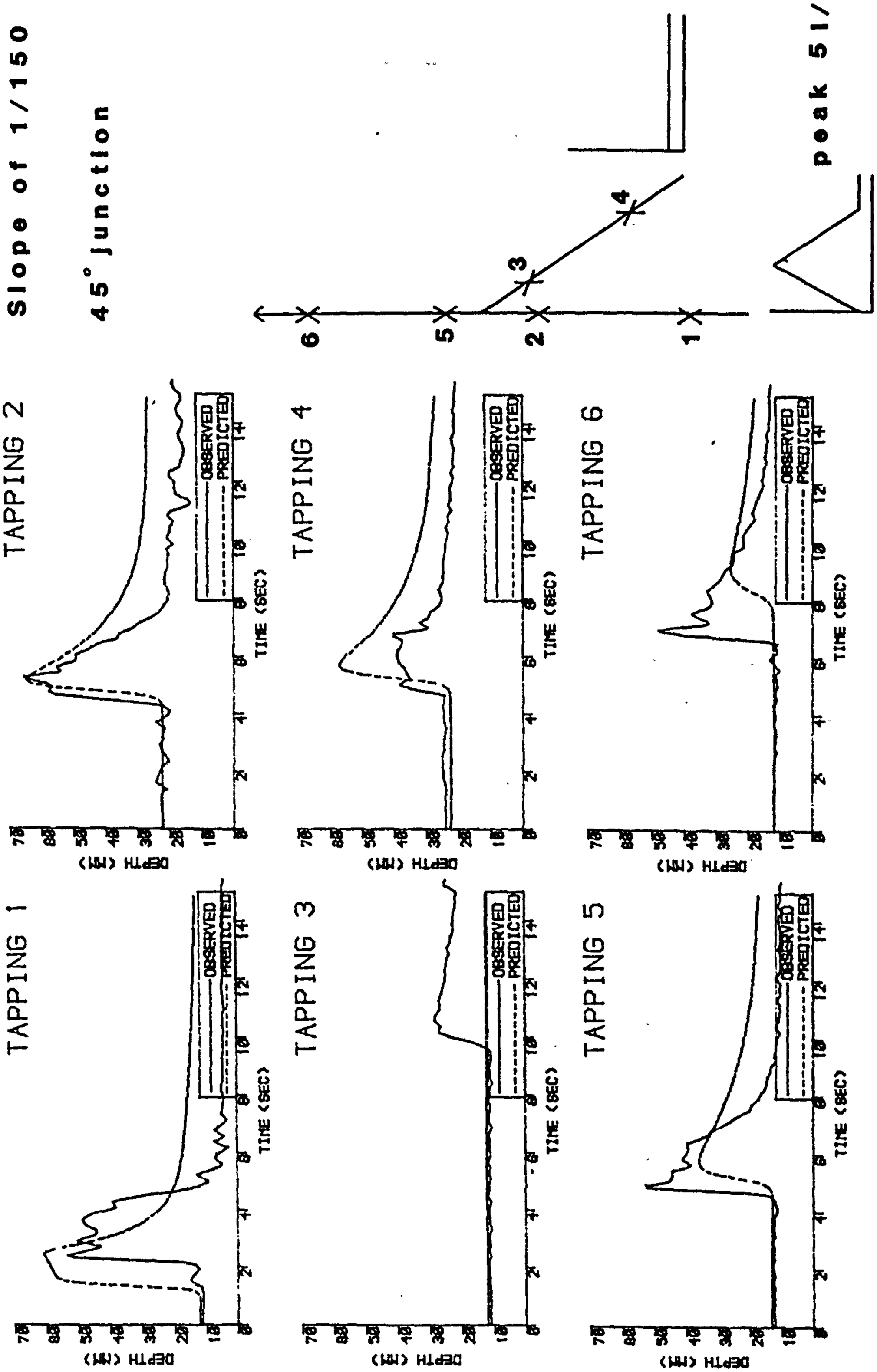

Figure 11.21 Attenuation of the wave through a junction (gradient of 1/150)

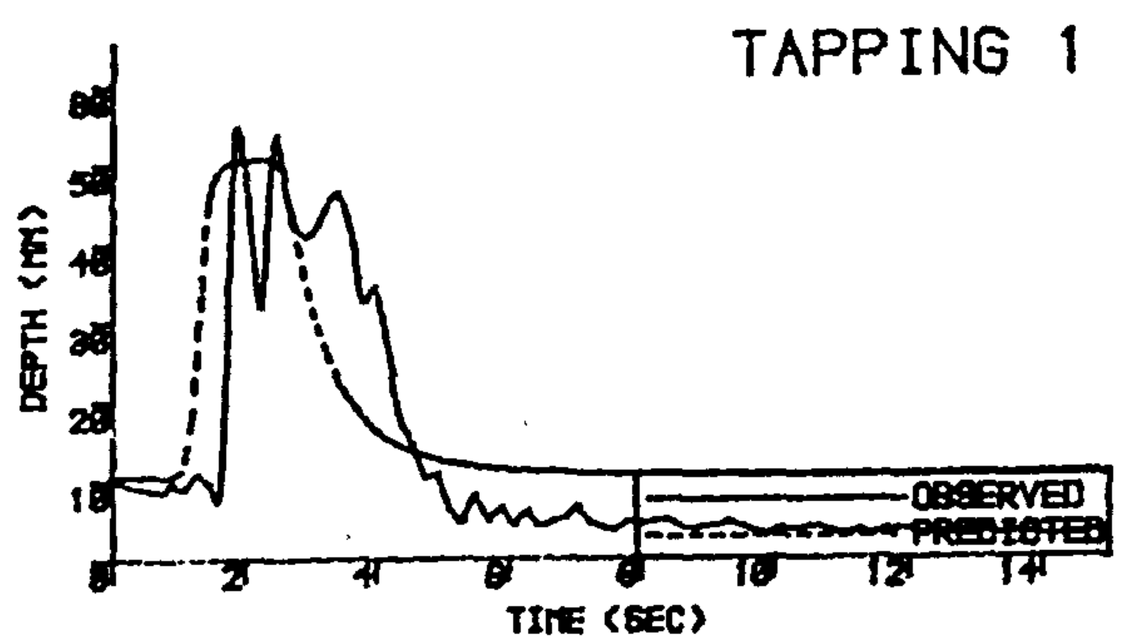

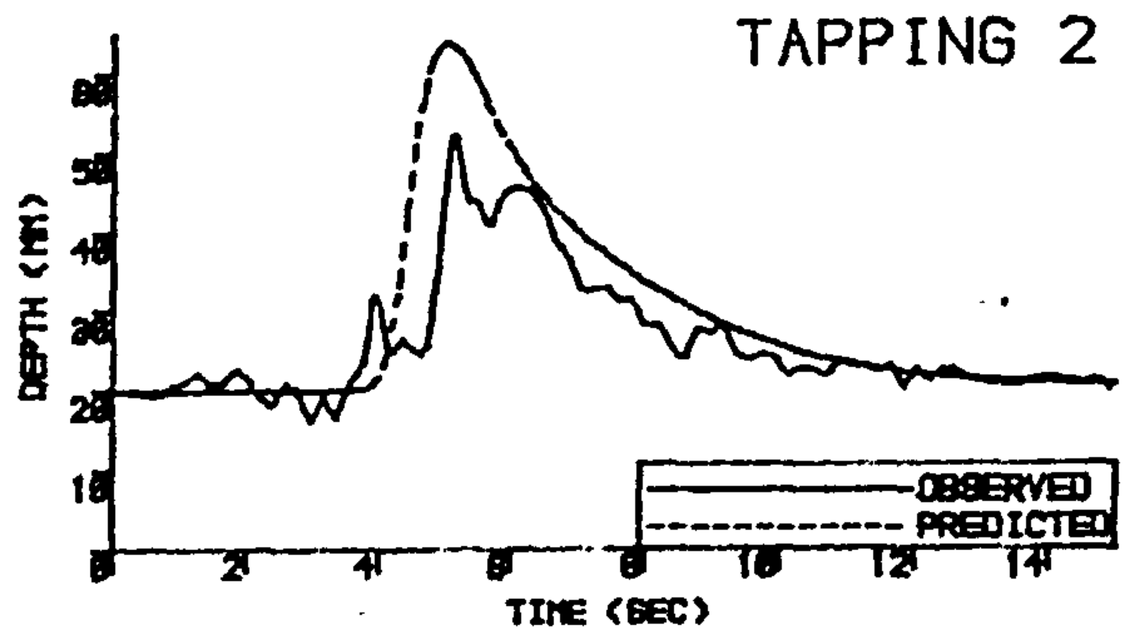

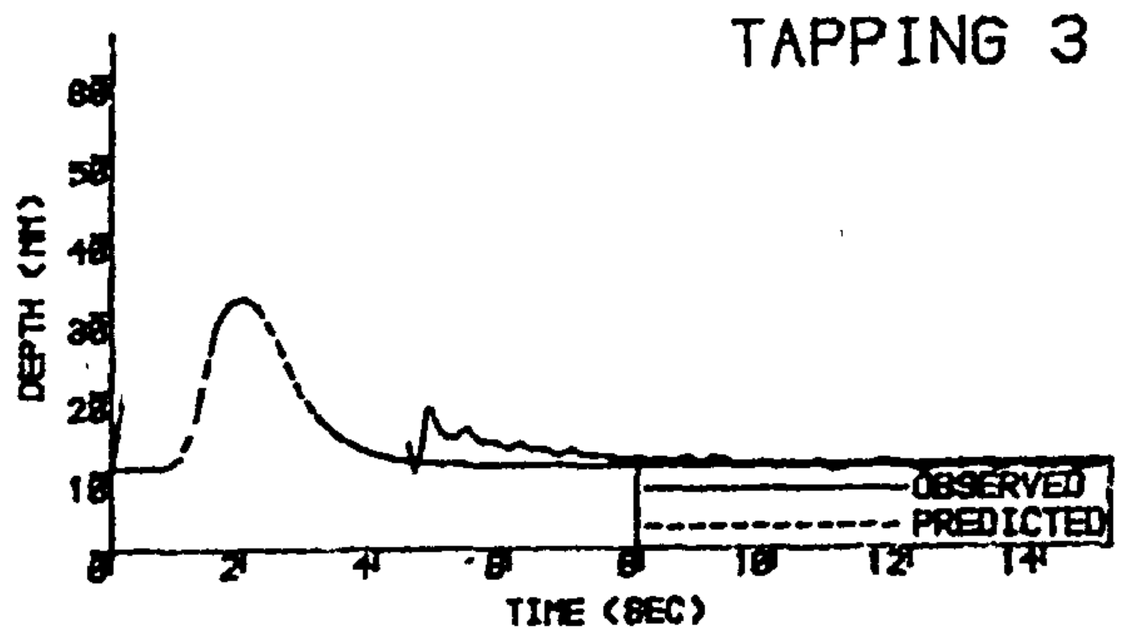

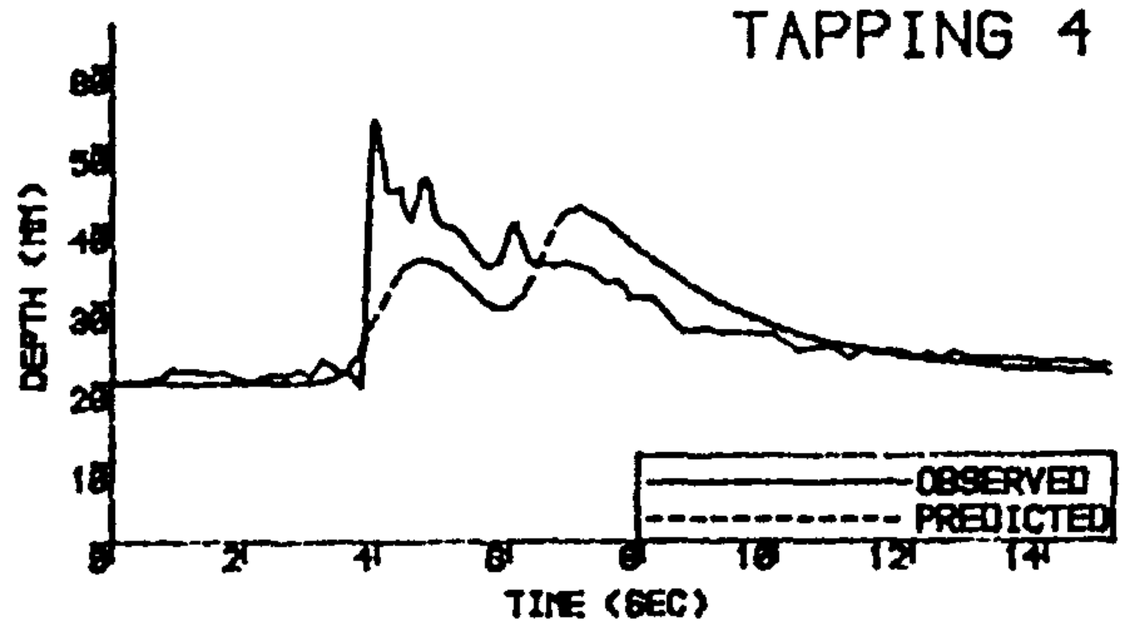

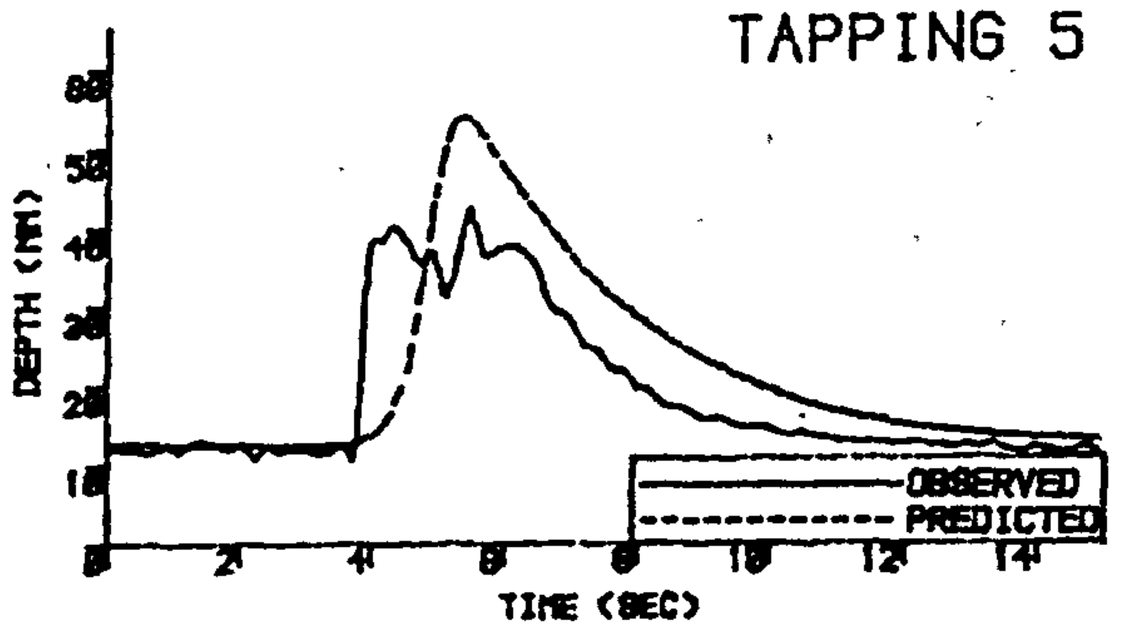

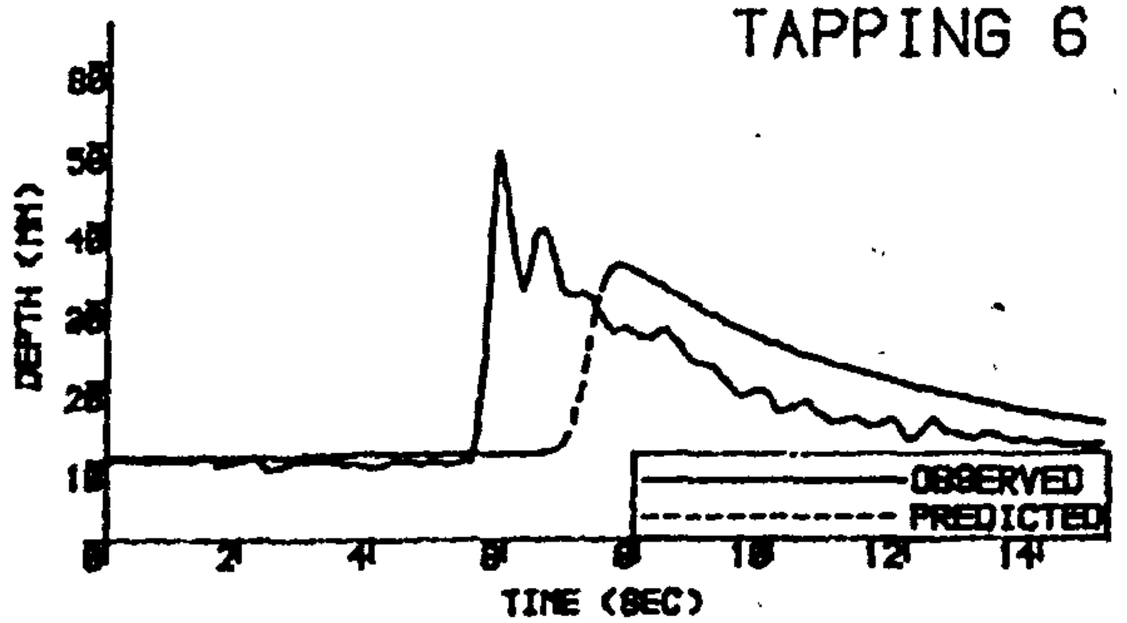

Slope of 1/80

90° junction

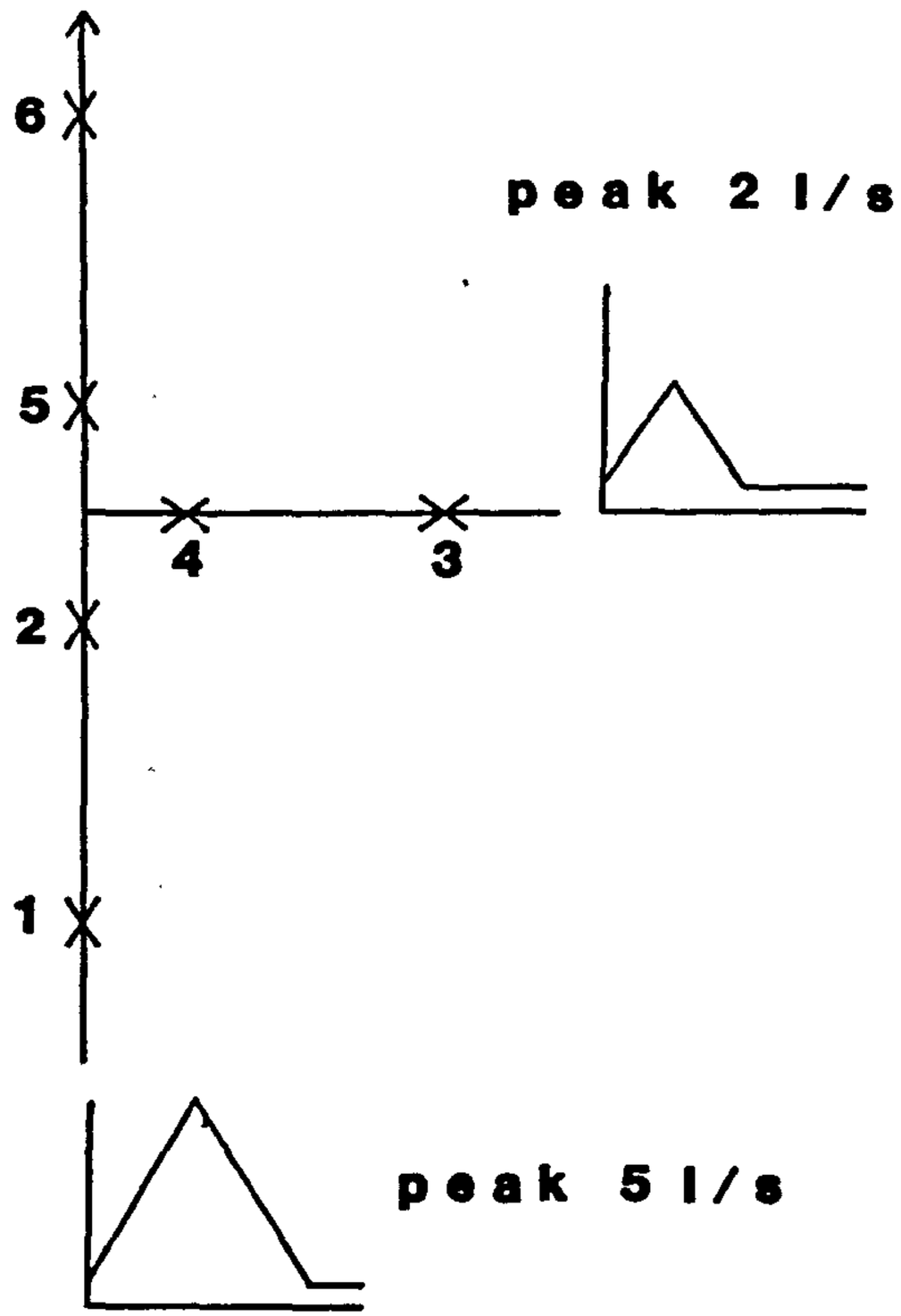

Figure 11.22 Attenuation of a wave through a junction (gradient of 1/80)

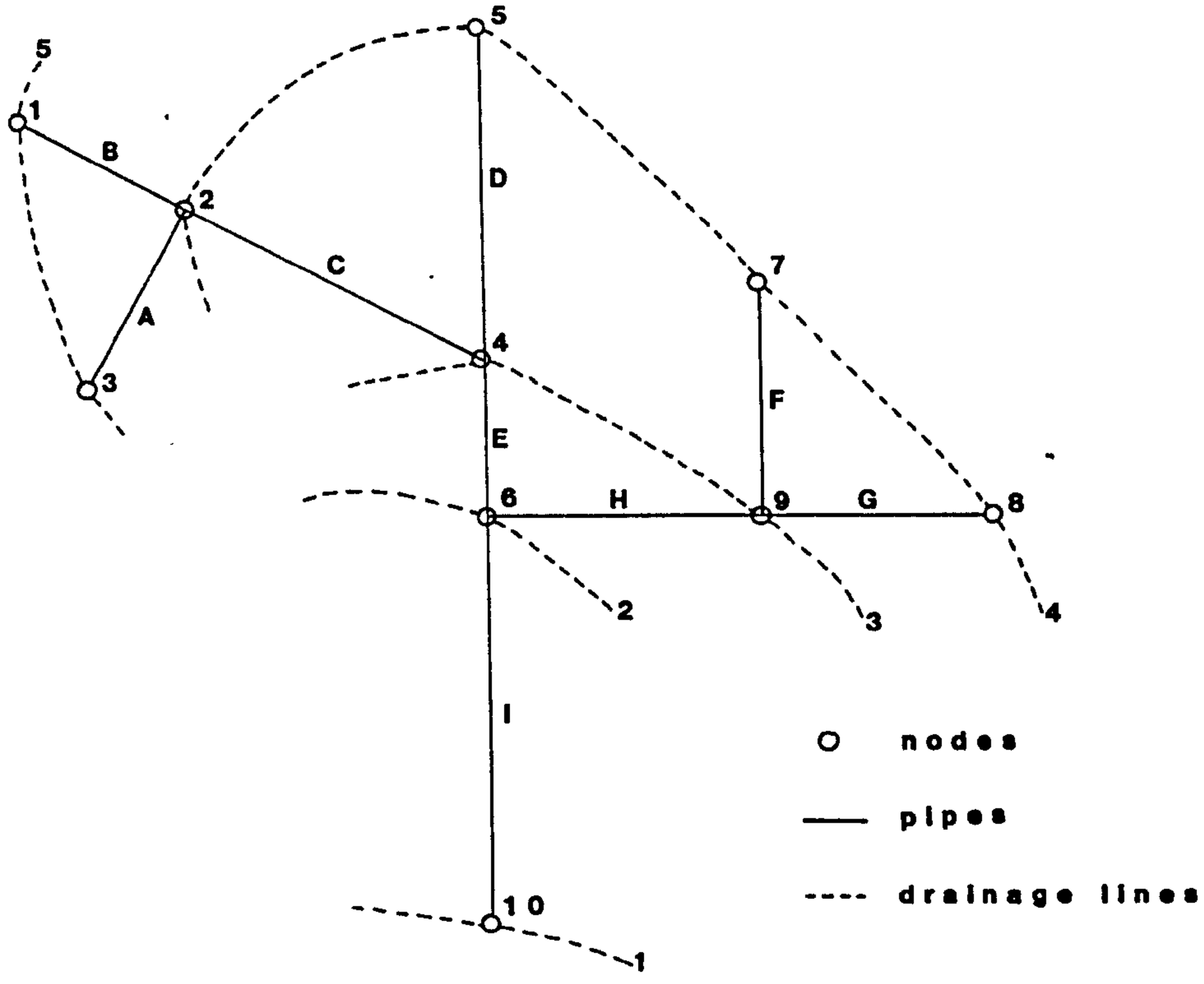

Figure 12.1 Network with drainage lines

node \ pipe	A	B	C	D	E	F	G	H	I	Pn	DL
1		X								1	5
2	X	X	X							3	4
3	X									1	5
4			X	X	X					3	3
5				X						1	4
6					X			X	X	3	2
7						X				1	4
8							X			1	4
9						X	X	X		3	3
10									X	1	1
β	1	1	1	1	1	1	1	1	1		

Figure 12.2 Node incidence matrix

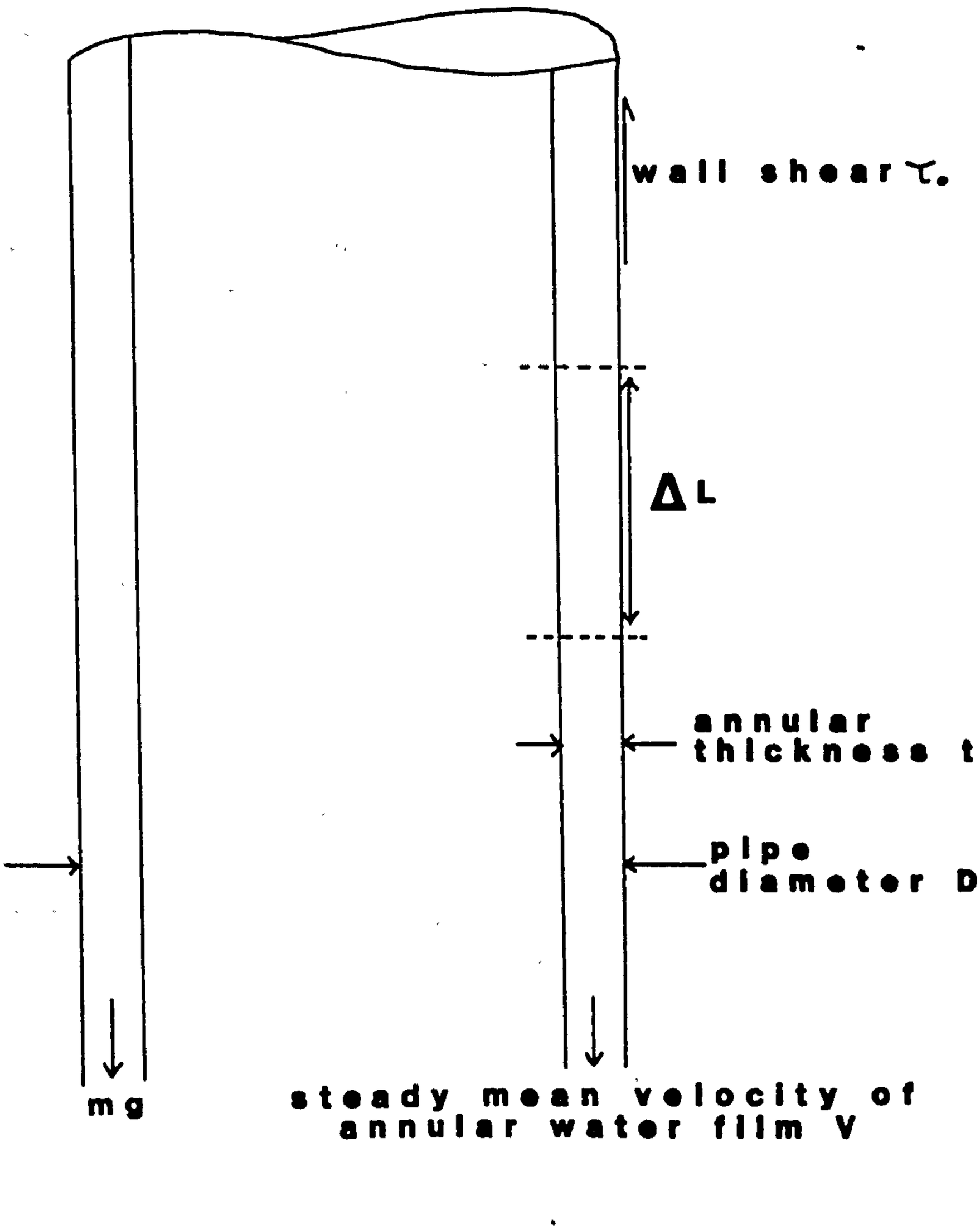

Figure 12.3 Fully developed annular flow in a vertical stack

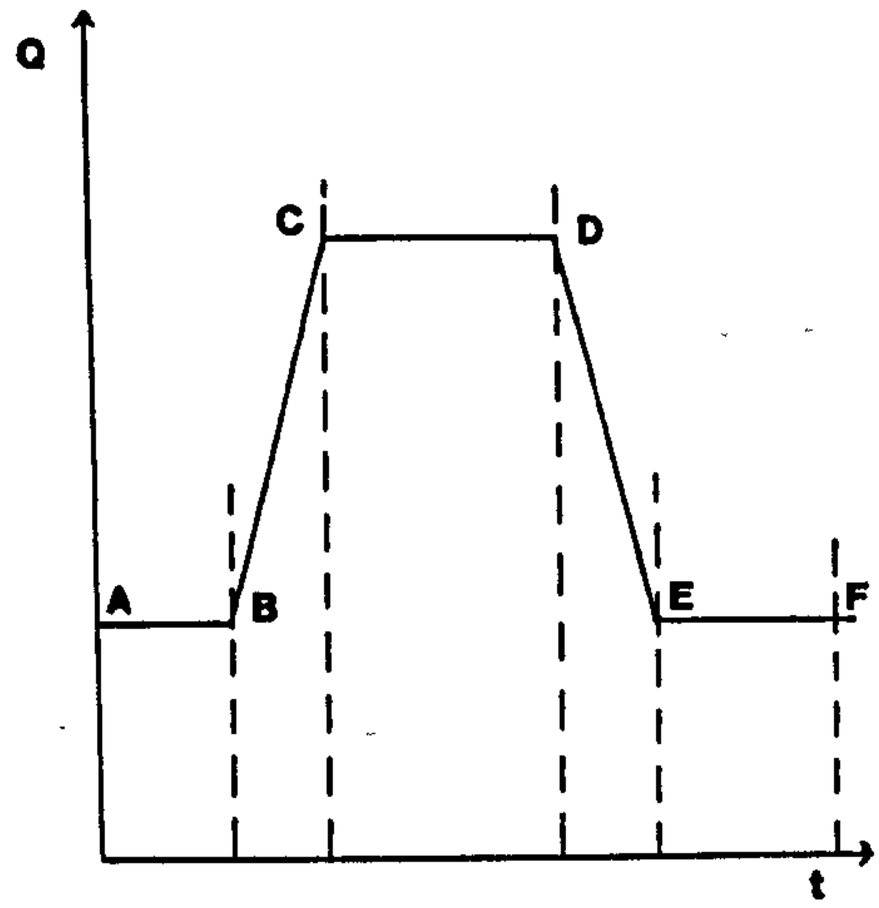

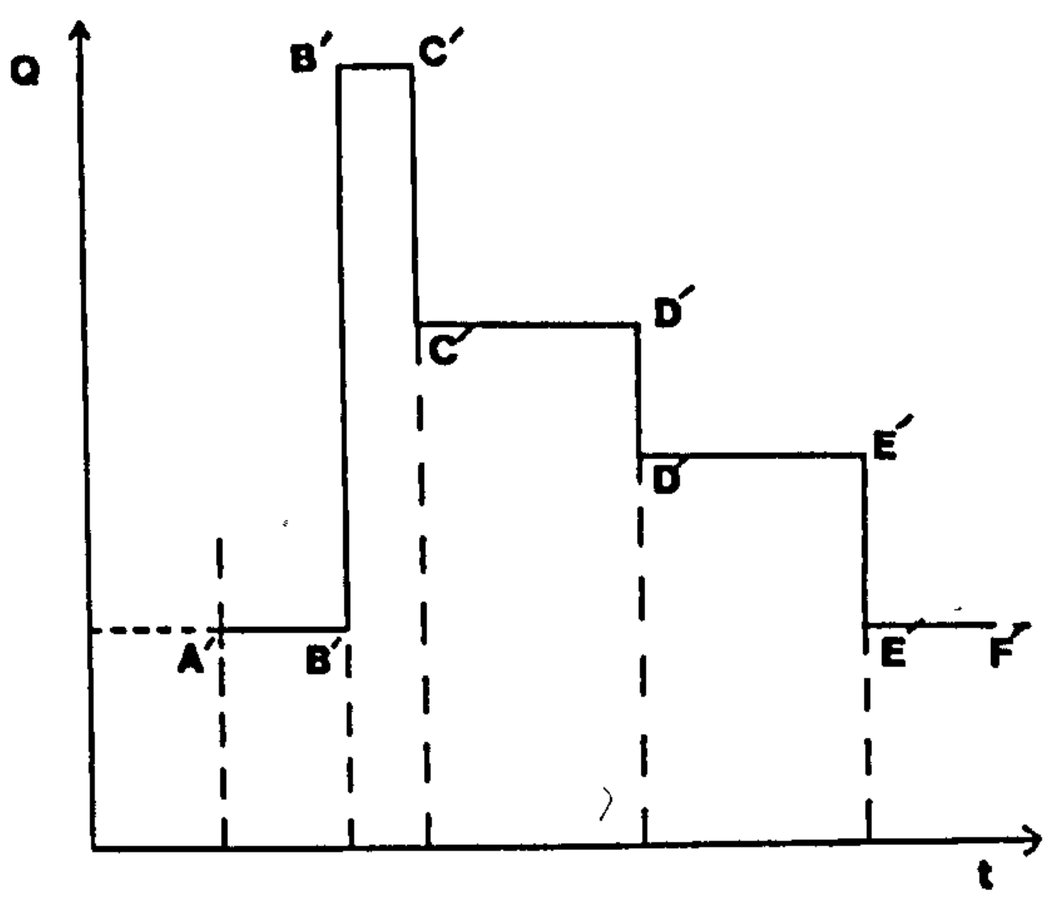

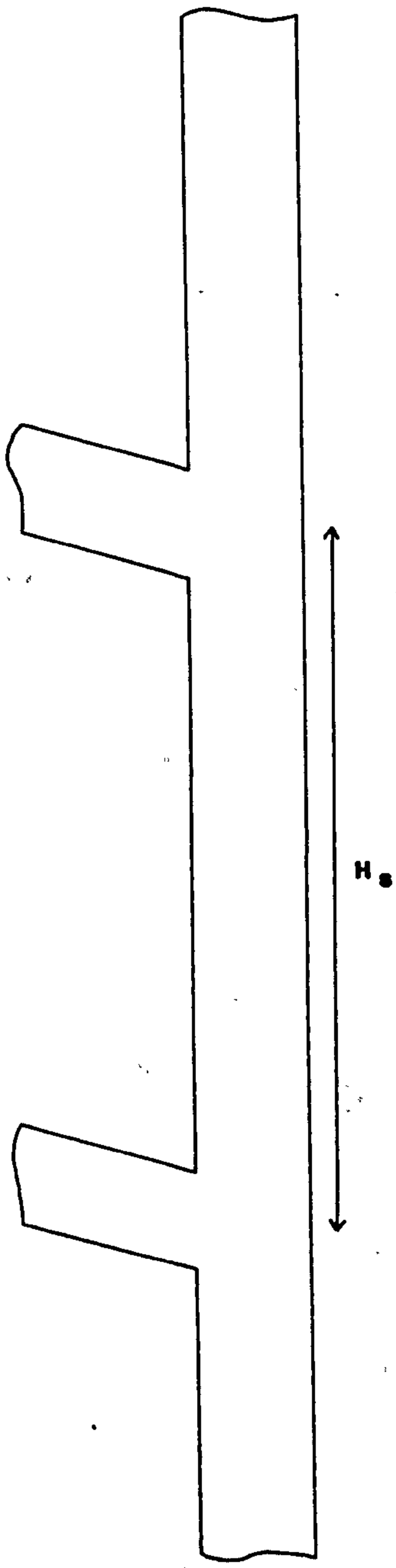

Figure 12.4 Input to the vertical stack

Q discharge in l/s
t time in s

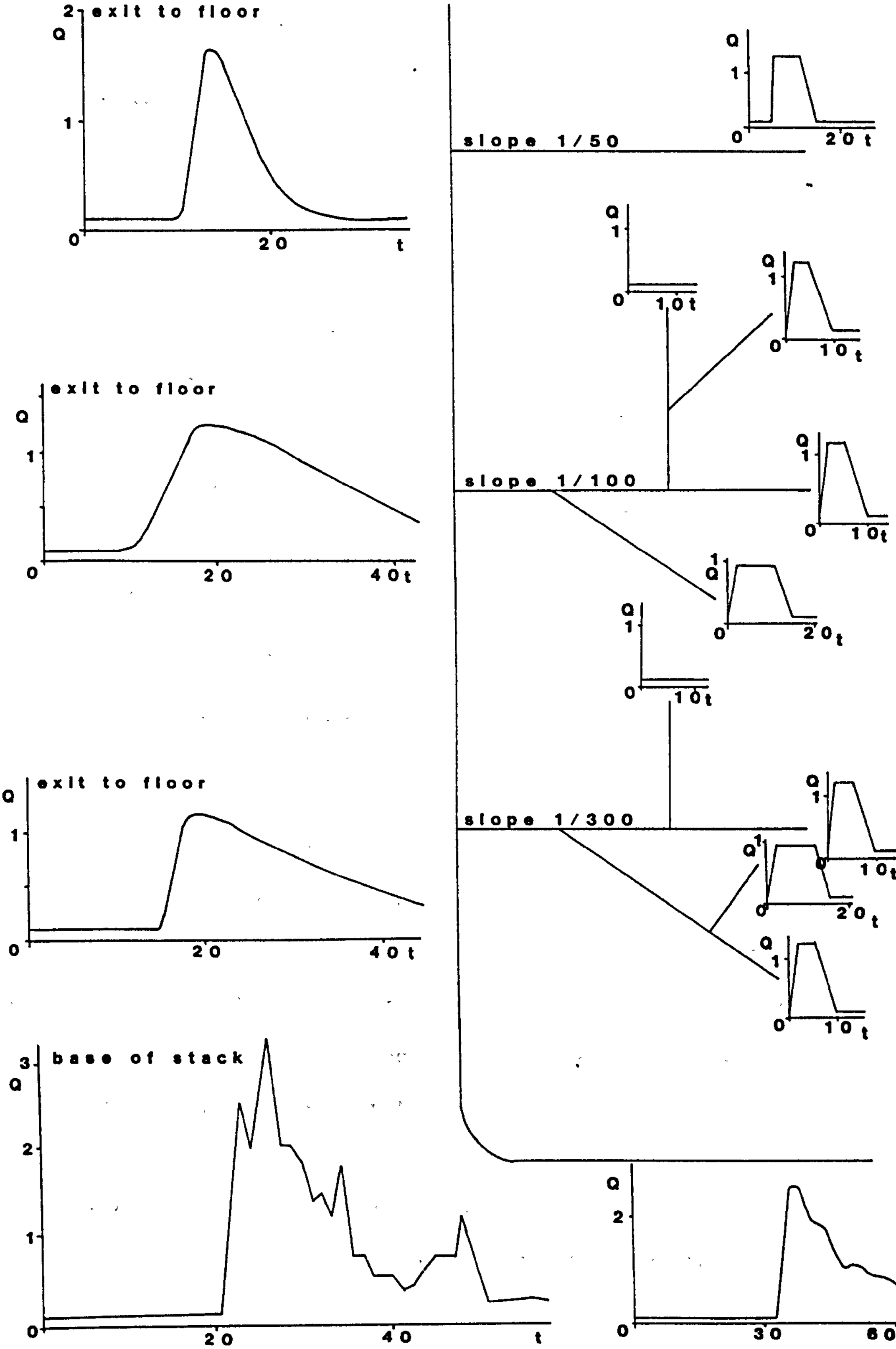

Figure 12.5 The multi-storey building drainage network model

Appendix I:

A1.1 The Energy Principle

The specific energy of the flow with reference to the channel bed as datum is defined as,

$$E = y + \frac{V^2}{2g} = y + \frac{Q^2}{2gA^2} \qquad (A1.1)$$

where E = specific energy of flow (m)

y = flow depth (m)

V = flow velocity (m/s)

g = acceleration due to gravity (m/s^2)

Q = discharge (m^3/s)

A = cross-sectional area (m^2)

For the simple case of a rectangular channel with a flow width b the specific energy may be expressed,

$$E = y + \frac{Q^2}{2g(yb)^2} \qquad (A1.2)$$

This may be rearranged to give,

$$y^3 - Ey^2 + \frac{Q^2}{2gb^2} = 0 \qquad (A1.3)$$

For given values of E and Q this equation has three roots, one of which is imaginary. Figure A1.1 shows the two possible alternate depths, one falling on the upper limb and one on the lower limb of the curve. Two possible flow régimes are therefore represented, slow and deep (tranquil) on the upper limb and fast and shallow (rapid) on the lower limb. The transition between these two régimes is known as critical flow which is defined as the state at which the specific energy E is a minimum for a given Q (Figure A1.1).

The critical depth is found by determining the minimum value of

the specific energy,

$$\frac{dE}{dy} = 0 = 1 - \frac{Q^2}{gA^3}\frac{dA}{dy} \qquad \text{(A1.4)}$$

Now dA = Tdy, where T is the surface width of flow in metres so the last equation may be expressed,

$$1 - \frac{Q^2T}{gA^3} = 0 \qquad \text{(A1.5)}$$

The value of y which will satisfy this equation is known as the critical depth of flow.

A1.2 Normal Depth

Under steady uniform flow conditions the force balance equation for an element of flow is usually expressed by the Chézy equation,

$$V = C\sqrt{RS_o} \qquad \text{(A1.6)}$$

where C = Chézy coefficient

R = hydraulic radius (m)

S_o = channel slope

Manning found the value of C to be dependent upon the hydraulic radius and the surface roughness of the channel; this gave rise to the well-known Manning equation,

$$V = \frac{R^{2/3}S_o^{1/2}}{n} \qquad \text{(A1.7)}$$

Where n = Manning's roughness coefficient

The depth value which will satisfy this equation is known as the normal depth. Critical depth is independent of pipe slope and pipe roughness whilst normal depth is dependent upon both of these factors. Thus a discharge in a particular channel may be tranquil or rapid depending upon the slope of the bed and in a series of channels at the same slope the flow régime will depend upon the surface roughness.

A1.3 Subcritical and Supercritical Flow

Equation A1.5 states that for critical flow the velocity may be expressed,

$$V = \sqrt{\frac{gA}{T}} \qquad (A1.8)$$

This term is equal to the velocity with which a long wave of low amplitude will move in a channel with a water depth y (where y = A/T). This velocity is known as the wavespeed c and is defined for a rectangular channel,

$$c = \sqrt{gy} \qquad (A1.9)$$

If the wavespeed is greater than the flow velocity then the flow is called subcritical (tranquil) and waves may propagate both upstream and downstream. If the wavespeed is less than the flow velocity then the flow is called supercritical (rapid) and waves may only be propagated downstream.

The ratio of the flow velocity to the wavespeed is called the Froude number Fr and it is less than unity for subcritical flow, equal to unity for critical flow and greater than unity for supercritical flow,

$$Fr = \frac{V}{\sqrt{gy}} \qquad (A1.10)$$

The simple approximation that A/T = y is used in Chapter Two to derive the characteristic form of the St. Venant equations. Figure A1.2 shows the difference in wavespeed which results from using this approximation. For flow depths up to 85% of the diameter of the pipe it will ensure that the positive and negative characteristics fall well within the domain of dependency of the calculation node.

A1.4 Bisection Method

The bisection method is used a number of times in the computer program to solve various equations (critical depth, normal depth, sequent depth of hydraulic jump, etc.). The critical depth equation will be used as an example to demonstrate the solution technique,

$$GG = 1 - \frac{Q^2 T}{gA^3} \qquad \text{(A1.11)}$$

GG has a value of zero for the depth of flow y which will satisfy this equation. The depth must lie between zero and the maximum possible depth which is equal to the diameter of the pipe. This interval is bisected and the value of y obtained used to calculate GG. If GG is positive then the root lies below the midpoint and the upper limit is reset to the y value just used and the new interval bisected. This process is repeated until an acceptable value of y is found. Acceptability is measured by comparing the old and new values of y; if they fall within, say, 1% of one another then the new value is deemed to be the solution.

A1.5 Gradually Varied Flow Profile

Gradually varied flow is steady non-uniform flow where the local head loss at any section is given by the Manning or Colebrook-White expression for the identical local flow depth and rate under assumed steady uniform conditions.

This may be expressed in terms of Figure A1.3 thus,

$$\frac{d}{dL}\left(\frac{V^2}{2g} + (Z_o - S_o L) + y\right) = -S_f \qquad \text{(A1.12)}$$

where $(Z_o - S_o L)$ = the elevation at distance L along the channel, measured in the downstream direction.

S_f = slope of the energy grade line

hence

$$\frac{-V}{g}\frac{dV}{dL} + S_o - \frac{dy}{dL} = S_f \qquad \text{(A1.13)}$$

and, as Q = VA

$$\frac{dV}{dL}A + V\frac{dA}{dL} = 0 \qquad \text{(A1.14)}$$

and as $\frac{dA}{dy} = T$ it follows that

$$\frac{dV}{dL} = \frac{V}{A}\frac{dA}{dL} = -\frac{VT}{A}\frac{dy}{dL} \qquad \text{(A1.15)}$$

Substituting in Equation A1.13

$$\frac{V^2T}{gA}\frac{dy}{dL} + S_o - \frac{dy}{dL} = S_f \qquad \text{(A1.16)}$$

$$dL = \frac{(1 - V^2T/gA)}{(S_o - S_f)}\,dy \qquad \text{(A.17)}$$

therefore

$$L = \int_{yo}^{y1} \frac{1 - V^2T/gA}{S_o - S_f}\,dy \qquad \text{(A1.18)}$$

where L = distance between two known depths y_1 and y_o

A1.6 Numerical Integration Using Simpson's Rule

The gradually varied flow profile defined by the following equation,

$$\Delta x = \int_{yo}^{y1} \frac{1 - V^2T/gA}{S_o - S_f}\,dy \qquad \text{(A1.19)}$$

where x = distance along the channel (m)

S_f = slope of the energy grade line

is integrated numerically using Simpson's Rule.

This rule states that if the integral is expressed thus,

$$X = \int_{yo}^{y_1} f(y)\,dy \qquad \text{(A1.20)}$$

and if the interval between y_1 and y_o is divided into two equal parts then the value of X is given by,

$$X = \frac{1}{3}dy(f(y_o) + 4f(y_o + dy) + f(y_o + 2dy)) \qquad \text{(A1.21)}$$

The depth differential covered by the gradually varied flow profile is divided into a number of small sections and the distance x is found for each section by repeatedly applying the last equation (Figure A1.4). As the integration proceeds the length traversed is accumulated until the length of the gradually varied flow profile is found.

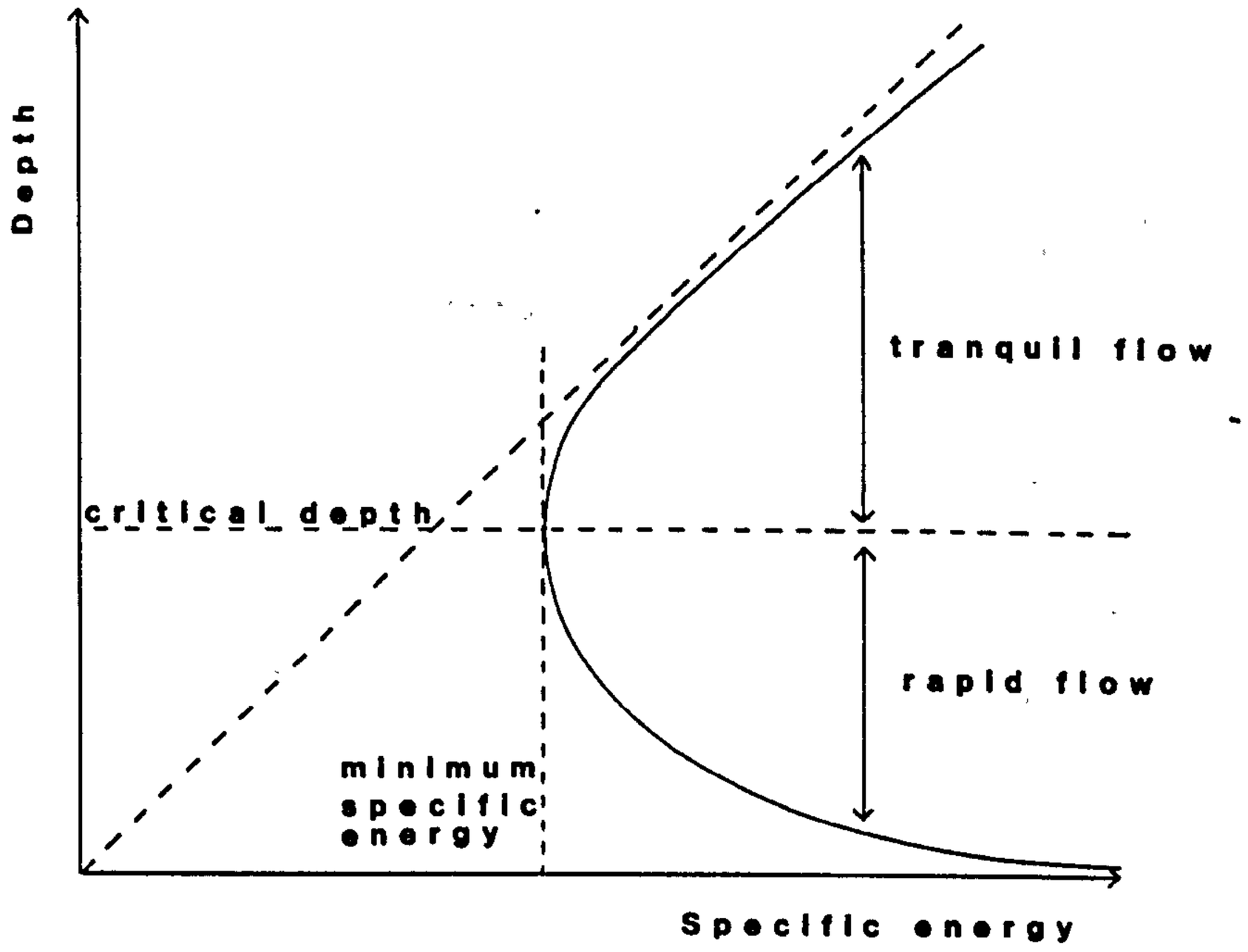

Figure A1.1 Specific energy of flow

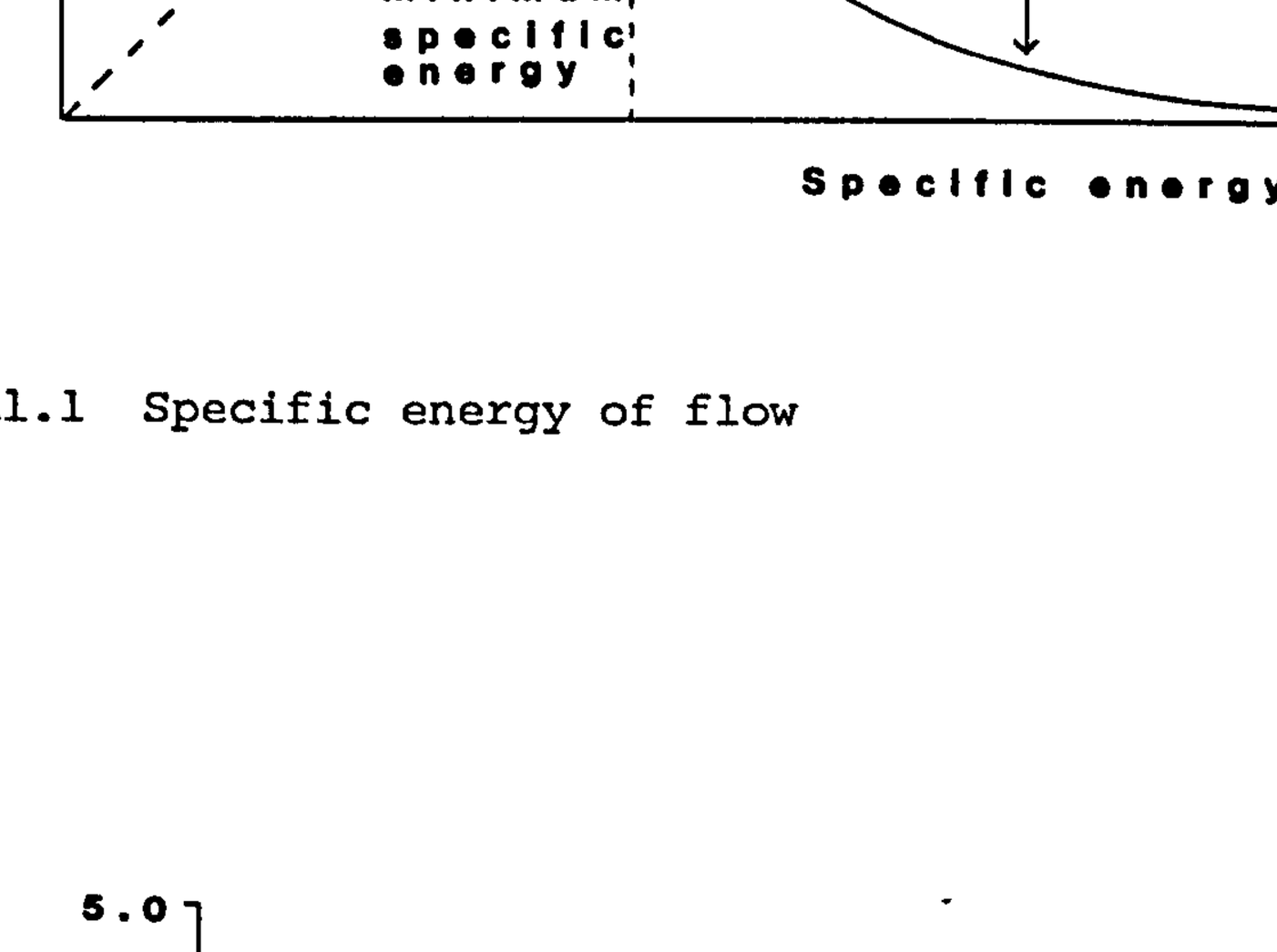

Figure A1.2 Wavespeed in a circular pipe

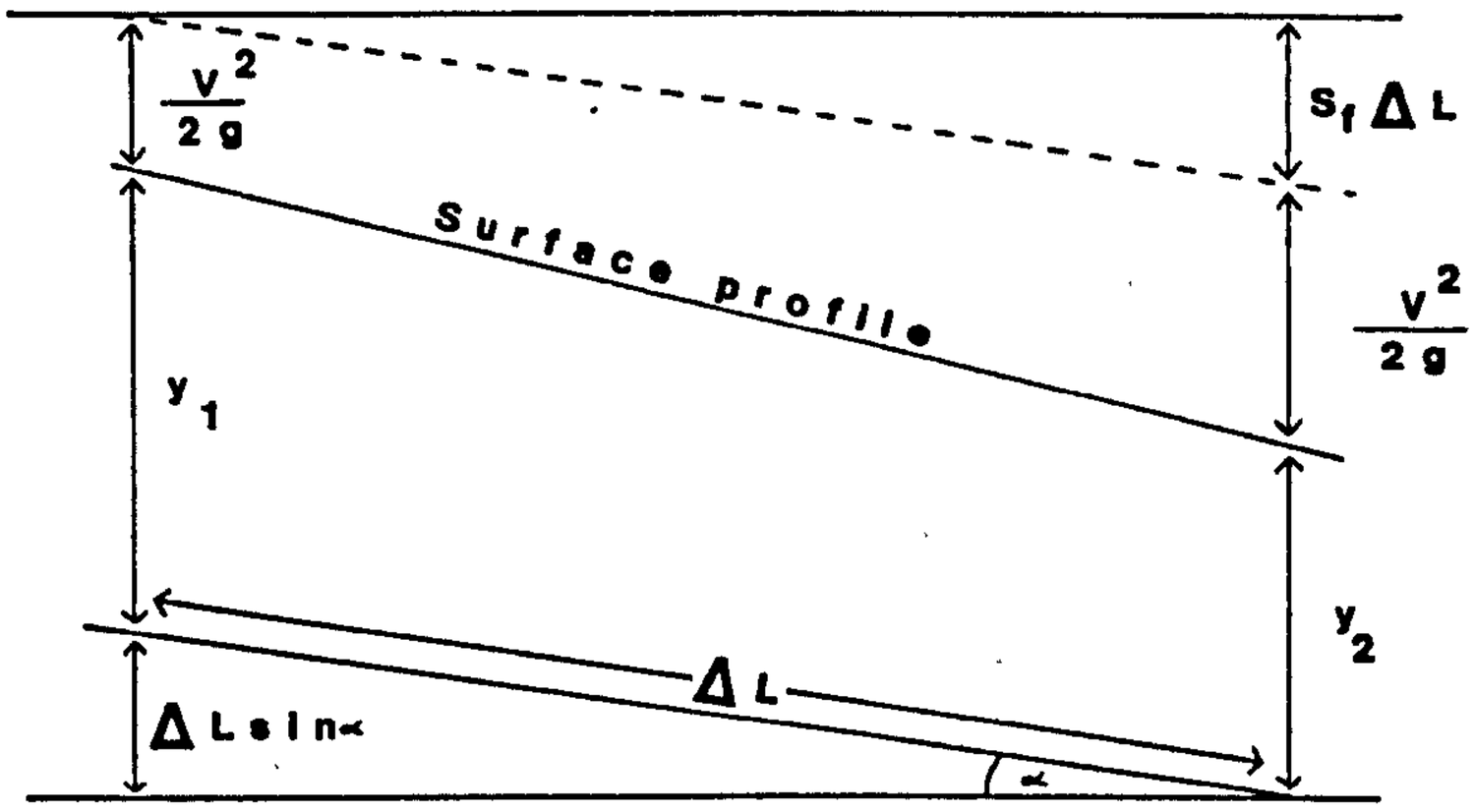

Figure A1.3 Basis of the gradually varied flow depth equation

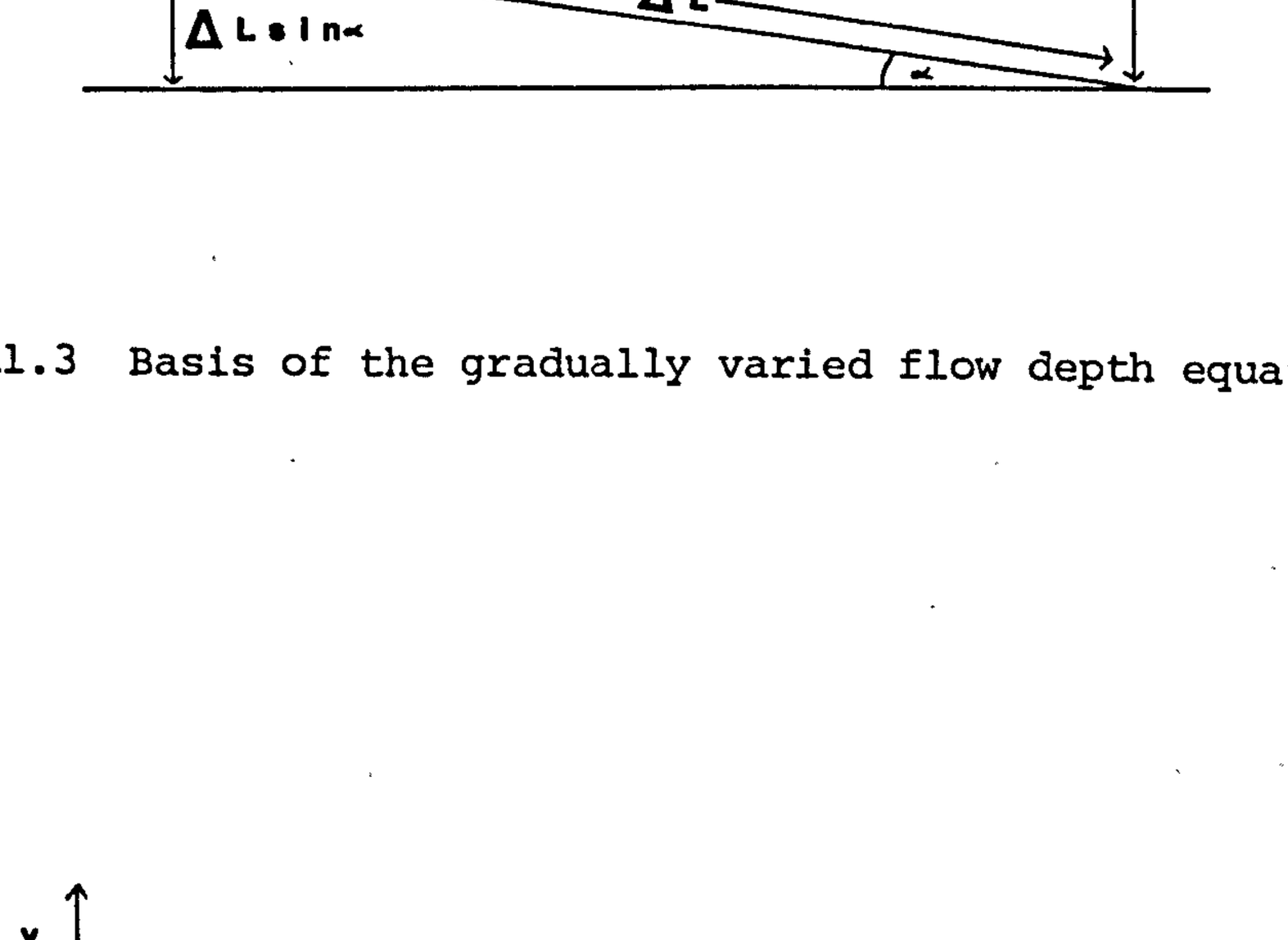

Figure A1.4 Numerical integration of the gradually varied flow profile using Simpson's Rule

Appendix II

Using BRUNET

General

The data describing the charateristics of the stack and the length of time for which the simulation is to run are read into the program first. The data describing the pipe network on each floor of the building are then input, starting with the highest network and working downwards.

Input and Output Files

The data are input in file25 and the results are output in file26 using NPRINT = 1 (input and output from each pipe in the network), file28 using NPRINT = 2 (depth and velocity at each node in the network at each time-step) and file29 using NPRINT = 3 (depth at the points specified in subroutine ASSIGN).

Stack Data

TMAX = duration of the simulation in seconds

DS = diameter of the stack in metres

SK = roughness coefficient of the stack in millimetres

NF = number of floors

HT = height between floors in metres starting with the highest floor and working downwards

Network Data

The pipe network on each floor of the building must have a tree structure with no loops and must drain to one sink node which must be specified. The pipes can be numbered in any order

but the numbers must start at one and continue consecutively upwards. The information about the pipes must be input in order, starting at one and working upwards.The nodes within the network may also be numbered in any way irrespective of the direction of flow, again the numbering must begin at one and continue consecutively upwards. The number assigned to the sink node must be specified seperately for each network.

The network at the lowest level ie that fed by the vertical stack, does not count as a floor and information about it is read in from the end of the data file. The format for the data is the same as that for a network but the pipe fed by the stack does not need to have a specified flow profile input.

NPIPE = total number of pipes in network

NSINK = number assigned to the sink node

NX = number of computational sections per metre

NPRINT = a code to define the output file. 1 = input and output from each pipe, 2 = depth and velocity at each node in the network at each time-step, 3 = depths at points specified in subroutine ASSIGN

TFAC = time-step factor, increases the number of time steps used from that calculated by a factor of TFAC

IPIPE(1) = number assigned to pipe

IPIPE(2) = node numbers at either

IPIPE(3) = end of pipe (order immaterial)

PL = length of pipe in metres

D = diameter of pipe in metres

RM = roughness coefficient k in millimetres

SO = slope of the pipe

DIAIN = diameter of input pipe for energy entry boundary condition in metres, zero for other entry boundary conditions

ANGLE = angle in degrees of junction at end of pipe, zero if no junction

IQN = pipe number of pipe with a flow input (upstream end of network)

NT = boundary condition of input pipe, 1 for a bath or basin, 2 for a w.c.

NPTS = number of points on the input flow profile

QIN = discharge in litres per second

TIN = time in seconds

File Format

TMAX,DS,SK,NF	(3F10.4,I3)		
HT	(F10.4)	repeat for NF	
NPIPE,NSINK,NX,NPRINT,TFAC	(4I3,F10.4)		repeat for number of floors plus network at lowest point in system
IPIPE(1),IPIPE(2),IPIPE(3),PL,D,RM,			
SO,DIAIN,ANGLE	(3I3,6F10.4)	repeat for NPIPE	
IQN,NT	(2I3)		
NPTS	(I3)		repeat for number of sanitary appliances
QIN,TIN	(2F10.4)	repeat for NPTS	

```
  50.0          0.15          0.0          1
    5.0
5    6    5    1          1.0
1    1    5          3.0          0.1          0.0          0.01          0.0          45.0
2    2    3          4.0          0.1          0.0          0.01          0.0          90.0
3    3    4          4.0          0.1          0.0          0.02          0.04         90.0
4    5    3          3.0          0.1          0.0          0.01          0.0          45.0
5    6    5          4.0          0.1          0.0          0.01          0.0           0.0
1    1
5
     0.0                0.0
     1.0                4.0
     1.0                8.0
     0.0               12.0
     0.0               50.0
2    1
5
     0.0                0.0
     1.0                4.0
     1.0                8.0
     0.0               12.0
     0.0               50.0
3    2
5
     0.0                0.0
     1.5                1.0
     1.5                2.0
     0.0                9.0
     0.0               50.0
1    2    5    1          1.0
1    1    2          8.0          0.1          0.0          0.01          0.0           0.0
```

Numbering of pipes and nodes

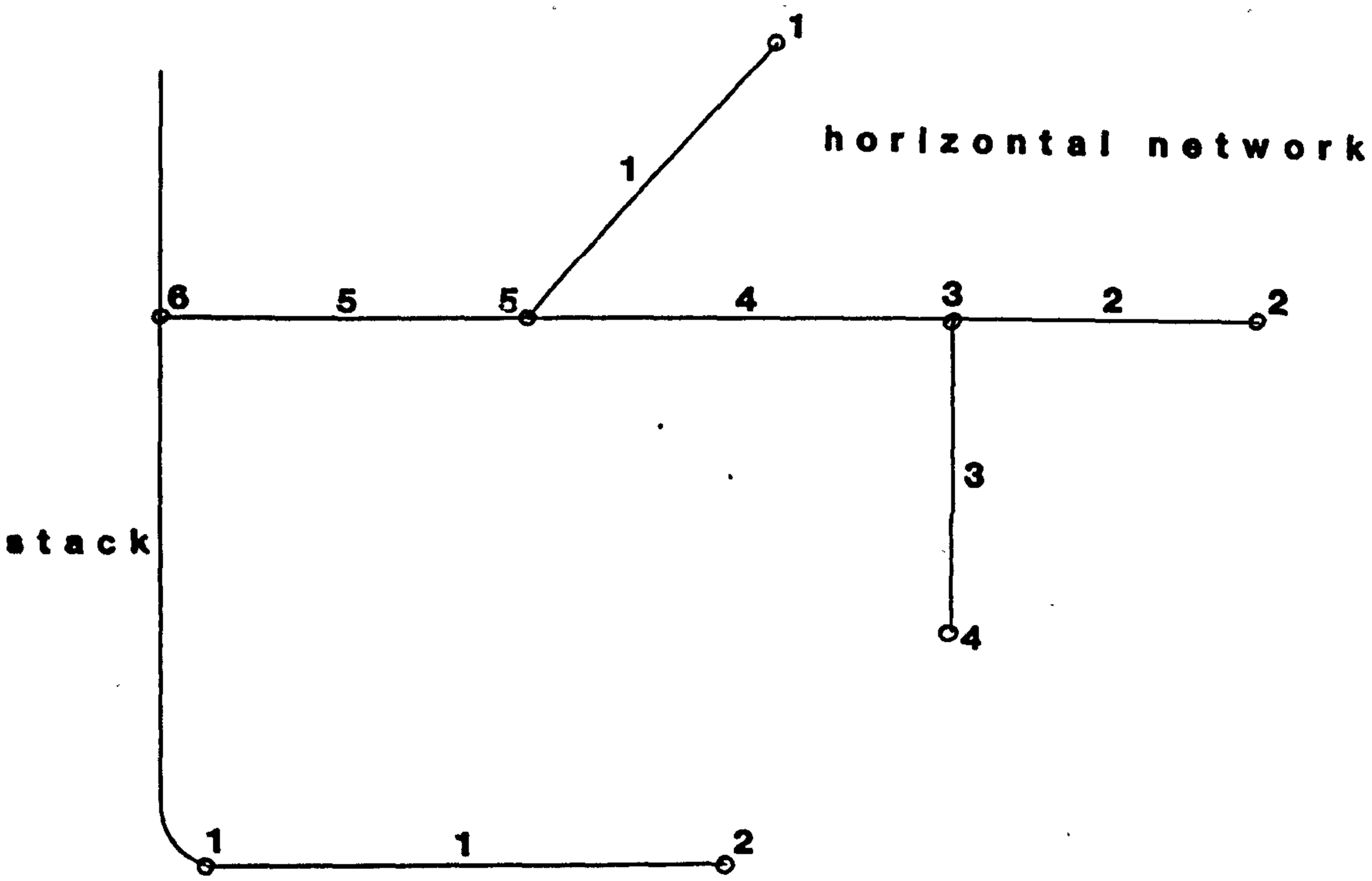

Example of input data file (file25)

```
 50.0          0.15          0.0        3
  5.0
  6.0
  5.0
1   2   5   1          1.0
1   1   2        9.0          0.1          0.0          0.02          0.043          0.0
1   2
5
    0.0                0.0
    1.3                1.0
    1.3                5.5
    0.0                9.5
    0.0               50.0
7   8   5   1          1.0
1   1   4        4.0          0.1          0.0          0.01          0.043         45.0
2   2   4        4.0          0.1          0.0          0.01          0.0           45.0
3   4   5        4.0          0.1          0.0          0.01          0.0           90.0
4   3   5        4.0          0.1          0.0          0.01          0.043         90.0
5   5   7        5.0          0.1          0.0          0.01          0.0           45.0
6   6   7        5.0          0.1          0.0          0.01          0.0           45.0
7   7   8        3.0          0.1          0.0          0.01          0.0            0.0
1   2
5
    0.0                0.0
    1.3                1.0
    1.3                5.5
    0.0                9.5
    0.0               50.0
2   1
2
    0.0                0.0
    0.0               50.0
4   2
5
    0.0                0.0
    1.3                1.0
    1.3                5.5
    0.0                9.5
    0.0               50.0
6   1
5
    0.0                0.0
    0.8                2.0
    0.8               10.0
    0.0               14.0
    0.0               50.0
7   8   5   1          1.0
1   3   2        5.0          0.1          0.0          0.0033        0.043         90.0
2   1   2        4.0          0.1          0.0          0.0033        0.0           90.0
3   2   4        4.0          0.1          0.0          0.0033        0.0           45.0
4   5   6        4.0          0.1          0.0          0.0033        0.0           90.0
5   6   7        4.0          0.1          0.0          0.0033        0.043         90.0
6   4   6        5.0          0.1          0.0          0.0033        0.0           45.0
7   4   8        3.0          0.1          0.0          0.0033        0.0            0.0
1   2
5
    0.0                0.0
    1.3                1.0
    1.3                5.5
    0.0                9.5
    0.0               50.0
2   1
2
    0.0                0.0
    0.0               50.0
4   1
5
    0.0                0.0
    0.8                2.0
    0.8               10.0
    0.0               14.0
    0.0               50.0
5   2
5
    0.0                0.0
    1.3                1.0
    1.3                5.5
    0.0                9.5
    0.0               50.0
1   2   5   1          1.0
1   1   2        8.0          0.15         0.0          0.01          0.0           0.0
```

Example of input data file (see Figure 12.5)

Appendix III

Program BRUNET

A short description of each subroutine is given to aid in the understanding of the program.

MAIN

The main program drives the calculation of unsteady flow through a multi-storey drainage system. Information about the system to be modelled is read in and subroutine PIPENET is then called for each floor of the system. When all the information about flows into the stack has been calculated then subroutine STACK is called to route the flow through to the base of the vertical stack. Subroutine PIPENET is called again to model the single pipe or network at the lowest level of the system.

STACK

STACK takes the discharge profile at each floor of the stack and uses the Colebrook-White equation to calculate the annular thickness of the flow. From this the velocity of the flow is calculated and used to route the discharge to the base of the stack. The input at each floor is added to the flow in the stack before it is routed to the next level. A discharge versus time profile is produced which can be used as the input profile to the network at the lowest level in the system (Chapter Twelve).

PIPENET

PIPENET is used to drive the calculation of unsteady flow

through the drainage network on a single floor of each building. Information about each network is read in and then the steady baseflow conditions at time zero are set up using the appropriate subroutines. The propagation of the unsteady input profile is then modelled for each pipe within the network through time until the maximum time specified is reached. The discharge versus time profile at the lowest point in the system is found and used as an input to the calculations in subroutine STACK.

PRINT

This subroutine prints out information about each network within the system, including the order in which the calculation of flow within each pipe of the network should proceed.

DRAIN

DRAIN calculates the drainage line number for each node within the network using information about the system input by the user. The drainage line number decides the order in which the pipe calculations are to take place so that flows can be accumulated at junctions at each time-step thus allowing backflow to occur and the calculations to proceed downstream through the network (Chapter Twelve).

OMEGA

OMEGA sets up a table of values of depth y and the stage variable ω which can be used to find the associated values of y and ω whenever required (Chapter Four).

DEPOM

DEPOM finds the value of the stage variable associated with a particular value of depth.

OMDEP

OMDEP finds the value of depth associated with a particular value of the stage variable.

TIMINC

TIMINC identifies the highest wavespeed c and the highest average flow velocity V in the simulated flow calculations in order to ensure that the time step chosen is the smallest possible thus ensuring stability (Chapter Four).

CBW

Subroutine CBW solves the Colebrook-White equation using the bisection method to find the steady-state loss associated with a particular depth y and velocity V of flow (Chapter Eight).

LOSS

LOSS uses subroutine CBW to find the loss at points R and S (or S') on the characteristic grid at each time-step.

DEPTH

DEPTH uses a section of subroutine ENTRY to calculate the normal and critical flow depths for the base flow (Chapter Four).

INFLOW

INFLOW calculates the inflow rate Q at the entry to each upstream pipe in the network based on the flow profile read into the program. The value of Q calculated is an average value for each time step.

SHAPE

SHAPE uses any depth of flow in the circular pipe to calculate the area, wetted perimeter, surface water width, depth to centroid and the ratio of normal depth to the steady-state loss. These values are frequently required throughout the program.

WAVSPD

WAVSPD calculates the wavespeed based on the depth and the cross-sectional shape.

PROFIL

PROFIL calculates the initial water surface for a pipe with a free outfall. The profile is based on critical depth at pipe exit with a gradually varied flow profile rising to normal depth if the flow is subcritical. The entry boundary conditions are calculated according to the code input for each pipe and the flow conditions at the head of the pipe adjusted accordingly (Chapter Four).

INTER

INTER sets up the base conditions for the next time-step using the values at each node on the space-time grid calculated at the current time-step. The values of depth, velocity and wavespeed are

calculated for points R and S (or S' in the supercritical case) on the characteristic grid using the interpolation equations given in Chapter Four. INTER also calculates the values at points A, B and D on the characteristic grid surrounding the discontinuity between the supercritical and subcritical flow upstream of the junction.

ENTRY

ENTRY is used by subroutine DEPTH to calculate the normal and critical depth for the base flow at time zero. ENTRY also calculates the depth at the entry boundary at all times after t = 0.0 using the codes input for each pipe. Four different entry boundary conditions are available; normal depth, critical depth, energy at entry and the energy at the base of a stack leading to the network at the lowest level in the system (Chapter Six).

NODAL

NODAL calculates the depth, flow velocity and wavespeed at each of the nodes between the upstream and downstream boundaries using the two wave equations. If a junction is present at the end of the pipe then NODAL does not calculate the flow conditions surrounding the discontinuity between the upstream supercritical flow and the downstream subcritical flow (Chapter Four).

EXIT

EXIT is called if the flow at the exit to the pipe is subcritical. If the end of the pipe is a free outfall then the critical depth equation and characteristic equation are solved to find the depth of flow at the exit. At a junction the equation describing

the relationship between depth and flow rate is solved with the characteristics equation to find the depth at the junction. EXIT is only called when the flow conditions at the ends of both pipes leading into the junction is known (Chapter Four).

ASSIGN

ASSIGN is used to set up the new base conditions along the pipe in preparation for the new time-step. The calculated values of depth, velocity and wavespeed are assigned to the variable names used for the base conditions.

JUMP

JUMP uses the normal depth of flow to calculate the sequent depth of the hydraulic jump formed at time zero by the presence of a junction at the end of the pipe. The velocity and wavespeed associated with the downstream sequent depth are also calculated (Chapter Eleven).

GRAD

GRAD uses Simpson's Rule to fit a gradually varied flow profile between the downstream side of the jump and the exit boundary, this gives the position of the jump in the pipe at time zero. GRAD also sets up the entry boundary conditions and the flow conditions upstream of the jump at time zero (Chapter Eleven).

JUNC

JUNC calculates the depth on the upstream side of the junction given the flows in the two pipes using the equations found by experimentation (Chapter Eleven).

JUMPMOVE

JUMPMOVE calculates the velocity of the jump (or steep-fronted wave) at each time-step subsequent to time zero using the technique described in Chapter Eleven. The depth, velocity and wavespeed upstream and downstream of the steep-fronted wave are calculated and also the depth, velocity and wavespeed at nodes upstream and downstream of the wavefront.

```
%global card
C
CCCCCC      ************************************************************
CCCCCC      BRUNET - THE BRUNEL MULTI-STOREY BUILDING DRAINAGE NETWORK
CCCCCC               ANALYSIS PROGRAM FOR PARTIALLY FILLED PIPE SYSTEMS.
CCCCCC               DEVELOPED AT BRUNEL UNIVERSITY,UXBRIDGE,MIDDX.
CCCCCC      ************************************************************
C
      DIMENSION HT(20),TIMEA(400),QSTACK(400),T(20,400),Q(20,400)
     + ,QEND(400),VEND(400),TEND(400),NDT(20)
C
      COMMON/CM441/ DT,DX,TMAX
      COMMON/CM452/ NTIME,TIMEA,QSTACK
      COMMON/CM453/ QEND,TEND,VEND,NPT
      COMMON/CM454/ Q,T
C
CC    THE MAIN PROGRAM DRIVES THE CALCULATION OF UNSTEADY FLOW
CC    IN A MULTI-STOREY BUILDING DRAINAGE SYSTEM USING THE
CC    METHOD OF CHARACTERISTICS TO SOLVE THE EQUATIONS OF
CC    OPEN-CHANNEL FLOW.
CC
C
      READ(25,100)TMAX,DS,SK,NF
  100 FORMAT(3F10.4,I3)
      DO 10 I=1,NF
      READ(25,200)HT(I)
  200 FORMAT(F10.4)
   10 CONTINUE
C
CC
C
      NS=0
      DO 20 I=1,NF
      CALL PIPEVET(NS)
      NDT(I)=NTIME-1
      WRITE(40,600)NDT(I)
  600 FORMAT(I4)
      DO 30 J=1,NDT(I)
      T(I,J)=TIMEA(J)
      Q(I,J)=QSTACK(J)
      WRITE(40,500)T(I,J),Q(I,J)
  500 FORMAT(2F12.6)
   30 CONTINUE
   20 CONTINUE
      IF(NF.EQ.1)GOTO 70
C
C
      QBASE=0.0001
      CALL STACK(QBASE,DS,SK,NF,HT,NDT)
      NNPT=0
      ICOUNT=0
      DO 50 J=1,NPT
      ICOUNT=ICOUNT+1
      IF(ICOUNT.EQ.1)NNPT=NNPT+1
      IF(ICOUNT.NE.1)GOTO 60
      TEND(NNPT)=TEND(J)
      QEND(NNPT)=QEND(J)
      VEND(NNPT)=VEND(J)
   60 IF(ICOUNT.EQ.1)ICOUNT=0
   50 CONTINUE
      NPT=NNPT
      WRITE(39,666)
  666 FORMAT("DISCHARGE AND VELOCITY AT THE BOTTOM OF THE STACK")
      DO 40 I=1,NPT
      WRITE(39,777)TEND(I),VEND(I),QEND(I)
   40 CONTINUE
  777 FORMAT(3F12.3)
      NS=1
      CALL PIPENET(NS)
C
   70 CONTINUE
      STOP
      END
```

```
C
      SUBROUTINE STACK(QBASE,DS,SK,NF,HT,NDT)
C
      DIMENSION HT(20),Q(20,400),T(20,400),NDT(20),TA(20,400),
     + QAV(20,400),VAV(20,400),TAV(20,400),DTAV(20,400)
      DIMENSION QEND(400),TEND(400),VEND(400)
      COMMON/CM453/ QEND,TEND,VEND,NPT
      COMMON/CM454/ Q,T
C
CC     THIS SUBROUTINE USES THE DICHARGE FROM EACH NETWORK IN THE
CC     SYSTEM AND ROUTES IT DOWN THE STACK IN ORDER TO PRODUCE
CC     AN INPUT PROFILE INTO THE LOWEST PIPE IN THE SYSTEM
C
      NDT(NF+1)=NDT(NF)
      NPT=NDT(NF+1)
      DO 100 I=1,NDT(NF+1)
      Q(NF+1,I)=0.0
      T(NF+1,I)=T(NF,I)
  100 CONTINUE
C
CC    CALCULATES ANNULAR THICKNESS USING COLEBROOK-WHITE AND
C     ALSO THE TERMINAL VELOCITY
      PI=3.142
      G=9.81
      DO 10 I=1,NF
      DO 20 K=1,NDT(I)
      JX0=1
      QX=Q(I,K)
      TT=0.0
   50 TT=TT+DS/1000.0
      IF(TT.GT.DS/1000.0)JX0=JX1
      XXL=QX/(12.568*DS*TT)*SQRT(1.0/(2.0*G*TT))
      XXR=-LOG10((SK/(14800.0*TT))+((0.3138*0.000001)/TT)*
     + SQRT(1.0/(2.0*G*TT)))
      XXX=XXL-XXR
      IF(XXX.LT.0.0)JX1=-1
      IF(XXX.GT.0.0)JX1=1
      IF(XXX.EQ.0.0)GOTO 30
      IF(TT.GT.(DS/1000.0).AND.(JX1*JX0).LT.0.0)GOTO 30
      GOTO 50
   30 TVEL=QX/(TT*PI*DS)
      IF(HT(I).LT.7.5)Z=HT(I)/7.5
      IF(HT(I).GE.7.5)Z=1.0
C
CC    USES THE VELOCITY OF FLOW IN THE STACK TO CALCULATE THE AVERAGE
C     DISCHARGE AND VELOCITY FOR EACH TIME STEP
      TA(I+1,K)=T(I,K)+HT(I)/(TVEL*Z)
      IF(K.EQ.1)GOTO 20
      QAV(I+1,K-1)=(Q(I,K)+Q(I,K-1))*0.5*(T(I,K)-T(I,K-1))/
     + (ABS(TA(I+1,K)-TA(I+1,K-1)))-QBASE
      IF(QAV(I+1,K-1).LT.0.0)QAV(I+1,K-1)=0.0
      VAV(I+1,K-1)=QAV(I+1,K-1)/(TT*PI*DS)
      TAV(I+1,K-1)=(TA(I+1,K)+TA(I+1,K-1))*0.5
      DTAV(I+1,K-1)=ABS((TA(I+1,K)-TA(I+1,K-1)))
   20 CONTINUE
C
C
C     CALCULATES THE TOTAL FLOW IN THE STACK AT EACH FLOOR
      DO 60 J=1,NDT(I+1)
      DO 70 K=1,NDT(I+1)
      A=TAV(I+1,K)+(DTAV(I+1,K)/2.0)

      B=TAV(I+1,K)-(DTAV(I+1,K)/2.0)
      IF(T(I+1,J).GT.B.AND.T(I+1,J).LT.A)Q(I+1,J)=Q(I+1,J)+QAV(I+1,K)
   70 CONTINUE
   60 CONTINUE
   10 CONTINUE
      DO 14 KKK=1,NF
      WRITE(39,543)KKK
  543 FORMAT("TOTAL FLOW IN STACK AT FLOOR ",I1)
      DO 13 JJJ=1,NDT(KKK+1)
      WRITE(39,987)T(KKK+1,JJJ),Q(KKK+1,JJJ)
   13 CONTINUE
   14 CONTINUE
  987 FORMAT(2F12.7)
C
C     CALCULATES THE TOTAL DISCHARGE AT THE BASE OF THE STACK
      DO 40 I=1,NPT
      JX0=1
      QX=Q(NF+1,I)+QBASE
      TT=0.0
   80 TT=TT+DS/1000.0
      IF(TT.GT.DS/1000.0)JX0=JX1
      XXL=QX/(12.566*DS*TT)*SQRT(1.0/(2.0*G*TT))
      XXR=-LOG10((SK/(14800.0*TT))+((0.3138*0.000001)/TT)*
     + SQRT(1.0/(2.0*G*TT)))
      XXX=XXL-XXR
      IF(XXX.LT.0.0)JX1=-1
      IF(XXX.GT.0.0)JX1=1
      IF(XXX.EQ.0.0)GOTO 90
      IF(TT.GT.(DS/1000.0).AND.(JX1*JX0).LT.0.0)GOTO 90
      GOTO 80
   90 VEND(I)=QX/(TT*PI*DS)
      QEND(I)=QX
      TEND(I)=T(NF+1,I)
   40 CONTINUE
      RETURN
      END
C
```

```
C
      SUBROUTINE PIPENET(NS)
C
C
      DIMENSION IPIPE(20,3),IQN(10),NT(10),NPTS(20),NTOP(10),NSEC(10)
      DIMENSION PL(10),D(10),RM(10),SO(10),DIAIN(10),ANGLE(10),
     + QUP(10),QTEMP(10)
      DIMENSION LIST(20,3),EXR(5,3),TIMEA(400),QSTACK(400),
     + QEND(400),TEND(400),VEND(400)
      DIMENSION HR(61),VR(61),CR(61),SR(61),XR(51),HS(61),VS(61)
     + ,CS(61),SS(61),XS(51)
      DIMENSION QP(61),VP(61),HP(61),CP(61)
      DIMENSION V(20,61),H(20,61),C(20,51),XN(20,61),CA(20)
      DIMENSION HC(20),HN(20),WTAB(10,100,2),C1(20,51),C2(20,61)
      DIMENSION VWAVE(20),XWAVE(20),XWZERO(20),NWAVE(20),VN(20),
     + CN(20)
      DIMENSION QIN(20,100),TIN(20,100)
      DIMENSION VUS(61),HUS(61),CUS(61),VDS(61),HDS(61),CDS(61)
C
      COMMON/CM441/ DT,DX,TMAX
      COMMON/CM442/ VR,HR,CR,XR,SR,VS,HS,CS,XS,SS
      COMMON/CM443/ QP,VP,HP,CP
      COMMON/CM444/ VPUS,HPUS,CPUS,VPDS,HPDS,CPDS
      COMMON/CM445/ THETA,VB,HB,CB
      COMMON/CM446/ V,H,C,XN
      COMMON/CM447/ QIN,TIN
      COMMON/CM448/ IPIPE,LIST,IADD
      COMMON/CM449/ EXR,WTAB
      COMMON/CM450/ C1,C2,CA
      COMMON/CM451/ NPRINT
      COMMON/CM452/ NTIME,TIMEA,QSTACK
      COMMON/CM453/ QEND,TEND,VEND,NPT
C
CC    THIS SUBROUTINE DRIVES THE UNSTEADY FLOW CALCULATION WITHIN
CC    THE PIPE NETWORK ON EACH STOREY OF THE BUILDING.
CC
CC    DATA FOR EACH NETWORK READ IN
C
      TIME=0.0
      NTIME=1
      TIMEA(1)=0.0
      READ(25,100)NPIPE,NSINK,NX,NPRINT,TFAC
C
  100 FORMAT(4I3,F10.4)
      NODE=NPIPE+1
C
      DO 65 I=1,NPIPE
      VWAVE(I)=0.0
   65 CONTINUE
C
CC
CC    NPIPE=NUMBER OF PIPES,NSINK=SINK NODE,NX=NUMBER OF COMPUTING
CC    SECTIONS PER METRE, NPRINT=1 OUTPUT IN FILE25(INPUT AND OUTPUT
CC    FROM EACH PIPE) NPRINT=2 OUTPUT IN FILE23(DEPTH AND VELOCITY AT
CC    EACH NODE AT EACH TIME) NPRINT=3 OUTPUT IN FILE29(DEPTH AT THE
CC    TAPPING POINTS SPECIFIED IN ASSIGN), TFAC= TIME STEP FACTOR
CC    (1 - 10)
C
      DO 10 I=1,NPIPE
      READ(25,200)(IPIPE(I,J),J=1,3),PL(I),D(I),RM(I),SO(I)
     + ,DIAIN(I),ANGLE(I)
  200 FORMAT(3I3,5F10.4)
   10 CONTINUE
C
CC    IPIPE=PIPE NUMBERS IN SEQUENCE(1,2,3 ETC),NODES AT EACH END OF
CC    PIPE,PL=PIPE LENGTH,D=PIPE DIAMETER,RM=PIPE ROUGHNESS,SO=PIPE
CC    SLOPE,DIAIN=DIAMETER OF INPUT PIPE,ANGLE=JUNCTION ANGLE AT
CC    END OF PIPE.
C
      DO 20 J=1,NPIPE
      NSEC(J)=INT(FLOAT(NX)*PL(J))
   20 CONTINUE
C
CC    DRAIN CALLED TO CALCULATE NUMBER OF INPUT FLOW PROFILES
      CALL DRAIN(NPIPE,NSINK)
C
      IF(NS.EQ.1)GOTO 70
      DO 30 K=1,IADD
      READ(25,300)IQN(K),NT(K)
  300 FORMAT(2I3)
      READ(25,300) NPTS(K)
      DO 40 L=1,NPTS(K)
      READ(25,400)QIN(K,L),TIN(K,L)
  400 FORMAT(2F10.4)
      QIN(K,L)=QIN(K,L)/1000.)
   40 CONTINUE
   30 CONTINUE
      GOTO 74
   70 IQN(1)=1
      NT(1)=3
      NPTS(1)=NPT
      DO 76 I=1,NPT
      QIN(1,I)=QEND(I)
      TIN(1,I)=TEND(I)
   76 CONTINUE
      IF(IADD.EQ.1)GOTO 74
      DO 27 K=2,IADD
      READ(25,300)IQN(K),NT(K)
      READ(25,300) NPTS(K)
      DO 37 L=1,NPTS(K)
      READ(25,400)QIN(K,L),TIN(K,L)
      QIN(K,L)=QIN(K,L)/1000.)
   37 CONTINUE
   27 CONTINUE
   74 CONTINUE
```

```
C
C       IQN=PIPE NUMBER OF INPUT PIPE,NT=BOUNDARY CONDITION OF INPUT
C       PIPE, 1=NORMAL DEPTH (PATH), 2=ENERGY ENTRY (J.C.), 3=ENERGY
C       ENTRY (STACK), 4=CRITICAL DEPTH (JUNCTION BOUNDARY),
C       NPTS=NUMBER OF POINTS ON INPUT PROFILE,QIN AND TIN=TIME
C       AND DISCHARGE PROFILES.
C
        ASSIGN BOUNDARY CONDITION FOR EVERY PIPE
        DO 45 JI=1,NPIPE
        NTOP(JI)=0
   46   CONTINUE
        DO 56 JI=1,IADD
        NTOP(IQN(JI))=NT(IADD)
   56   CONTINUE
        DO 66 JI=1,NPIPE
        IF(NTOP(JI).EQ.0)NTOP(JI)=4
   66   CONTINUE
C
        QBASE=0.0001
C       FIND BASEFLOW FOR EACH PIPE
   86   DO 25 I=1,NPIPE
        QUP(I)=0.0
   25   CONTINUE
        DO 35 J=1,IADD
        QUP(IQN(J))=QBASE
   35   CONTINUE
        DO 55 I=1,NPIPE
        DO 45 J=1,IADD
        IF(I.EQ.IQN(J))GOTO 55
   45   CONTINUE
        DO 75 K=1,NPIPE
        IF(I.EQ.LIST(K,1))GOTO 87
   75   CONTINUE
   87   DO 95 L=1,NPIPE
        IF(LIST(K,3).EQ.LIST(L,2))QUP(I)=QBASE
   95   CONTINUE
   55   CONTINUE
        QSTACK(1)=QBASE
C
        IF(NPRINT.EQ.1)CALL PRINT(NPIPE,P_,D,RM,SO,ANGLE,NSEC,NTOP
     +  ,IQN,NPTS)
        IF(NPRINT.EQ.2)WRITE(23,910)TIME
        IF(NPRINT.EQ.3)WRITE(29,910)TIME
        IF(NPRINT.EQ.3)WRITE(31,944)TIME
  944   FORMAT(F6.2)
  910   FORMAT(//5X,"TIME = ",F6.2)
        WRITE(0,123)TIME
  123   FORMAT("TIME= ",F7.3)
C
C       CALCULATE CONDITIONS AT TIME ZERO USING THE EQUATION FOR
C       STEADY FLOW
        DO 50 I=1,NPIPE
        NP=LIST(I,1)
        N=NSEC(NP)
        Q=QUP(NP)
        QB=0.0
        IF(NPRINT.EQ.2)WRITE(28,911)NP
  911   FORMAT(/5X,"PIPE NUMBER= ",I3)
        CALL DEPTH(TIME,HC(NP),HN(NP),NTOP(NP),RM(NP),SO(NP),DIAM(NP)
     +  ,D(NP),NP,Q,V,NPTS(NP))
        DO 19 LL=1,IADD
        IF(NTOP(NP).EQ.3)GOTO 19
        IF(HC(NP).GT.HN(NP).AND.NP.EQ.IQN(LL))NTOP(NP)=1
   19   CONTINUE
        IF(NPRINT.EQ.2)WRITE(28,941)HN(NP),HC(NP)
  941   FORMAT(/5X,"NORMAL DEPTH= ",F6.4,"     CRITICAL DEPTH= ",F6.4/)
        IF(ANGLE(NP).EQ.0.0)CALL PROFIL(N,HN(NP),HC(NP),TIME,PL(NP),D(NP)
     +  ,NTOP(NP),NP,Q,SO(NP))
        IF(ANGLE(NP).EQ.0.0)GOTO 60
        IF(HN(NP).LE.HC(NP))CALL JUMP(NP,HN(NP),TIME,D(NP),HTOP,
     +  SO(NP),QUP(NP),RM(NP))
        DO 18 JJ=1,NPIPE
        IF(LIST(I,2).EQ.LIST(JJ,2))QB=QB+QUP(LIST(JJ,1))
   18   CONTINUE
        CALL JUNC(QB,ANGLE(NP),HJUNC,0)
        IF(HN(NP).GT.HC(NP))HTOP=HN(NP)
        CALL GRAD(N,NP,PL(NP),HN(NP),HC(NP),XWAVE(NP),XWZERO(NP),
     +  YWAVE(NP),NTOP(NP),D(NP),HJUNC,HTOP,Q,TIME,SO(NP))
   60   CALL ASSIGN(TIME,N,NP,VJS(NP),HJS(NP),CJS(NP),VDS(NP),HDS(NP)
     +  ,CDS(NP),NWAVE(NP),XWAVE(NP),ANGLE(NP),HN(NP),HC(NP),NPRINT,IT)
        CALL TIMINC(N,YWAVE(NP),VN(NP),CN(NP))
        CALL SHAPE(TIME,NP,D(NP),SO(NP),H(NP,N+1),A,T,PER,HBAR,
     +  DL,DY,QUP(NP),RM(NP))
        CALL OMEGA(TIME,NP,D(NP),SO(NP),QUP(NP),RM(NP))
   50   CONTINUE
        DX=1.0/FLOAT(NX)
        ICOUNT=0
  450   CMAX=CN(1)
C
C       FIND MAXIMUM VELOCITY AND WAVESPEED IN ORDER TO CALCULATE
C       THE TIME STEP SIZE
        VMAX=VN(1)
        DO 16 K=2,NPIPE
        IF(CN(K).GT.CMAX)CMAX=CN(K)
        IF(VN(K).GT.VMAX)VMAX=VN(K)
   16   CONTINUE
        DT=DX/(TFAC*(CMAX+VMAX))
        IF(TIME.EQ.0.0)DT=DX/(TFAC*5.0*(CMAX+VMAX))
```

```
      IF(DT.GT.DTO)DT=DTO
      TIME=TIME+DT
      ICOUNT=ICOUNT+1
      IF(ICOUNT.EQ.1)NTIME=NTIME+1
      IF(ICOUNT.EQ.1)TIMEA(NTIME)=TIME
      IF(TIME.GT.TMAX)GOTO 550
      WRITE(0,234)TIME
  234 FORMAT("TIME= ",F7.3)
      DO 17 KL=1,NPIPE
      QUP(KL)=0.0
   17 CONTINUE
      IDOWN=0
      IF(NPRINT.EQ.2)WRITE(28,910)TIME
      IF(NPRINT.EQ.3)WRITE(29,910)TIME
      IF(NPRINT.EQ.3)WRITE(31,944)TIME
C
C     BEGIN UNSTEADY FLOW CALCULATION FOR EACH PIPE IN THE NETWORK
C     AT EACH TIME STEP IN THE SIMULATION
      DO 150 J=1,NPIPE
      NP=LIST(J,1)
      IF(J.GT.1)NP2=LIST(J-1,1)
      N=NSEC(NP)
      IF(J.GT.1)NTWO=NSEC(NP2)
      Q=QUP(NP)
      QB=0.0
      IF(NPRINT.EQ.2)WRITE(28,911)NP
      DO 26 K=1,IADD
      IF(NP.EQ.IQN(K))CALL INFLOW(TIME,K,NPTS(K),2)
      IF(NP.EQ.IQN(K).AND.NTOP(NP).NE.3)Q=Q+QBASE
   26 CONTINUE
      CALL INTER(N,NP,NWAVE(NP),XWAVE(NP),VUS(NP),HUS(NP),CUS(NP),
     + VDS(NP),HDS(NP),CDS(NP),ANGLE(NP),HN(NP),HC(NP),VWAVE(NP))
      CALL LOSS(N,RM(NP),HN(NP),HC(NP),ANGLE(NP),NP,D(NP),SO(NP),
     + TIME,XWAVE(NP))
      CALL ENTRY(TIME,HC(NP),HN(NP),NTOP(NP),RM(NP),SO(NP),DIAIN(NP)
     + ,D(NP),NP,Q,N,NPTS(NP))
      CALL NODAL(N,HN(NP),HC(NP),ANGLE(NP),XWAVE(NP),NWAVE(NP),
     + TIME,NP,D(NP),SO(NP))
      IF(ANGLE(NP).EQ.0.0)GOTO 24
      IF(NWAVE(NP).EQ.0)GOTO 34
      IF(HN(NP).LE.HC(NP))CALL JUMPMOVE(TIME,N,NP,NWAVE(NP),XWAVE(NP),
     + XWZERO(NP),D(NP),VDS(NP),HDS(NP),CDS(NP),RM(NP),VWAVE(NP),
     + SO(NP))
   34 IF(LIST(J,2).EQ.NSINK)GOTO 24
      IF(IDOWN.NE.LIST(J,2))GOTO 14
      EXR(1,2)=HR(J+1)
      EXR(2,2)=VR(J+1)
      EXR(3,2)=CR(J+1)
      EXR(4,2)=SR(J+1)
      EXR(5,2)=SO(NP)
      GOTO 24
   14 EXR(1,1)=HR(J+1)
      EXR(2,1)=VR(J+1)
      EXR(3,1)=CR(J+1)
      EXR(4,1)=SR(J+1)
      EXR(5,1)=SO(NP)
      IDOWN=LIST(J,2)
   24 CALL ASSIGN(TIME,N,NP,VUS(NP),HUS(NP),CUS(NP),VDS(NP),HDS(NP)
     + ,CDS(NP),NWAVE(NP),XWAVE(NP),ANGLE(NP),HN(NP),HC(NP),NPRINT,IT)
      IF(LIST(J,2).EQ.NSINK)CALL SHAPE(TIME,NP,D(NP),SO(NP),H(NP,N+1),
     + A,T,PER,HBAR,DL,DY,Q,RM(NP))
      IF(LIST(J,2).EQ.NSINK.AND.ICOUNT.EQ.1)QSTAR(NTIME)=V(NP,N+1)*A
      IF(ICOUNT.EQ.10)ICOUNT=0
      IF(IDOWN.NE.LIST(J-1,2))GOTO 250
      IF(V(NP,N).LT.C(NP,N).OR.ANGLE(NP).GT.0.0)CALL EXIT(TIME,
     + ANGLE(NP),NP,N,D(NP),SO(NP),NP2,NTWO)
      CALL SHAPE(TIME,NP,D(NP),SO(NP),H(NP2,NTWO+1),A2,T,PER,HBAR,
     + DL,DY,Q,RM(NP))
      QOUT1=V(NP2,NTWO+1)*A2
      CALL SHAPE(TIME,NP,D(NP),SO(NP),H(NP,N+1),A1,T,PER,HBAR,
     + DL,DY,Q,RM(NP))
      QOUT2=V(NP,N+1)*A1
      IF(NPRINT.EQ.2)WRITE(28,918)NP2,H(NP2,NTWO+1)
      IF(NPRINT.EQ.2)WRITE(28,916)NP,H(NP,N+1)
  918 FORMAT(/"PIPE",I3,"     DEPTH AT EXIT = ",F7.4)
      DO 85 I=1,NPIPE
      IF(LIST(I,3).NE.IDOWN)GOTO 85
      IF(LIST(I,3).EQ.IDOWN)QUP(LIST(I,1))=QOUT1+QOUT2-QBASE
      GOTO 250
   85 CONTINUE

  250 CALL TIMINC(J,NWAVE(NP),VN(NP),CN(NP))
  150 CONTINUE
      GOTO 450
  550 RETURN
      END
C
C
```

```
C
      SUBROUTINE DRAIN(NPIPE,NSINK)
C
      DIMENSION KARRAY(20,20),IPIPE(20,3),LIST(20,3)
      COMMON/CM448/ IPIPE,LIST,IADD
C
C     THIS SUBROUTINE SETS UP A NODE INCIDENCE MATRIX TO CALCULATE THE
C     DRAINAGE LINE NUMBER FOR EACH NODE AND THEREFORE THE ORDER IN


C     WHICH THE CALCULATION IS TO PROCEED
C
      NODE=NPIPE+1
      DO 60 I=1,NODE
      DO 70 J=1,NPIPE
      KARRAY(I,J)=0
   70 CONTINUE
   60 CONTINUE
C
C     RECORD NODE NUMBERS FOR EACH PIPE
      DO 10 I=1,NPIPE
      JX=IPIPE(I,1)
      JY=IPIPE(I,2)
      JZ=IPIPE(I,3)
      KARRAY(JY,JX)=1
      KARRAY(JZ,JX)=1
   10 CONTINUE
C
C     SUM NUMBER OF PIPES MEETING AT EACH NODE
      ISUM=0
      DO 30 K=1,NODE
      DO 20 J=1,NPIPE
      ISUM=ISUM+KARRAY(K,J)
   20 CONTINUE
      KARRAY(K,NPIPE+1)=ISUM
      ISUM=0
   30 CONTINUE
      IADD=0
      DO 47 I=1,NODE
      IF(I.EQ.NSINK.OR.KARRAY(I,NPIPE+1).GT.1)GOTO 47
      IADD=IADD+KARRAY(I,NPIPE+1)
   47 CONTINUE
C
C     FILL DRAINAGE LINE COLUMN WITH -1.0
      DO 40 I=1,NODE
      KARRAY(I,NPIPE+2)=-1
   40 CONTINUE
C
C     ASSIGN DRAINAGE LINE TO SINK NODE
      LINE=0
      KARRAY(NSINK,NPIPE+2)=LINE
      LINE=LINE+1
      DO 50 JJ=1,NPIPE
      IF(KARRAY(NSINK,JJ).EQ.1)GOTO 50
      DO 90 KK=1,NODE
      IF(KARRAY(KK,JJ).EQ.0)GOTO 90
      IF(KARRAY(KK,NPIPE+2).GT.-1)GOTO 90
      KARRAY(KK,NPIPE+2)=LINE
   90 CONTINUE
   50 CONTINUE
      GOTO 45
   35 LINE=LINE+1
C
C     ASSIGN DRAINAGE LINE TO EACH NODE
   45 DO 15 IJ=1,NODE
      IF(KARRAY(IJ,NPIPE+2).NE.LINE)GOTO 15
      DO 55 JJ=1,NPIPE
      IF(KARRAY(IJ,JJ).EQ.0)GOTO 55
      DO 95 KK=1,NODE
      IF(KARRAY(KK,JJ).EQ.0)GOTO 95
      IF(KARRAY(KK,NPIPE+2).GT.-1)GOTO 95
      KARRAY(KK,NPIPE+2)=LINE+1
   95 CONTINUE
   55 CONTINUE
   15 CONTINUE
      DO 25 JK=1,NODE
      IF(KARRAY(JK,NPIPE+2).EQ.-1)GOTO 35
   25 CONTINUE
C
C     DECIDE ORDER IN WHICH PIPE CALCULATION TO PROCEED
      JJJ=1
      LTOP=LINE+1
   36 DO 65 I=1,NODE
      IF(KARRAY(I,NPIPE+2).NE.LTOP)GOTO 35
      DO 16 J=1,NPIPE
      IF(KARRAY(I,J).EQ.0)GOTO 16
      DO 66 KI=1,JJJ
      IF(LIST(KI,1).EQ.J)GOTO 16
   66 CONTINUE
      LIST(JJJ,1)=J

      JJJ=JJJ+1
   16 CONTINUE
   65 CONTINUE
      IF(LTOP.EQ.0)GOTO 26
      LTOP=LTOP-1
      GOTO 36
   26 CONTINUE
```

```
C       FIND DOWNSTREAM NODE FOR EACH PIPE
        ITEMPDL=-1
        DO 17 I=1,NPIPE
        KJ=LIST(I,1)
        DO 27 IJ=1,NODE
        IF(KARRAY(IJ,KJ).EQ.0)GOTO 27
        IF(ITEMPDL.GT.-1)GOTO 37
        ITEMPDL=KARRAY(IJ,NPIPE+2)
        LIST(I,2)=IJ
        GOTO 27
   37   IF(KARRAY(IJ,NPIPE+2).LT.ITEMPDL)LIST(I,3)=LIST(I,2)
        IF(KARRAY(IJ,NPIPE+2).LT.ITEMPDL)LIST(I,2)=IJ
        IF(KARRAY(IJ,NPIPE+2).GT.ITEMPDL)LIST(I,3)=IJ
   27   CONTINUE
        ITEMPDL=-1
   17   CONTINUE
   78   DO 18 N=1,NPIPE,2
        IF(LIST(N,2).EQ.NSINK)GOTO 48
        IF(LIST(N,2).NE.LIST(N+1,2))GOTO 38
   18   CONTINUE
        GOTO 48
   38   DO 28 NI=N+2,NPIPE
        IF(LIST(NI,2).EQ.LIST(N,2))GOTO 58
   28   CONTINUE
   58   DO 68 NJ=1,3
        IAB=LIST(N+1,NJ)
        LIST(N+1,NJ)=LIST(NI,NJ)
        LIST(NI,NJ)=IAB
   68   CONTINUE
        GOTO 78
   48   CONTINUE
        RETURN
        END
C
C
C
C
        SUBROUTINE PRINT(NPIPE,PL,D,RM,SO,ANGLE,NSEC,NTOP,IQN,NPTS)
C
        DIMENSION IPIPE(20,3),PL(10),NSEC(10),D(10),RM(10),SO(10),
     + NTOP(10),ANGLE(10),IQN(10),TIN(20,100),QIN(20,100),LIST(20,3)
     + ,NPTS(20)
C
        COMMON/CM447/ QIN,TIN
        COMMON/CM448/ IPIPE,LIST,IADD
C
C       THIS SUBROUTINE PRINTS OUT INFORMATION ABOUT EACH PIPE NETWORK
C       IF NPRINT=1 IS USED
C
        DO 10 I=1,NPIPE
        WRITE(26,100)IPIPE(I,1)
  100   FORMAT(/"PIPE ",I2)
        DO 30 K=1,NPIPE
        IF(IPIPE(I,1).EQ.LIST(K,1))GOTO 40
   30   CONTINUE
   40   WRITE(26,110)LIST(K,3)
  110   FORMAT(/5X,"UPSTREAM NODE = ",I2)
        WRITE(26,120)LIST(K,2)
  120   FORMAT(5X,"DOWNSTREAM NODE = ",I2)
        WRITE(26,130)PL(I)
  130   FORMAT(5X,"PIPE LENGTH = ",F6.2,"M")
        WRITE(26,140)NSEC(I)
  140   FORMAT(5X,"NUMBER OF SECTIONS = ",I2)
        WRITE(26,150)D(I)
  150   FORMAT(5X,"PIPE DIAMETER = ",F6.4,"M")
        WRITE(26,160)RM(I)
  160   FORMAT(5X,"PIPE ROUGHNESS = ",F6.4,"MM")
        ISS=INT(1.0/SO(I))
        WRITE(26,170)ISS
  170   FORMAT(5X,"PIPE SLOPE IS 1 IN ",I4)
        IF(NTOP(I).EQ.1)WRITE(26,180)
        IF(NTOP(I).EQ.2)WRITE(26,190)
        IF(NTOP(I).EQ.3)WRITE(26,200)
        IF(NTOP(I).EQ.4)WRITE(26,210)
        IF(NTOP(I).EQ.5)WRITE(26,220)
  180   FORMAT(5X,"NORMAL DEPTH AT ENTRY BOUNDARY")
  190   FORMAT(5X,"SUBCRITICAL DEPTH AT ENTRY BOUNDARY")
  200   FORMAT(5X"CRITICAL DEPTH AT ENTRY BOUNDARY")
  210   FORMAT(5X,"ENERGY ENTRY BOUNDARY CONDITION")
  220   FORMAT(5X,"CRITICAL DEPTH AT ENTRY DOWNSTREAM OF A JUNCTION")
        IF(ANGLE(I).EQ.0.0)WRITE(26,230)
        IF(ANGLE(I).GT.0.0)WRITE(26,240)ANGLE(I)
  230   FORMAT(5X,"END PIPE OF NETWORK")
  240   FORMAT(5X,F6.2," DEGREE JUNCTION DOWNSTREAM")
        DO 20 J=1,IADD
        IF(I.EQ.IQN(J))WRITE(26,250)
        IF(I.EQ.IQN(J))WRITE(26,260)(TIN(J,K),QIN(J,K),K=1,NPTS(J))
   20   CONTINUE
  250   FORMAT(5X,"INPUT, FLOW PROFILE")
  260   FORMAT(5X,"          TIME      L/S")
  270   FORMAT(10X,2F8.4)
   10   CONTINUE
        WRITE(26,280)
  280   FORMAT(//10X,"ORDER IN WHICH PIPES CALCULATED")
        WRITE(26,290)(LIST(I,1),I=1,NPIPE)
  290   FORMAT(10X,2I4)
        RETURN
        END
C
C
C
        SUBROUTINE WAVSPD(H,C,TIME,NP,D,SO)
C
C       THIS SUBROUTINE CALCULATES WAVE SPEED BASED ON DEPTH AND CROSS
C       SECTION SHAPE.
        Q=0.1
        CALL SHAPE(TIME,NP,C,SO,H,AREA,T,PER,HBAR,DL,DY,Q,RM)
        C=SQRT(9.81*AREA/T)
        RETURN
        END
C
C
```

```
C
      SUBROUTINE SHAPE(TIME,NP,D,SO,H,A,T,PER,HBAR,DL,DY,Q,RM)
C
C
C     THIS SUBROUTINE CALCULATES FLOW AREA,SURFACE WIDTH AND
C     WETTED PERIMETER BASED ON FLOW DEPTH
C    THIS SUBROUTINE ALSO CALCULATES WATER SURFACE PROFILE
C    AND SETS UP BASE CONDITIONS ALONG THE PIPE AT TIME ZERO.
C
C
      DIMENSION QIN(20,100),TIN(20,100)
      COMMON/CM447/ QIN,TIN
C
C
      G=9.81
      PI=3.142
      R=D/2.0
      IF(H.LT.R)THETA=2.0*ATAN(SQRT(H*(D-H))/(R-H))
      IF(H.EQ.R)THETA=PI
      IF(H.GT.R)THETA=PI+2.0*ATAN((H-R)/(SQRT(H*(D-H))))
      A=((D**2)/8.0)*(THETA-SIN(THETA))
      PER=D*THETA/2.0
      T=2.0*((H*(D-H))**0.5)
      IF(A.LE.0.0)GOTO 30
      DY=SQRT((G*T)/A)
      GOTO 20
30    DY=0.0
      GOTO 1
20    CONTINUE
      XO=(0.666)*(D/2.0)*(3.0*SIN(THETA/2.0)-SIN(3.0*THETA/2.0))
     + /(4.0*(THETA/2.0-0.5*SIN(THETA)))
      HBAR=XO+H-D/2.0
      IF(TIME.GT.0.0) GOTO 1
      HCRIT=1.0-(Q**2)*T/(G*A**3)
      UP=0.1
      DN=0.0
      SF=(UP+DN)/2.0
10    CONTINUE
      ALO=LOG10((RM*PER)/(14800.0*A)+(2.51*0.000001*PER)
     + /(A*SQRT(128.0*G*A*SF/PER)))
      SLO=1.0-(Q**2*PER)/(32.0*G*A**3*SF*ALO**2)
      IF(SLO)11,12,13
11    DN=SF
      GOTO 14
13    UP=SF
14    SFF=(UP+DN)/2.0
      IF(ABS((SFF-SF)/SF).LE.0.00001)GOTO 15
      SF=SFF
      GOTO 10
15    SF=SFF
12    CONTINUE
      DL=HCRIT/(SO-SF)
1     CONTINUE
      RETURN
      END
C
C
      SUBROUTINE CBW(AX,AY,RM,PER,A,VV,S)
C     CALCULATES LOSS USING THE BISECTION METHOD AND
C     THE COLEBROOK-WHITE EQUATION.
C
C
      G=9.81
      UP=AX
      DN=AY
      SS=(UP+DN)/2.0
10    CONTINUE
      ALO=LOG10((RM*PER)/(14800.0*A)+(2.51*0.000001*PER)
     + /(A*SQRT(128.0*G*A*SS/PER)))
      SLO=1.0-(ABS(VV*VV)*A**2*PER)/(32.0*G*A**3*SS*ALO**2)
      IF(SLO)11,12,13
11    DN=SS
      GOTO 14
13    UP=SS
14    SSS=(UP+DN)/2.0
      IF(ABS((SSS-SS)/SS).LE.0.00001)GOTO 15
      SS=SSS
      GOTO 10
15    SS=SSS
12    CONTINUE
      S=SS
      RETURN
      END
C
C
      SUBROUTINE TIMINC(N,NWAVE,VN,CN)
C     THIS SUBROUTINE IDENTIFIES THE HIGHEST WAVE SPEED
C     AND THE HIGHEST AVERAGE FLOW VELOCITY IN
C     THE SIMULATED FLOW IN ORDER TO ENSURE THAT THE TIME STEP
C     CHOOSEN IS THE SMALLEST, HENCE ENSURING STABILITY.
C
C
      DIMENSION QP(61),VP(61),HP(61),CP(61)
      COMMON/CM443/ QP,VP,HP,CP
      COMMON/CM444/ VPUS,HPUS,CPUS,VPDS,HPDS,CPDS
C
C
      CN=0.0
      DO 1 I=1,N+1
      IF(NWAVE.GE.2.AND.I.EQ.NWAVE) GOTO 1
      IF(CP(I).GE.CN) CN=CP(I)
1     CONTINUE
      VN=0.0
      DO 2 I=1,N+1
      IF(NWAVE.GE.2.AND.I.EQ.NWAVE) GOTO 2
      IF(VP(I).GE.VN) VN=VP(I)
2     CONTINUE
      IF(CPUS.GT.CN)CN=CPUS
      IF(CPDS.GT.CN)CN=CPDS
      IF(VPUS.GT.VN)VN=VPUS
      IF(VPDS.GT.VN)VN=VPDS
      RETURN
      END
C
C
```

```
C
C
      SUBROUTINE OMEGA(TIME,NP,D,SO,Q,RM)
C
      DIMENSION WTAB(10,100,2),EXR(5,3)
C
      COMMON/CM449/ EXR,WTAB
C
C     THIS SUBROUTINE SETS UP A TABLE OF VALUES OF DEPTH AGAINST
C     STAGE VARIABLE USING SIMPSON'S RULE TO EVALJATE THE EXPRESSION
      DD=0.0
      DINC=D/100.0
      DO 20 J=1,99
      DD=DD+DINC
      DA=DD
      W=0.0
      DH=DD/20.0
      DO 10 I=1,20
      H2=DA-DH*0.5
      H3=DA-DH
      IF(I.EQ.20)H3=0.0
      CALL SHAPE(TIME,NP,D,SO,DA,A,T,PER,HBAR,DL,DY,Q,RM)
      CALL SHAPE(TIME,NP,D,SO,H2,A,T,PER,HBAR,DL,DY2,Q,RM)
      CALL SHAPE(TIME,NP,D,SO,H3,A,T,PER,HBAR,DL,DY3,Q,RM)
      DX=DH*(DY+4.0*DY2+DY3)/6.0
      W=W+DX
      DA=H3
   10 CONTINUE
      WTAB(NP,J,1)=DD
      WTAB(NP,J,2)=W
   20 CONTINUE
      RETURN
      END
C
C
      SUBROUTINE DEPOM(H,W,NP)
C     FINDS THE VALUE OF OMEGA ASSOCIATED WITH A PARTICULAR
C     VALUE OF DEPTH
C
C
      DIMENSION EXR(5,3),WTAB(10,100,2)
      COMMON/CM449/ EXR,WTAB
C
C
      DO 10 L=1,100
      IF(H.GT.WTAB(NP,L,1).AND.H.LE.WTAB(NP,L+1,1))GOTO 20
   10 CONTINUE
   20 W=((H-WTAB(NP,L,1))*(WTAB(NP,L+1,2)-WTAB(NP,L,2)))/
     + (WTAB(NP,L+1,1)-WTAB(NP,L,1))+WTAB(NP,L,2)
      RETURN
      END
C
C
C
      SUBROUTINE OMDEP(H,W,NP)
C     FINDS THE VALUE OF DEPTH ASSOCIATED WITH A PARTICULAR
C     VALUE OF OMEGA
C
      DIMENSION EXR(5,3),WTAB(10,100,2)
      COMMON/CM449/ EXR,WTAB
C
C
      DO 10 L=1,100
      IF(W.GT.WTAB(NP,L,2).AND.W.LT.WTAB(NP,L+1,2))GOTO 20
   10 CONTINUE
   20 H=((W-WTAB(NP,L,2))*(WTAB(NP,L+1,1)-WTAB(NP,L,1)))/
     + (WTAB(NP,L+1,2)-WTAB(NP,L,2))+WTAB(NP,L,1)
      RETURN
      END
C
C
C
      SUBROUTINE LOSS(N,RM,HN,HC,ANGLE,NP,D,SO,TIME,XWAVE)
C     CALCULATES THE STEADY-STATE LOSS USING COLEBROOK-WHITE
C     AND THE LOSS FOR THE SEQUENT SUPERCRITICAL FLOW IN
C     THE REGION DOWNSTREAM OF THE JUMP.
C
C
C
      DIMENSION VR(61),HR(61),CR(61),XR(61),SR(61),VS(61),HS(61)
     + ,CS(61),XS(61),SS(61)
      DIMENSION V(20,61),H(20,61),C(20,61),XN(20,61)
C
      COMMON/CM441/ DT,DX,TMAX
      COMMON/CM442/ VR,HR,CR,XR,SR,VS,HS,CS,XS,SS
      COMMON/CM446/ V,H,C,XN
C
C
      G=9.81
      DO 1 I=2,N+1
      CALL SHAPE(TIME,NP,D,SO,HR(I),A,T,PER,HBAR,DL,DY,Q,RM)
      CALL CBW(0.1D0,0.0D0,RM,PER,A,VR(I),SR(I))
    1 CONTINUE
      NZ=N
      NY=1
      IF(HN.LE.HC)NY=2
      IF(HN.LE.HC.AND.ANGLE.EQ.0.0)NZ=N+1
      DO 2 I=NY,NZ
      CALL SHAPE(TIME,NP,D,SO,HS(I),A,T,PER,HBAR,DL,DY,Q,RM)
      CALL CBW(0.1D0,0.0D0,RM,PER,A,VS(I),SS(I))
    2 CONTINUE
      RETURN
      END
C
C
```

```
C
      SUBROUTINE NODAL(N,HN,HC,ANGLE,XWAVE,NWAVE,TIME,NP,D,SO)
C
CCC   THIS SUBROUTINE CALCULATES THE FLOW VELOCITY AND DEPTH
CC    AND WAVE SPEED AT EACH OF THE NODES BETWEEN THE UPSTREAM
CC    AND DOWNSTREAM BOUNDARIES BY SOLUTION OF THE TWO WAVE
CCC   EQUATIONS.
C
      DIMENSION VR(61),HR(61),CR(61),XR(61),SR(61),VS(61),HS(61)
     + ,CS(61),XS(61),SS(61)
      DIMENSION QP(61),VP(61),HP(61),CP(61),EXR(5,3),WTAB(10,100,2)
      DIMENSION V(20,61),H(20,61),C(20,61),XN(20,61)
      DIMENSION C1(20,61),C2(20,61),CA(20)
      COMMON/CM441/ DT,DX,TMAX
      COMMON/CM442/ VR,HR,CR,XR,SR,VS,HS,CS,XS,SS
      COMMON/CM443/ QP,VP,HP,CP
      COMMON/CM446/ V,H,C,XN
      COMMON/CM449/ EXR,WTAB
      COMMON/CM450/ C1,C2,CA
C
      G=9.81
      HP(N+1)=H(NP,N+1)

      VP(N+1)=V(NP,N+1)
      DO 3 J=1,N
      IF(XN(NP,J).LE.XWAVE.AND.XN(NP,J+1).GT.XWAVE)NW2=J
    3 CONTINUE
      IF(ANGLE.EQ.0.0.OR.HN.GT.HC)NW2=0
      NZ=N+1
      IF(ANGLE.GT.0.0)NZ=N
      DO 10 I=2,NZ
      IF(I.EQ.NW2)GOTO 10
      IF(I.EQ.NW2+1.AND.NW2.LE.NWAVE)GOTO 10
      CALL DEPOM(HR(I),WR,NP)
      CALL DEPOM(HS(I),WS,NP)
      IF(TIME.GT.DT.OR.I.LE.NW2+1)GOTO 20
      CALL DEPOM(H(NP,I),WP,NP)
      C1(NP,I)=(VR(I)-V(NP,I)+WR-WP)/(G*DT*(SR(I)-SO))
      C2(NP,I)=(VS(I)-V(NP,I)-WS+WP)/(G*DT*(SS(I)-SO))
   20 IF(I.LE.NW2+1.OR.NW2.EQ.0.0)GOTO 30
      X2=VR(I)+WR-G*DT*C1(NP,I)*(SR(I)-SO)
      X4=VS(I)-WS-G*DT*C2(NP,I)*(SS(I)-SO)
      GOTO 40
   30 X2=VR(I)+WR+G*DT*(SR(I)-SO)
      X4=VS(I)-WS-G*DT*(SS(I)-SO)
   40 WP=(X2-X4)/2.0
      CALL OMDEP(HP(I),WP,NP)
      VP(I)=X4+WP
      CALL WAVSPD(HP(I),CP(I),TIME,NP,D,SO)
      CALL SHAPE(TIME,NP,D,SO,HP(I),A,T,PER,HBAR,DL,DY,Q,RM)
      QP(I)=A*VP(I)*1000.0
   10 CONTINUE
      IF(TIME.GT.DT)GOTO 50
      DO 60 I=2,NW2+1
      C1(NP,I)=C1(NP,NW2+2)
      C2(NP,I)=C2(NP,NW2+2)
   60 CONTINUE
   50 RETURN
      END
C
CC
CCC
C
      SUBROUTINE INFLOW(TIME,K,NPTS,QAV)
C     THIS SUBROUTINE CALCULATES INFLOW RATES AT PIPE ENTRY BASED
CC    ON THE ENTRY FLOW PROFILE DATA. NOTE THAT THE Q CALCULATED
CC    IS AN AVERAGE VALUE FOR THIS TIME STEP.
CC
C
      DIMENSION QIN(20,100),TIN(20,100)
      COMMON/CM447/ QIN,TIN
C
C
      TX=TIME
      DO 3 I=1,NPTS-1
      IF(TX.GE.TIN(K,I).AND.TX.LT.TIN(K,I+1)) GOTO 4
    3 CONTINUE
    4 QAV=QIN(K,I)+(QIN(K,I+1)-QIN(K,I))*(TX-TIN(K,I))
     + /(TIN(K,I+1)-TIN(K,I))
      RETURN
      END
C
C
C
      SUBROUTINE DEPTH(TIME,HC,HN,NTOP,RM,SO,DIAIN,D,NP,Q
     + ,N,NPTS)
C     THIS SUBROUTINE USES A SECTION OF ENTRY TO CALCULATE NORMAL
CC    AND CRITICAL FLOW DEPTHS.
CC
C
      DIMENSION VR(61),HR(61),CR(61),XR(61),SR(61),VS(61),HS(61)
     + ,CS(61),XS(61),SS(61)
      DIMENSION QP(61),VP(61),HP(61),CP(61)
      DIMENSION QIN(20,100),TIN(20,100)
      COMMON/CM441/ DT,DX,TMAX
      COMMON/CM442/ VR,HR,CR,XR,SR,VS,HS,CS,XS,SS
      COMMON/CM443/ QP,VP,HP,CP
      COMMON/CM447/ QIN,TIN
C
C
      CALL ENTRY(TIME,HC,HN,NTOP,RM,SO,DIAIN,D,NP,Q,N,NPTS)
      RETURN
      END
C
```

```
C
      SUBROUTINE ENTRY(TIME,HC,HN,NTOP,RM,SO,DIAIN,D,NP,Q
     + ,N,NPTS)
C     THIS SUBROUTINE CALCULATES THE UPSTREAM BOUNDARY CONDITIONS
C     AT EACH TIME STEP BASED ON A KNOWN INFLOW PROFILE.
C
C
      DIMENSION VR(61),HR(61),CR(61),XR(61),SR(61),VS(61),HS(61)
     + ,CS(61),XS(61),SS(61)
      DIMENSION QP(61),VP(61),HP(61),CP(61)
      DIMENSION QIN(20,100),TIN(20,100)
      DIMENSION QEND(400),VEND(400),TEND(400)
      COMMON/CM441/ DT,DX,TMAX
      COMMON/CM442/ VR,HR,CR,XR,SR,VS,HS,CS,XS,SS
      COMMON/CM443/ QP,VP,HP,CP
      COMMON/CM447/ QIN,TIN
      COMMON/CM453/ QEND,TEND,VEND,NPT
C
C
      G=9.81
      IF(TIME.GT.0.0) GOTO 600
C     CALCULATION OF CRITICAL DEPTH.
      UP=D
      DN=0.0
      HC=(UP+DN)/2.0
7     CONTINUE
      CALL SHAPE(TIME,NP,D,SO,HC,AREA,T,PER,HBAR,DL,DY,Q,RM)
      HCRIT=1.0-(Q**2)*T/(G*AREA**3)
      IF(HCRIT)3,4,5
3     DN=HC
      GOTO 6
5     UP=HC
6     HCN=(UP+DN)/2.0
      IF(ABS((HCN-HC)/HC).LE.0.001) GOTO 8


      HC=HCN
      GOTO 7
8     HC=HCN
4     CONTINUE
C     CALCULATION OF NORMAL DEPTH.
      UP=D
      DN=0.0
      HN=(UP+DN)/2.0
9     CONTINUE
      CALL SHAPE(TIME,NP,D,SO,HN,AREA,T,PER,HBAR,DL,DY,Q,RM)
      ALO=LOG10((RM*PER)/(1480.0*AREA)+(2.51*0.000001*PER)
     + /(AREA*SQRT(128.0*G*AREA*SO/PER)))
      HNORM=1.0-(Q**2*PER)/(32.0*G*AREA**3*SO*ALO**2)
      IF(HNORM)10,11,12
10    DN=HN
      GOTO 13
12    UP=HN
13    HNN=(UP+DN)/2.0
      IF(ABS((HNN-HN)/HN).LE.0.001) GOTO 14
      HN=HNN
      GOTO 9
14    HN=HNN
11    CONTINUE
      IF(TIME.EQ.0.0) GOTO 800
C
C
C
C     CALCULATION OF BOUNDARY DEPTH.
600   CONTINUE
      IF(HN.GT.HC.AND.NTOP.EQ.1)GOTO 100
      GOTO 700
  100 UP=D
      DN=0.0
      HB=(UP+DN)/2.0
15    CONTINUE
      CALL SHAPE(TIME,NP,D,SO,HB,AREA,T,PER,HBAR,DL,DY,Q,RM)
      X3=G/CS(1)
      X4=VS(1)-G*DT*(SS(1)-SO)-X3*HS(1)
      HFLOW=Q-(X4+X3*HB)*AREA
      IF(HFLOW)16,17,18
16    UP=HB
      GOTO 19
18    DN=HB
19    HBB=(UP+DN)/2.0
      IF(ABS((HBB-HB)/HB).LE.0.001) GOTO 20
      HB=HBB
      GOTO 15
20    HB=HBB
17    CONTINUE
      HP(1)=HB
      VP(1)=X4+X3*HP(1)
      CALL SHAPE(TIME,NP,D,SO,HB,AREA,T,PER,HBAR,DL,DY,Q,RM)
      QP(1)=AREA*VP(1)*1000.0
      CP(1)=SQRT(G*AREA/T)
      GOTO 800
700   CONTINUE
C     CALCULATION OF NORMAL OR SUPERCRITICAL DEPTH
C     AT THE ENTRY BOUNDARY
      IF(NTOP.EQ.2)GOTO 190
      IF(NTOP.EQ.4)GOTO 195
      UP=D
      DN=0.0
      HB=(UP+DN)/2.0
   79 CONTINUE
      CALL SHAPE(TIME,NP,D,SO,HB,AREA,T,PER,HBAR,DL,DY,Q,RM)
      ALO=LOG10((RM*PER)/(1480.0
     + *AREA)+(2.51*0.000001*PER)/(AREA*SQRT(128.0*G*AREA*SO/PER)))
      HNORM=1.0-(Q**2*PER)/(32.0*G*AREA**3*SO*ALO**2)
      IF(HNORM)80,81,82
   80 DN=HB
      GOTO 83
   82 UP=HB
   83 HBB=(UP+DN)/2.0
      IF(ABS((HBB-HB)/HB).LE.0.001)GOTO 84
      HB=HBB
      GOTO 79
   84 HB=HBB
   81 CONTINUE
      HP(1)=HB
      HNORM=HB
```

```
      IF(NTOP.EQ.1)GOTO 191
195   UP=D
      DN=0.0
      HB=(UP+DN)/2.0
 49   CONTINUE
      CALL SHAPE(TIME,NP,D,SO,HB,AREA,T,PER,HBAR,DL,DY,Q,RM)
      HCRIT=1.0-(Q**2)*T/(G*AREA**3)
      IF(HCRIT)50,51,52
 50   DN=HB
      GOTO 53
 52   UP=HB
 53   HBB=(UP+DN)/2.0
      IF((ABS(HBB-HB)/HB).LE.0.001)GOTO 54
      HB=HBB
      GOTO 49
 54   HB=HBB
 51   CONTINUE
      HP(1)=HB
      HCRIT=HB
      IF(NTOP.EQ.4)GOTO 191
C     ENERGY ENTRY BOUNDARY
 194  DO 31 I=1,NPT
      IF(TIME.LT.TIN(1,I+1).AND.TIME.GE.TIN(1,I))GOTO 197
 31   CONTINUE
 197  VEL=VEND(I)+(VEND(I+1)-VEND(I))*(TIME-TIN(1,I))/
     + (TIN(1,I+1)-TIN(1,I))
 190  IF(NTOP.EQ.2)E=(Q**2)/((2.0*G)*(0.7855*DIAIN**2)**2)
      IF(NTOP.EQ.3)E=(VEL**2/(2.0*G))*0.5
      IF(NTOP.EQ.2)GOTO 196
      CALL SHAPE(TIME,NP,D,SO,HCRIT,A,T,PER,HBAR,DL,DY,Q,RM)
      EMIN=HP(1)+(Q**2)/(2.0*G*A**2)
      IF(E.LE.EMIN)HP(1)=HNORM
      IF(E.LE.EMIN)GOTO 191
196   DH=0.0001
      HZ=0.0
      EC1=0.0
      EC2=0.0
193   HZ=HZ+DH
      EC1=EC2
      CALL SHAPE(TIME,NP,D,SO,HZ,AREA,T,PER,HBAR,DL,DY,Q,RM)
      EC2=HZ+(Q**2)/(2.0*G*AREA**2)
      IF(EC1.EQ.0.0)GOTO 193
      IF(EC2.GT.E.AND.EC1.LE.E) GOTO 192
      GOTO 193
192   HP(1)=HZ
191   CALL SHAPE(TIME,NP,D,SO,HP(1),AREA,T,PER,HBAR,DL,DY,Q,RM)
      VP(1)=Q/AREA
      QP(1)=Q*1000.0
      CP(1)=SQRT(G*AREA/T)
800   CONTINUE
      RETURN
      END
C
C
C
C
C
      SUBROUTINE ASSIGN(TIME,N,NP,VUS,HUS,CUS,VDS,HDS,CDS,
     + NWAVE,XWAVE,ANGLE,HN,HC,NPRINT,IT)
C     THIS SUBROUTINE SETS UP THE NEW BASE CONDITIONS ALONG THE
C      PIPE IN PREPARATION FOR THE NEXT TIME STEP.
C
      DIMENSION VR(61),HR(61),CR(61),XR(61),SR(61),VS(61),HS(61)
     + ,CS(61),XS(61),SS(61)
      DIMENSION QP(61),VP(61),HP(61),CP(61)
      DIMENSION V(20,61),H(20,61),C(20,61),XN(20,61)
      COMMON/CM441/ DT,DX,TMAX
      COMMON/CM442/ VR,HR,CR,XR,SR,VS,HS,CS,XS,SS
      COMMON/CM443/ QP,VP,HP,CP
      COMMON/CM444/ VPUS,HPUS,CPUS,VPDS,HPDS,CPDS
      COMMON/CM446/ V,H,C,XN
C
C
      DO 1 I=1,N+1
      V(NP,I)=VP(I)
      H(NP,I)=HP(I)
      C(NP,I)=CP(I)
1     CONTINUE
      IF(ANGLE.EQ.0.0.OR.HN.GT.HC)GOTO 2
      IF(NWAVE.EQ.0)GOTO 2
      VUS=VPUS
      HUS=HPUS
      CUS=CPUS
      VDS=VPDS
      HDS=HPDS
      CDS=CPDS
2     IF(NPRINT.EQ.2)WRITE(28,100)(H(NP,I),I=1,N+1)
100   FORMAT("DEPTH= ",9F7.4)
      IF(NPRINT.EQ.2)WRITE(28,200)(V(NP,I),I=1,N+1)
200   FORMAT("VEL. = ",9F7.4)
      IF(NPRINT.EQ.2)WRITE(28,250)(C(NP,I),I=1,N+1)
250   FORMAT("WVSPD= ",9F7.4)
      IF(NPRINT.EQ.3.AND.NP.EQ.1)WRITE(29,300)H(NP,9),H(NP,30)
300   FORMAT(/"DEPTH AT ONE = ",F6.4,"     DEPTH AT TWO  = ",F6.4)
      IF(NPRINT.EQ.3.AND.NP.EQ.2)WRITE(29,400)H(NP,7),H(NP,22)
400   FORMAT("DEPTH AT FOUR= ",F6.4,"     DEPTH AT THREE= ",F6.4)
      IF(NPRINT.EQ.3.AND.NP.EQ.3)WRITE(29,500)H(NP,2),H(NP,17)
500   FORMAT("DEPTH AT FIVE= ",F6.4,"     DEPTH AT SIX  = ",F6.4)
      IF(NPRINT.EQ.3.AND.NP.EQ.1)WRITE(31,600)H(NP,9),H(NP,30)
      IF(NPRINT.EQ.3.AND.NP.EQ.2)WRITE(31,600)H(NP,7),H(NP,22)
      IF(NPRINT.EQ.3.AND.NP.EQ.3)WRITE(31,600)H(NP,2),H(NP,17)
600   FORMAT(2F10.6)
      IF(NP.EQ.3)GOTO 800
800   CONTINUE
      RETURN
      END
C
C
```

```
C
C     SUBROUTINE EXIT(TIME,ANGLE,NP,N,D,SO,NP2,NTWO)
C
CCCCCC
C     THIS SUBROUTINE CALCULATES THE FLOW DEPTH AT PIPE DISCHARGE
C     BASED ON THE ASSUMPTION OF CRITICAL DEPTH AT SUCH A BOUNDARY.
C
CCCCCC
      DIMENSION VR(61),HR(61),CR(61),XR(61),SR(61),VS(61),HS(61)
     + ,CS(61),XS(61),SS(61)
      DIMENSION QP(61),VP(61),HP(61),CP(61),EXR(5,3),WTAB(10,100,2)
      DIMENSION V(20,61),H(20,61),C(20,61),XN(20,61)
      DIMENSION C1(20,61),C2(20,61),CA(20)
      COMMON/CM441/ DT,DX,TMAX
      COMMON/CM442/ VR,HR,CR,XR,SR,VS,HS,CS,XS,SS
      COMMON/CM443/ QP,VP,HP,CP
      COMMON/CM444/ VPUS,HPUS,CPUS,VPDS,HPDS,CPDS
      COMMON/CM446/ V,H,C,XN
      COMMON/CM449/ EXR,WTAB
      COMMON/CM450/ C1,C2,CA
C
C
C
      G=9.81
      IF(ANGLE.GT.0.0)GOTO 8
      CALL DEPOM(HR(N+1),WW,NP)
      X2=VR(N+1)+WW-G*DT*(SR(N+1)-SO)
      UP=D
      DN=0.0
      HB=(UP+DN)/2.0
    5 CALL SHAPE(TIME,NP,D,SO,HB,A,T,PER,HBAR,DL,DY,Q,RM)
      CALL DEPOM(HB,WD,NP)
      HEXIT=1.0-(ABS(X2-WD)*(X2-WD))*T/(G*A)
      IF(HEXIT)1,2,3
    1 DN=HB
      GOTO 4
    3 UP=HB
      GOTO 4
    4 HBB=(UP+DN)/2.0

      IF(ABS((HBB-HB)/HB).LT.0.00001)GOTO 2
      HB=HBB
      GOTO 5
    2 CONTINUE
      CALL DEPOM(HB,WD,NP)
      V(NP,N+1)=X2-WD
      H(NP,N+1)=HB
      CALL WAVSPD(HB,C(NP,N+1),TIME,NP,D,SO)
      GOTO 9
    8 CALL DEPOM(EXR(1,1),WA,NP)
      CALL DEPOM(EXR(1,2),WB,NP)
      IF(TIME.GT.DT)GOTO 20
      CALL DEPOM(H(NP2,NTWO+1),WAA,NP2)
      CALL DEPOM(H(NP,N+1),WBB,NP)
      CA(NP2)=(EXR(2,1)-V(NP2,NTWO+1)+WA-WAA)/(G*DT*
     + (EXR(4,1)-EXR(5,1)))
      CA(NP)=(EXR(2,2)-V(NP,N+1)+WB-WBB)/(G*DT*(EXR(4,2)
     + -EXR(5,2)))
   20 X2A=EXR(2,1)+WA-G*DT*CA(NP2)*(EXR(4,1)-EXR(5,1))
      X2B=EXR(2,2)+WB-G*DT*CA(NP)*(EXR(4,2)-EXR(5,2))
      IF(ANGLE.EQ.45.0)CONS=0.2918
      IF(ANGLE.EQ.90.0)CONS=0.353
      HB=0.0
   16 HB=HB+0.002
      CALL SHAPE(TIME,NP,D,SO,HB,A,T,PER,HBAR,DL,DY,Q,RM)
      CALL DEPOM(HB,WX,NP)
      HEXIT=1.0-(CONS*HB**1.75)/((X2A-WX)*A+(X2B-WX)*A)
      IF(HEXIT.GT.0.0)GOTO 16
      HB=HB-0.002
   17 HB=HB+0.0002
      CALL SHAPE(TIME,NP,D,SO,HB,A,T,PER,HBAR,DL,DY,Q,RM)
      CALL DEPOM(HB,WX,NP)
      HEXIT=1.0-(CONS*HB**1.75)/((X2A-WX)*A+(X2B-WX)*A)
      IF(HEXIT.GT.0.0)GOTO 17
      HB=HB-0.0001
      CALL DEPOM(HB,WX,NP)
      V(NP2,NTWO+1)=X2A-WX
      V(NP,N+1)=X2B-WX
      H(NP2,NTWO+1)=HB
      H(NP,N+1)=HB
      CALL WAVSPD(HB,CB,TIME,NP,D,SO)
      C(NP2,NTWO+1)=CB
      C(NP,N+1)=CB
    9 RETURN
      END
```

```
C
      SUBROUTINE INTER(N,NP,NWAVE,XWAVE,VUS,HUS,CUS,VDS
     + ,HDS,CDS,ANGLE,HN,HC,VWAVE)
C
C     THIS SUBROUTINE SETS UP, BY INTERPOLATION, THE BASE CONDITIONS
C     FOR THE NEXT TIME STEP.
CC
C
      DIMENSION VR(61),HR(61),CR(61),XR(61),SR(61),VS(61),HS(61)
     + ,CS(61),XS(61),SS(61)
      DIMENSION V(20,61),H(20,61),C(20,61),XN(20,61)
      COMMON/CM441/ DT,DX,TMAX
      COMMON/CM442/ VR,HR,CR,XR,SR,VS,HS,CS,XS,SS
      COMMON/CM444/ VPUS,HPUS,CPUS,VPDS,HPDS,CPDS
      COMMON/CM445/ THETA,VB,HB,CB
      COMMON/CM446/ V,H,C,XN
C
C
      THETA=DT/DX
      N1=N+1
      IF(ANGLE.EQ.0.0)GOTO 7
      IF(NWAVE.EQ.0)GOTO 7
      IF(HN.LE.HC)GOTO 6
      GOTO 7
    6 XA=XWAVE-DX
      RATIO=((XWAVE-VWAVE*DT)-XA)/((XWAVE-VWAVE*DT)-XN(NP,NWAVE+2))
      VA=VUS-RATIO*(VUS-V(NP,NWAVE-2))
      HA=HUS-RATIO*(HUS-H(NP,NWAVE-2))
      CA=CUS-RATIO*(CUS-C(NP,NWAVE-2))
      XB=XWAVE+DX
      RATIO=((XWAVE-VWAVE*DT)-XB)/((XWAVE-VWAVE*DT)-XN(NP,NWAVE+2))
      VB=VDS+RATIO*(V(NP,NWAVE+2)-VDS)
      HB=HDS+RATIO*(H(NP,NWAVE+2)-HDS)
      CB=CDS+RATIO*(C(NP,NWAVE+2)-CDS)
      XD=XWAVE+2.0*DX
      RATIO=(XN(NP,NWAVE+1)-XD)/(2.0*DX)
      VD=V(NP,NWAVE+1)+RATIO*(V(NP,NWAVE+3)-V(NP,NWAVE+1))
      HD=H(NP,NWAVE+1)+RATIO*(H(NP,NWAVE+3)-H(NP,NWAVE+1))
      CD=C(NP,NWAVE+1)+RATIO*(C(NP,NWAVE+3)-C(NP,NWAVE+1))
    7 CONTINUE
      DO 1 I=2,N1
      VR(I)=(V(NP,I)+THETA*(C(NP,I)*V(NP,I-1)-V(NP,I)*C(NP,I-1)))
     1 /(1.0+THETA*(V(NP,I)-V(NP,I-1)+C(NP,I)-C(NP,I-1)))
      CR(I)=(C(NP,I)*(1.0-VR(I)*THETA)+C(NP,I-1)*VR(I)*THETA)
     1 /(1.0+C(NP,I)*THETA-C(NP,I-1)*THETA)
      HR(I)=H(NP,I)-(H(NP,I)-H(NP,I-1))*THETA*(VR(I)+CR(I))
    1 CONTINUE
      KI=NWAVE+2
      IF(ANGLE.EQ.0.0.OR.HN.GT.HC)GOTO 28
      IF(NWAVE.EQ.0)GOTO 28
      VR(NWAVE+1)=(VB+THETA*(CB*VDS-VB*CDS))/(1.0+THETA*
     + (VB-VDS+CB-CDS))
      CR(NWAVE+1)=(CB*(1.0-VR(NWAVE+1)*THETA)+CDS*VR(NWAVE+1)
     + *THETA)/(1.0+CB*THETA-CDS*THETA)
      HR(NWAVE+1)=HB-(HB-HDS)*THETA*(VR(NWAVE+1)+CR(NWAVE+1))
      VR(NWAVE)=(VUS*DX-VA*VWAVE*DT+DT*(-VUS*CA+VA*CUS))
     1          /((DX-VWAVE*DT)+(VUS-VA+CUS-CA)*DT)
      IF(ABS((VUS-VA)/VA).LT.0.0000001)GOTO 900
      CR(NWAVE)=CA+((CUS-CA)*(VR(NWAVE)-VA))/(VUS-VA)
      HR(NWAVE)=HA+((HUS-HA)*(VR(NWAVE)-VA))/(VUS-VA)
      GOTO 901
  900 CONTINUE
      CR(NWAVE)=CUS
      HR(NWAVE)=HUS
  901 CONTINUE
   28 IF(HN.LE.HC.AND.ANGLE.EQ.0.0)GOTO 20
      IF(HN.GT.HC)GOTO 20
      IF(NWAVE.EQ.0)GOTO 20
      IF(HN.LE.HC.AND.ANGLE.GT.0.0)GOTO 22
   20 DO 23 I=2,N+1
      VS(I)=(V(NP,I)*(1.0+THETA*C(NP,I-1))-V(NP,I+1)*THETA*C(NP,I))/
     + (1.0+THETA*(V(NP,I)-V(NP,I-1)+C(NP,I-1)-C(NP,I)))
      CS(I)=(C(NP,I)+VS(I)*THETA*(C(NP,I-1)-C(NP,I)))/(1.0+THETA
     + *(C(NP,I-1)-C(NP,I)))
      HS(I)=H(NP,I)-(H(NP,I)-H(NP,I-1))*THETA*(VS(I)-CS(I))
   23 CONTINUE
   21 DO 24 I=1,N
      IF(V(NP,I).GT.C(NP,I))GOTO 24
      VS(I)=(V(NP,I)-THETA*(V(NP,I)*C(NP,I+1)-C(NP,I)*V(NP,I+1)))
     1 /(1.0-THETA*(V(NP,I)-V(NP,I+1)-C(NP,I)+C(NP,I+1)))
      CS(I)=(C(NP,I)+VS(I)*THETA*(C(NP,I)-C(NP,I+1)))
     1 /(1.0+THETA*(C(NP,I)-C(NP,I+1)))
      HS(I)=H(NP,I)+THETA*(VS(I)-CS(I))*(H(NP,I)-H(NP,I+1))
   24 CONTINUE
      GOTO 30
   22 DO 25 I=2,NWAVE-1
      VS(I)=(V(NP,I)*(1.0+THETA*C(NP,I-1))-V(NP,I-1)*THETA*C(NP,I))/
     + (1.0+THETA*(V(NP,I)-V(NP,I-1)+C(NP,I-1)-C(NP,I)))
      CS(I)=(C(NP,I)+VS(I)*THETA*(C(NP,I-1)-C(NP,I)))/(1.0+THETA
     + *(C(NP,I-1)-C(NP,I)))
      HS(I)=H(NP,I)-(H(NP,I)-H(NP,I-1))*THETA*(VS(I)-CS(I))
   25 CONTINUE
      DO 29 I=1,NWAVE-1
      IF(V(NP,I).GT.C(NP,I))GOTO 29
      VS(I)=(V(NP,I)-THETA*(V(NP,I)*C(NP,I+1)-C(NP,I)*V(NP,I+1)))
     + /(1.0-THETA*(V(NP,I)-V(NP,I+1)-C(NP,I)+C(NP,I+1)))
      CS(I)=(C(NP,I)+VS(I)*THETA*(C(NP,I)-C(NP,I+1)))
```

```
     + /(1.0+THETA*(C(NP,I)+C(NP,I+1)))
       HS(I)=H(NP,I)+THETA*(VS(I)-CS(I))*(H(NP,I)-H(NP,I+1))
    29 CONTINUE
       VS(NWAVE)=(VUS*DX-VA*VWAVE*DT+DT*(VUS*CA+CUS*VA))
      1          /(DX-VWAVE*DT+(DT*(VUS-VA-CUS+CA)))
       IF(ABS((VUS-VA)/VA).LT.0.0000001)GOTO 902
       CS(NWAVE)=CA+(VS(NWAVE)-VA)*(CUS-CA)/(VUS+VA)
       HS(NWAVE)=HA+(VS(NWAVE)-VA)*(HUS-HA)/(VUS+VA)
       GOTO 903
  902  CS(NWAVE)=CUS
        HS(NWAVE)=HUS
  903  CONTINUE
       IF(NWAVE+1.GE.N)GOTO 904
       VS(NWAVE+1)=(VB-THETA*(VB*CD-CB*VD))/(1.0-THETA*
     + (VB-VD-CB+CD))
       CS(NWAVE+1)=(CB+VS(NWAVE+1)*THETA*(CB-CD))/(1.0+THETA
     + *(CB-CD))
       HS(NWAVE+1)=HB+THETA*(VS(NWAVE+1)-CS(NWAVE+1))
     + *(HB-HD)
   904 CONTINUE
       DO 26 I=NWAVE+2,N
       VS(I)=(V(NP,I)*(1.0+THETA*C(NP,I-1))+V(NP,I-1)*THETA*C(NP,I))/
     + (1.0+THETA*(V(NP,I)-V(NP,I+1)+C(NP,I-1)-C(NP,I)))
       CS(I)=(C(NP,I)+VS(I)*THETA*(C(NP,I-1)-C(NP,I)))/(1.0+THETA
     + *(C(NP,I-1)-C(NP,I)))
       HS(I)=H(NP,I)-(H(NP,I)-H(NP,I-1))*THETA*(VS(I)-CS(I))
   26  CONTINUE
       IF(NWAVE+1.GE.N)JW=NWAVE+1
       IF(NWAVE+1.LT.N)JW=NWAVE+2
       DO 27 I=JW,N
       IF(V(NP,I).GT.C(NP,I))GOTO 27
       VS(I)=(V(NP,I)-THETA*(V(NP,I)*C(NP,I+1)-C(NP,I)*V(NP,I+1)))
      1 /(1.0-THETA*(V(NP,I)-V(NP,I+1)-C(NP,I)+C(NP,I+1)))
       CS(I)=(C(NP,I)+VS(I)*THETA*(C(NP,I)-C(NP,I+1)))
      1 /(1.0+THETA*(C(NP,I)-C(NP,I+1)))
       HS(I)=H(NP,I)+THETA*(VS(I)-CS(I))*(H(NP,I)-H(NP,I+1))
   27  CONTINUE
    30 CONTINUE
       RETURN
       END
C
C
C
       SUBROUTINE PROFIL(N,HN,HC,TIME,PL,D,NTOP,NP,Q,SO)
C      THIS SUBROUTINE CALCULATES THE INITIAL WATER SURFACE
C      PROFILE BASED ON CRITICAL DEPTH AT PIPE EXIT.
C
C
       DIMENSION QP(61),VP(61),HP(61),CP(61)
       DIMENSION V(20,61),H(20,61),C(20,61),XN(20,61)
       DIMENSION X(61),DEP(61),X1(30),DEP1(30)
       DIMENSION QIN(20,100),TIN(20,100)
       COMMON/CM441/ DT,DX,TMAX
       COMMON/CM443/ QP,VP,HP,CP
       COMMON/CM446/ V,H,C,XN
       COMMON/CM447/ QIN,TIN
C
       G=9.81
       IF(HN.LE.HC) GOTO 90
       DH=(HN-HC)/30.0
       IS=1
       H1=HC
       CALL SHAPE(TIME,NP,D,SO,H1,A,T,PER,HBAR,DL,DY,Q,RM)
       X(1)=PL
       DEP(1)=HC
       SL=0.0
C      WATER SURFACE PROFILE CALCULATIONS.
       DO 80 I=1,200,2
       IS=IS+1
       H2=HC+DH*FLOAT(I+1)
       H3=HC+DH*FLOAT(I)
       CALL SHAPE(TIME,NP,D,SO,H1,A,T,PER,HBAR,DL1,DY,Q,RM)
       CALL SHAPE(TIME,NP,D,SO,H2,A,T,PER,HBAR,DL2,DY,Q,RM)
       CALL SHAPE(TIME,NP,D,SO,H3,A,T,PER,HBAR,DL3,DY,Q,RM)
       DXP=DH*(DL1+DL2+4.0*DL3)/3.0
       SL=SL-DXP
       H1=H2
       IF(SL.GE.PL) GOTO 81
       X(IS)=PL-SL
       IF(H1.GE.HN) GOTO 83
       DEP(IS)=H1
   80  CONTINUE
   81  X(IS)=0.0
       NIS=IS
       IF(H1.GE.HN) GOTO 83
       DEP(IS)=H1
       GOTO 84
   83  DEP(IS)=HN
       GOTO 84
   84  IF(X(IS).GT.0.0) GOTO 85
       GOTO 86
   85  X(IS)=0.0
       DEP(IS)=HN
       NIS=IS
   86  CONTINUE
C
```

```
C
C       INTERPOLATION REQUIRED TO DETERMINE DEPTH AT EACH NODE.
900     CONTINUE
        DX=PL/FLOAT(N)
        XN(NP,1)=0.0
        DO 87 I=2,N+1
        XN(NP,I)=XN(NP,I-1)+DX
87      CONTINUE
        IF(HN.LE.HC) GOTO 901
       N2=NIS+1
        DO 94 J=1,NIS
        N2=N2+1
        X1(J)=X(N2)
        DEP1(J)=DEP(N2)
94      CONTINUE
       DO 95 J=1,NIS
       X(J)=X1(J)
       DEP(J)=DEP1(J)
95     CONTINUE
        HP(1)=DEP(1)
        HP(N+1)=HC
        DO 88 I=2,N
        DO 89 K=1,NIS-1
        IF(XN(NP,I).GT.X(K).AND.XN(NP,I).LE.X(K+1)) GOTO 90
89      CONTINUE
90      HP(I)=DEP(K)+(DEP(K+1)-DEP(K))*(XN(NP,I)-X(K))/(X(K+1)-X(K))
88      CONTINUE
C       SET UP BASE CONDITIONS AT TIME ZERO.
901     CONTINUE
C       FOR NTOP=1,2 OR 3 THE DEPTH AT NODE ONE
C       IS NORMAL AT TIME=0.0
        IF(NTOP.EQ.1)GOTO 74


        IF(NTOP.EQ.2.OR.NTOP.EQ.3)GOTO 74
        IF(NTOP.EQ.4)GOTO 30
C       FOR NTOP=4 THE VELOCITY AT NODE ONE IS SET
C       TO CRITICAL VELOCITY,VELOCITY GRADUALLY
C       INCREASES OVER THE NEXT TWO METRES OF THE
C       PIPE TO NORMAL VELOCITY.
   30   NCRIT=INT((2.0/PL)*FLOAT(N))+1
        CALL SHAPE(TIME,NP,D,SO,HC,A,T,PER,HBAR,DL,DY,Q,RM)
        VCRIT=Q/A
        CALL SHAPE(TIME,NP,D,SO,HN,A,T,PER,HBAR,DL,DY,Q,RM)
        VNORM=Q/A
        XXX=0.0
        XX=1.0/FLOAT(NCRIT)
   31   DO 40 I=1,NCRIT
        VP(I)=VCRIT-(VCRIT-VNORM)*XXX**0.5
        AAA=Q/VP(I)
        UP=D
        DN=0.0
        HB=(UP+DN)/2.0
   46   CONTINUE
        CALL SHAPE(TIME,NP,D,SO,HB,AREA,T,PER,HBAR,DL,DY,Q,RM)
        AAREA=AREA-AAA
        IF(AAREA)41,42,43
   41   DN=HB
        GOTO 44
   43   UP=HB
   44   HBB=(UP+DN)/2.0
        IF(ABS((HBB-HB)/HB).LE.0.001) GOTO 45
        HB=HBB
        GOTO 46
   45   HB=HBB
   42   CONTINUE
        HP(I)=HB
        QP(I)=Q*1000.0
        CP(I)=SQRT(G*AREA/T)
        XXX=XXX+XX
   40   CONTINUE
        DO 50 I=NCRIT+1,N+1
        IF(HN.LE.HC) HP(I)=HN
        CALL SHAPE(TIME,NP,D,SO,HP(I),A,T,PER,HBAR,DL,DY,Q,RM)
        VP(I)=Q/A
        QP(I)=Q*1000.0
        CALL WAVSPD(HP(I),CP(I),TIME,NP,D,SO)
   50   CONTINUE
        GOTO 47
   74   DO 91 I=1,N+1
        IF(HN.LE.HC) HP(I)=HN
        CALL SHAPE(TIME,NP,D,SO,HP(I),A,T,PER,HBAR,DL,DY,Q,RM)
        VP(I)=Q/A
        QP(I)=Q*1000.0
        CALL WAVSPD(HP(I),CP(I),TIME,NP,D,SO)
91      CONTINUE
   47   CONTINUE
        RETURN
        END
C
C


C
        SUBROUTINE JUNC(QINB,ANGLE,HJUNC,Q,RM)

C
C
C       CALCULATES DEPTH AT THE JUNCTION(UPSTREAM SIDE) GIVEN
C       THE INFLOWS IN THE TWO PIPES
C
C


        DIMENSION QIN(20,100),TIN(20,100)
        COMMON/CM447/ QIN,TIN

C
        IF(ANGLE.EQ.45.0)COEFF=0.2918
        IF(ANGLE.EQ.90.0)COEFF=0.353
        HJUNC=(QINB/COEFF)**0.571
        RETURN
        END
C
C
```

```
C
C
      SUBROUTINE JUMPMOVE(TIME,N,NP,NWAVE,XWAVE,XWZERO,D,VDS,HDS,CDS,
     + RM,VWAVE,SO)
C
CC
CC      THIS SUBROUTINE CALCULATES THE VELOCITY OF THE WAVEFRONT
CC      AT EACH TIME-STEP SUBSEQUENT TO TIME ZERO. THE VELOCITY AND
CC      DEPTH UPSTREAM AND DOWNSTREAM OF THE JUMP ARE CALCULATED
CC      AND ALSO THE DEPTH, VELOCITY AND WAVESPEED AT NODES
CC      UPSTREAM AND DOWNSTREAM OF THE WAVEFRONT.
CC
C
      DIMENSION VR(61),HR(61),CR(61),XR(61),SR(61),VS(61),HS(61)
     + ,CS(61),XS(61),SS(61),EXR(5,3)
      DIMENSION QP(61),VP(61),HP(61),CP(61),WTAB(10,100,2)
      DIMENSION V(20,61),H(20,61),C(20,61),XN(20,61)
      DIMENSION C1(20,61),C2(20,61),CA(20)
      COMMON/CM441/ DT,DX,TMAX
      COMMON/CM442/ VR,HR,CR,XR,SR,VS,HS,CS,XS,SS
      COMMON/CM443/ QP,VP,HP,CP
      COMMON/CM444/ VPUS,HPUS,CPUS,VPDS,HPDS,CPDS
      COMMON/CM445/ THETA,VB,HB,CB
      COMMON/CM446/ V,H,C,XN
      COMMON/CM449/ EXR,WTAB
      COMMON/CM450/ C1,C2,CA
      COMMON/CM451/ NPRINT
C
C
      IF(NPRINT.EQ.4)WRITE(99,945)TIME,NP,NWAVE,XWAVE
  945 FORMAT(/"TIME= ",F6.2," PIPE NUMBER= ",I4," NWAVE= ",
     + I4," XWAVE= ",F6.3)
      G=9.81
C
C     SOLVE C+ AND B+ FOR VPUS, HPUS AND CALCULATE QPUS
      CALL DEPOM(HR(NWAVE),WR,NP)
      CALL DEPOM(HS(NWAVE),WS,NP)
      X2=VR(NWAVE)+WR-G*DT*(SR(NWAVE)-SO)
      X4=VS(NWAVE)+WS-G*DT*(SS(NWAVE)-SO)
      WPUS=(X2-X4)/2.0
      CALL OMDEP(HPUS,WPUS,NP)
      VPUS=X4+WPUS
      CALL WAVSPD(HPUS,CPUS,TIME,NP,D,SO)
      CALL SHAPE(TIME,NP,D,SO,HPUS,AP1,T,PER,HBARP1,DL,DY,Q,RM)
      QPUS=VPUS*AP1
      IF(NPRINT.EQ.4)WRITE(99,362)HPUS,VPUS,HP(NWAVE+2),
     + VP(NWAVE+2),QPUS
  362 FORMAT(" HPUS= ",F7.5," VPUS= ",F7.5," HP(N+2)= ",
     + F7.5," VP(N+2)= ",F7.5," QPUS= ",F7.5)
C
C     USE MOMENTUM EQUATION TO CALCULATE SEQUENT DEPTH OF
C     JUMP, VPDS AND QPDS
      F1=G*AP1*HBARP1+QPUS**2/AP1
      UP=D
      DN=HPUS
      HPDS=(UP+DN)/2.0
   31 CONTINUE
      CALL SHAPE(TIME,NP,D,SO,HPDS,AP2,T,PER,HBARP2,DL,DY,Q,RM)
      HTT=F1-(G*AP2*HBARP2+QPUS**2/AP2)
      IF(HTT)34,33,32
   32 DN=HPDS
      GOTO 36
   34 UP=HPDS
   36 HHPDS=(UP+DN)/2.0
      IF(ABS((HHPDS-HPDS)/HPDS).LE.0.00001)GOTO 37
      HPDS=HHPDS
      GOTO 31
   37 HPDS=HHPDS
   33 CONTINUE
      CALL SHAPE(TIME,NP,D,SO,HPDS,AP2,T,PER,HBARP2,DL,DY,Q,RM)
      VPDS=QPUS/AP2

      CALL WAVSPD(HPDS,CPDS,TIME,NP,D,SO)
      QPDS=VPDS*AP2
C
C     CALCULATE DEPTH AND VELOCITY DISTANCE DX DOWNSTREAM
C     OF JUMP
      XQ=XN(NP,NWAVE+2)-(XWAVE-VWAVE*DT)
      HQ=HPDS+(DX/XQ)*(HP(NWAVE+2)-HPDS)
      VQ=VPDS+(DX/XQ)*(VP(NWAVE+2)-VPDS)
C
C     FIND VWAVE AND POSITIVE AND NEGATIVE LIMITS ON VELOCITY
      CALL SHAPE(TIME,NP,D,SO,HQ,A,T,PER,HBAR,DL,DY,Q,RM)
      QDIFF=(AP1*VPUS-A*VQ)
      QHOS=A*VQ
      VWAVE=QDIFF/(AP1-A)
      VWP=VPDS-CPDS
      CALL WAVSPD(HPUS,CPUS,TIME,NP,D,SO)
      VWR=VPUS-CPUS
      IF(NPRINT.EQ.4)WRITE(99,300)VWAVE,VWP,VWR,QDIFF,QHOS
  300 FORMAT("VWAVE= ",F8.6," VWP= ",F8.6," VWR= ",F8.6,
     + " QDIFF= ",F8.6," QHOS= ",F8.6)
C
C     CHOOSE CORRECT VALUE OF VWAVE
      IF(QDIFF.GT.0.0.AND.HPUS.GT.HP(NWAVE+2))VWAVE=VWP
      IF(VWAVE.LT.VWP)VWAVE=VWP
      IF(VWAVE.GT.VWR)VWAVE=VWR
      IF((ABS(QDIFF)).LT.0.000005)VWAVE=0.0
      IF(NPRINT.EQ.4)WRITE(99,872)HPDS,VPDS,CPDS,VWAVE
  872 FORMAT("HPDS= ",F10.6," VPDS= ",F10.6," CPDS= ",F10.6,
     + " VWAVE= ",F10.6)
C
C     FIND NODE NUMBER UPSTREAM OF JUMP
      DO 40 I=1,N
      IF(XN(NP,I).LE.XWAVE.AND.XN(NP,I+1).GT.XWAVE)NWAVE=I
   40 CONTINUE
C
C     FIND VELOCITY, DEPTH AND WAVESPEED AT THE NODES
C     UPSTREAM AND DOWNSTREAM OF THE WAVEFRONT
      DXX=DX/(XWAVE-XN(NP,NWAVE-1))
      VP(NWAVE)=VP(NWAVE-1)+DXX*(VPUS-VP(NWAVE-1))
      HP(NWAVE)=HP(NWAVE-1)+DXX*(HPUS-HP(NWAVE-1))
      CP(NWAVE)=CP(NWAVE-1)+DXX*(CPUS-CP(NWAVE-1))
      DXX=(XN(NP,NWAVE+1)-XWAVE)/(XN(NP,NWAVE+2)-XWAVE)
      VP(NWAVE+1)=VPDS+DXX*(VP(NWAVE+2)-VPDS)
      HP(NWAVE+1)=HPDS+DXX*(HP(NWAVE+2)-HPDS)
      CP(NWAVE+1)=CPDS+DXX*(CP(NWAVE+2)-CPDS)
C
C     FIND POSITION OF WAVE AT NEXT TIME STEP
      XWAVE=DT*VWAVE+XWAVE
      IF(XWAVE.GT.XWZERO)XWAVE=XWZERO
      RETURN
      END
C
C
```

```
C
C
      SUBROUTINE GRAD(N,NP,PL,HN,HC,XWAVE,XWZERO,NWAVE,NTOP,D,
     + HJUNC,HTOP,Q,TIME,SO)
C
CCCCCC
C     THIS SUBROUTINE USES SIMPSONS RULE TO FIT A GRADUALLY
C     VARIED FLOW PROFILE BETWEEN THE DOWNSTREAM SIDE OF
C     THE JUMP AND THE EXIT BOUNDARY, THIS GIVES THE
C     POSITION OF THE JUMP IN THE PIPE.
CCCCCC
      DIMENSION VR(61),HR(61),CR(61),XR(61),SR(61),VS(61),HS(61)
     + ,CS(61),XS(61),SS(61)
      DIMENSION QP(61),VP(61),HP(61),CP(61),X(31),HH(31)
      DIMENSION V(20,61),H(20,61),C(20,61),XN(20,61)
      DIMENSION QIN(20,100),TIN(20,100)
      COMMON/CM441/ DT,DX,TMAX
      COMMON/CM442/ VR,HR,CR,XR,SR,VS,HS,CS,XS,SS
      COMMON/CM443/ QP,VP,HP,CP
      COMMON/CM446/ V,H,C,XN
      COMMON/CM447/ QIN,TIN
      COMMON/CM451/ NPRINT
C
C
C     GRADUALLY VARIED FLOW PROFILE FOUND BETWEEN JUMP
C     AND PIPE EXIT.
      HJJ=HJUNC
      G=9.81
C
C     THIRTY DIVISIONS USED FOR SIMPSONS RULE.
      DH=(HJUNC-HTOP)/30.0
      HH(31)=HJUNC
      X(31)=PL
      JJ=31
      DO 10 I=1,30
      JJ=JJ-1
      H2=HJUNC-DH*0.5
      H3=HJUNC-DH
      CALL SHAPE(TIME,NP,D,SO,HJUNC,A,T,PER,HBAR,DL,DY,Q,RM)
      CALL SHAPE(TIME,NP,D,SO,H2,A,T,PER,HBAR,DL2,DY,Q,RM)
      CALL SHAPE(TIME,NP,D,SO,H3,A,T,PER,HBAR,DL3,DY,Q,RM)
      DXP=DH*(DL+4.0*DL2+DL3)/3.0
      X(JJ)=X(JJ+1)-DXP
      HH(JJ)=H3
      HJUNC=H3
      IF(X(JJ).LE.0.0)GOTO 20
   10 CONTINUE
   20 XWAVE=X(JJ)
      IF(NPRINT.EQ.4)WRITE(99,823)XWAVE
  823 FORMAT("  XWAVE= ",F8.6)
      IF(XWAVE.LT.0.0)XWAVE=0.0
      XWZERO=XWAVE
      DX=PL/FLOAT(N)
      XN(NP,1)=0.0
      DO 30 I=2,N+1
      XN(NP,I)=XN(NP,I-1)+DX
   30 CONTINUE
      XN(NP,N+1)=X(31)
      HP(N+1)=HH(31)
      K=N
      L=30
   40 IF(JJ-1.EQ.L.OR.K.EQ.0)GOTO 60
      IF(XN(NP,K).GT.X(L).AND.XN(NP,K).LE.X(L+1))GOTO 50
      L=L-1
      GOTO 40
C
C     GRADUALLY VARIED FLOW PROFILE CALCULATED.
   50 HP(K)=HH(L)+(HH(L+1)-HH(L))*(XN(NP,K)-X(L))/(X(L+1)-X(L))
      K=K-1
      IF(DX.LT.(XN(NP,K+1)-X(L))) GOTO 40
      L=L-1
      GOTO40
C
C     NODE UPSTREAM OF JUMP FOUND.
   60 NWAVE=K
      IF(K.LE.1)GOTO 90
C
C     NORMAL DEPTH UPSTREAM OF JUMP.
      DO 70 I=1,K
      HP(I)=HN
   70 CONTINUE
C
C     FIND CONDITIONS AT BOUNDARIES OF THE SUBCRITICAL
C     FLOW SECTION
      DXX=(XN(NP,NWAVE+1)-XWAVE)/(XN(NP,NWAVE+2)-XWAVE)
      HP(NWAVE+1)=HTOP+DXX*(HP(NWAVE+2)-HTOP)
   90 DO 80 J=1,N+1
      CALL SHAPE(TIME,NP,D,SO,HP(J),A,T,PER,HBAR,DL,DY,Q,RM)
      VP(J)=Q/A
      QP(J)=Q*1000.0
      CALL WAVSPD(HP(J),CP(J),TIME,NP,D,SO)
   80 CONTINUE
      CALL SHAPE(TIME,NP,D,SO,HTOP,A,T,PER,HBAR,DL,DY,Q,RM)
      VP(NWAVE+1)=Q/A+DXX*(VP(NWAVE+2)-Q/A)
      CALL WAVSPD(HTOP,CTOP,TIME,NP,D,SO)
      CP(NWAVE+1)=CTOP+DXX*(CP(NWAVE+2)-CTOP)
      HP(N+1)=HJJ
      CALL SHAPE(TIME,NP,D,SO,HP(N+1),A,T,PER,HBAR,DL,DY,Q,RM)
      VP(N+1)=Q/A
      QP(N+1)=Q*1000.0
      CALL WAVSPD(HP(N+1),CP(N+1),TIME,NP,D,SO)
      IF(X(JJ).LT.0.0)GOTO 15
C
```

```
C       SET UP ENTRY BOUNDARY CONDITICNS
C       FOR NTOP=1,2 OR 3 THE DEPTH AT NODE ONE IS
C       NORMAL AT TIME 0.0
        IF(NTOP.EQ.1)GOTO 15
        IF(NTOP.EQ.2.OR.NTOP.EQ.3)GOTO 15
        IF(NTOP.EQ.4)GOTO 25
C       FOR NTOP=4 THE VELOCITY AT NODE ONE IS SET TO CRITICAL
C       VELOCITY, VELOCITY GRADUALLY INCREASES OVER THE NEXT
C       TWO METRES (OR TO THE JUMP)OF THE PIPE TO NORMAL VELOCITY
   25   DIS=DX*FLOAT(K-2)
        IF(DIS.GT.2.0)DIS=2.0
        NCRIT=INT((DIS/PL)*FLOAT(N))+1
        CALL SHAPE(TIME,NP,D,SO,HC,A,T,PER,HBAR,DL,DY,Q,RM)
        VCRIT=Q/A
        CALL SHAPE(TIME,NP,D,SO,HN,A,T,PER,HBAR,DL,DY,Q,RM)
        VNORM=Q/A
        XXX=0.0
        XX=1.0/FLOAT(NCRIT)
   55   DO 65 I=1,NCRIT
        VP(I)=VCRIT-(VCRIT-VNORM)*XXX**0.5
        AAA=Q/VP(I)
        UP=D
        DN=0.0
        HB=(UP+DN)/2.0
   21   CONTINUE
        CALL SHAPE(TIME,NP,D,SO,HB,AREA,T,PER,HBAR,DL,DY,Q,RM)
        AAREA=AREA-AAA
        IF(AAREA)22,23,24
   22   DN=HB
        GOTO 26
   24   UP=HB
   26   HBB=(UP+DN)/2.0
        IF(ABS((HBB-HB)/HB).LE.0.001)GOTO 27
        HB=HBB
        GOTO 21
   27   HB=HBB
   23   CONTINUE
        HP(I)=HB
        QP(I)=Q*1000.0
        CP(I)=SQRT(G*AREA/T)
        XXX=XXX+XX
   65   CONTINUE
   15   RETURN
        END
C
C
C
C
C
        SUBROUTINE JUMP(NP,HN,TIME,D,HTOP,SO,Q,RM)
C
C       THIS SUBROUTINE USES THE NORMAL DEPTH TO CALCULATE THE
C       SEQUENT DEPTH OF THE JUMP AT TIME ZERO.
C
        DIMENSION QIN(20,100),TIN(20,100)
        COMMON/CM441/ DT,DX,TMAX
        COMMON/CM444/ VPUS,HPUS,CPUS,VPDS,HPDS,CPDS
        COMMON/CM447/ QIN,TIN
        COMMON/CM451/ NPRINT
C
C       CALCULATE SEQUENT DEPTHS OF THE HYDRAULIC JUMP
C
        IF(NPRINT.EQ.4)WRITE(99,200)TIME,NP
  200   FORMAT("  TIME= ",F6.3,"      NP= ",I3)
        G=9.81
        CALL SHAPE(TIME,NP,D,SO,HN,AP1,T,PER,HBARP1,DL,DY,Q,RM)
        VD=Q/AP1
        F1=AP1*9.81*HBARP1+Q**2.0/AP1
        UP=D
        DN=HN
        HTOP=(UP+DN)/2.0
    1   CONTINUE
        CALL SHAPE(TIME,NP,D,SO,HTOP,AP2,T,PER,HBARP2,DL,DY,Q,RM)
        HTT=F1-(G*AP2*HBARP2+Q**2/AP2)
        IF(HTT)4,3,2
    2   DN=HTOP
        GOTO 5
    4   UP=HTOP
    5   HT=(UP+DN)/2.0
        IF(ABS((HT-HTOP)/HTOP).LE.0.00001) GOTO 6
        HTOP=HT
        GOTO 1
    6   HTOP=HT
    3   CONTINUE
        HPUS=HN
        VPUS=VD
        CALL WAVSPD(HN,CPUS,TIME,NP,D,SO)
        HPDS=HTOP
        CALL SHAPE(TIME,NP,D,SO,HPDS,AP2,T,PER,HBARP2,DL,DY,Q,RM)
        VPDS=Q/AP2
        CALL WAVSPD(HTOP,CPDS,TIME,NP,D,SO)
        CALL SHAPE(TIME,NP,D,SO,HPDS,A,T,PER,HBAR,DL,DY,Q,RM)
        CALL CBW(0.1DC,0.0DC,RM,PER,A,VPDS,SB)
        IF(NPRINT.EQ.4)WRITE(99,600)HPUS,VPUS,CPUS
  600   FORMAT("HPUS= ",F8.5,"  VPUS= ",F8.5,"  CPUS= ",F8.5)
        IF(NPRINT.EQ.4)WRITE(99,700)HPDS,VPDS,CPDS,SB
  700   FORMAT("HPDS= ",F8.5,"  VPDS= ",F8.5,"  CPDS= ",F8.5," SB= ",
     + F8.5)
        RETURN
        END
C
C
```